

**Compressive strength of rectangular columns made with ECC  
and confined with rectangular stirrups**

by

Wai Man Wong

A thesis submitted in partial fulfillment of the requirements for the degree of

**Master of Science**

in

**Structural Engineering**

Department of Civil and Environmental Engineering  
University of Alberta

© Wai Man Wong, 2018

## ABSTRACT

Engineered Cementitious Composites (ECC) is a type of high-performance fiber-reinforced cementitious composites (HPFRCC) which is designed to achieve high tensile strain capacity with strain hardening effect during the post-cracking response. The high tensile ductility of ECC with steady-state crack width has the potential to reduce the wide cracks and fracture problems associated with critical loads and large imposed deformations in structural members made with conventional concrete. Previous studies have demonstrated that the unique characteristics of ECC offer high damage tolerance capacity in tension – increasing the durability, safety, and sustainability of structures subjected to severe loading.

Under compression, however, there is a lack of data regarding confinement effects on reinforced-ECC (RECC) members. Thus, the design of ECC structures is usually made by assuming the ECC behaves in the same way as conventional concrete under compression, which can be inaccurate, uneconomical, or unsafe.

An experimental test program on confined ECC columns is performed in this study. Sixteen 100 mm x 100 mm x 300 mm ECC square columns, consisting of one set of unconfined ECC and three sets of confined ECC with 1%, 1.5% and 2% transverse steel content were fabricated and tested under monotonic compressive load until failure. The force-displacement and stress-strain relationships in the longitudinal direction were measured. An empirical stress-strain model for rectangularly confined high-strength ECC was developed based on an existing model for high-strength conventional concrete. The model was validated with the experimental results using an off-the-shelf material concrete model implemented into an open-source finite-element (FE) software, OpenSEES. After validation, a parametric study was conducted on a reinforced-ECC (RECC) frame and a reinforced-concrete (RC) control frame to evaluate their ductility capacities and cracking responses.

**Keywords** – Engineered Cementitious Composites (ECC), square columns, rectangular confinement model, finite-element (FE) analysis, dynamic analysis, static pushover analysis

## **DEDICATION**

To:

Mother 媽媽

Father 在天堂的爸爸

God.

媽媽·多謝你一直地愛我！

爸爸·你的女兒我長大了！

For God so loved the world that he gave his one and only Son, that whoever believes in him shall not perish but have eternal life.

**John 3:16**

## ACKNOWLEDGEMENTS

This project was funded by the Natural Sciences and Engineering Research Council of Canada (NSERC) and LafargeHolcim through an Engage Grant. Special thanks go to LafargeHolcim for the help in casting concrete for the experiment. The experimental program of this project was performed at the I.F Morrison Structures Laboratory and Concrete Laboratory at the University of Alberta. Thanks to Kuraray Co., for donating a portion of the PVA fibres, and to BASF for donating the high-range water-reducing admixture MasterGlenium 7700 for this research.

I would like to thank Dr. Carlos Cruz Noguez for all the support since the third year of my undergraduate degree. Dr. Carlos inspired me to continue with structural engineering in his Civ E 374 class. For my graduate studies, Dr. Carlos strongly supported me in my academic studies and research projects. Dr. Carlos is very passionate in structural engineering and he has been a great teacher, supervisor, and friend.

I would like to thank professors Dr. Roger Cheng, Dr. Samer Adeeb, Dr. Robert Driver, Mustafa Gul, Dr. Vivek Bindiganavile, Dr. Yong Li, and Dr. Douglas Tomlinson for their help and for sharing their experiences and knowledge with me. Special thanks to the AutoCAD and Surveying professor, Doug Booth, for sharing his advice with me.

I also would like to thank the concrete technician, Rizaldy Mariano, for helping me in the material casting and testing for this research, as well as the structural technicians, Greg Miller and Cameron West, who assisted in the test set-up, design, and testing, providing valuable advice all the way.

At the end, I would like to give unlimited thanks to my friends and fellow graduate students, who helped me with material casting, performing experimental tests, academic studies, sharing ideas and experiences, making me laugh, giving me great memories and moments, and so much more.

All this has been given by God. I would like thank God who never abandoned me and also made all this happen. Amen.



## TABLE OF CONTENTS

<b>CHAPTER 1. Introduction .....</b>	<b>1</b>
1.1 Background .....	1
1.2 Problem Statement .....	3
1.3 Scope and Objectives .....	5
1.4 Thesis Outline .....	6
<b>CHAPTER 2. Literature Review .....</b>	<b>7</b>
2.1 Background .....	7
2.2 ECC Material Design .....	9
2.3 ECC General Characteristics .....	12
2.3.1 Generalities .....	12
2.3.2 Tensile Characteristics.....	13
2.3.3 Compressive Characteristics.....	14
2.3.4 Flexural Characteristics .....	14
2.4 Structural Properties and Durability .....	15
2.4.1 Flexural Elements.....	15
2.4.2 Shear-critical Members .....	17
2.4.3 Axial Compression Elements .....	18
2.4.4 Beam-Column Connection Element.....	18
2.4.5 Durability under Various Environments.....	20
2.5 Structural Use of ECC .....	20
2.6 ECC Confinement research.....	22
2.6.1. Motaref et al. (2011) Confinement Model for ECC .....	22

<b>CHAPTER 3. ECC Fabrication and Characterization .....</b>	<b>25</b>
3.1 Scope.....	25
3.2 Engineered Cementitious Composite (ECC) .....	25
3.3 Material Components.....	26
3.3.1 Cement.....	26
3.3.2 Fly Ash .....	26
3.3.3 Aggregate .....	27
3.3.5 Superplasticizer .....	27
3.3.5 Water .....	27
3.3.6 PVA fibres .....	28
3.4 ECC Fabrication.....	28
3.4.1 Methodology.....	28
3.5 ECC Characterization .....	30
3.5.1 Uniaxial Compression Test .....	30
3.5.2 Uniaxial Tensile Test.....	31
3.6 ECC Mix Trials.....	34
3.6.1 ECC Mix Trial # 1 (ECC01) .....	34
3.6.2 ECC Mix Trial # 2 (ECC02) .....	38
3.6.3 ECC Mix Trial # 3 (ECC03) .....	42
3.6.4 ECC Mix Trial # 4 (ECC04) .....	46
3.6.5 ECC Mix Trial # 5 (ECC05) .....	50
3.6.6 ECC Mix Trial # 6 (ECC06) .....	54
3.6.7 ECC Mix Trial # 7 (ECC07) .....	58
3.6.8 ECC Mix Trial # 8 (ECC08) .....	62
3.6.9 ECC Mix Trial # 9 (ECC09) .....	66

3.6 Discussion .....	70
3.6.1 ECC mixes .....	70
3.6.2 Comparison of Tensile and Compressive Properties.....	72
3.7 Summary .....	78
<b>CHAPTER 4. Confinement on ECC .....</b>	<b>81</b>
4.1 Scope.....	81
4.2 Confinement.....	82
4.2.1 Confinement Models – Background .....	85
4.2.1.1 Mander et al. (1988) Model.....	85
4.2.1.2 Yong et al. (1988) Model .....	90
4.2.1.3 Bjerkeli et al. (1990) Model .....	93
4.3 Experimental Program .....	97
4.3.1 Geometry .....	97
4.3.2 Material.....	99
4.3.4 Instrumentation and Testing Procedure.....	103
4.3.5 Result and Discussion.....	106
4.4 Empirical Model for Stress-strain Relationship.....	120
4.4.1 Parameters of Stress-Strain Relationship .....	120
4.4.2 Summary of Empirical Model for Rectangularly Confined High-Strength ECC in Square Columns.....	123
Notation for the proposed ECC confinement model.....	128
<b>CHAPTER 5. VALIDATION AND PARAMETRIC ANALYSIS.....</b>	<b>130</b>
5.1 Scope.....	131
5.1 OpenSEES Software .....	132

5.2 OpenSEES Modelling.....	132
5.2.1 Frame Elements .....	132
5.2.2 Material.....	133
5.2.3 Section Modelling .....	136
5.2.4 Applying Mass and Load.....	137
5.2.5 Analysis Command .....	138
5.3 Validation.....	139
5.4 Frame Modelling.....	144
5.4.1 Building the Frame .....	145
5.4.2 Applying Mass and Gravity Load .....	152
5.4.3 Applying External Load .....	153
5.4.4 Recorder of Analysis Result.....	154
5.3 Finite-Element Analysis Results.....	155
5.3.1 Static Pushover Analysis .....	156
5.4.1 Dynamic Analysis .....	160
<b>CHAPTER 6. Summary and Conclusions .....</b>	<b>163</b>
6.1 Summary.....	163
6.2 Conclusions.....	164
6.2.1 ECC Fabrication and Characterization.....	164
6.2.2 Confinement effect on ECC .....	165
6.2.3 Parametric Study .....	166
6.3 Recommendations for Future Work.....	167
<b>References.....</b>	<b>168</b>
<b>Appendix A – Variation in mechanical properties of ECC09 .....</b>	<b>176</b>

<b>Appendix B – Poisson’s ratio of ECC09 .....</b>	<b>177</b>
<b>Appendix C – Averaging process and test variations .....</b>	<b>178</b>

## LIST OF TABLES

Table 2-1: Typical mix design for PVA-ECC (M45).....	12
Table 3-1: PVA-ECC M45 sample engineered cementitious composite mix design.....	25
Table 3-2: Material density for PVA-ECC M45.....	29
Table 3-3: Original Mixing Procedure for PVA-ECC M45 (Li, 2008).....	29
Table 3-4: Mix proportion of ECC01 .....	34
Table 3-5: Mixing sequence of ECC01 .....	34
Table 3-6: Mix proportion of ECC02 .....	38
Table 3-7: Mixing sequence of ECC02 .....	38
Table 3-8: Mix proportion of ECC03 .....	42
Table 3-9: Mixing sequence of ECC03 .....	42
Table 3-10: Mix proportion of ECC04 .....	46
Table 3-11: Mixing sequence of ECC04 .....	46
Table 3-12: Mix proportion of ECC05 .....	50
Table 3-13: Mixing Sequence of ECC05.....	50
Table 3-14: Mix proportion of ECC06 .....	54
Table 3-15: Mixing sequence of ECC06 .....	54
Table 3-16: Mix proportion of ECC07 .....	58
Table 3-17: Mixing sequence of ECC07 .....	58
Table 3-18: Mix proportion of ECC08 .....	62
Table 3-19: Mixing sequence of ECC08 .....	62
Table 3-20: Mix proportion of ECC09 .....	66
Table 3-21: Mixing sequence of ECC09 .....	66

Table 3-22: Summary of ECC trial mixes for compressive responses .....	74
Table 3-23: Summary of ECC trial mixes for tensile responses.....	77
Table 3-24: Optimized ECC-M45 mix proportion .....	80
Table 3-25: Optimized ECC-M45 mixing procedures.....	80
Table 4-1: Specimen geometry and material properties .....	99
Table 4-2: Summary of axial compressive test results .....	119
Table 4-3: Equations of Bjerkeli et al. model with the original and modified coefficients.....	122
Table 5-1: Summary of RC and RECC base columns cracking .....	160

## LIST OF FIGURES

Figure 1-1: Uniaxial tensile stress–deformation relation of concrete, FRC, and HPFRCC. (Li, 2008).....	1
Figure 1-2: A tensile stress–strain curve of an ECC (Li, 2008).....	2
Figure 1-3: Bendable Concrete ECC (Moore, 2009).....	2
Figure 1-4: Probability of having to demolish a building that has not collapsed as a function of the peak residual (EDP, engineering demand parameter; RIDR, residual interstorey drift ratio).....	4
Figure 2-1: The $\sigma$ – $\delta$ curve and the concept of complementary (Li, 2008).....	8
Figure 2-2: Tensile stress-strain relationship for ductile (a) PVA-ECC and (b) PE-ECC (Li, 2008).....	9
Figure 2-3: The $\sigma$ – $\delta$ curve and the concept of complementary (Li, 2003).....	10
Figure 2-4: (a) Low complementary results in Griffith type cracking, b) High complementary energy results in steady-state flat crack (Li, 2003).....	11
Figure 2-5: Uniaxial tensile stress-strain curve of an ECC (Li, 2008).....	13
Figure 2-6: Cracking mechanisms of (a) concrete, and (b) ECC (Li, 2003).....	14
Figure 2-7: Specimen configurations of the tested flexural elements: (a) RC; (b) RECC (Fischer and Li, 2002a).....	15
Figure 2-8: Hysteretic responses of flexural members (a) RC; and (b) RECC (Fischer and Li, 2002a).....	16
Figure 2-9: Flexural fatigue testing of ECC link-slab element (Kim et al., 2004).....	16
Figure 2-10: Hysteretic responses for shear beams (Fukuyama et al. 2000).....	17
Figure 2-11: Damage pattern in shear beams: (a) R/C, and (b) R/ECC (Fukuyama et al. 2000). ..	17
Figure 2-12: Small-scale circular column with spirals (Motaref et al., 2011).....	18
Figure 2-13: Crack pattern in beam-column interior connection: (a) RC, and (b) RECC (Qudah & Maalej, 2014).....	19



Figure 2-14: Cracking patterns of the tested column-to-steel beam: (a) RC, and (b)RECC (Parra-Montesinos and Wight, 2000).....	19
Figure 2-15: (a) Glorio Tower Roppongi, (b) Nabule Yokohama Tower and Residence (Kanda et. al 2011) .....	20
Figure 2-16: Placement of ECC on Mihara Bridge (Mitamura et al. 2005) .....	21
Figure 2-17: ECC link slab in Michigan (Li, 2006).....	21
Figure 2-18: Motaref et al. (2011) model for circular confined ECC.....	23
Figure 3-1: (a) ELRICH intensive mixer RV02E, (b) ECC Cylinders and Coupon specimen ....	30
Figure 3-2: (a) ECC Cylinder in compressometer, (b) Compressive test in MTS 815 machine ..	31
Figure 3-3: ECC coupon preparation - surface grinding .....	32
Figure 3-4: ECC coupon preparation - gluing aluminum plates.....	32
Figure 3-5: Tensile test setup in MTS 810 machine: (a) 2-D view, (b) 3-D view.....	33
Figure 3-6: (a) RECS-15 fibre before mixing, (b) ECC01 trial mix, (c) ECC01 cylinder .....	35
Figure 3-7: Uniaxial compressive stress-strain graph of ECC01.....	36
Figure 3-8: Uniaxial tensile stress-strain graph of ECC01 .....	36
Figure 3-9: Tensile cracking on ECC01 coupon specimen .....	37
Figure 3-10: (a) RECS-15 fibre before mixing, (b) ECC02 trial mix, (c) ECC02 specimens.....	39
Figure 3-11: Uniaxial compressive stress-strain graph of ECC02.....	40
Figure 3-12: Uniaxial tensile stress-strain graph of ECC02 .....	40
Figure 3-13: Tensile cracking on ECC02 coupon specimen .....	41
Figure 3-14: (a) RECS-15 fibre before mixing, (b) ECC03 trial mix, (c) ECC03 specimens.....	43
Figure 3-15: Uniaxial compressive stress-strain graph of ECC03.....	44
Figure 3-16: Uniaxial tensile stress-strain graph of ECC03 .....	44

Figure 3-17: Tensile cracking on ECC03 coupon specimen .....	45
Figure 3-18: (a) RECS-15 fibre before mixing, (b) ECC04 trial mix, (c) ECC04 specimen .....	47
Figure 3-19: Uniaxial compressive stress-strain graph of ECC04.....	48
Figure 3-20: Uniaxial tensile stress-strain graph of ECC04 .....	48
Figure 3-21: Tensile cracking on ECC04 coupon specimen .....	49
Figure 3-22: (a) RECS-15 fibre before mixing, (b) ECC05 trial mix, (c) ECC05 specimens.....	51
Figure 3-23: Uniaxial compressive stress-strain graph of ECC05.....	52
Figure 3-24: Uniaxial tensile stress-strain graph of ECC05 .....	52
Figure 3-25: Tensile cracking on ECC05 coupon specimen .....	53
Figure 3-26: (a) RECS-15 fibre before mixing, (b) ECC06 trial mix, (c) ECC06 specimens.....	55
Figure 3-27: Uniaxial compressive stress-strain graph of ECC06.....	56
Figure 3-28: Uniaxial tensile stress-strain graph of ECC06 .....	56
Figure 3-29: Tensile cracking on ECC06 coupon specimen .....	57
Figure 3-30: (a) RECS-15 fibre before mixing, (b) ECC07 trial mix, (c) ECC07 specimens.....	59
Figure 3-31: Uniaxial compressive stress-strain graph of ECC07.....	60
Figure 3-32: Uniaxial tensile stress-strain graph of ECC07 .....	60
Figure 3-33: Tensile cracking on ECC07 coupon specimen .....	61
Figure 3-34: (a) RECS-15 fibre before mixing, (b) ECC08 trial mix, (c) ECC08 specimen .....	63
Figure 3-35: Uniaxial compressive stress-strain graph of ECC08.....	64
Figure 3-36: Uniaxial tensile stress-strain graph of ECC08 .....	64
Figure 3-37: Tensile cracking on ECC08 specimen .....	65
Figure 3-38: (a) RECS-15 fibre before mixing, (b) ECC09 trial mix, (c) ECC09 specimens.....	67
Figure 3-39: Uniaxial compressive stress-strain graph of ECC09.....	68

Figure 3-40: Uniaxial tensile stress-strain graph of ECC09 .....	68
Figure 3-41: Tensile cracking of ECC09 specimen .....	69
Figure 3-42: Uniaxial tensile stress-strain graph of all ECC trial mixes .....	72
Figure 3-43: Uniaxial compressive stress-strain graph of all ECC trial mixes.....	75
Figure 3-44: Tensile stress-strain response of ECC09 and conventional concrete.....	79
Figure 3-45: Tensile stress-strain response of ECC09 and conventional concrete (close-up) .....	79
Figure 4-1: Stress-strain curves for concrete cylinders tested by Iyenfar et al. (1970) .....	82
Figure 4-2: Effect of spacing of transverse steel on efficiency of confinement (Park and Paulay 1975) .....	83
Figure 4-3: Confinement by square hoops and circular spirals (Park and Paulay 1975).....	83
Figure 4-4: Mander et al. (1988) model for confined and unconfined concrete.....	85
Figure 4-5: Effectively confined core for circular hoop reinforcement (Mander et al. 1988).....	88
Figure 4-6: Effectively confined core for rectangular hoop reinforcement (Mander et al. 1988)	89
Figure 4-7: Confined strength determination from lateral confining stresses for rectangular sections (Mander et al. 1988).....	89
Figure 4-8: Yong et al. (1988) model for confined high-strength concrete.....	90
Figure 4-9: Bjerkeli et al. (1990) model for confined high-strength concrete.....	93
Figure 4-10: Idealized “confining pressures” $f_r$ (Bjerkeli et al. 1990).....	94
Figure 4-11: Vertical and horizontal section with compressive axes between reinforcement (Bjerkeli et al. 1990) .....	94
Figure 4-12: Cross-sectional details of specimens.....	98
Figure 4-13: cross-sectional details of specimens with 0%, 1%, 1.5%, and 2% transverse steel content.....	98
Figure 4-14: Steel cage preparation .....	100

Figure 4-15: Steel cages of ECC-0%.....	100
Figure 4-16: Steel cage of ECC-1%.....	101
Figure 4-17: Steel cage of ECC-1.5%.....	101
Figure 4-18: Steel cage of ECC-2%.....	102
Figure 4-19: Specimen fabrication.....	103
Figure 4-20: Overall 2-D view of instrumentation of specimen.....	104
Figure 4-21: Overall 3-D view of instrumentation of specimen.....	104
Figure 4-22: General view of specimen testing in MTS 815 machine .....	105
Figure 4-23: Averaged load-displacement response for 0% confinement concrete square column .....	106
Figure 4-24: Averaged load-displacement response for 0% confinement ECC square column.	107
Figure 4-25: Averaged stress-strain response for 0% confinement concrete square column (Concrete-0%).....	108
Figure 4-26: Averaged stress-strain response for 0% confinement ECC square column (ECC-0%) .....	109
Figure 4-27: Ultimate cracking of (a) concrete-0% and (b) ECC-0% .....	110
Figure 4-28: Stress-strain graph of concrete cylinder and concrete square columns .....	112
Figure 4-29: Stress-strain graph of ECC cylinder and ECC square columns .....	112
Figure 4-30: Averaged load-displacement response for 1% confinement ECC square column.	113
Figure 4-31: Averaged load-displacement response for 1.5% confinement ECC square column .....	114
Figure 4-32: Averaged load-displacement response for 2% confinement ECC square column.	114
Figure 4-33: Averaged stress-strain response for 1% confinement ECC square column.....	115
Figure 4-34: Averaged stress-strain response for 1.5% confinement ECC square column.....	116

Figure 4-35: Averaged stress-strain response for 2% confinement ECC square column.....	117
Figure 4-36: Microcracks and boundary conditions at peak load on (a) ECC-1%, (b) ECC-1.5%, and (c) ECC-1.5%.....	118
Figure 4-37: Averaged stress-strain response for all square column.....	119
Figure 4-38: Proposed confinement model for Rectangular Confined High-Strength ECC in Square Columns .....	123
Figure 4-39: Comparison between ECC-1% test result and proposed model .....	126
Figure 4-40: Comparison between ECC-1.5% test result and proposed model .....	126
Figure 4-41: Comparison between ECC-2% test result and proposed model .....	127
Figure 4-42: Ideal "confining pressures" $f_r$ .....	129
Figure 4-43: Horizontal and vertical column cross-section.....	129
Figure 5-1: Uniaxial material Steel02 in OpenSEES (Mazzoni et al. 2006) .....	133
Figure 5-2: Uniaxial material Concrete02 in OpenSEES (Mazzoni et al. 2006).....	134
Figure 5-3: Uniaxial material ECC01 (Tension) (Mazzoni et al. 2006).....	135
Figure 5-4: Uniaxial material ECC01 (Compression) (Mazzoni et al. 2006).....	136
Figure 5-5: Example of fibre sections (Mazzoni et al. 2006) .....	137
Figure 5-6: Concrete cantilever column with ECC plastic hinge (Motaref et al. 2011).....	140
Figure 5-7: Displacement and base shear of a tested column with ECC plastic hinge (Motaref et al. 2011) .....	140
Figure 5-8: Configuration of the tested four-span bridge (Cruz-Noguez and Saiidi, 2010).....	141
Figure 5-9: Displacement and base shear of SMA Bent. Black line: measured; purple line: calculated (Cruz-Noguez and Saiidi, 2010).....	142
Figure 5-10: Load-displacement curve of ECC square columns with (a) unconfined material, (b) 1% confinement, (c) 1.5% confinement, (d) 2% confinement .....	143

Figure 5-11: Geometry of a 7-storey building with cross sections of columns and beams .....	145
Figure 5-12: Compressive and tensile behaviours of steel bars for OpenSEES .....	146
Figure 5-13: Compressive behaviour of unconfined concrete material in OpenSEES.....	147
Figure 5-14: Compressive behaviour of confined concrete material in OpenSEES.....	148
Figure 5-15: Tensile behaviour of concrete material in OpenSEES.....	148
Figure 5-16: Compressive behaviour of unconfined ECC material in OpenSEES .....	150
Figure 5-17: Compressive behaviour of confined ECC material in OpenSEES .....	151
Figure 5-18: Tensile behaviour of ECC material in OpenSEES.....	151
Figure 5-19: Lateral loads on a 7-Storey building in pushover analysis .....	153
Figure 5-20: Rinaldi record from the Northridge earthquake (1994) .....	154
Figure 5-21: Overall view of base column sections for cracking study .....	156
Figure 5-22: Shear-drift graph of RC building with associated cracking conditions .....	157
Figure 5-23: Base shear – Roof drift of RECC building .....	158
Figure 5-24: Shear-Drift graph of RECC (RECC01-19) building with associated cracking conditions.....	159
Figure 5-25: Roof Displacement of RC Building with associated Cracking Conditions .....	161
Figure 5-26: Roof Displacement of RECC Building with associated Cracking Conditions .....	161

## CHAPTER 1. INTRODUCTION

### 1.1 Background

Conventional concrete has a high compressive strength, which is an attractive material property in structural engineering. However, due to its low tensile strength and strain, significant cracks develop rapidly in the tension region (Fig. 1-1). To overcome this limitation, fibre-reinforced concrete (FRC) materials have been developed to gain post-cracking and tensile strain capacity (Fig. 1-1) by adding certain types of fibres such as steel, glass, carbon, synthetics, and natural fibres to the concrete mix. High-performance fibre-reinforced cementitious composites (HPFRCC) are a type of FRC designed to achieve higher tensile strain capacity with strain hardening effect during the post-cracking response (Fig. 1-1). Two main classes of HPFRCC have been developed in the recent years. One is Ductal®, a commercial HPFRCC that has a typical tensile strength of 12 MPa and a ductility of 0.02 to 0.06%. The other one is called Engineered Cementitious Composites (ECC), which has a typical moderate tensile strength of 4 to 6 MPa and a higher ductility of 3 to 5%. One of the best-known types of ECC was originally developed at the University of Michigan in the early 1990s. This was a micromechanical-based material made of cement, fly ash, silica sand, water and polymeric polyvinyl alcohol (PVA) fibres. By using micromechanical theory, this particular type of ECC has been successfully tailored to exhibit microcracking behaviour and achieving high tensile ductility (Li, 2008).

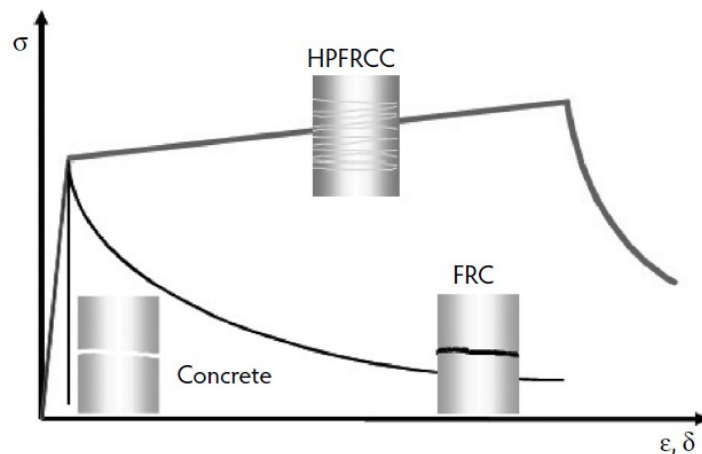


Figure 1-1: Uniaxial tensile stress–deformation relation of concrete, FRC, and HPFRCC. (Li, 2008)

The utilization of fibres in ECC leads to multiple fine cracks with crack widths below 100µm. The microcracking behaviour prevents localized crack openings and allows the development of larger tensile strain capacities. The uniaxial tensile stress-strain curve in Fig 1-2 shows that ECC is able to reach ultimate tensile strains up to 500 times higher than traditional concrete. Due to the “yielding” response in tension after the elastic stage, ECC exhibits a strain-hardening response after cracking (Fig. 1-2). Due to its high tensile capacity, ECC is also referred as “bendable concrete” (Fig. 1-3) because of the ultra-ductile behaviour which enables a large degree of curvature under bending without significant cracks in the tension region (Li, 2008).

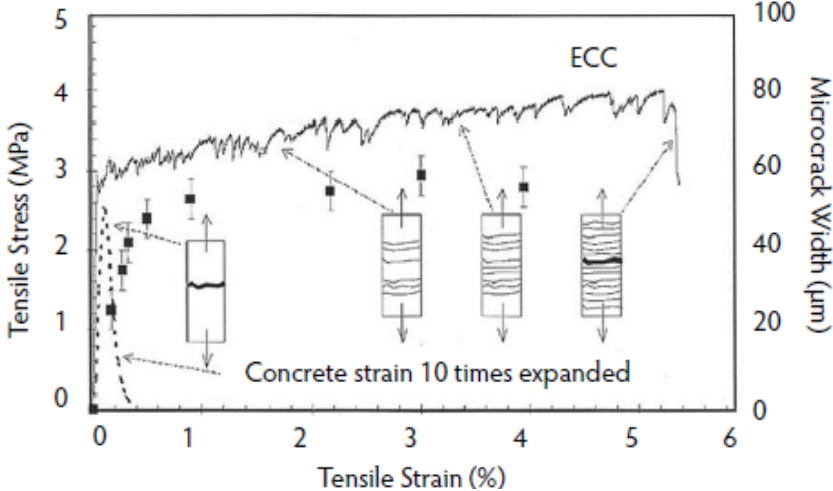


Figure 1-2: A tensile stress–strain curve of an ECC (Li, 2008)

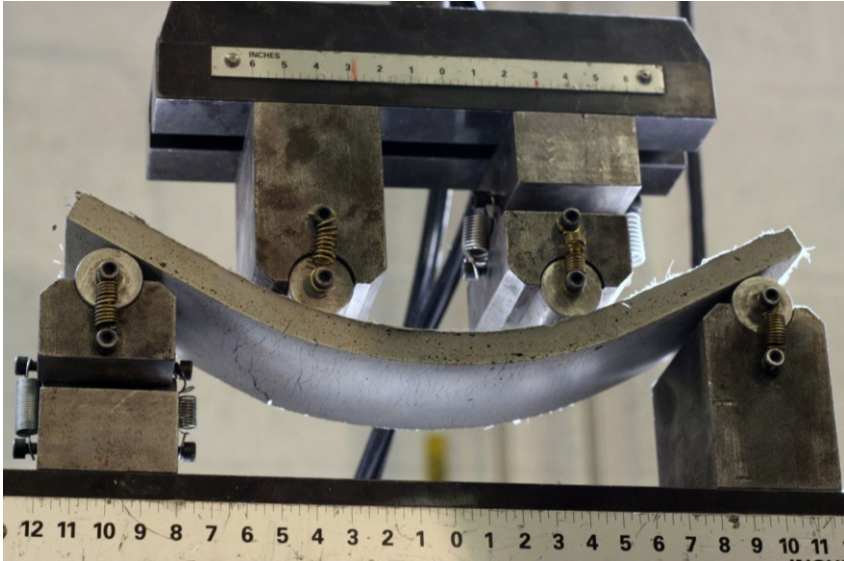


Figure 1-3: Bendable Concrete ECC (Moore, 2009)



The compression characteristics of ECC such as compressive strength and strain capacity are similar to the conventional compressive response of normal or high-strength concrete. While preserving the compressive behaviour of conventional concrete, the tensile ductility of ECC reduces cracking and fracture problems associated with overloads and large imposed deformations. The high damage tolerance capacity of ECC can increase durability, safety, and sustainability of structures subjected to severe loading. Past studies and structural experience in Japan and the U.S. have shown that structural elements made with ECC have superior structural performance than the concrete elements, in terms of resistance to cracking mechanism, damage mitigation, energy absorption, and resilience (Li, 2008).

## **1.2 Problem Statement**

When structures experience extreme loads such as earthquakes, conventional reinforced-concrete members will experience damage consisting of yielding of reinforcement steel, concrete cracking or spalling, and concrete crushing in compression. Severe economic losses due to earthquakes can result from building collapse or reparation and retrofitting activities. As shown in Fig. 1-4, the probability of having to demolish a reinforced-concrete building is approximately 10% if the maximum residual interstorey drift is about 1.0%. The probability graph also suggests that a building would have to be demolished if it experiences a residual interstorey drift of 3.0% or more (Ramirez & Miranda, 2012). For buildings that exhibit residual drifts lower than 1.0% and do not have to be demolished (the vast majority of structures under service seismic motions) costly repairs are usually required to address concrete spalling and cracking. Due to its high tensile ductility and microcracking capabilities, ECC is therefore an attractive alternative to reduce the cost of repairs at the service level due to seismic excitation.

To date, ECC has been used at the coupling beams of two high-rise reinforced concrete residential buildings (Kanda et al., 2011), a replacement overlay on a bridge in Japan (Mitamura et al., 2005), and a link-slab in a bridge in the U.S. (Lepech and Li, 2009). However, the use of this remarkable material for structural purposes and research studies in North America is very limited. Therefore, a pilot project on ECC characterization and use in confined columns is useful for future application in Canada and to develop resilient infrastructure with lower repair costs after critical events.

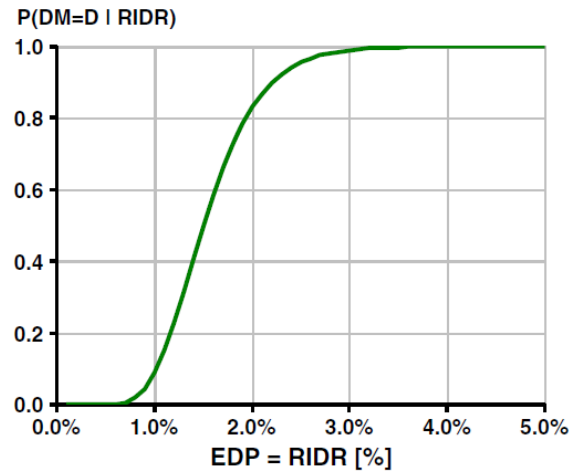


Figure 1-4: Probability of having to demolish a building that has not collapsed as a function of the peak residual (EDP, engineering demand parameter; RIDR, residual interstorey drift ratio) (Ramirez & Miranda, 2012)

During an earthquake, the extreme ground movement induces stresses in structures and damage is concentrated at critical regions in structural members, developing “plastic hinges” at those locations when the stresses enter into the inelastic stage. A sequential formation of plastic hinges will guarantee a ductile behaviour of the structure. In order to prevent brittle failure at the plastic hinges, the ductility of a structure is a significant consideration in seismic design since the ductile response can provide a warning of failure by producing large deformation. One of the approaches to increase the ductility of a structure is to detail the confinement of concrete materials under compression (Park and Paulay, 1975). Although there are many existing models for concrete confinement (Park and Paulay, 1975; Mander et al., 1988; Sheikh and Uzumeri, 1980; etc), confinement models for ECC are scarce. The only available model is the one developed by Motaref et al. (2011), which proposed for circular columns made with ECC and reinforced with transverse steel spirals. Due to the difference in behaviour between the confinement by circular steel spirals and confinement by rectangular or square hoops, it is essential to study the confinement effect on rectangular columns made with ECC with different quantities of transverse reinforcement.

### 1.3 Scope and Objectives

In this research, material fabrication and characterization of ECC material are investigated experimentally, and the confinement effects in rectangular columns made with ECC are studied. A confinement model for rectangular columns made with high-strength ECC is developed based on a model originally proposed for high-strength concrete. The model is validated with a finite-element analysis (FEA) and a parametric study of a full-scale ECC structure is presented.

The confinement effects study on ECC columns are conducted on small-scale specimens and square columns with transverse reinforcement ratios ranging from 1 to 2 % only. This research is conducted on one type of high-strength ECC material only. The parametric study is developed based on the empirical results from ECC characterization and confinement experimental test program.

The objectives of this research are as follows:

1. Fabricate and characterize the ECC material

*Specific Aim 1:* Investigate the feasibility of fabricating ECC with local Western Canada raw materials with PVA fibres from Japan

*Specific Aim 2:* Determine mechanical properties of the ECC through material tests such as compression tests and tensile tests.

2. Propose and validate a confinement model for ECC square columns

*Specific Aim 1:* Conduct an experimental test program on short square columns with different volumetric ratios of transverse reinforcement.

*Specific Aim 2:* Develop a confinement model which includes confined ECC behaviour through an analytical study on the test results and based on an existing model for high-strength concrete.

3. Develop a parametric analysis on a full-scale ECC structure.

*Specific Aim 1:* Validate the confinement model through FEA by comparing the predicted compressive load-deformation response of the tested specimens with the experimental results

*Specific Aim 2:* Develop a full-scale RECC structure in a finite-element software, OpenSEES.

*Specific Aim 3:* Develop a static pushover analysis and dynamic analysis for RECC structure to investigate the seismic performance of ECC material.

## **1.4 Thesis Outline**

This thesis is organized in 6 chapters. The outline of each chapter is as follows:

Chapter 1 presents a brief background of ECC and explains the motivation for this research. Objectives and organization of this thesis are also included.

Chapter 2 consists of a comprehensive literature review on ECC including the history, material design, mechanical properties, structural application, an introduction of confinement, and an overview of the available confinement models for ECC.

Chapter 3 discusses an experimental program for ECC fabrication and characterization. Experimental methodologies, test setup and empirical results are included. The optimized ECC mix proportion and mixing procedure for the ECC with the best performance are presented.

Chapter 4 introduces confinement and different existing confinement models for normal and high-strength concrete. This chapter also discusses an experimental program of confinement effect on ECC square columns with rectangular steel stirrups. The experimental methodology, test setup and empirical results are included. An empirical confinement model for rectangularly confined ECC in square column is developed.

Chapter 5 presents the validation of the confinement model developed in Chapter 4 with test results through FEA. A parametric analysis of a full-scale reinforced ECC structure is conducted in a finite-element software, OpenSEES. A static pushover analysis and a dynamic analysis using empirical results from chapter 3 and 4 are included, as well as an evaluation of the structural performance of ECC in terms of cracking.

Chapter 6 summarizes the studies and conclusions of this research. Recommendation for continue research and future work are also included.

## CHAPTER 2. LITERATURE REVIEW

This chapter summarizes the background for fibre-reinforced concrete and the development of Engineered Cementitious Composite (ECC). An introduction to ECC in regards to its mixture design and mechanical behaviour is presented. Structural performances and material durability of ECC are discussed along with the structural applications of ECC around the world.

### 2.1 Background

The effectiveness of short steel fibres in reducing the brittleness of concrete was first demonstrated by Romualdi and Batson (1963) and Romualdi and Mandel (1964). This led to the continued development of a variety of other fibre reinforcement in concrete, such as glass, carbon, synthetics, natural fibres, or even combination of different lengths and types of fibres (Li, 2008). These fibre-reinforced-concrete types (FRCs) possess a “ductile” tensile stress-strain response which provides a descending post-peak reserve of strength in tension (so-called tension softening), in comparison with the brittle response of conventional concrete. Aveston et al. (1971) and Krenchel and Stang (1989) studied the use of continuous aligned fibres and showed that the composite material could achieve hundreds of times higher tensile ductility than conventional concrete. Textile-reinforced FRCs studied by Curbach and Jesse (1999) and Reinhardt et al. (2003) and pultruded continuous fibre reinforced concrete studied by Mobasher et al. (2006) exhibit an ascending post-peak tensile response, which is distinct from the tension-softening response of FRC. Naaman and Reinhardt (2003) classified these materials as high-performance fibre-reinforced cementitious composites (HPFRCC). The differences in tensile response between normal concrete, FRC, and HPFRCC are illustrated in Fig. 2-1. Tensile strain capacity of conventional concrete is limited and gives a typical brittle failure. FRC have an improved response in reducing the brittleness of concrete. However, the deformation in FRC is localized onto a single fracture crack during tension softening. In contrast, the deformation in HPFRCC is composed of the opening of multiple fine cracks which allows elastic stretching of the material between these cracks.

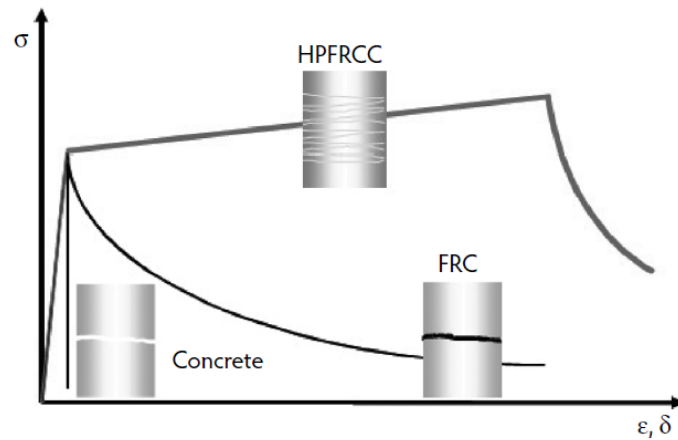


Figure 2-1: The  $\sigma$ - $\delta$  curve and the concept of complementary (Li, 2008)

A type of HPFRCC called Engineered Cementitious Composite (ECC), which incorporates polyvinyl alcohol (PVA) fibres, was originally developed at the University of Michigan. It has a typical tensile strength of 4 to 6 MPa and a tensile ductility of 3 to 5%. The tensile stress-strain responses shown in Figs. 2-1 and 2-2 illustrate that the steady-state fine cracks and high tensile ductility that allow ECC to exhibit the desired tensile ductility properties that are lacking in conventional concrete or in FRC.

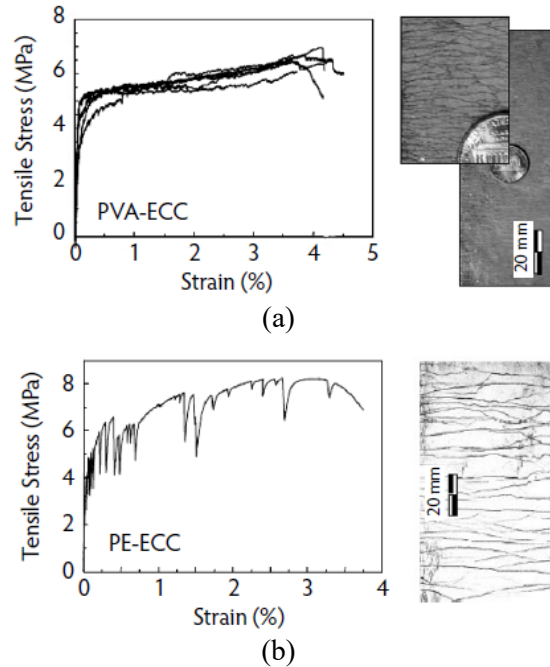


Figure 2-2: Tensile stress-strain relationship for ductile (a) PVA-ECC and (b) PE-ECC (Li, 2008)

## 2.2 ECC Material Design

The design approach of ECC seeks to create synergistic interactions between multiple microcracks while minimizing the fibre content (generally 2% or less by volume) which switches the material from a normal tension-softening FRC behaviour to a ductile ECC behaviour. Li et al. (2001), Li et al. (2002), Li, (2003), and Li (2008) have optimized ECC through micromechanics at the material constituent level to take advantage of the mechanical interactions between the fibre, mortar matrix, and fibre-matrix interface.

The fundamental property of a fibre reinforced cementitious material is found to be the fibre bridging property across a matrix crack (Li, 2003; Li, 1992; Li et al., 1993; Lin and Li, 1997). The fibres can be represented by non-linear springs connecting the opposite surfaces of a crack and provide forces acting against the opening of the crack when the composite is in tension. At the crack opening, a  $\sigma$ - $\delta$  relationship (Fig. 2-3) can be established where the averaged tensile stress  $\sigma$  is transmitted across a crack with crack opening  $\delta$ . In order to optimize the  $\sigma$ - $\delta$  relationship, two criteria related to strength and energy must be achieved (Li, 2003).

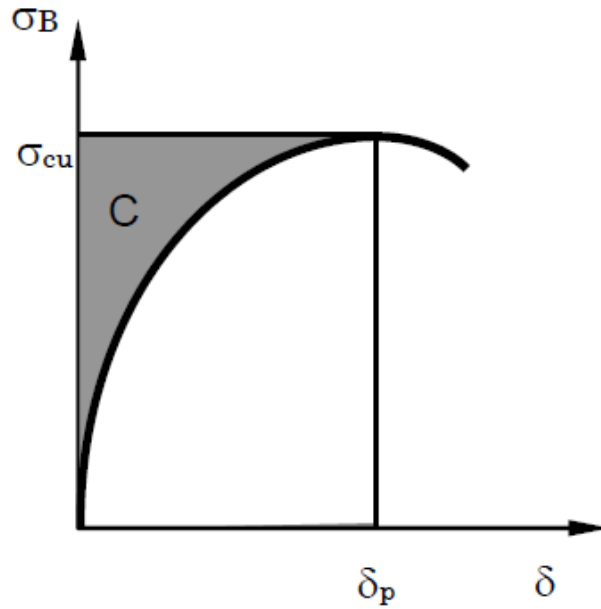


Figure 2-3: The  $\sigma$ - $\delta$  curve and the concept of complementary (Li, 2003)

In the strength criterion, the formation of a crack is governed by the bridging stress of fibre. When loading cannot be supported by the fibre bridging stress, the springs will be soften or break and lead to Griffith crack (Fig. 2-4a). Therefore, the matrix cracking strength must not exceed the maximum bridging stress  $\sigma_{cu}$  in order to achieve the steady-state flat crack shown in Fig. 2-4b (Li, 2003).

In the energy criterion, the mode of crack propagation is governed by the complementary energy, which is shown as the shaded area C in the  $\sigma$ - $\delta$  curve in Fig. 2-3. Steady-state crack analysis conducted by Li and Leung (1992) indicates that when the complementary energy is small, the crack will behave like a typical Griffith crack (Fig. 2-4a). When the fibre/matrix interface is too weak, fibre pull-out occurs and results in a low peak strength  $\sigma_{cu}$ . When the interface is too strong, fibre rupture occurs due to the stiff springs and results in a small value of critical opening  $\delta_p$ . In either case, the complementary energy will be small and leads to the tension-softening behaviour in a normal FRC where the formation of Griffith cracking can reduce the tensile loading capacity. In order to attain a steady-state crack with crack opening smaller than  $\delta_p$  (Fig. 2-4b), large complementary energy must be achieved so that the crack can remain flat as it propagates. In such case, springs across the steady-state flat crack are able to maintain and transfer the tensile load



back into the matrix and cause the formation of another crack. The repetition of this process results in the desired phenomenon of multiple microcracking for ECC (Li, 2003).

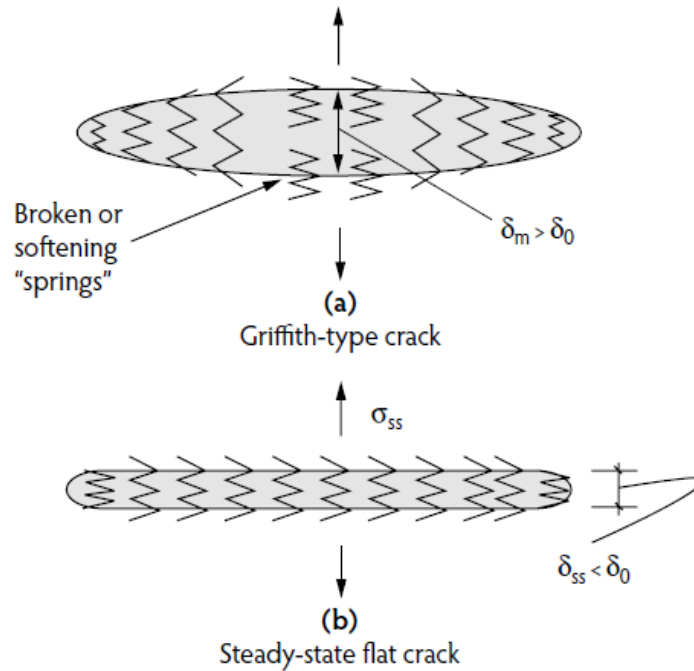


Figure 2-4: (a) Low complementary results in Griffith type cracking, b) High complementary energy results in steady-state flat crack (Li, 2003)

Lin et al. (1999) demonstrated that the shape of the  $\sigma$ - $\delta$  curve is governed by the fibre volume fraction, diameter, length, strength, and modulus, as well as the fibre/matrix interaction in terms of interfacial chemical and frictional bond properties. To control the  $\sigma$ - $\delta$  curve for ECC, Li et al. (2001), Li et al. (2002), Li (2003), and Li (2008) tailored a special type of PVA-ECC in which a proprietary surface coating agent is used to lower the interface chemical and frictional bond of the fibres.

Other than PVA fibres, other fibres such as high-modulus polyethylene (PE) fibres (Kamal et al., 2007; Li, 1993; Li and Wang, 2002) and polypropylene (PP) fibres (Takashima et al., 2003; Yang and Li, 2010) have been also successfully utilized to fabricate ECC and develop its unique tensile ductility characteristics.

## 2.3 ECC General Characteristics

### 2.3.1 Generalities

ECC is a general term to describe a family of composite materials which exhibits the unique characteristics of high tensile ductility and microcracking. Different classes of ECC have been developed to accommodate specific structural requirements and perform different functions in addition to high tensile ductility. For example, 1) high-early-strength ECC (HES-ECC) is designed for applications that require rapid strength gain (Wang and Li, 2006a); 2) lightweight ECC (LW-ECC) is designed for applications that require small dead load (Wang and Li, 2003); 3) Green ECC (G-ECC) is designed to maximize infrastructure sustainability (Lepech et al., 2007; Li et al., 2004b); 4) self-healing ECC (SHECC) offers recovery ability in mechanical properties after experiencing damage (Li and Yang, 2007; Yang et al., 2005). Polyvinyl Alcohol Fibre ECC with a minimum strength of 45 MPa (PVA-ECC [M45]), is the most commonly used type of ECC (Li, 2008).

The typical mix design for conventional PVA-ECC, so-called M45 has been optimized to satisfy the multiple cracking criteria reported in Li (2008) and Li et al. (2002) and to exhibit a minimum compressive strength of 45 MPa, even though it often reaches 60-80 MPa. The type, size, and amount of fibre and matrix ingredients, along with interface characteristics are tailored for multiple cracking and controlled crack width, and its minimum strength makes it a good candidate for use in structural applications. Therefore, the feasibility of fabricating PVA-ECC (45M) with materials available locally in western Canada and the material characterization will be investigated in this study. The optimized mix design for PVA-ECC (M45) given by Li (2008) is shown in Table 2-1.

Table 2-1: Typical mix design for PVA-ECC (M45)

Mix Designation	Cement	Fly Ash	Sand	Water	SP (Superplasticizer)	Fibre (Vol.)
M45	1.0	1.2	0.8	0.56	0.012	0.02

### 2.3.2 Tensile Characteristics

High tensile ductility and fine multiple cracking are the most important tensile characteristics of ECC. The uniaxial tensile stress-strain curve of ECC in Fig. 2-5 from Li (2008) illustrates the high tensile strain capacity (up to 5%) that ECC can achieve. The general tensile behaviour of ECC presents a metal-like response with “yielding” after the elastic stage when the first microcrack appears on the specimen. Multiple microcracking continues on ECC as the tensile load increases, until one of the multiple cracks forms a fracture plane. At that point, ECC reaches failure and behaves as normal FRC with tension-softening response (Li, 2008).

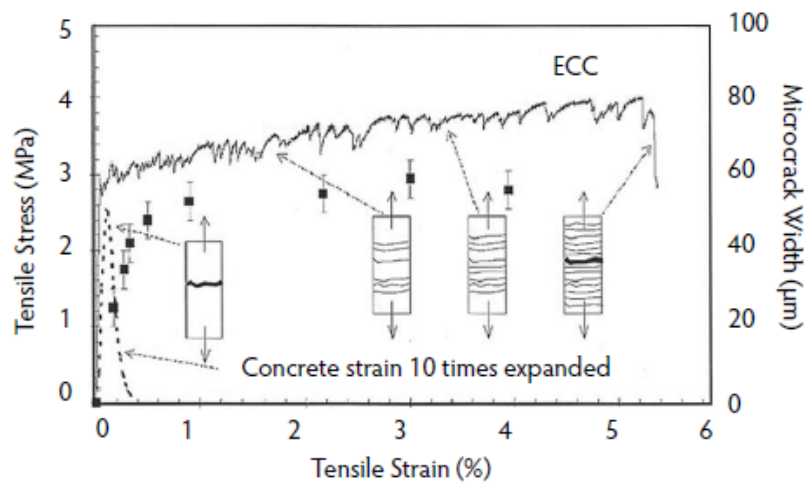


Figure 2-5: Uniaxial tensile stress-strain curve of an ECC (Li, 2008)

Developing multiple microcracks is necessary for ECC to achieve high tensile ductility. Li (2008) reported that the microcrack opening reaches about 60 µm by 1% strain. Continue loading beyond 1% strain causes multiple cracks but with no crack opening greater than the steady-state value of 60 µm. Li (2003) compared the crack localization in reinforced concrete element and the microcracking in reinforced ECC element (Fig. 2-6).

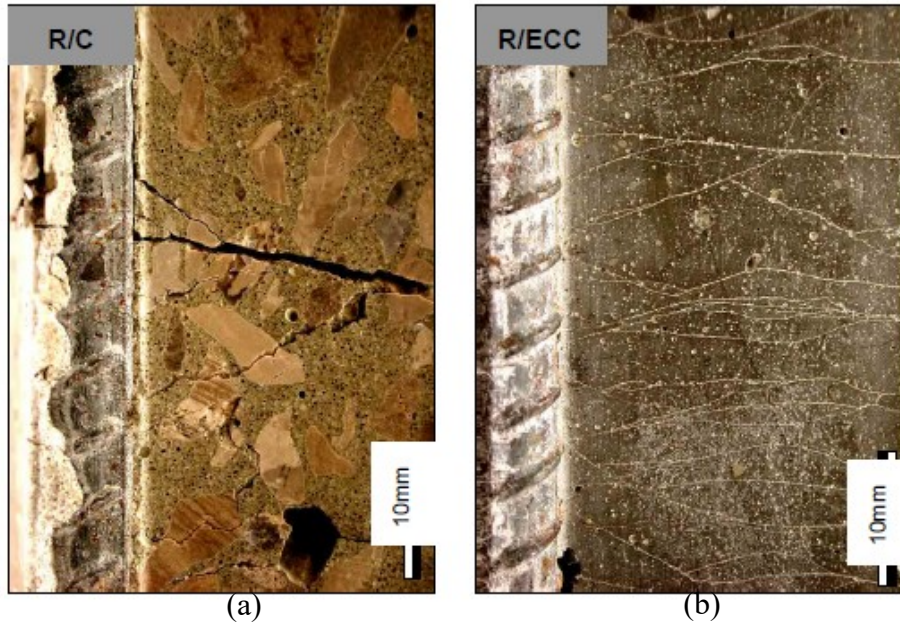


Figure 2-6: Cracking mechanisms of (a) concrete, and (b) ECC (Li, 2003)

### 2.3.3 Compressive Characteristics

Li (2008) reported that the compressive properties of ECC are similar to normal- to high-strength concrete. Compressive strengths of ECC which range from 20 to 95 MPa and Elastic modulus of 15 to 34 GPa are reported. The lower elastic modulus of ECC in comparison to concrete is due to the absence of coarse aggregates. The compressive strain capacity at peak-strength of ECC ranges from 0.45 to 0.65%, which is slightly higher than concrete. In comparison to high-strength concrete, a gentler degradation behaviour for ECC during the post-peak stage was observed. ECC also presents a gradual bulging failure rather than an explosive crushing failure (Li, 2008).

### 2.3.4 Flexural Characteristics

The studies of Kunieda and Rokugo (2006a), Maalej and Li (1994), Wang (2005), Wang and Li (2006b) have demonstrated that multiple microcracks form at the tension zone of the flexural element under bending (Fig. 1-3) allows deformation under a large degree of curvature. As a result, ECC is also known as bendable concrete (Li, 2008). Li (2008) reported a flexural strength (modulus of rupture, or MOR) of 10 to 15 MPa for ECC.

## 2.4 Structural Properties and Durability

### 2.4.1 Flexural Elements

Fischer and Li (2002) studied the behaviour of reinforced-ECC (RECC) flexural elements under reversed cyclic loading and compared to the reinforced-concrete (RC) elements (Fig. 2-7). The resulted hysteretic responses showed that the RECC beam achieved a significant larger energy dissipation (Fig. 2-8). There was no spalling observed on RECC element, while the control RC beam experienced loss of concrete cover and spalling. This demonstrated significant damage tolerance under severe loading.

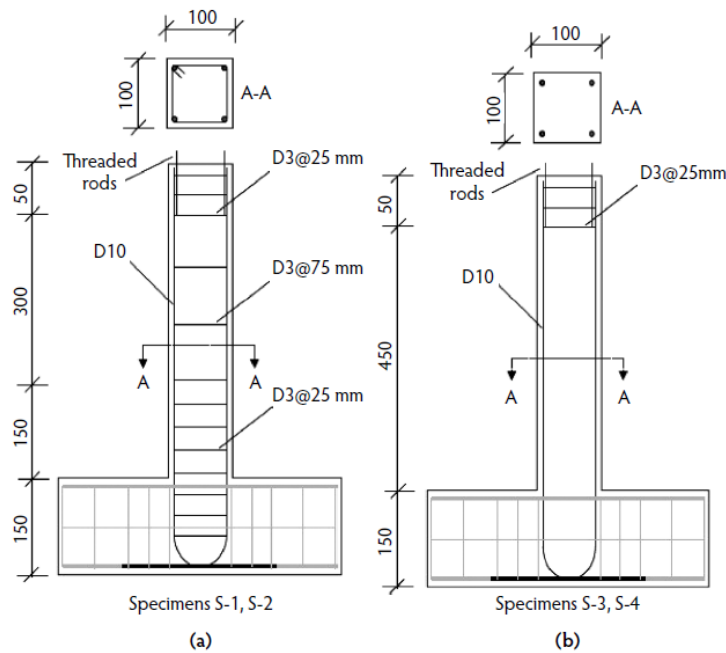


Figure 2-7: Specimen configurations of the tested flexural elements: (a) RC; (b) RECC (Fischer and Li, 2002a)

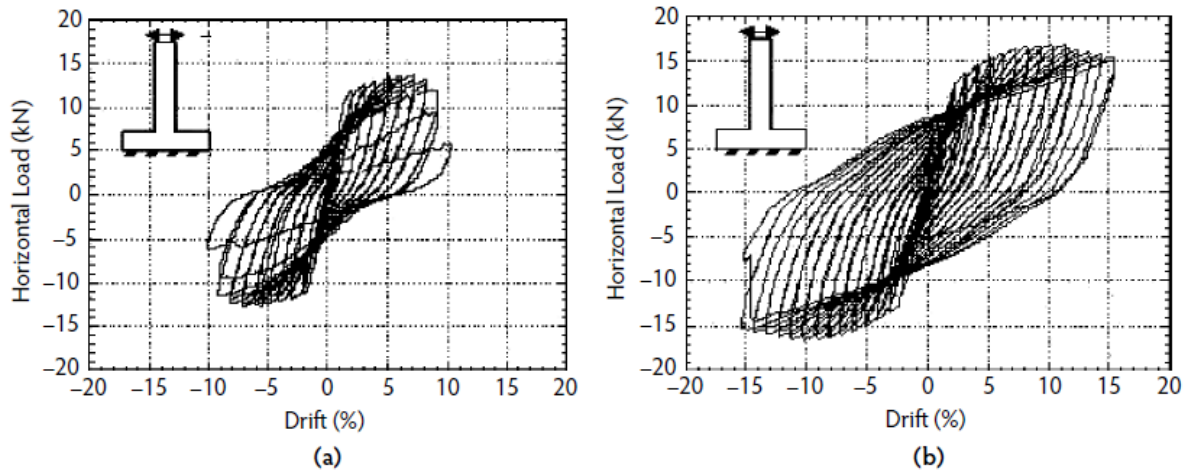


Figure 2-8: Hysteretic responses of flexural members (a) RC; and (b) RECC (Fischer and Li, 2002a)

Kim et al. (2004) studied the high cycle fatigue response of RECC flexural elements. A ECC link-slab element was tested over 100,000 cycles (Fig 2-9). The test results showed the RECC element had only microcracks of approximately 50  $\mu\text{m}$  while the control RC element had localized cracks at 0.6 mm at the end of the test.

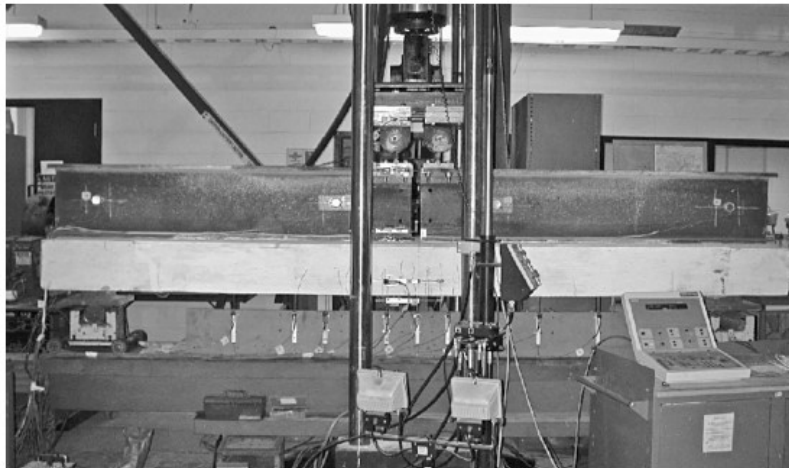


Figure 2-9: Flexural fatigue testing of ECC link-slab element (Kim et al., 2004)

## 2.4.2 Shear-critical Members

Varela and Saiidi (2013) and Fukuyama et al. (2000) studied the shear behaviour of ECC elements. Varela and Saiidi (2013) performed 40 shear tests on simply supported ECC beam and found that the shear strength of ECC is higher than the shear strength of concrete. Fukuyama et al. (2000) tested RECC shear elements under reversed cyclic loading and compared to the RC elements. The hysteretic responses showed that RECC achieved greater stability and ability to dissipate energy (Fig. 2-10), and significantly greater shear strength compared to conventional concrete having the same peak compressive strength. There was significant lower shear damage on RECC element while RC element suffered from extensive bond splitting and large diagonal cracks (Fig. 2-11).

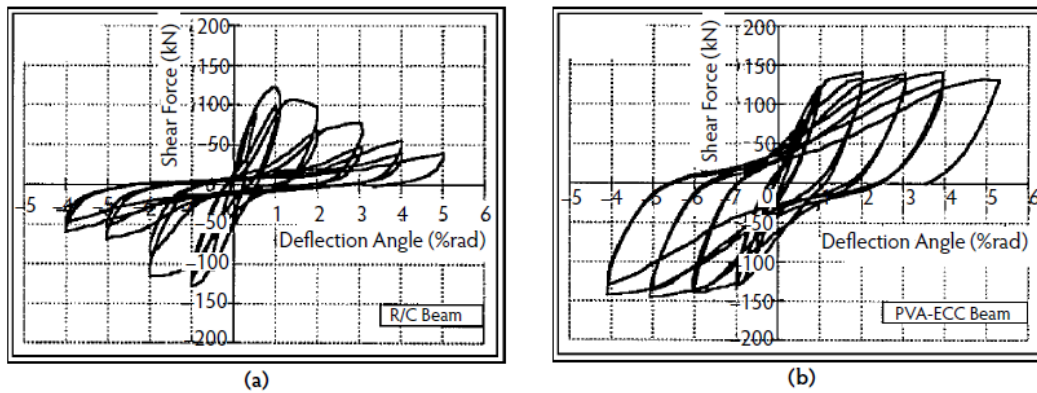


Figure 2-10: Hysteretic responses for shear beams (Fukuyama et al. 2000)

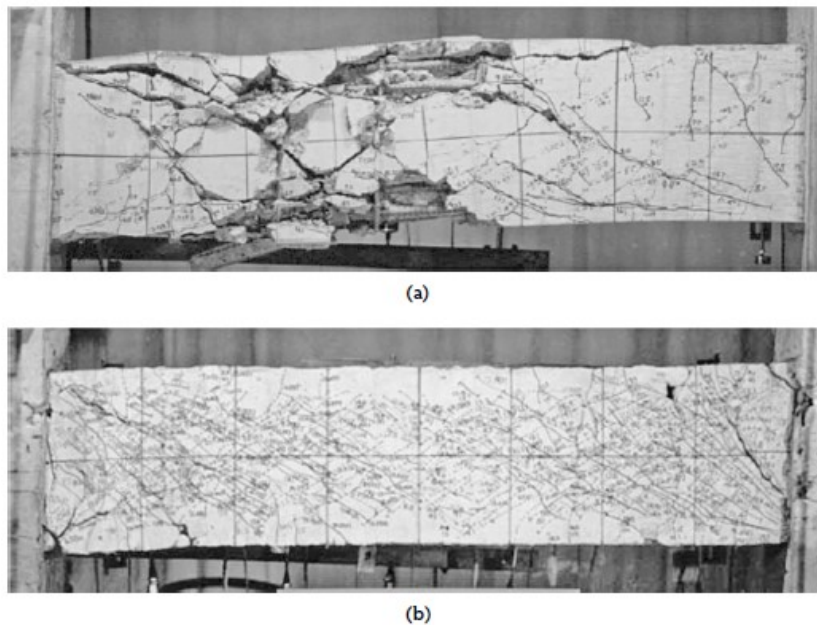


Figure 2-11: Damage pattern in shear beams: (a) R/C, and (b) R/ECC (Fukuyama et al. 2000)



### 2.4.3 Axial Compression Elements

Motaref et al. (2011) tested small-scale ECC circular column under axial load (Fig. 2-12). The test results demonstrated transverse steel confinement improved the compressive strength capacity and strength of ECC. The strength gained from confinement of ECC was lower in comparison to a similarly-confined concrete. The detail of the study is presented in section 2.6.1.



Figure 2-12: Small-scale circular column with spirals (Motaref et al., 2011)

### 2.4.4 Beam-Column Connection Element

Qudah & Maalej (2014) and Parra-Montesinos and Wight (2000) studied the structural behaviour of beam-column connection with ECC. Qudah & Maalej (2014) performed a test on ECC beam-column connections under reverse cyclic loading. The results demonstrated that ECC enhanced the joint seismic resistance at the plastic zones in terms of the shear resistance, energy absorption capacity and damage tolerance (Fig. 2-13). Parra-Montesinos and Wight (2000) tested a RECC column-to-steel beam under reversed cyclic loading. There was no surface spalling observed on RECC element while the larger crack widths which lead to edge spalling were found on the RC element (Fig. 2-14).

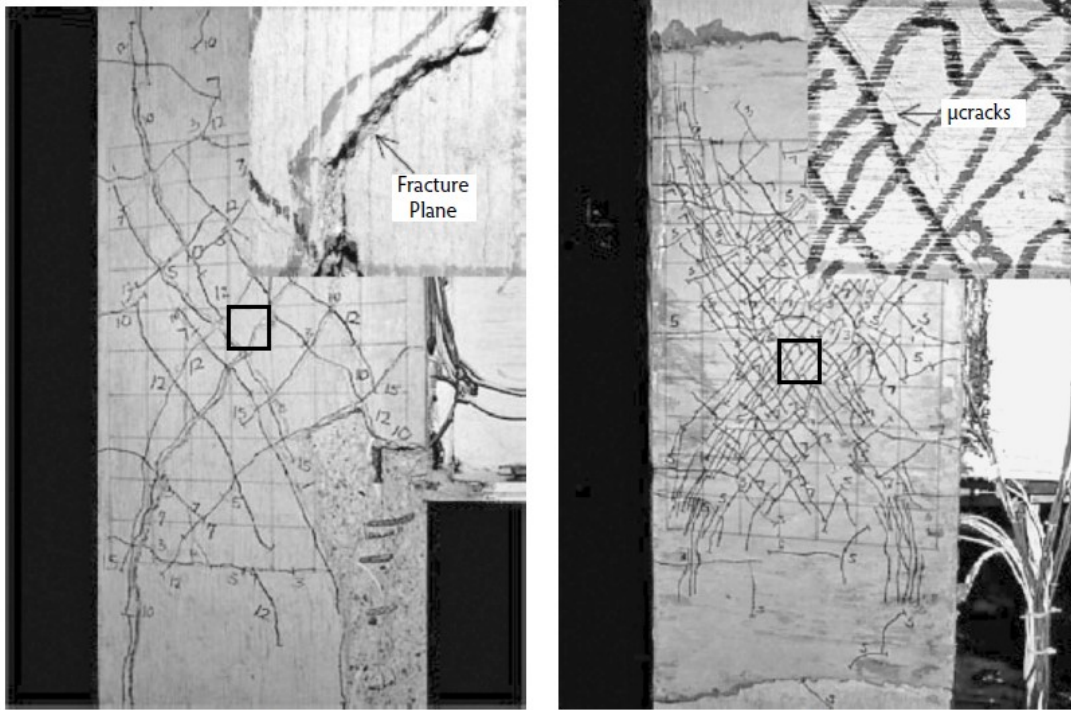




(a)

(b)

Figure 2-13: Crack pattern in beam-column interior connection: (a) RC, and (b) RECC (Qudah & Maalej, 2014)



(a)

(b)

Figure 2-14: Cracking patterns of the tested column-to-steel beam: (a) RC, and (b) RECC (Parra-Montesinos and Wight, 2000)

### 2.4.5 Durability under Various Environments

Freeze-thaw durability tests (ASTM C 666) by Li et al. (2003) demonstrated that ECC specimens survived a test duration of 300 cycles while conventional concrete specimens had severely deteriorated after 110 cycles. Chloride immersion tests by Şahmaran et al. (2007a) demonstrated that ECC can effectively reduce chloride penetration depth, which can cause corrosion on steel reinforcement. De-icing salt scaling test (ASTM C 672) by Şahmaran and Li (2007b) demonstrated that ECC specimens presented a good salt resistance while the mortar specimens deteriorated severely. Other studies such as long-term aging (Li and Lepech, 2004), tropical climate exposure (Li et al., 2004a), alkali-silica reaction (Şahmaran and Li, 2008), fatigue (Suthiwarapirak et al. 2002), creep under constant load (Boshoff and van Zijl, 2007), have also shown that ECC has superior durability properties compare to conventional concrete.

### 2.5 Structural Use of ECC

A number of full-scale structural applications can be found in Japan and the United States (Li, 2008). In Japan, ECC coupling beams were used in two high-rise reinforced concrete (RC) buildings: (1) Glorio Tower Roppongi, a 93 m high, 27-story building in Tokyo (Fig. 2-14a) and (2) Nabule Yokohama Tower and Residence, a 150 m high, 41-story building in Yokohama (Fig. 2-15b) to provide high seismic energy absorption and minimize repair work after earthquakes (Kanda et al., 2011).



Figure 2-15: (a) Glorio Tower Roppongi, (b) Nabule Yokohama Tower and Residence (Kanda et. al 2011)

Mitamura et al. (2005) reported an ECC replacement overlay on steel deck on Mihara Bridge in Hokkaido (Japan) in 2004 to improve the load bearing capacity and fatigue resistance of the stiffener for the steel deck (Fig. 2-16) (Mitamura et al. 2005; Kunieda and Rokugo, 2006b).



Figure 2-16: Placement of ECC on Mihara Bridge (Mitamura et al. 2005)

Lepech and Li (2009) reported a demonstration project of ECC bridge deck links slabs by the Michigan Department of Transportation in 2005 (Fig. 2-17). The performance of the ECC link slab was reported to be an effective replacement of conventional expansion joints which significantly reduced bridge deck maintenance needs.



Figure 2-17: ECC link slab in Michigan (Li, 2006)

ECC has also been used for the surface repair of damaged structures such as reparation of the Mitaka Dam in Japan (Kunieda and Rokugo 2006b; Kojima et al., 2004), Central Main Channel in Shiga Prefecture, Japan (Kunieda and Rokugo, 2006b; JSCE 2005a), Seridanno Channel in Toyama Prefecture, Japan (Kunieda and Rokugo, 2006b), retaining wall in Gifu Prefecture, Japan (Kunieda and Rokugo, 2006b; Rokugo et al. 2005), and railway viaduct girders (Kunieda and Rokugo, 2006b; Suda and Rokugo 2005; Inaguma et al. 2006)

## **2.6 ECC Confinement research**

Confinement provides ductility to reinforced-concrete structures and ensures that they can provide a warning of failure by producing large deformation instead of brittle failures. Through active or passive confinement, the lateral expansion of the concrete subjected to axial stresses is restrained, and the resulting triaxial state of stresses increase the crushing strain of the concrete in the longitudinal direction. Transverse reinforcement is widely used to provide passive confinement to concrete (which is activated only until the concrete starts expanding laterally), commonly through the use of closely spaced steel spirals or hoops (Park and Paulay, 1975). Although confined concrete has been intensively studied (Park and Paulay, 1975; Mander et al., 1988; Sheikh and Uzumeri, 1980), studies of confinement effect on ECC are scarce. The only available study of confined ECC was conducted by Motaref et al. (2011), who proposed a confined model for circular ECC cylinders reinforced with steel spirals. There are no models for rectangular columns made of ECC and confined with rectangular steel ties, to the knowledge of the author.

### **2.6.1. Motaref et al. (2011) Confinement Model for ECC**

Motaref et al. (2011) proposed a confinement model of ECC with circular confinement subjected to axial compressive load. Motaref et al. (2011) tested four groups of small-scale  $100 \times 200$  mm circular ECC columns, one group with no confinement and other groups with the confining spiral spacing of 2 in (51mm), 1.5in (38mm) and, 1 in (25mm). The model proposed by Motaref et al. (2011) was developed based on existing confinement models for conventional concrete (i.e: Mander et al., 1988; Popovics, 1973). The coefficients of the confinement model were found through statistical regression, providing the best fit with the measured response.

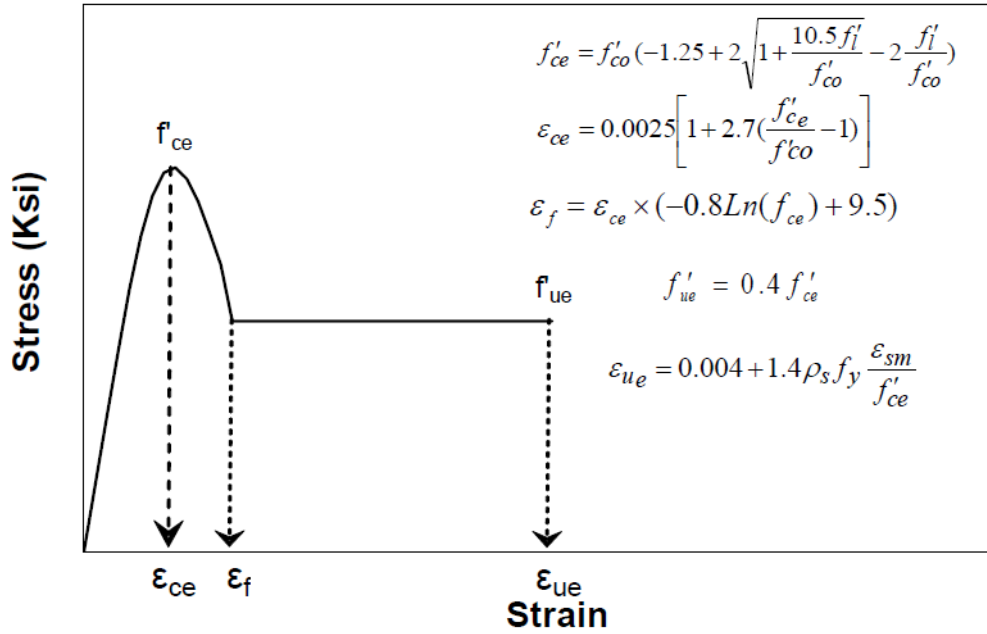


Figure 2-18: Motaref et al. (2011) model for circular confined ECC

The maximum strength ( $f'_{ce}$ ), strain ( $\varepsilon_{ce}$ ) at maximum strength, and ultimate strain ( $\varepsilon_{ue}$ ) of confined ECC are defined based on Mander et al. (1988), which are shown as follow:

$$\text{For } \frac{f'_l}{f'_{co}} \leq 0.035 \quad f'_{ce} = f'_{co} \quad (1-1)$$

$$\text{For } \frac{f'_l}{f'_{co}} > 0.035 \quad f'_{ce} = f'_{co} \left( -1.25 + 2 \sqrt{1 + \frac{10.5 f'_l}{f'_{co}} - 2 \frac{f'_l}{f'_{co}}} \right) \quad (1-2)$$

$$\varepsilon_{ce} = 0.0025 \left[ 1 + 2.7 \left( \frac{f'_{ce}}{f'_{co}} - 1 \right) \right] \quad (1-3)$$

$$\varepsilon_{ue} = 0.004 + 1.4 \rho_s f_y \frac{\varepsilon_{sm}}{f'_{ce}} \quad (1-4)$$

Where

$f'_l$  = confinement stress

$f'_{co}$  = unconfined strength

$f'_{ce}$  = maximum confined strength

$\varepsilon_{ce}$  = strain at maximum confined strength  $f'_{ce}$

$\varepsilon_{ue}$  = ultimate strain

$f_y$  = yield stress pf transverse steel

$\varepsilon_{sm}$  = steel strain at maximum tensile stress

$\rho_s$  = volumetric transverse steel ratio

$\rho_s = \frac{4A_{sp}}{d_s s}$  , and  $A_{sp}$  = transverse steel area,  $d_s$ = core diameter (center of spirals to center),  
 $s$ = spacing of transverse steel

The proposed overall stress-strain curve for confined ECC was defined based on that suggested by Popovics (1973), which is shown as follow:

$$\text{For } 0 \leq \varepsilon \leq \varepsilon_f \quad f = f'_{ce} \frac{\varepsilon}{\varepsilon_{ce}} \frac{n}{n - 1 + \left(\frac{\varepsilon}{\varepsilon_{ce}}\right)^n} \quad (1-5)$$

$$\text{For } \varepsilon_f \leq \varepsilon \leq \varepsilon_{ue} \quad f = 0.4f'_{ce} \quad (1-6)$$

Where

$\varepsilon$  = longitudinal strain

$f$  = confinement stress

$\varepsilon_f$  = longitudinal strain when the residual stress begins

$n$  = an approximate function of the compressive strength of cement mortars =  $0.2 \times 10^{-3} f'_{ce} + 2$

## CHAPTER 3. ECC FABRICATION AND CHARACTERIZATION

The unique mechanical properties of Engineered Cementitious Composite (ECC) materials have the potential to benefit the infrastructure in Canada by enhancing their durability, safety, and sustainability. However, widespread adoption of this promising material is hindered by the lack of experimental data on fabrication, material characterization, and consistency in material properties. The feasibility of ECC fabrication and ECC characterization are discussed in this chapter. The development of a practical ECC mix is presented, investigating the feasibility of fabricating ECC with local Western Canada raw materials and PVA fibres from Japan, in the context of large-scale manufacturing processes. The results from material characterization tests in tension and compression are discussed as well.

### 3.1 Scope

The fabrication and characterization studies are conducted on one type of high-strength ECC material only. The objective of ECC characterization is to obtain the behaviour of tensile ductility in terms of tensile strain capacity, regardless of the tensile strain hardening response.

### 3.2 Engineered Cementitious Composite (ECC)

PVA-ECC (M45) is the most commonly used type of ECC, a material with a minimum compressive strength of 45 MPa. The mix design for conventional PVA-ECC (M45) was developed by Li (2008) and Li et al. (2002). Due to the extensive literature data on this mix type, PVA-ECC (M45) was selected as the study object for this investigation. The optimized mix design for PVA-ECC (M45) given by Li (2008) is summarized in Table 3-1.

Table 3-1: PVA-ECC M45 sample engineered cementitious composite mix design

Mix Designation	Cement	Fly Ash	Sand	Water	SP (Superplasticizer)	Fibre (Vol.)
M45	1.0	1.2	0.8	0.56	0.012	0.02



### **3.3 Material Components**

#### **3.3.1 Cement**

Cement is a fine, dry mineral material which develops binding properties by a chemical reaction between cement mineral and water called hydration. Cements that are used in construction can be classified into hydraulic cement and non-hydraulic cement. The most commonly used cementitious material for concrete making is Portland cement, which is a hydraulic cement that consists of reactive calcium silicates (Monteiro, 2008). The Portland cement used in this study is Type Gu (ASTM Type I) Portland Cement from LafargeHolcim in Edmonton. This type of cement is designed for general use which is suitable for typical structural applications.

#### **3.3.2 Fly Ash**

Fly ash is a by-product of coal-burning in power plants, which is a commonly used mineral admixture that is added to concrete as a supplementary cementitious material (SCM). Besides cost reduction and improvement of workability of fresh concrete, natural pozzolanic material such as fly ash also helps to resist thermal cracking by lowering the hydration heat. It decreases permeability, enhances plasticity, and increases durability to sulfate attack and alkali-aggregate expansion. Thus, fly ash can substitute a portion of the Portland cement in concrete mix. Fly ash is classified into 3 classes of mineral admixture according to ASTM: Class N fly ash is raw or calcined pozzolans, Class F fly ash is pozzolanic, and Class C fly ash is both pozzolanic and cementitious (Monteiro, 2008).

Wang and Li (2007) suggested that Class F fly ash or even bottom ash is an important component in an ECC mixture. The use of low reactive ash in ECC reduce the high interfacial bond in terms of chemical bonding and frictional bonding that formed between the fibres and the cementitious matrix due to the hydrophilic nature of PVA fibres. A high interfacial bond may cause rupture of the PVA fibres, and thereby, limit the tensile ductility of ECC. Lowering the interfacial bonds facilitates fibre pullout instead of fibre rupture to attain high tensile strain capacity of ECC (Wang and Li, 2007). The fly ash used in this study is the ASTM Class F fly ash from LafargeHolcim in Edmonton.



### **3.3.3 Aggregate**

Aggregates in normal concrete are used as an economical filler to occupy a significant volume of a concrete mix, and played an important role in the mechanical properties and dimensional stability or durability of concrete (Monteiro, 2008). However, the addition of aggregates with a particle size larger than the average spacing between fibres in a mixture tends to affect fibre dispersion in the mixture and leads to fibre balling (De Koker and Van Zijl, 2004). The aggregate effect becomes more significant as the maximum size of particles increases, and consequently affects the fibre bridging properties of ECC and limits the ductility (De Koker and Van Zijl, 2004; Sahmaran et al., 2009). Sahmaran et al. (2009) reported that the presence of large aggregates in a mixture also tends to increase the tortuosity of the fracture path of the composite, potentially increasing crack propagation. In order to achieve uniform fibres dispersion, Sahmaran et al. (2009) suggested that fine sands such as microsilica instead of large aggregate particles should be used in a standard ECC mixture. Therefore, the fine aggregate used in this study is the silica sand from Alberta, which has a maximum grain size of 250  $\mu\text{m}$  and an average size of 110  $\mu\text{m}$ .

### **3.3.5 Superplasticizer**

Superplasticizers, also known as high-range water reducers, are chemical admixtures that reduce the water content in a concrete mixture and enhance the fluidity of the system without adding water (Monteiro, 2008). Superplasticizer containing a polycarboxylate chemical composite is recommended for ECC mixes that incorporate PVA fibres to reduce the viscosity of the mix and facilitate pouring (Li, 2008). The superplasticizer used in this study is Glenium 7700 from the manufacturer B-ASF. This is used to control the workability and setting time of ECC mixtures without weakening the mechanical properties caused by the addition of water.

### **3.3.5 Water**

Water is an important element to react with cement and fly ash to form hydration products of cementing binders. Therefore, there is a direct relationship between the water-cement ratio (w/c ratio) and concrete strength. When the mixing water is excessive in a mixture, not only the concrete

strength may be affected but also the setting time (Monteiro, 2008). Water is used in this study to control the desired workability of ECC mixture as well as ECC strength.

### **3.3.6 PVA fibres**

Different fibres have been successfully utilized to date in reinforcing ECC mixtures, such as high-modulus polyethylene (PE) fibres and polypropylene (PP) fibres, but polyvinyl alcohol (PVA) fibres are the most commonly used (Li, 2008). PVA fibres are synthetic fibres made from poval resin, and they display high tenacity, low elongation, hydrophilic properties, weather resistance, and alkali resistance. The PVA fibre used in PVA-ECC (M45) is RECS-15, a fibre manufactured by Kuraray Co. from Japan. RECS-15 fibres have a diameter of 40 $\mu$ m and a length of 12mm with a proprietary oil coating on the surface. The oil coating decreases the possibility of fibre fracture by preventing the development of the high interfacial bond, allowing slipping (Wang and Li, 2007). RECS-15 fibres have a tensile strength of 1560 MPa, elastic modulus of 40 GPa, and strain capacity of 6.5%.

## **3.4 ECC Fabrication**

### **3.4.1 Methodology**

The feasibility of ECC fabrication with Western Canada raw materials was investigated through ECC mix trials and material characterization. Different trial mixes were carried out to optimize the mixing procedures and material proportions of ECC-M45 for future large-scale ECC fabrication. Trial mixes with the raw material listed in Table 3-2 were started based on the mix proportion shown in Table 3-1 and the mixing procedure in Table 3-3 as suggested by Li (2008). Modifications and adjustments were made to accommodate the use of local materials for ECC-M45. In this chapter, material preparation, mixing procedures and observation were recorded for each trial mix to investigate the feasibility of ECC fabrication.

All raw materials were first measured and recorded in mix proportion summary for each trial. The prepared materials were then mixed in an ELRICH intensive mixer model RV02E (Fig. 3-1a) in the Concrete Laboratory at the University of Alberta. The volume of each mix trial was designed to be 4L in order to reach the minimum capacity of the mixer. In each mix trial, at least four

Ø75x150 mm ECC cylinders and four 304.8 mm x 76.2 mm x 12.7 mm ECC coupon specimens (Fig. 3-1b) were cast and vibrated to consolidate the mix. The mix proportion and mixing procedure of each trial mix were recorded. Material testing was conducted on all the cast samples from each trial mix to characterize the material properties.

Table 3-2: Material density for PVA-ECC M45

Material	Type	Density (g/cm <sup>3</sup> )
Cement	Type GU	3.15
Fly Ash	ASTM Class F	2.04
Sand	SIL-CO-SIL® 250	2.65
Water	-	1
Superplasticizer	Glenium 7700	1.064
Fibres	RECS-15	1.3

Table 3-3: Original Mixing Procedure for PVA-ECC M45 (Li, 2008)

Sequence no.	Activity	Time (min)
1	Charge all sand.	2
2	Charge approximately 90% of mixing water and all superplasticizer	2
3	Charge all fly ash	2
4	Charge all cement	2
5	Charge remaining mixing water	4
6	Mix at high RPM* until material is homogenous	5
7	Charge all fibres	2
8	Mix at high RPM until material is homogenous	5

\*RPM = Revolution(s) Per Minute



Figure 3-1: (a) ELRICH intensive mixer RV02E, (b) ECC Cylinders and Coupon specimen

### **3.5 ECC Characterization**

ECC is designed to exhibit microcracking behaviour and achieve high tensile ductility while preserving the conventional compressive response of normal or high-strength concrete (Li, 2008). Material characterization is conducted to determine the tensile and compressive properties of ECC. Uniaxial compressive tests and uniaxial tensile tests were performed. The strain-strain responses of ECC specimens under the uniaxial compressive tests, tensile tests, and cracking behaviour, are reported in this chapter.

#### **3.5.1 Uniaxial Compression Test**

##### **3.5.1.1 Test Specimens and Testing Method**

A standard compression test was conducted on the  $\text{Ø}75 \times 150$  mm cylinders cast from each trial mix as per ASTM C469/C469M – 14. All cylinders were end-grinded using a grinding machine to obtain parallel flat surface for compressive testing. The prepared cylinder was placed in a compressometer and tested in a hydraulic MTS 815 machine (Fig. 3-2a & 3-2b). The compressive responses in terms of 28-day compressive strength, strain, modulus of elasticity, and Poisson's ratio (at the strain corresponding to 40% of peak compressive strength) of ECC from each trial mix are discussed and compared in section 3.6.

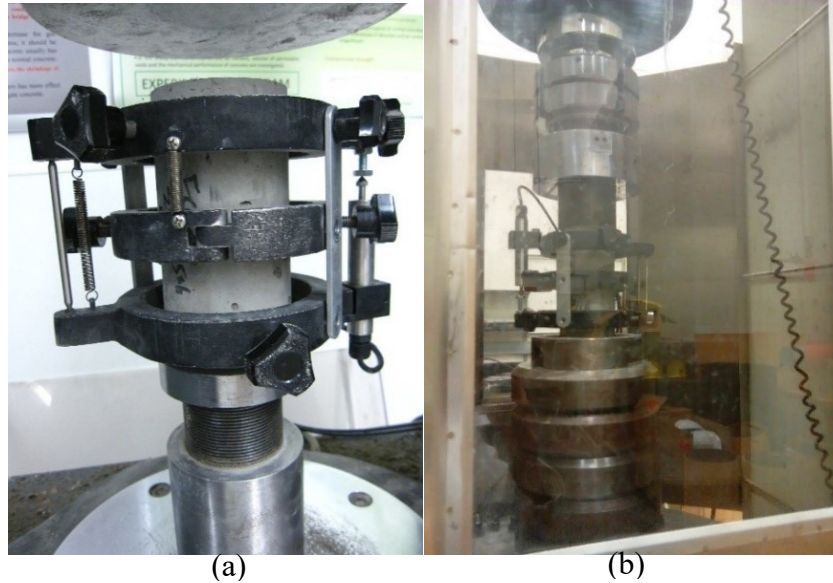


Figure 3-2: (a) ECC Cylinder in compressometer, (b) Compressive test in MTS 815 machine

### **3.5.2 Uniaxial Tensile Test**

#### **3.5.2.1 Test Specimens and Testing Method**

The uniaxial tensile test on ECC was conducted according to the procedures suggested by Zhou et al. (2012). The uniaxial tensile test was performed in an hydraulic MTS 810 machine by clamping the ends of 304.8 mm x 76.2 mm x 12.7 mm coupon specimens (Fig. 3-5). The grip pressure for clamping was set to be 27.6 – 34.4 MPa (4000 – 5000 psi) depending the maximum compressive strength of each ECC specimen. All specimens were grinded using grinding tool to obtain flat surfaces for testing (Fig. 3-3). Four aluminum plates were glued to the two ends of each specimens using plaster, preventing crushing the specimens from clamping (Fig. 3-4). A diagram of tensile fixture which was designed to provide a pin-pin boundary condition for the specimens is presented in Fig. 3-5. An LVDT was mounted on the tensile fixture at a gauge length of 80 mm for recording the longitudinal strain. The uniaxial tensile stress-strain responses and tensile cracking of specimens from each trial mix are discussed in section 3.6.

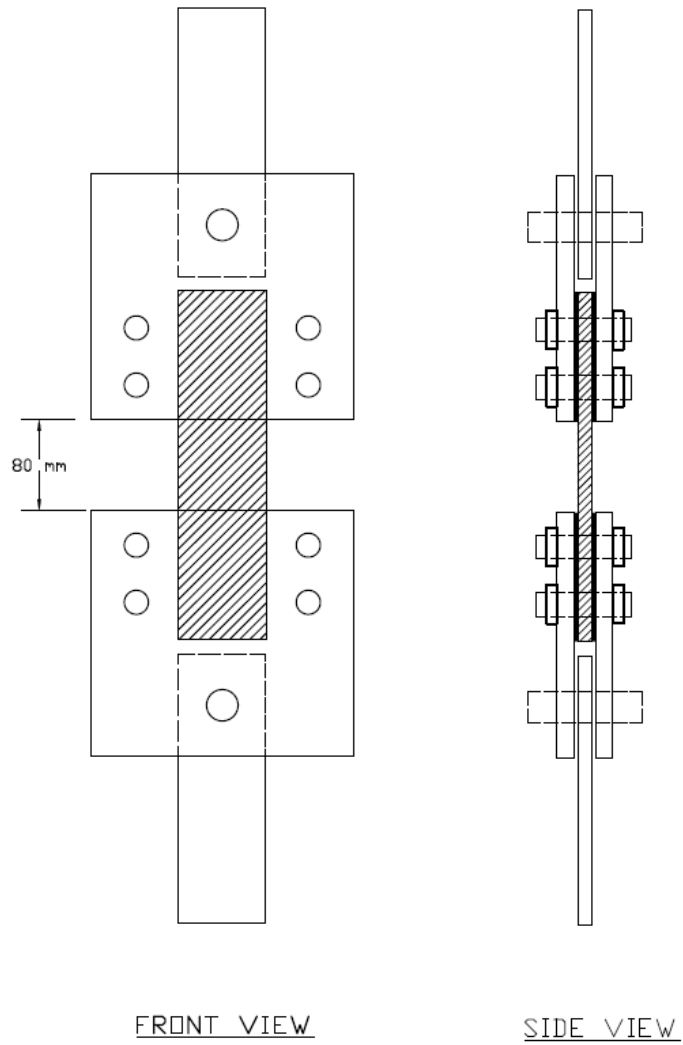


Figure 3-3: ECC coupon preparation - surface grinding



Figure 3-4: ECC coupon preparation - gluing aluminum plates





(a)



(b)

Figure 3-5: Tensile test setup in MTS 810 machine: (a) 2-D view, (b) 3-D view

### 3.6 ECC Mix Trials

#### 3.6.1 ECC Mix Trial # 1 (ECC01)

Table 3-4: Mix proportion of ECC01

ID: ECC01	Cement	Fly Ash	Sand	Water	SP (Superplasticizer)	Fibre	Stabilizer
Weight (g)	2012	2412	1608	1574.6	24.16	104	0
Weight Ratio	1	1.2	0.8	0.78	0.012	2%Vol	0

Table 3-5: Mixing sequence of ECC01

Sequence no.	Activity	Time (min)
1	Charge all sand.	2
2	Charge approximately 90% of mixing water and all superplasticizer	2
3	Charge all fly ash	2
4	Charge all cement	2
5	Charge remaining mixing water	4
6	Mix at high RPM until material is homogenous	5
7	Charge all fibres	2
8	Mix at high RPM until material is homogenous	6

##### **3.6.1.1 ECC Fabrication – Mix Trial # 1 (ECC01)**

###### Mix proportion/Mix procedure:

ECC01 mix was conducted based on the mix proportion in Table 3-1 and the mixing procedure in Table 3-3 with only minor deviations. Only superplasticizer was used to increase the workability and no stabilizer was used. Fibres were untreated before mixing (Fig. 3-6a). The mix proportion and mixing procedure of ECC01 are summarized in Table 3-4 and 3-5 respectively.



### Observations:

The mix became dry after charging all fly ash and cement, at only 0.56 w/c ratio with superplasticizer. An additional amount of water before charging fibres to maintain a good workability of the mixture and achieved a w/c ratio of 0.68. The mixture turned dry again after charging all the fibres in Step 7 which required an additional amount of water to increase the workability. The finished ECC01 mixture exhibited good workability and achieved an overall w/c ratio of 0.78 (Fig. 3-6b). The finished mix presented no bleeding (Fig. 3-6b). The specimens demonstrated no cold joint problems after de-molding (Fig. 3-6c). All molded specimens were hardened and set normally during initial curing period (i.e. 24 hrs) (Fig. 3-6c).

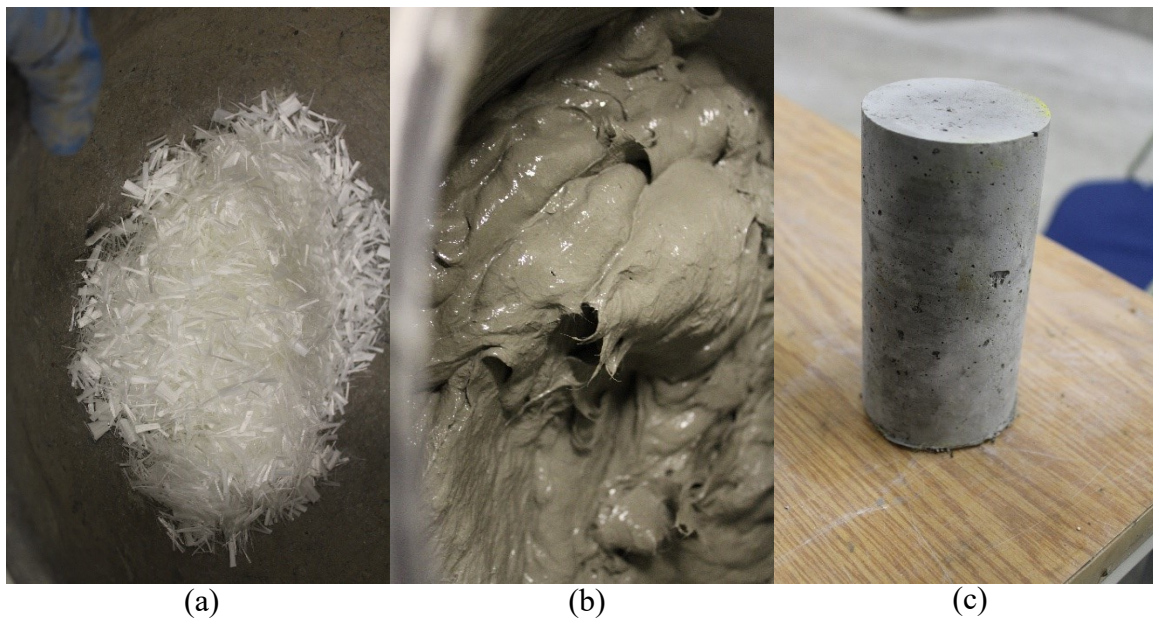


Figure 3-6: (a) RECS-15 fibre before mixing, (b) ECC01 trial mix, (c) ECC01 cylinder

### **3.6.1.2 ECC Characterization – Mix Trial # 1 (ECC01)**

ECC01 resulted in a compressive strength ( $f'_c$ ) of 39.83 MPa, modulus of elasticity (E) of 17093 MPa, and Poisson's ratio of 0.200 (Fig. 3-7). ECC01 resulted in a tensile strength of 2.44 MPa and an ultimate tensile strain of 0.0040 (Fig. 3-8). The cracking on ECC 01 showed one localized crack during the tensile test (Fig. 3-9) with very few microcracks.

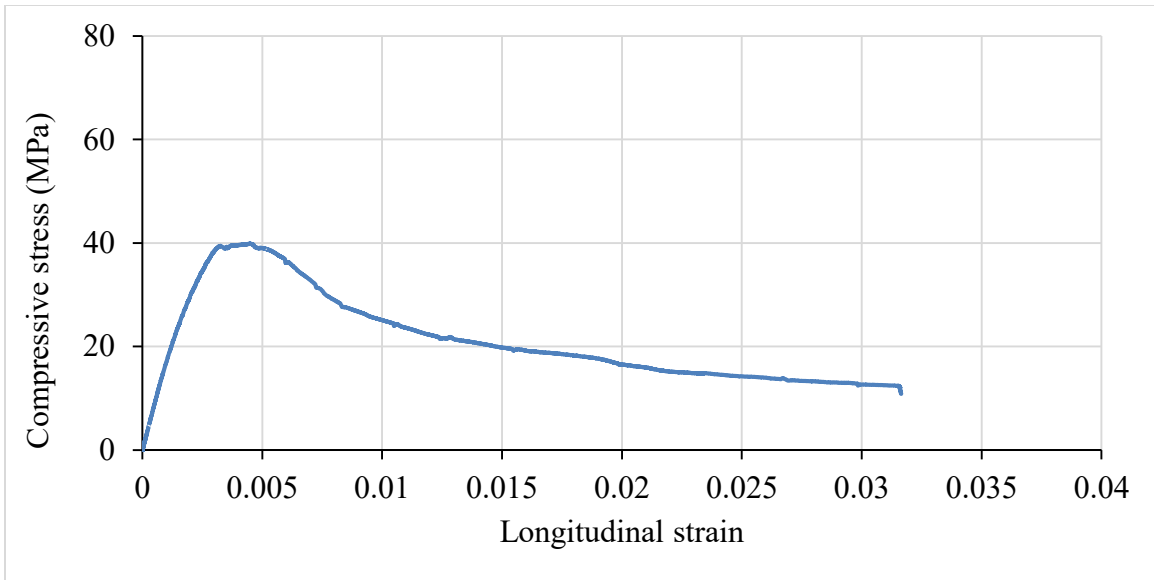


Figure 3-7: Uniaxial compressive stress-strain graph of ECC01

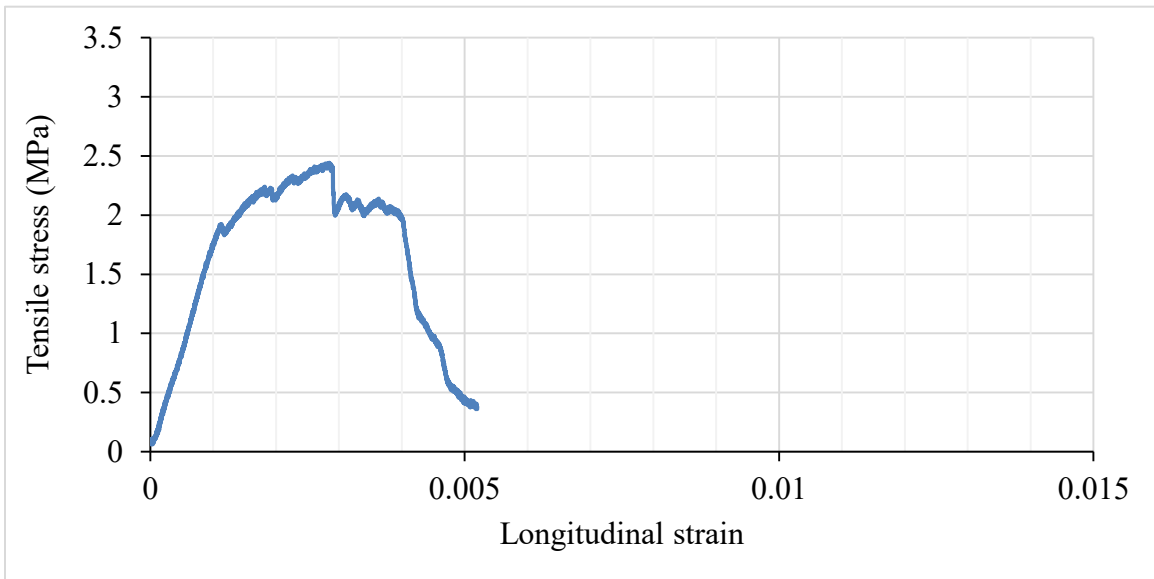


Figure 3-8: Uniaxial tensile stress-strain graph of ECC01



Figure 3-9: Tensile cracking on ECC01 coupon specimen

### 3.6.2 ECC Mix Trial # 2 (ECC02)

Table 3-6: Mix proportion of ECC02

ID: ECC02	Cement	Fly Ash	Sand	Water	SP (Superplasticizer)	Fibre	Stabilizer
Weight (g)	2225	2670	1780.2	1407.4	53.4	104.2	47
Weight Ratio	1	1.2	0.8	0.63	0.024	2% Vol	0.0211

Table 3-7: Mixing sequence of ECC02

Sequence no.	Activity	Time (min)
1	Charge all sand.	2
2	Charge approximately 90% of mixing water	2
3	Charge all fly ash	2
4	Charge all cement	2
5	Charge remaining mixing water, all superplasticizer and stabilizer	4
6	Mix at high RPM until material is homogenous	6
7	Charge all fibres	2
8	Mix at high RPM until material is homogenous	6

#### **3.6.2.1 ECC Fabrication – Mix Trial # 2 (ECC02)**

##### Mix proportion/Mix procedure:

ECC02 mix was conducted based on the mix proportion of ECC01 but the mixing procedure was altered from ECC01. Stabilizer was used together with doubled the amount of superplasticizer to control the workability without adding excess water. Superplasticizer and stabilizer were added after the dry material mixed with 90% of water in sequence no. 5. Fibres were untreated before mixing (Fig. 3-10a). The mix proportion and mixing procedure of ECC02 are summarized in Table 3-6 and 3-7 respectively.

### Observations:

The mix was workable after charging all fly ash and cement at only 0.58 w/c ratio with doubled amount of superplasticiser and stabilizer. No additional amount of water was added before charging fibres. The mixture turned dry after charging all the fibres in Step 7 which required additional amount of water and stabilizer to increase the workability. The finished ECC02 mixture exhibited good workability and achieved an overall w/c ratio of 0.63 (Fig. 3-10b) and stabilizer-cement ratio of 0.0211. The finished mix presented no bleeding (Fig. 3-10b). The specimens demonstrated no cold joint problems after de-molding (Fig. 3-10c). All molded specimens remained wet and soft after initial curing period (i.e. 24 hrs) which led to a longer time for hardening (Fig. 3-10c).

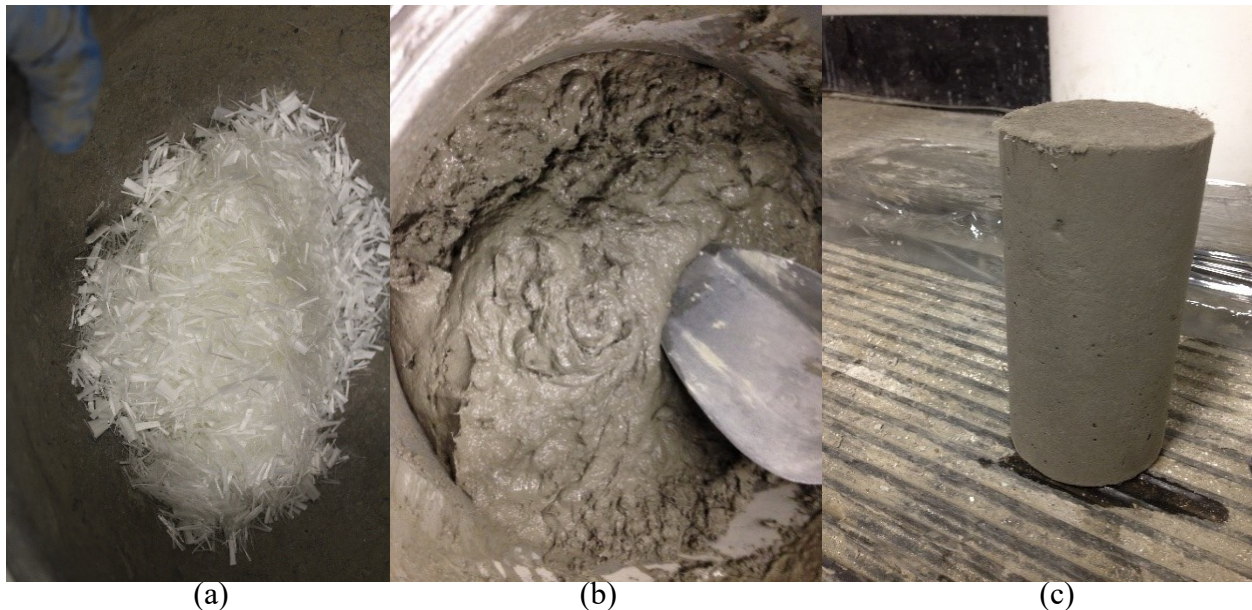


Figure 3-10: (a) RECS-15 fibre before mixing, (b) ECC02 trial mix, (c) ECC02 specimens

### **3.6.2.2 ECC Characterization – Mix trial # 2 (ECC02)**

ECC02 resulted in a compressive strength ( $f'_c$ ) of 80.26 MPa, modulus of elasticity (E) of 20865 MPa, and Poisson's ratio of 0.165 (Fig. 3-11). ECC02 resulted in a tensile strength of 3.045 MPa and an ultimate strain of 0.011 (Fig. 3-12). Cracking on ECC02 illustrated one localized crack with a few microcracks developing along the specimen after the tensile test (Fig 3-13).



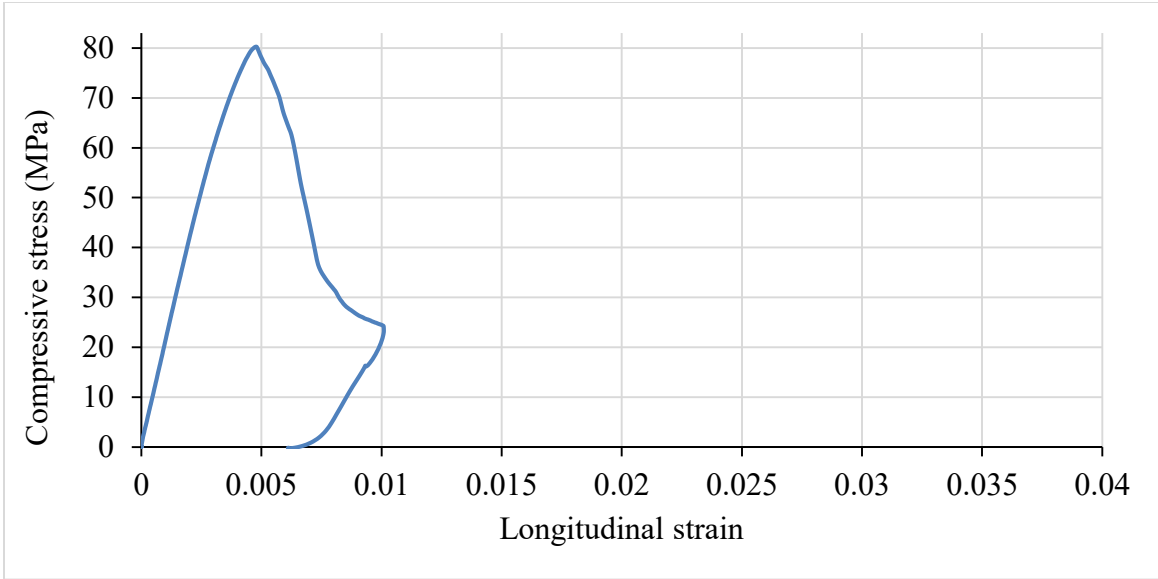


Figure 3-11: Uniaxial compressive stress-strain graph of ECC02

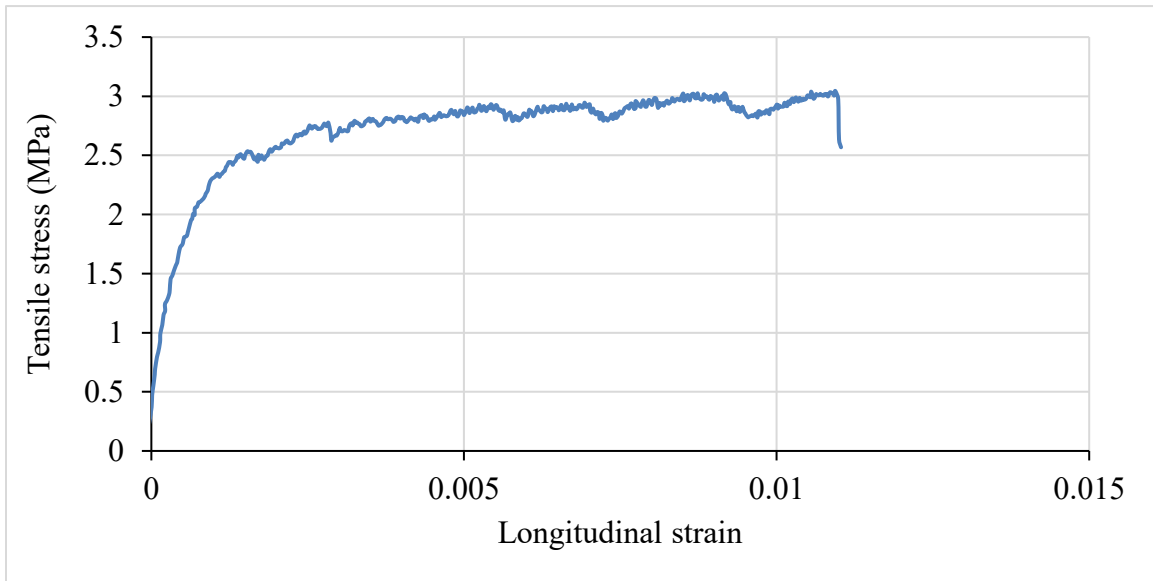


Figure 3-12: Uniaxial tensile stress-strain graph of ECC02



Figure 3-13: Tensile cracking on ECC02 coupon specimen

### 3.6.3 ECC Mix Trial # 3 (ECC03)

Table 3-8: Mix proportion of ECC03

ID: ECC03	Cement	Fly Ash	Sand	Water	SP (Superplasticizer)	Fibre	Stabilizer
Weight (g)	2225	2670	1780	1451	53.8	104	70.6
Weight Ratio	1	1.2	0.8	0.65	0.024	2% Vol	0.032

Table 3-9: Mixing sequence of ECC03

Sequence no.	Activity	Time (min)
1	Charge all sand, fly ash, and cement	4
2	Charge approximately 90% of mixing water, all superplasticizer and stabilizer	4
3	Mix until material is homogenous	2
4	Charge remaining mixing water	2
5	Mix at high RPM until material is homogenous	5
6	Charge all fibres	3
7	Mix at high RPM until material is homogenous	5

#### **3.6.3.1 ECC Fabrication – Mix Trial # 3 (ECC03)**

Mix proportion/Mix procedure:

ECC03 mix was conducted based on the mix proportion of ECC02 with double amount of superplasticizer and stabilizer to increase the workability without adding excess water. The mixing procedure of ECC03 was based on that from ECC02. All the dry materials such as sand, fly ash, and cement were mixed before adding any water. Fibres were untreated before mixing (Fig. 3-14a). The mix proportion and the mixing procedure of ECC03 are summarized in Table 3-8 and 3-9 respectively.



### Observations:

The mix was workable after charging all sand, fly ash, cement at only 0.56 w/c ratio with superplasticiser and stabilizer. No additional amount of water before charging fibres was provided. The mixture turned dry after charging all the fibres in Step 7 which required an additional amount of water and stabilizer to increase the workability. The finished ECC03 mixture exhibited good workability and achieved an overall w/c ratio of 0.63 (Fig. 3-14b). The extra stabilizer added resulted in 1.4 times more than the amount used in ECC02 mix. The finished mix presented no bleeding (Fig. 3-14b). The specimens demonstrated no cold joint problem after de-molding (Fig. 3-14c). All molded specimens were hardened and set normally during the initial curing period (i.e. 24 hrs) (Fig. 3-14c).

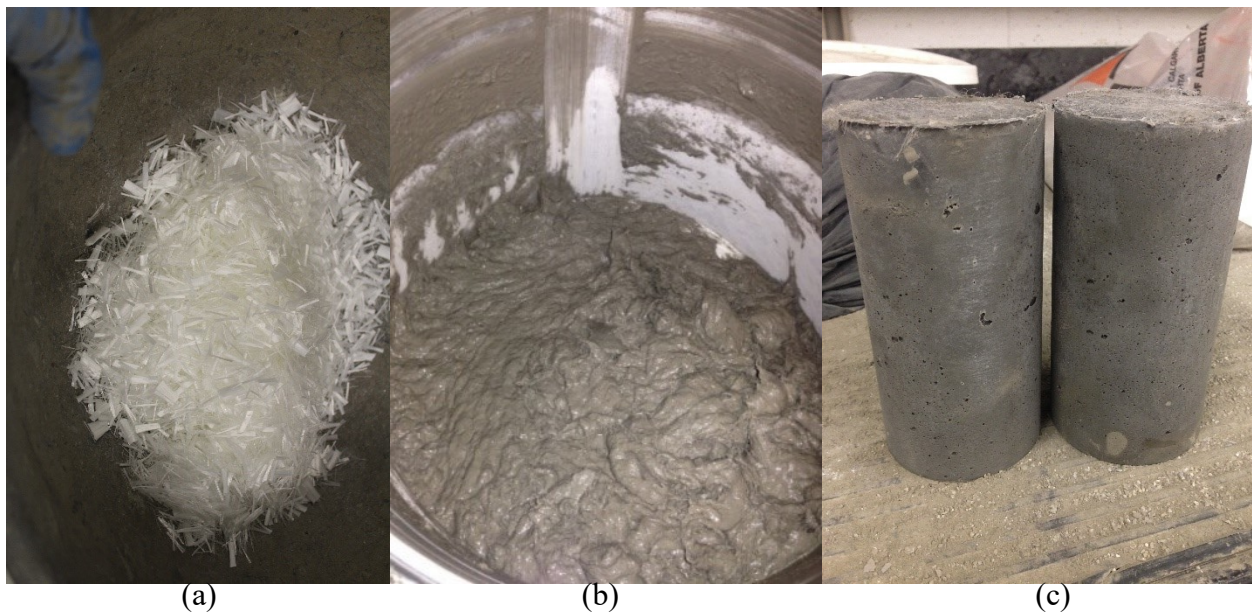


Figure 3-14: (a) RECS-15 fibre before mixing, (b) ECC03 trial mix, (c) ECC03 specimens

### **3.6.3.2 ECC Characterization – Mix trial # 3**

ECC03 resulted in a compressive strength ( $f'_c$ ) of 36.08 MPa, modulus of elasticity (E) of 8827 MPa, and Poisson's ratio of 0.046 (Fig. 3-15). ECC03 resulted in a tensile strength of 2.34 MPa

and an ultimate strain of 0.008 (Fig. 3-16). Cracking on ECC03 consisted of some microcracks developed near the failure crack after the tensile test (Fig. 3-17).

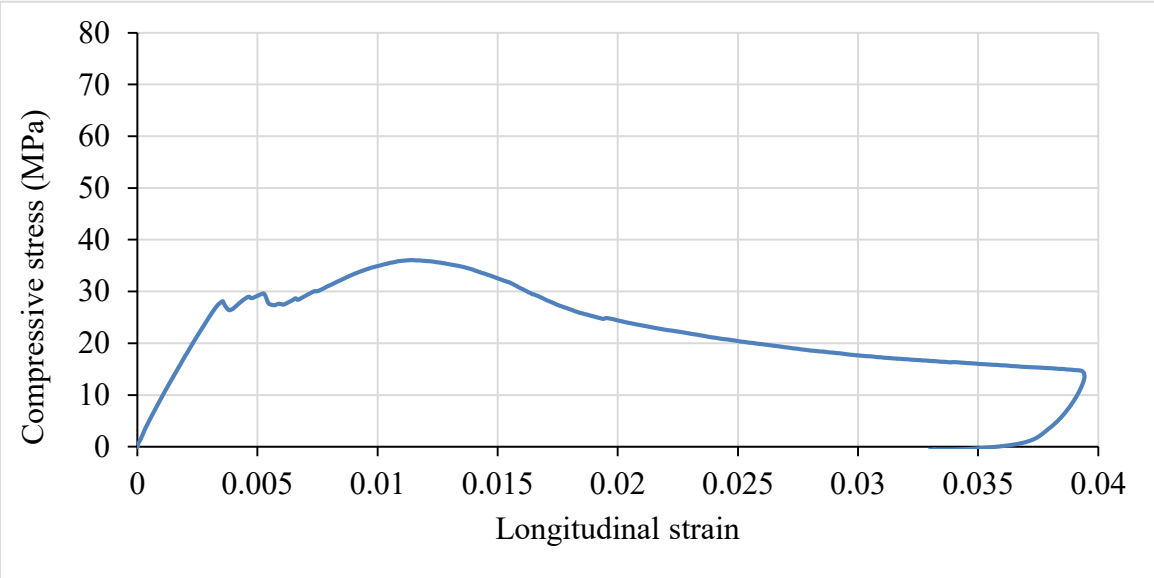


Figure 3-15: Uniaxial compressive stress-strain graph of ECC03

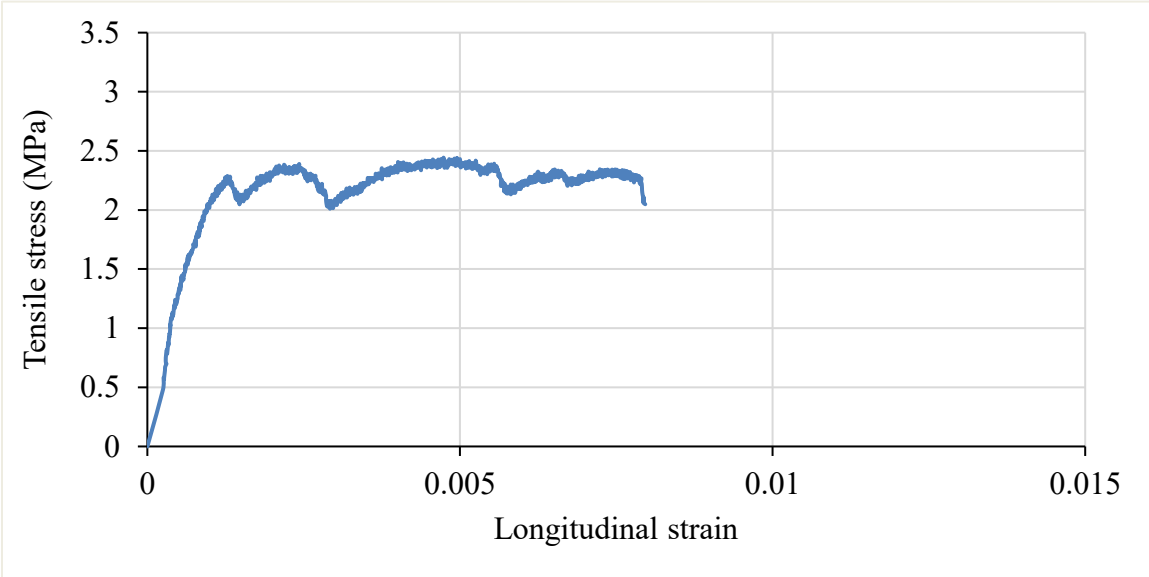


Figure 3-16: Uniaxial tensile stress-strain graph of ECC03



Figure 3-17: Tensile cracking on ECC03 coupon specimen

### 3.6.4 ECC Mix Trial # 4 (ECC04)

Table 3-10: Mix proportion of ECC04

ID: ECC04	Cement	Fly Ash	Sand	Water	SP (Superplasticizer)	Fibre	Stabilizer
Weight (g)	2225	2670	1780	1246.4	53.8	104	0
Weight Ratio	1	1.2	0.8	0.56	0.024	2% Vol	0

Table 3-11: Mixing sequence of ECC04

Sequence no.	Activity	Time (min)
1	Charge all sand, fly ash, and cement	4
2	Charge approximately 90% of mixing water and all superplasticizer	2
3	Mix until material is homogenous	4
5	Charge remaining mixing water	2
6	Mix until material is homogenous	3
7	Charge all fibres	3
8	Mix at high RPM until material is homogenous	5

#### **3.6.4.1 ECC Fabrication – Mix Trial # 4 (ECC04)**

##### Mix proportion/Mix procedure:

ECC04 mix was conducted based on the mix proportion of ECC03 with only superplasticizer to control the workability. The mixing procedure of ECC04 was based on that of ECC03. Fibres were untreated before mixing (Fig. 3-18a). The mix proportion and mixing procedure of ECC04 are summarized in Table 3-10 and 3-11 respectively.

##### Observations:

The mix was workable after charging all sand, fly ash, cement at only 0.56 w/c ratio with superplasticizer. No additional amount of water was provided before charging fibres. The mixture remained workable after charging all the fibres in Step 7. No additional amount of water was added after charging fibres. The finished ECC04 mixture exhibited good workability and achieved an



overall w/c ratio of 0.56 (Fig. 3-18b). The finished mix presented bleeding (Fig. 3-18b). The specimens demonstrated no cold joint problem after de-molding (Fig. 3-18c). All molded specimens hardened and set normally during the curing period (i.e. 24 hrs) (Fig. 3-18c).

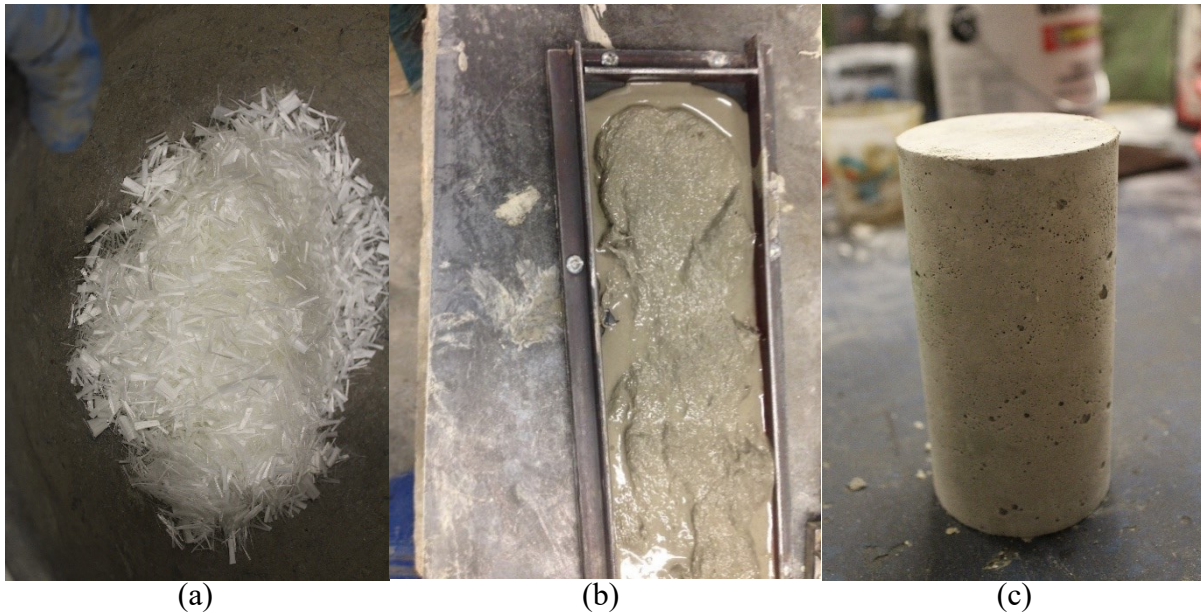


Figure 3-18: (a) RECS-15 fibre before mixing, (b) ECC04 trial mix, (c) ECC04 specimen

#### **3.6.4.2 ECC Characterization – Mix trial # 4 (ECC04)**

ECC04 resulted in a compressive strength ( $f'_c$ ) of 62.47 MPa, modulus of elasticity (E) of 24786 MPa, and Poisson's ratio of 0.204 (Fig. 3-19). ECC04 resulted in a tensile strength of 2.86 MPa and an ultimate strain of 0.00529 (Fig. 3-20). Cracking on ECC04 illustrated one failure crack with a few microcracks developing along the specimen during the tensile test (Fig. 3-21).

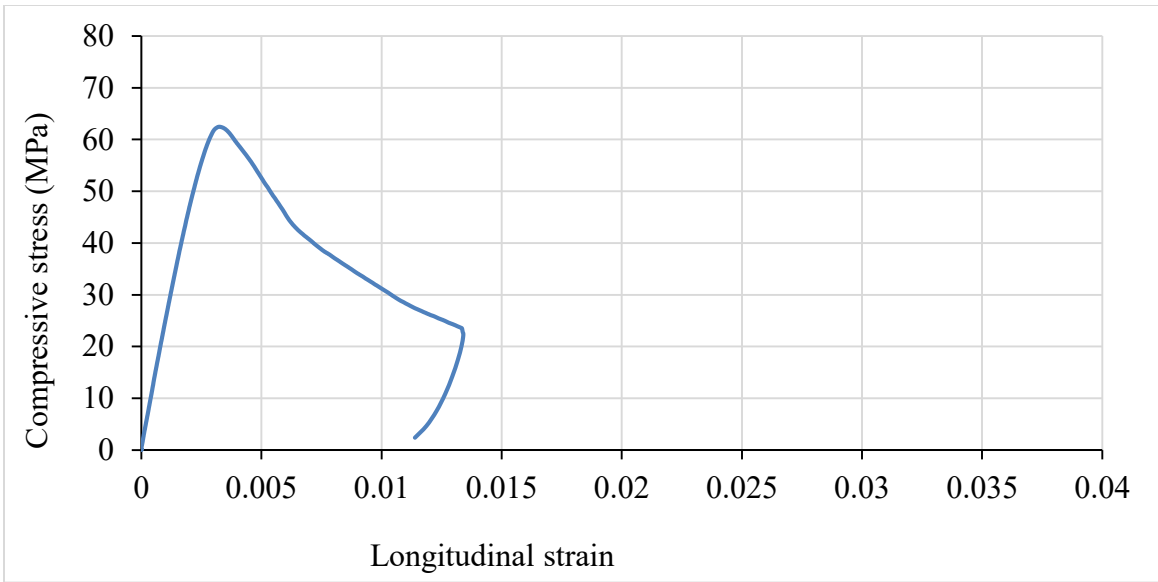


Figure 3-19: Uniaxial compressive stress-strain graph of ECC04

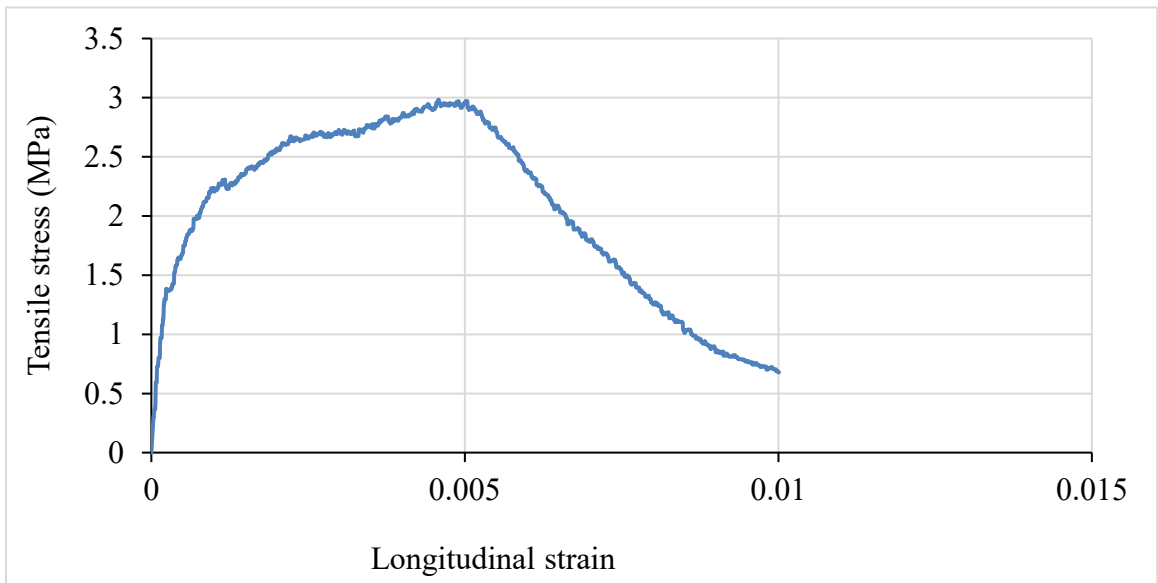


Figure 3-20: Uniaxial tensile stress-strain graph of ECC04



Figure 3-21: Tensile cracking on ECC04 coupon specimen

### 3.6.5 ECC Mix Trial # 5 (ECC05)

Table 3-12: Mix proportion of ECC05

ID: ECC05	Cement	Fly Ash	Sand	Water	SP (Superplasticizer)	Fibre	Stabilizer
Weight (g)	2225.8	2674	1783.6	1246	59.4	104	0
Weight Ratio	1	1.2	0.8	0.56	0.027	2% Vol	0

Table 3-13: Mixing Sequence of ECC05

Sequence no.	Activity	Time (min)
0	Spin all fibres at high RPM	3
1	Charge all sand.	2
2	Charge approximately 90% of mixing water	2
3	Charge all fly ash	2
4	Charge all cement	2
5	Charge remaining mixing water and all superplasticizer	4
6	Mix until material is homogenous	5
7	Charge all fibres	2
8	Mix at high RPM until material is homogenous	8

#### **3.6.5.1 ECC Fabrication – Mix Trial # 5 (ECC05)**

##### Mix proportion/Mix procedure:

ECC05 mix was conducted based on the mix proportion of ECC04. ECC05 mixing was based on the mixing producer of ECC02. Fibres were treated by spinning before mixing (Fig. 3-22a). The mix proportion and mixing procedure of ECC05 are summarized in Table 3-12 and 3-13 respectively.

##### Observation:

The mix was workable after charging all sand, fly ash, cement at only 0.56 w/c ratio with superplasticiser. No additional amount of water was provided before charging fibres. The mixture turned dry after charging all the fibres in Step 7. No additional amount of water was added after



charging fibres but extra amount of superplasticizer. The finished ECC05 mixture exhibited dry and stiff condition when achieved an overall w/c ratio of 0.56 (Fig. 3-22b). The finished mix presented no bleeding (Fig. 3-22b). All specimens demonstrated a cold joint problem after demolding (Fig. 3-22c). All molded specimens were hardened and set normally during initial curing (i.e. 24 hrs) period (Fig. 3-22c).

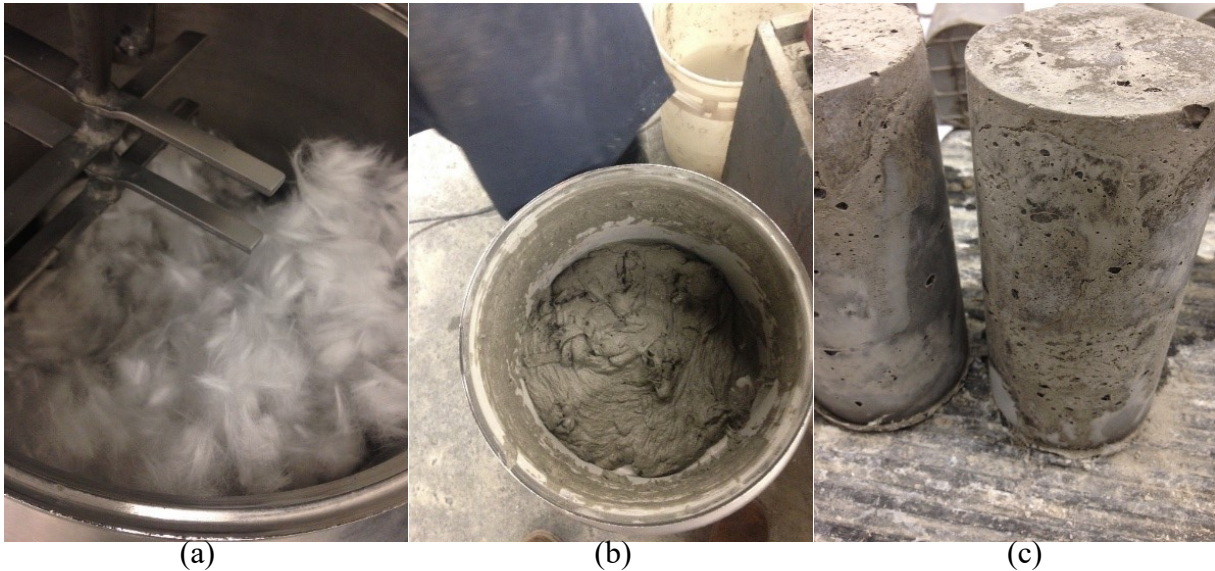


Figure 3-22: (a) RECS-15 fibre before mixing, (b) ECC05 trial mix, (c) ECC05 specimens

### **3.6.5.2 ECC Characterization – Mix trial # 5 (ECC05)**

ECC05 resulted in a compressive strength ( $f'_c$ ) of 64.78 MPa, modulus of elasticity (E) of 16285 MPa, and Poisson's ratio of 0.240 (Fig. 3-23). ECC05 resulted in a tensile strength of 1.68 MPa and an ultimate strain of 0.00751 (Fig. 3-24). Cracking on ECC05 consisted of a few microcracks developing near the failure crack after the tensile test (Fig. 3-25).

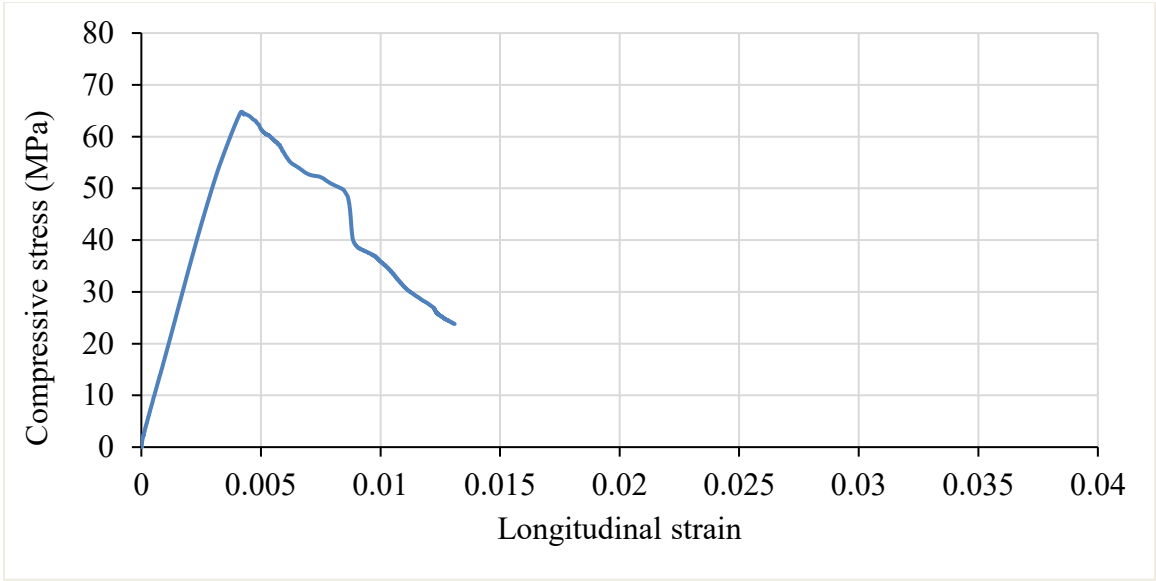


Figure 3-23: Uniaxial compressive stress-strain graph of ECC05

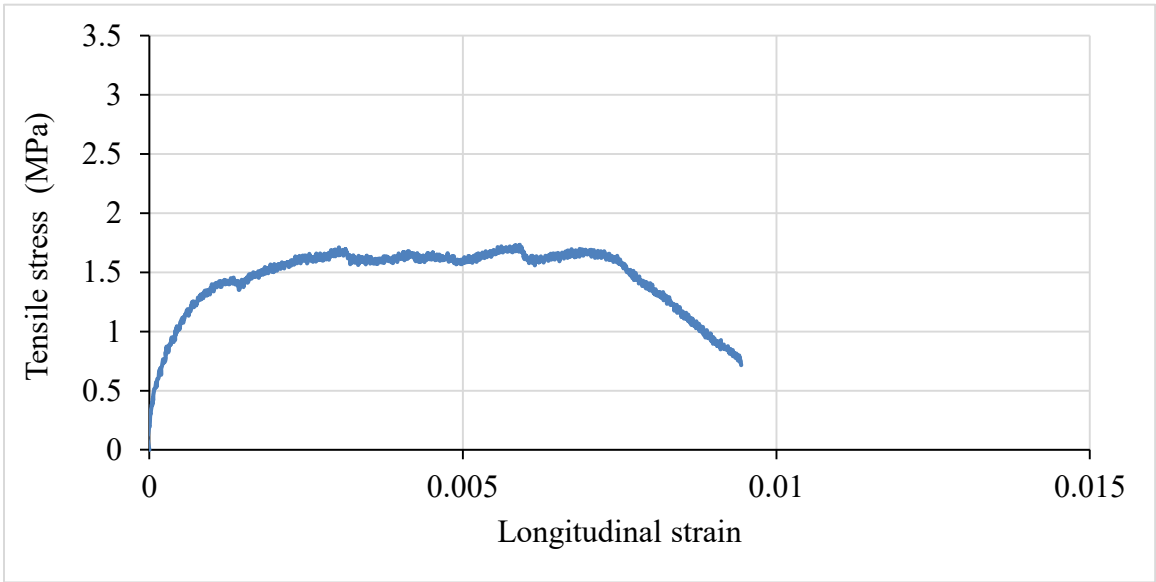


Figure 3-24: Uniaxial tensile stress-strain graph of ECC05

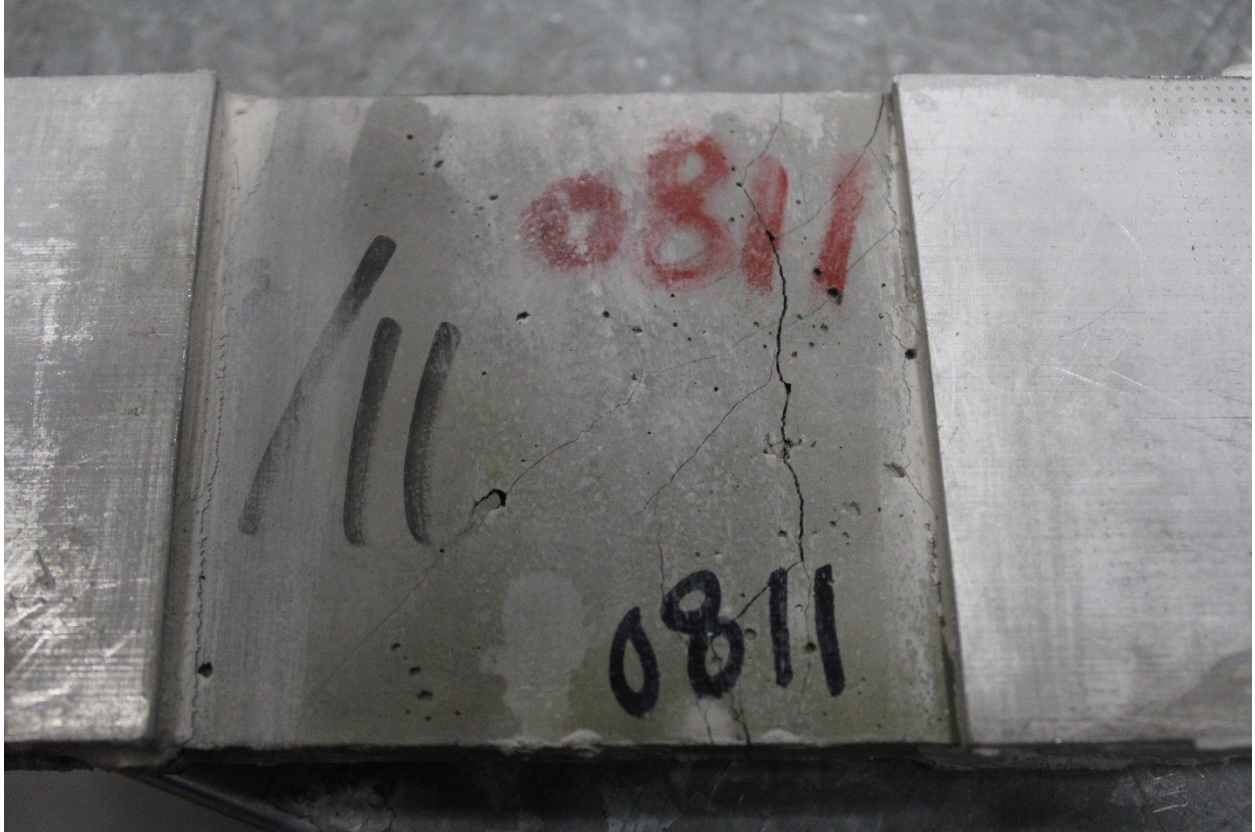


Figure 3-25: Tensile cracking on ECC05 coupon specimen

### 3.6.6 ECC Mix Trial # 6 (ECC06)

Table 3-14: Mix proportion of ECC06

ID: ECC06	Cement	Fly Ash	Sand	Water	SP (Superplasticizer)	Fibre	Stabilizer
Weight (g)	2225	2670	1780	1247	53.8	104	0
Weight Ratio	1	1.2	0.8	0.56	0.024	2% Vol	0

Table 3-15: Mixing sequence of ECC06

Sequence no.	Activity	Time (min)
0	Spin all fibres at high RPM	3
1	Charge all sand.	2
2	Charge approximately 90% of mixing water	2
3	Charge all fly ash	2
4	Charge all cement	2
5	Charge remaining mixing water, and all superplasticizer	4
6	Mix at high RPM until material is homogenous	3
7	Charge all fibres	2
8	Mix at high RPM until material is homogenous	3

#### **3.6.6.1 ECC Fabrication – Mix Trial # 6 (ECC06)**

Mix proportion/Mix procedure:

ECC06 mix was conducted based on the mix proportion of ECC05. ECC06 mixing was based on the mixing procedure of ECC05 but with lesser mixing time at step 8. Fibres were treated by spinning before mixing (Fig. 3-26a). The mix proportion and mixing procedure of ECC06 are summarized in Table 3-14 and 3-15 respectively.

Observation:

The mix was workable after charging all sand, fly ash, cement at only 0.56 w/c ratio with superplasticizer. No additional amount of water was provided before charging fibres. The mixture



remained workable after charging all the fibres in step 7. No additional amount of water or superplasticizer was added after charging fibres. The finished ECC06 mixture exhibited satisfactory workability when achieved an overall w/c ratio of 0.56 (Fig. 3-26b). The finished mix presented bleeding (Fig. 3-26b). The specimens demonstrated no cold joint problem after demolding (Fig. 3-26c). All molded specimens were hardened and set normally during initial curing (i.e. 24 hrs) period (Fig. 3-26c).

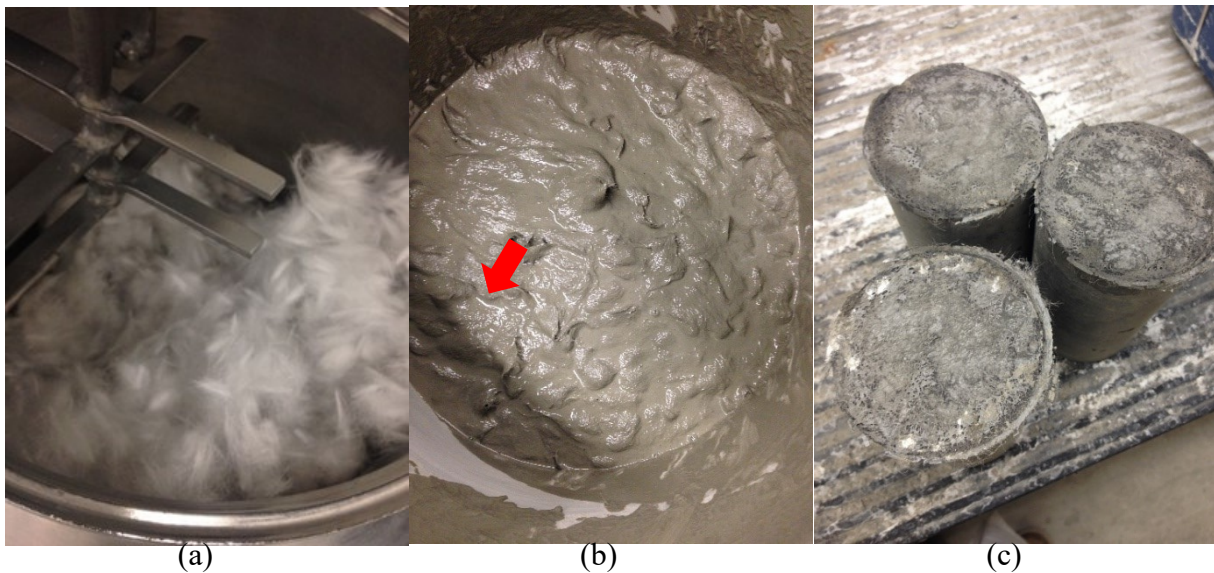


Figure 3-26: (a) RECS-15 fibre before mixing, (b) ECC06 trial mix, (c) ECC06 specimens

### **3.6.6.2 ECC Characterization – Mix trial # 6 (ECC06)**

ECC06 resulted in a compressive strength ( $f'_c$ ) of 33.23 MPa, modulus of elasticity ( $E$ ) of 14034 MPa, and Poisson's ratio of 0.094 (Fig. 3-27). ECC06 resulted in a tensile strength of 2.82 MPa and an ultimate strain of 0.00658 (Fig. 3-28). Cracking on ECC06 illustrated few microcracks developed near the failure crack after the tensile test (Fig. 3-29).

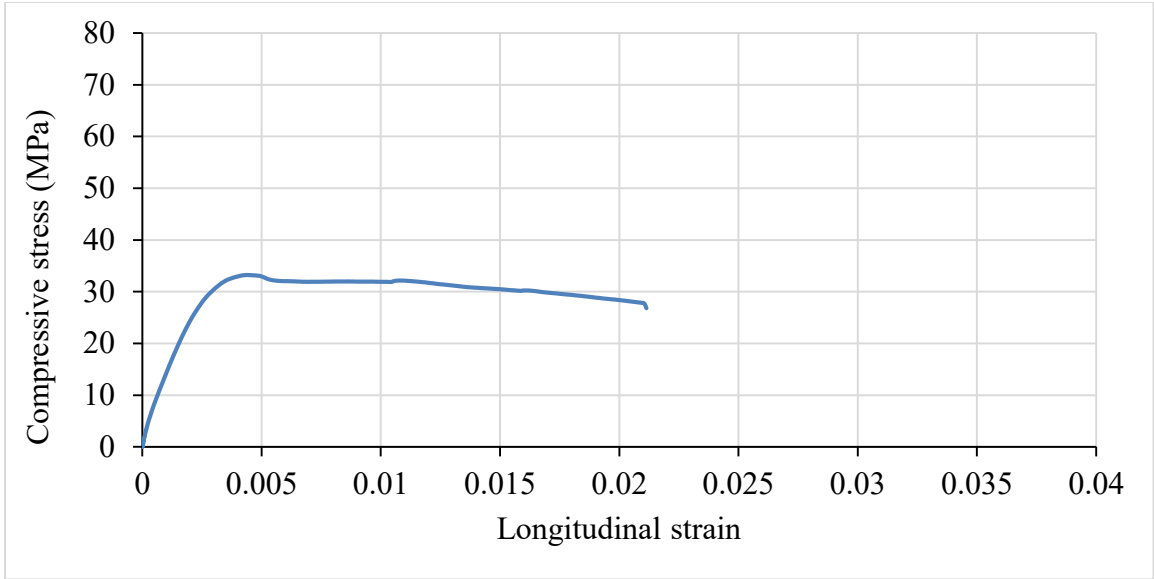


Figure 3-27: Uniaxial compressive stress-strain graph of ECC06

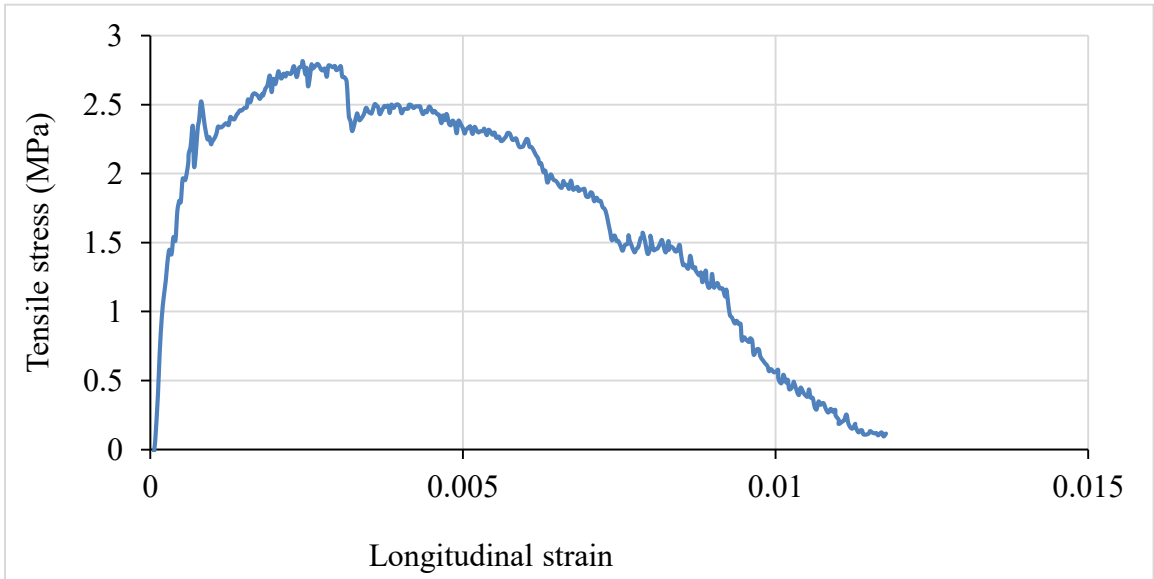


Figure 3-28: Uniaxial tensile stress-strain graph of ECC06

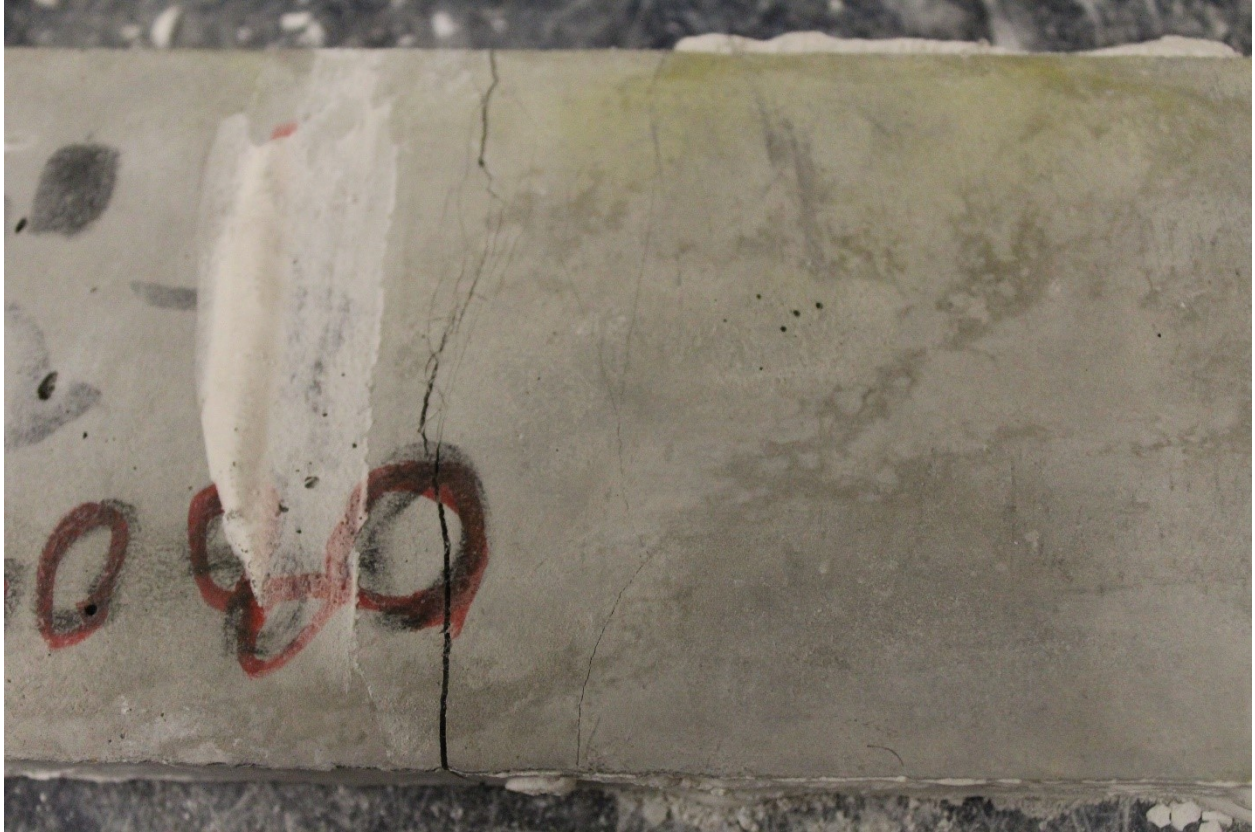


Figure 3-29: Tensile cracking on ECC06 coupon specimen

### 3.6.7 ECC Mix Trial # 7 (ECC07)

Table 3-16: Mix proportion of ECC07

ID: ECC07	Cement	Fly Ash	Sand	Water	SP (Superplasticizer)	Fibre	Stabilizer
Weight (g)	2226	2670.6	1780	1299	40	104	0
Weight Ratio	1	1.2	0.8	0.58	0.018	2% Vol	0

Table 3-17: Mixing sequence of ECC07

Sequence no.	Activity	Time (min)
1	Charge all sand.	2
2	Charge approximately 90% of mixing water	2
3	Charge all fly ash	2
4	Charge all cement	2
5	Charge remaining mixing water, and all superplasticizer	4
6	Mix at high RPM until material is homogenous	5
7	Charge all fibres	2
8	Mix at high RPM until material is homogenous (add water or superplasticizer if necessary)	5

#### **3.6.7.1 ECC Fabrication – Mix Trial # 7 (ECC07)**

##### Mix proportion/Mix procedure:

ECC07 mix was conducted based on the mix proportion and the mixing procedure of ECC06. Fibres were not treated before mixing (Fig. 3-30a). The mix proportion and mixing procedure of ECC07 are summarized in Table 3-16 and 3-17 respectively.

##### Observation:

The mix was workable after charging all sand, fly ash, cement at only 0.56 w/c ratio with superplasticiser. No additional amount of water before charging fibres. The mixture remained workable after charging all the fibres in Step 7. Little portion of additional water and superplasticizer was added after charging fibres to maintain the workability. The finished ECC07



mixture exhibited dry and stiff when achieved an overall w/c ratio of 0.56 (Fig. 3-30b). The finished mix presented no bleeding (Fig. 3-30b). The specimens demonstrated no cold joint problem after de-molding (Fig. 3-30c). All molded specimens were hardened and set normally during initial curing period (i.e. 24 hrs) (Fig. 3-30c).

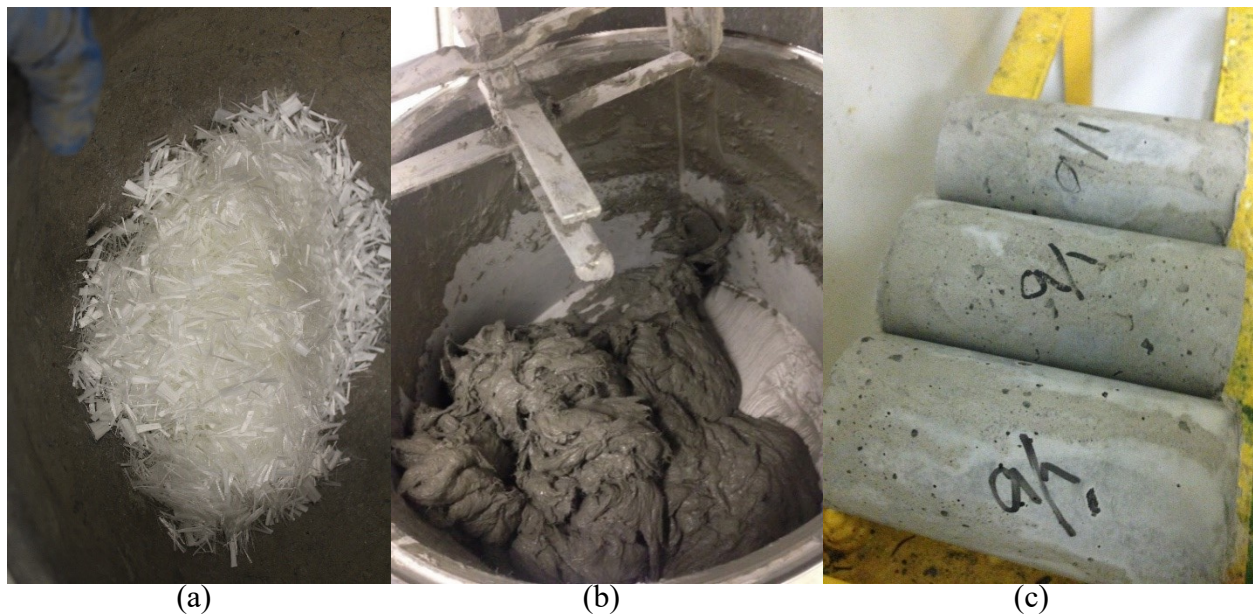


Figure 3-30: (a) RECS-15 fibre before mixing, (b) ECC07 trial mix, (c) ECC07 specimens

### **3.6.7.2 ECC Characterization – Mix trial # 7 (ECC07)**

ECC07 resulted in a compressive strength ( $f'_c$ ) of 78.86 MPa, modulus of elasticity (E) of 16479 MPa, and Poisson's ratio of 0.152 (Fig. 3-31). ECC07 resulted in a tensile strength of 2.27 MPa and an ultimate strain of 0.01 (Fig. 3-32). Cracking on ECC07 consisted of one failure crack with several microcracks developing along the specimen after the tensile test (Fig. 3-33).

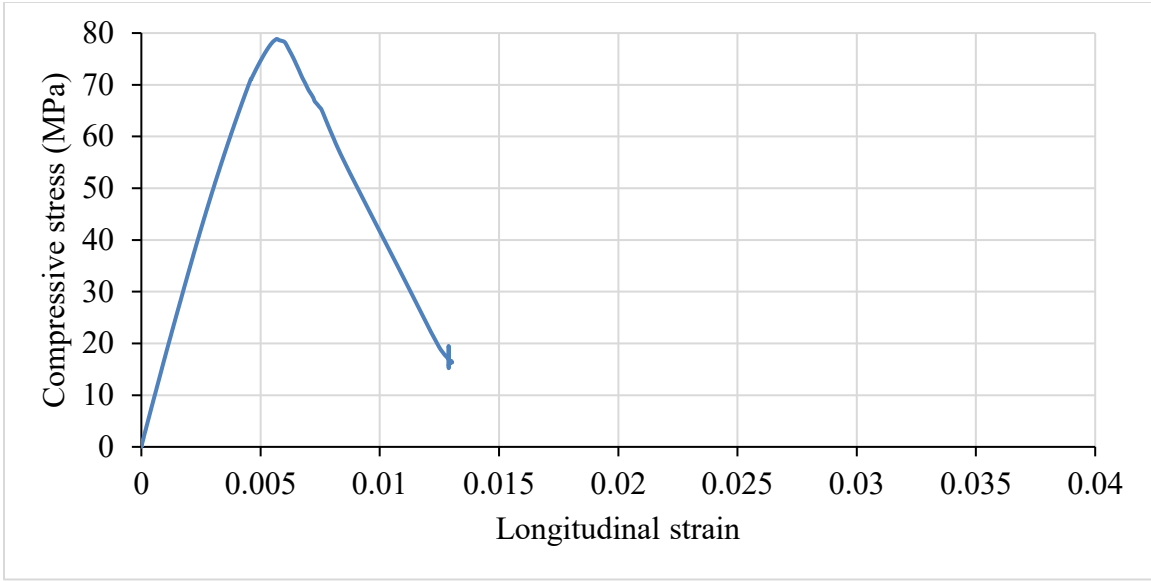


Figure 3-31: Uniaxial compressive stress-strain graph of ECC07

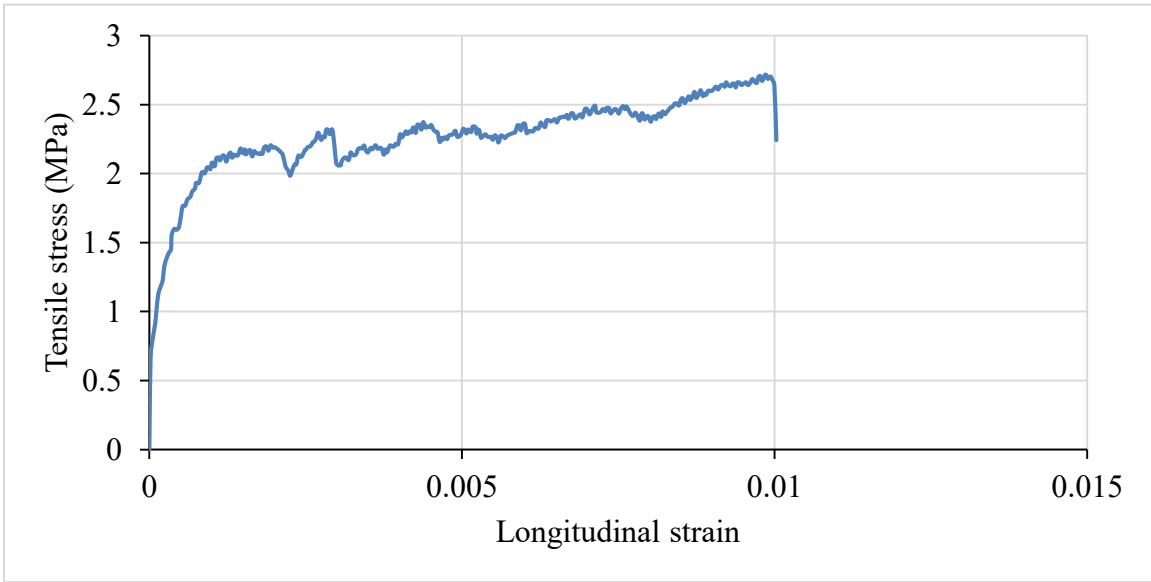


Figure 3-32: Uniaxial tensile stress-strain graph of ECC07

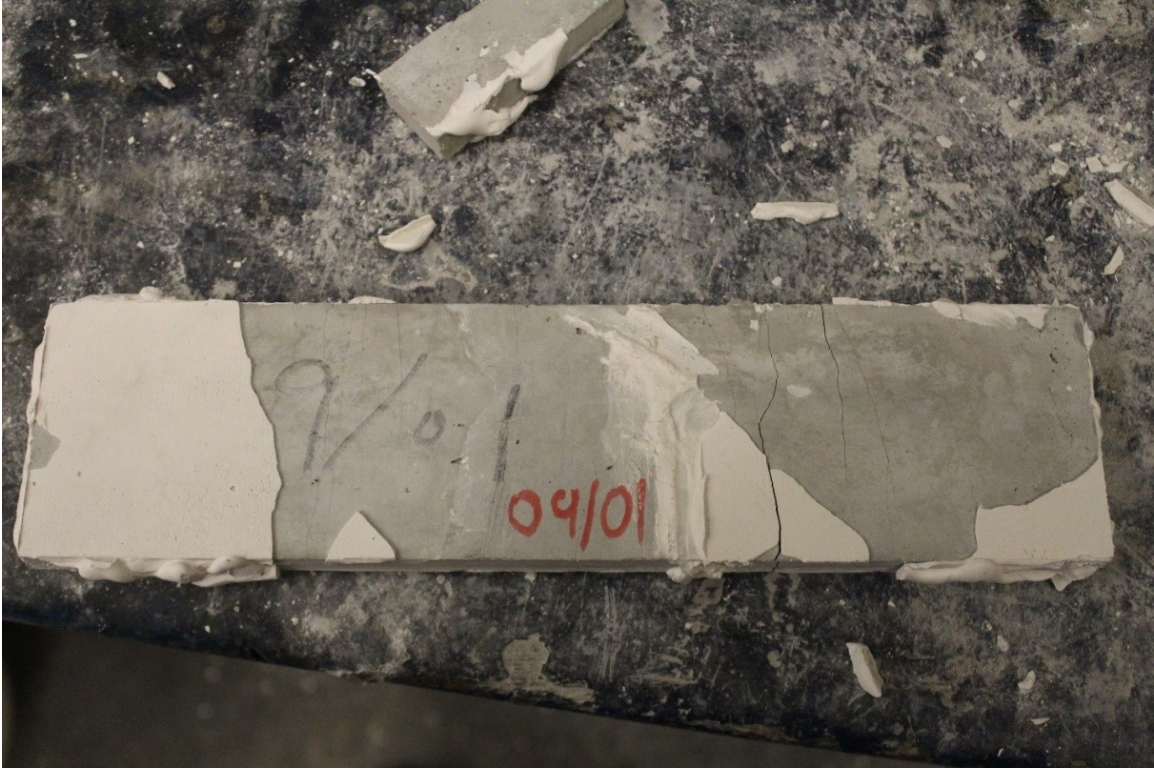


Figure 3-33: Tensile cracking on ECC07 coupon specimen

### 3.6.8 ECC Mix Trial # 8 (ECC08)

Table 3-18: Mix proportion of ECC08

ID: ECC09	Cement	Fly Ash	Sand	Water	SP (Superplasticizer)	Fibre	Stabilizer
Weight (g)	2226	2670.6	1780	1432	32.4	104	0
Weight Ratio	1	1.2	0.8	0.64	0.015	2% Vol	0

Table 3-19: Mixing sequence of ECC08

Sequence no.	Activity	Time (min)
1	Charge all sand, fly ash, and cement	3
2	Charge approximately 90% of mixing water and all superplasticizer	2
3	Mix until material is homogenous	4
4	Charge remaining mixing water	4
5	Mix at high RPM until material is homogenous	4
6	Charge all fibres	2
7	Mix at high RPM until material is homogenous	4

#### **3.6.8.1 ECC Fabrication – Mix Trial # 8 (ECC08)**

##### Mix proportion/Mix procedure:

ECC08 mix was conducted based on the mix proportion of ECC07. ECC08 mixing was based on the mixing procedure of ECC04 in which all the dry materials such as sand, fly ash, and cement were mixed before adding any water. Fibres were not treated before mixing (Fig. 3-34a). The mix proportion and mixing procedure of ECC08 are summarized in Table 3-18 and 3-19 respectively.

##### Observation:

The mix was workable after charging all sand, fly ash, cement at 0.60 w/c ratio with superplasticizer. No additional amount of water before charging fibres. The mixture remained workable after charging all the fibres in Step 7. Little additional amount of water was added after charging fibres to maintain the workability. The finished ECC08 mixture exhibited dry and stiff



when achieved an overall w/c ratio of 0.64 (Fig. 3-34b). The finished mix presented no bleeding (Fig. 3-34b). The specimens demonstrated minor cold joint problem after de-molding (Fig. 3-34c). All molded specimens were hardened and set normally during initial curing period (i.e. 24 hrs) (Fig. 3-34c).

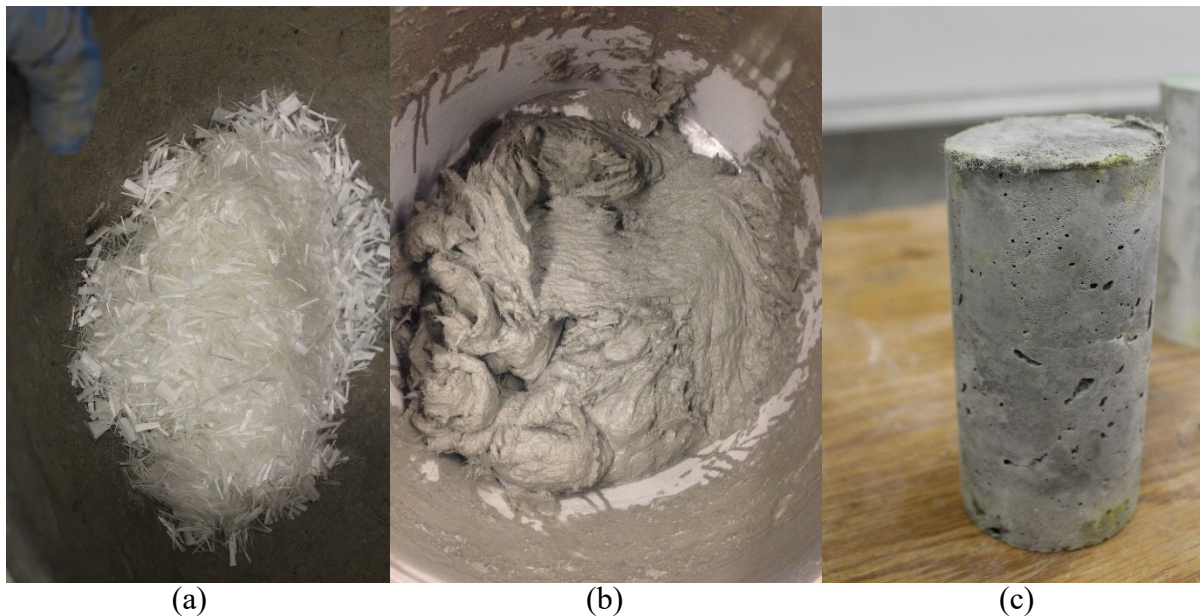


Figure 3-34: (a) RECS-15 fibre before mixing, (b) ECC08 trial mix, (c) ECC08 specimen

### **3.6.8.2 ECC Characterization – Mix Trial # 8 (ECC08)**

ECC08 resulted in a compressive strength ( $f_c$ ) of 57.91 MPa, modulus of elasticity (E) of 0.141 MPa, and Poisson's ratio of 15107 (Fig. 3-35). ECC09 resulted in a tensile strength of 2.43 MPa and an ultimate strain of 0.00465 (Fig. 3-36). Cracking on ECC08 consisted of one failure crack with several microcracks developing along the specimen after the tensile test (Fig. 3-27).

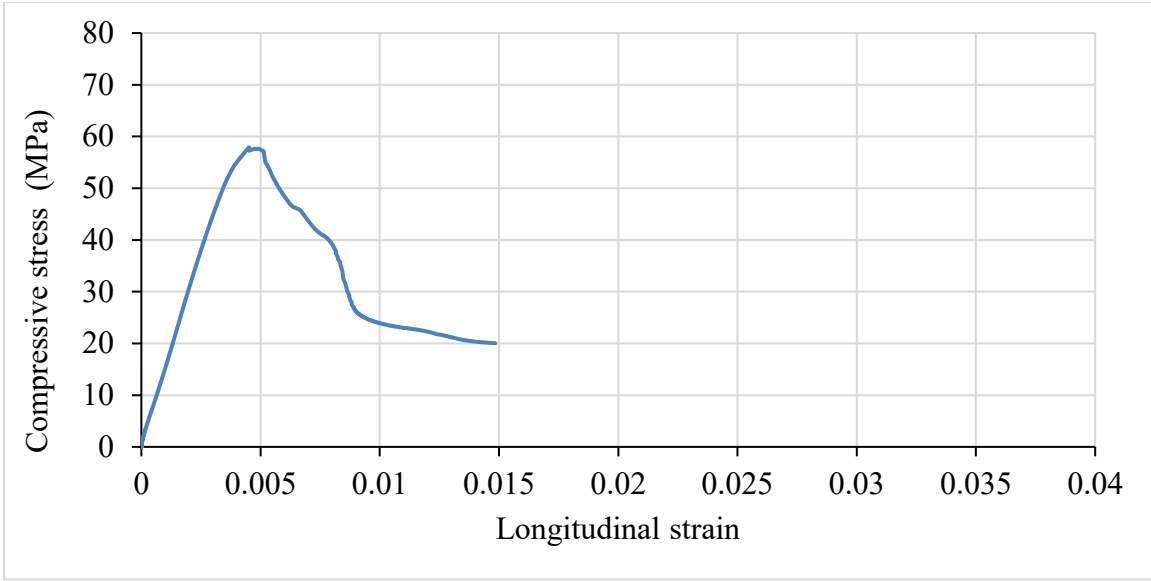


Figure 3-35: Uniaxial compressive stress-strain graph of ECC08

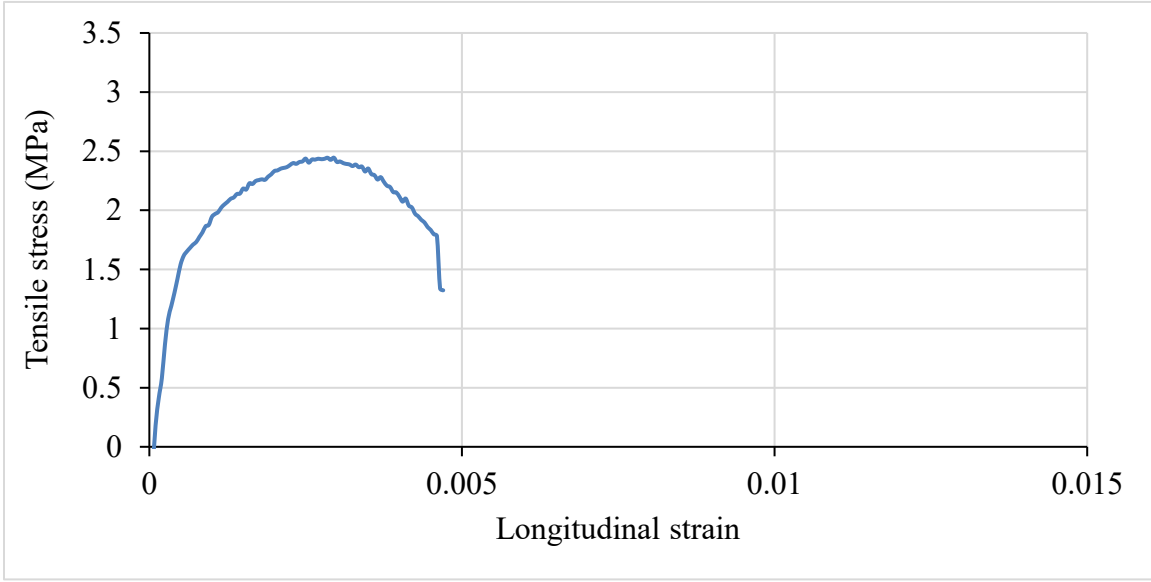


Figure 3-36: Uniaxial tensile stress-strain graph of ECC08

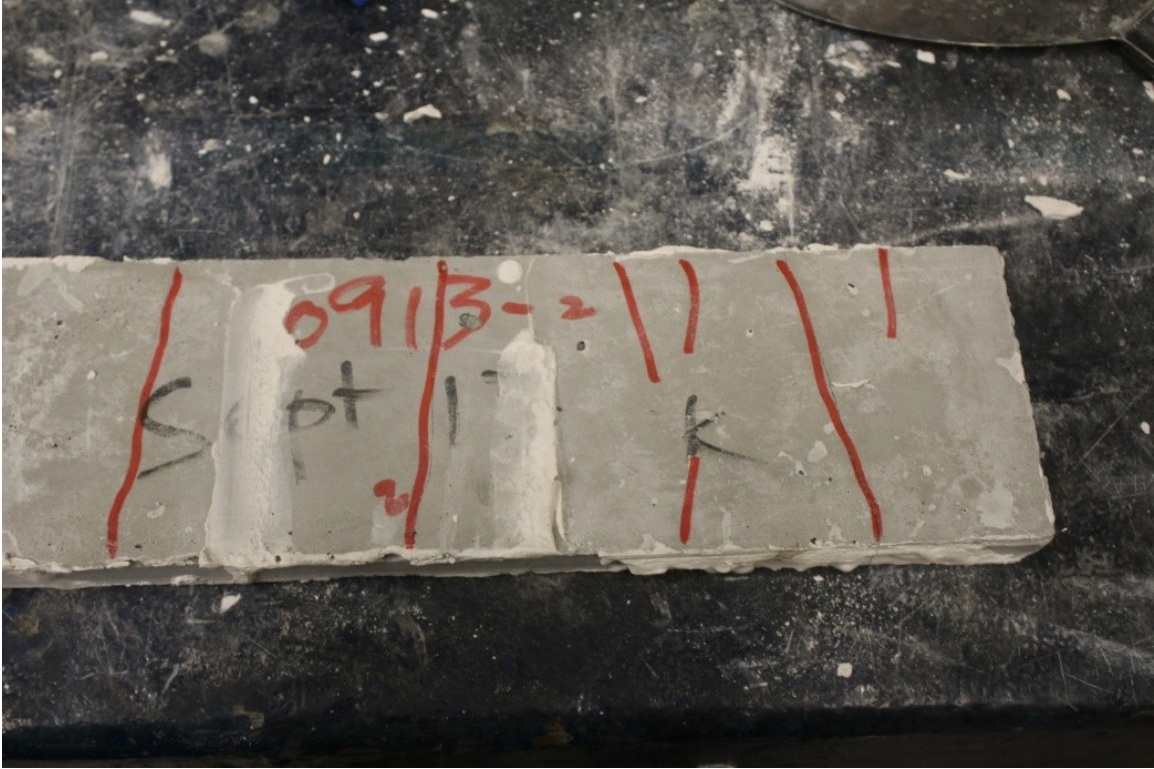


Figure 3-37: Tensile cracking on ECC08 specimen

### 3.6.9 ECC Mix Trial # 9 (ECC09)

Table 3-20: Mix proportion of ECC09

ID: ECC09	Cement	Fly Ash	Sand	Water	SP (Superplasticizer)	Fibre	Stabilizer
Weight (g)	2226.2	2670	1781	1387.2	37.8	104	0
Weight Ratio	1	1.2	0.8	0.62	0.017	2% Vol	0

Table 3-21: Mixing sequence of ECC09

Sequence no.	Activity	Time (min)
1	Charge all sand, fly ash, and cement	3
2	Charge approximately 90% of mixing water	4
3	Mix until material is homogenous	2
4	Charge remaining mixing water and all superplasticizer	4
5	Mix at high RPM until material is homogenous	4
6	Charge all fibres	2
7	Mix at high RPM until material is homogenous	4

#### **3.6.9.1 ECC Fabrication – Mix Trial # 9 (ECC09)**

##### Mix proportion/Mix procedure:

ECC09 mix was conducted based on the mix proportion and the mixing procedure of ECC08. Fibres were not treated before mixing (Fig. 3-38a). The mix proportion and the mixing procedure of ECC09 are summarized in Table 3-20 and 3-21 respectively.

##### Observation:

The mix was workable after charging all sand, fly ash, cement at 0.60 w/c ratio with superplasticizer. No additional amount of water before charging fibres. The mixture remained workable after charging all the fibres in step 7. Little additional amount of water and superplasticizer was added after charging fibres to maintain the workability. The finished ECC09 mixture exhibited well workability when achieved an overall w/c ratio of 0.62 (Fig. 3-38b). The finished mix presented no bleeding (Fig. 3-38b). The specimens demonstrated no cold joint



problems after de-molding (Fig. 3-38c). All molded specimens were hardened and set normally during initial curing period (i.e. 24 hrs) (Fig. 3-38c).

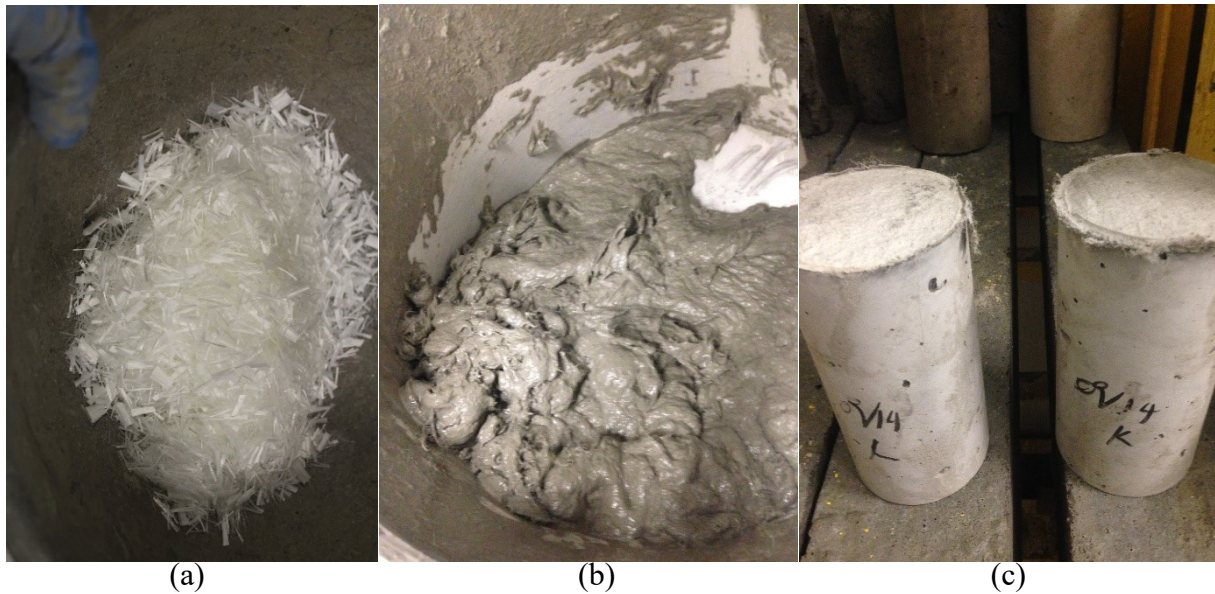


Figure 3-38: (a) RECS-15 fibre before mixing, (b) ECC09 trial mix, (c) ECC09 specimens

### **3.6.9.2 ECC Characterization – Mix trial # 9 (ECC09)**

ECC09 resulted in a compressive strength ( $f'_c$ ) of 74.13 MPa, modulus of elasticity (E) of 16399 MPa, and Poisson's ratio of 0.153 (Fig 3-39). ECC09 resulted in a tensile strength of 2.6 MPa and an ultimate strain of 0.015 (Fig. 3-40). Cracking on ECC09 consisted of one large crack with several microcracks developing along the specimen after the tensile test (Fig. 3-41).

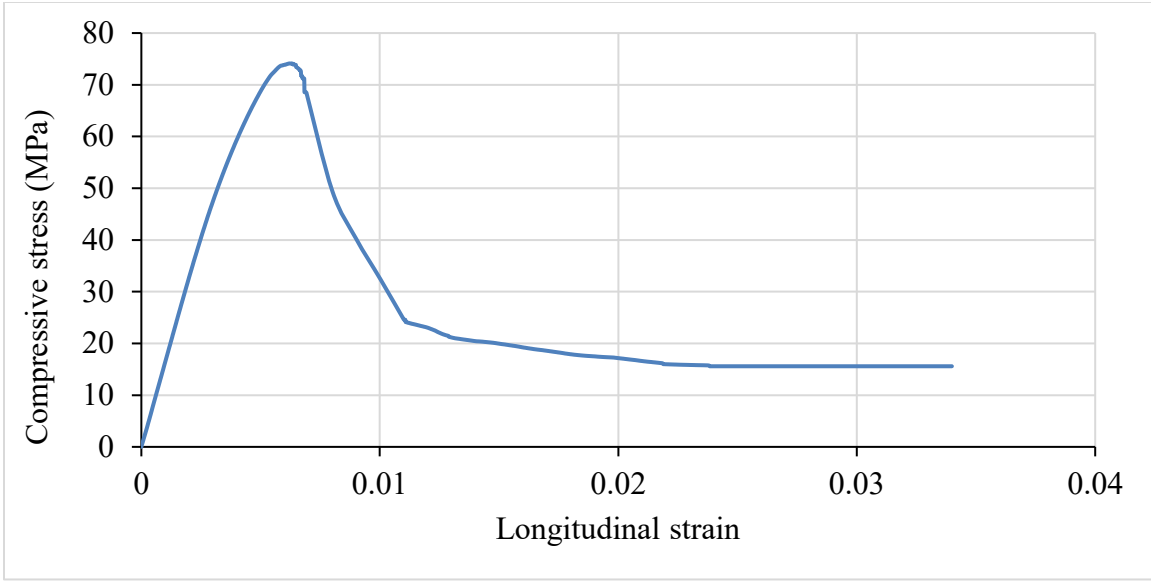


Figure 3-39: Uniaxial compressive stress-strain graph of ECC09

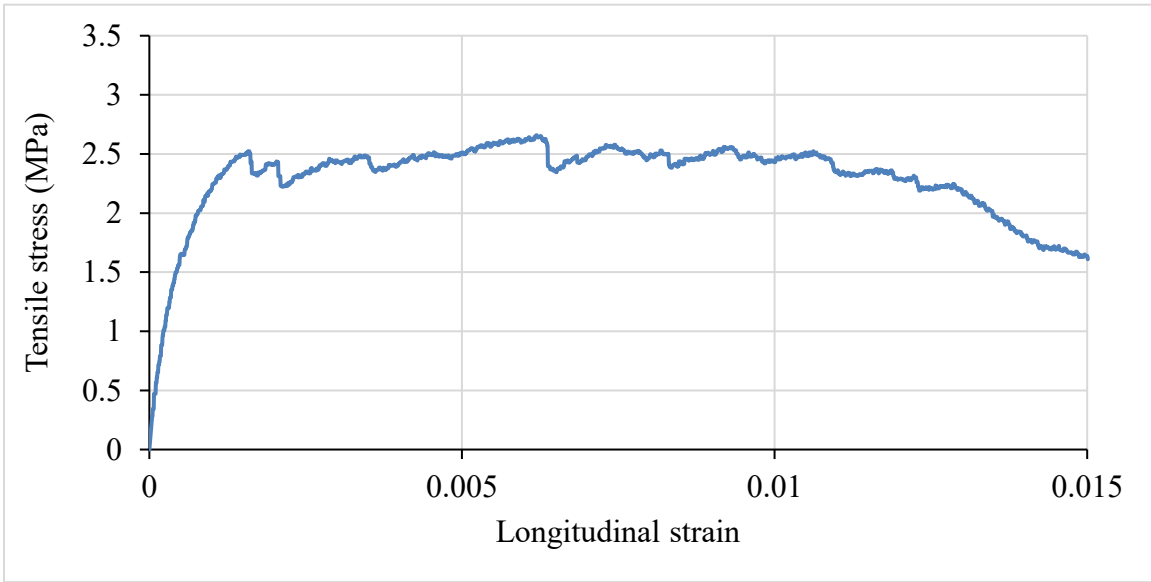


Figure 3-40: Uniaxial tensile stress-strain graph of ECC09



Figure 3-41: Tensile cracking of ECC09 specimen

## **3.6 Discussion**

The feasibility of ECC-M45 fabrication with Western Canada raw materials was investigated through ECC mix trials. Mechanical properties of the fabricated ECC were characterized through uniaxial tensile tests and uniaxial compressive tests. The study has demonstrated that ECC-M45 can be successfully fabricated to exhibit high tensile ductility and fine multiple cracking (mix ECC09). The resulting composite has a high compressive strength.

### **3.6.1 ECC mixes**

Different issues related to workability, bleeding, and cold joints were observed during the trial mixes. Alteration and modification on mix proportions and mixing procedures were made to optimize the process.

As mentioned in section 3.3.5, mixing water can be used to increase the workability of a mixture. However, the water-cement (w/c) ratio has a direct influence on concrete strength. The original mix proportion of ECC-M45 from Table 3-1 (Li, 2008) suggested a 0.56 w/c ratio which resulted in low workability. To increase the workability, chemicals such as superplasticizer and stabilizer were utilized. The use of stabilizer led to a slower curing time for ECC02 (Fig. 3-11c) and affected the compressive behaviour of ECC03 (Fig. 3-15c). Therefore, stabilizer was omitted in the ECC mix design. The optimal mix (ECC09) had a 0.63 w/c ratio with superplasticizer added to obtain a satisfactory workability.

Bleeding is a phenomenon which water appears on the surface after the concrete mixture has been placed and compacted but before it has set. Since the weight of water is the lightest among the mixing component in a concrete mixture, the heavier component tends to move downward under the gravity force and causes segregation. Bleeding occurs when the material fails to hold all the mixing water in a dispersed state due to the settlement of the relatively heavy solid (Monteiro, 2008). To overcome the bleeding problem, fibres were spun in the mixer in ECC05 and ECC06 mixes to loosen the fibres before mixing to achieve better fibre dispersion in mixing. However, bleeding still occurred in the ECC06 mix. Moreover, fibre preparation before mixing was considered not practical in an industrial and large-scale operation, therefore it was omitted in mixing procedure. Utilizing large amounts of superplasticizer was found to be a factor that

increased the tendency of bleeding such as in ECC04 and ECC06 mixes. ECC04 and ECC06 mixes were fabricated with 0.024 sp/c ratio, which is 1.4 times more than the amount of superplasticizer used in the optimal ECC09. The ECC09 mix was successfully fabricated with only 0.017 sp/c (superplasticizer/cement ratio) and no bleeding occurred.

Dry mixes can cause difficulty in molding and lead to cold joints problems such as ECC05 and ECC08. Cold joints may cause defects or discontinuity in a specimen and affect the material properties. To avoid dry mixes, water and superplasticizer were utilized together to control workability as discussed previously. Mixing procedures were found to have influence in the workability of the mixture. The original mixing procedure for ECC-M45 (Table 3-3) suggested mixing sand and water before adding other dry components. However, silica fine sands used in the ECC mixes caused high water absorption and resulted in insufficient water for cement and fly ash. This phenomenon was observed in ECC01, ECC02, ECC05, ECC06, and ECC07. To prevent water absorption in silica sands, the mixing procedures in ECC03, ECC04, ECC08, and ECC09 were altered where water and superplasticizer were mixed together with all dry components such as silica sands, cement, and fly ash. Although some minor cold joints still occurred on ECC08 cylinders, it was due to the insufficient water content in the mixture. The optimal ECC09 mix was made using the same procedure of ECC08 but adding more water. As a result, ECC09 exhibited good workability with no cold joints in cylinder specimens.

ECC09 mix was cast using the following components: (1) Type GU portland cement (1.0 weight ratio), (2) ASTM Class F fly ash (1.2 weight ratio), (3) Silica sand (0.8 weight ratio), (4) Superplasticizer Glenium 7700 (0.017 weight ratio), (5) water (0.63 weight ratio), and (6) PVA fibres (2% of the volume). The procedure to fabricate the ECC09 mix consisted of: (1) mix all sand, fly ash, and cement, (2) add 90% of water, (3) add the remaining water together with the superplasticizer, (4) add fibres.

### 3.6.2 Comparison of Tensile and Compressive Properties

#### 3.6.2.1 Uniaxial tensile properties

Uniaxial tensile tests were performed on 304.8 mm x 76.2 mm x 12.7 mm coupon specimens from all 9 ECC trial mixes. Tensile behaviours such as tensile strength, strain, and cracking mechanism of the ECC were obtained. Although the tensile responses (Fig. 3-42) demonstrate that all ECC specimen have exhibited higher tensile strain than conventional concrete, the effect of workability, bleeding, and cold joints on the material performance under tension are discussed below.

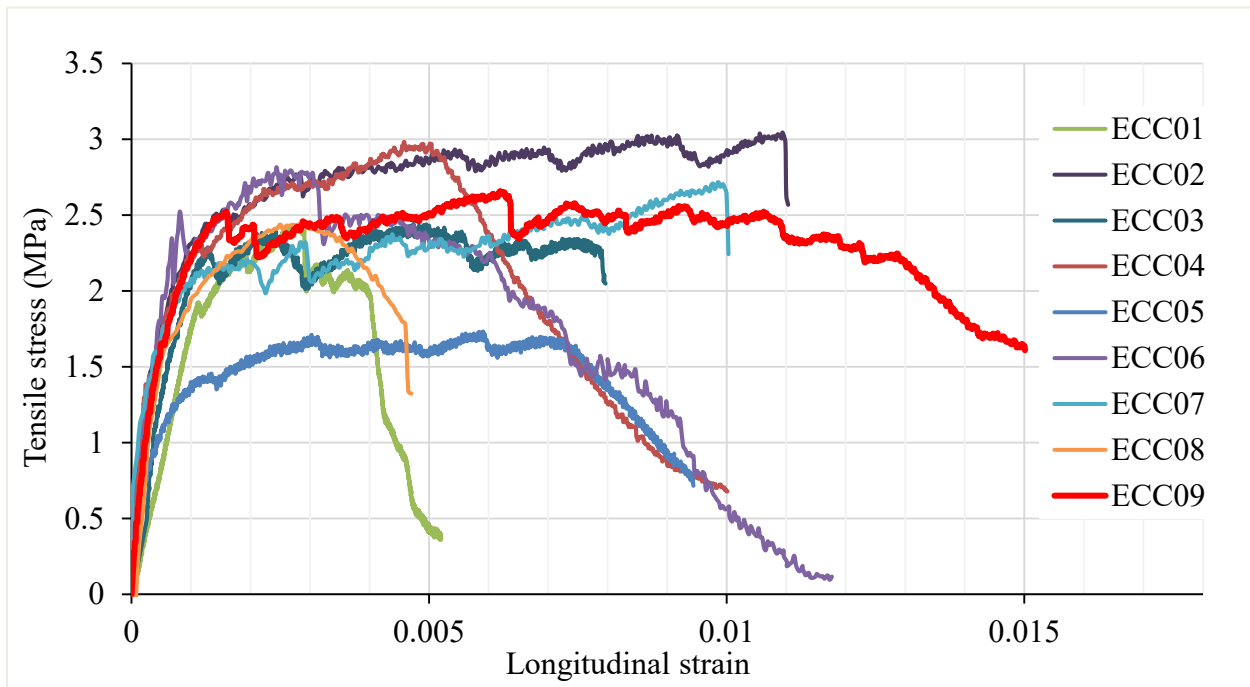


Figure 3-42: Uniaxial tensile stress-strain graph of all ECC trial mixes

Although mixing water provides workability to the mixture, w/c ratio brings effect to the material properties. The ECC tensile responses suggested that w/c ratio of the mix influences tensile strain of the material, where the tensile stress or strain tends to decrease as the w/c ratio decrease. ECC01 which was fabricated with the highest w/c of 0.78, resulted in the lowest tensile strain capacity of 0.004. The limited ductility of ECC01 was due to the crack localization and failure in forming the microcracks (Fig. 3-9). Mixing chemical such as stabilizer and superplasticizer were used to control workability. The effect of stabilizer on tensile responses are not significant in ECC02 and

ECC03, which reached the ultimate tensile strain capacity at 0.011 and 0.008 respectively. The optimal ECC09 mix with only 0.63 w/c achieved the highest tensile strain capacity of 0.015 while successfully developing microcracks (Fig. 3-41).

Bleeding, which due to the separation of material components in a specimen, can affect material performance. Fibre preparation was attempted to reduce the possibility of bleeding in ECC05 and ECC06 mixes. The effect of fibre preparation on the tensile responses of ECC05 and ECC06 is not comparable since bleeding still occurred in ECC06. Bleeding due to the overuse of superplasticizer in ECC04 and ECC06 led to a lower tensile strain capacity of 0.00529 and 0.00658 respectively. The optimal ECC09 mix with lesser amount of superplasticizer which resulted in no bleeding had achieved the highest tensile strain capacity.

Cold joints cause defects in the specimen and affect tensile behaviour. Mixing procedures were modified to reduce the possibility of having a dry mixture. Trials consisting of mixing silica sand with water were conducted in ECC01, ECC02, ECC05, ECC06, and ECC07. Trials consisting of mixing dry components such as cement, fly ash, and cement with water were conducted in ECC03, ECC04, ECC08, and ECC09. Cold joints only occurred in ECC05 and ECC08 and led to a lower tensile strain capacity of 0.00658 and 0.00465. The optimal mix (ECC09) was conducted based on that of ECC08 with more mixing water to mitigate the cold joint problem.

Microcrack formation is one of the essential properties for ECC-M45 to develop ductility. Most of the ECC specimens exhibited microcracking except ECC01 which had a high w/c ratio. ECC specimen developed microcracking only near the failure cracks in ECC03, ECC05, and ECC06. Microcracking along the entire specimen occurred in ECC02, ECC04, ECC07, ECC08, and ECC09. The best performance was deemed to occur when multiple microcracking developed along the length of the specimen, such as in mixes ECC07, ECC08 and ECC09.

Table 3-22: Summary of ECC trial mixes for tensile responses

Mix ID	Workability		Bleeding		Cold Joints		Tensile Strength (MPa)	Tensile Strain capacity	Microcracking	Issue
	c/w* ratio	c/s* ratio	Fibre preparation	c/sp* ratio	Original Mixing procedure	Modified Mixing procedure				
ECC01	0.78			0.012	✓		2.44	0.004	No	
ECC02	0.63	0.0211		0.024	✓		3.045	0.011	along the specimen	slower curing time
ECC03	0.65	0.032		0.024		✓	2.34	0.008	only near the failure cracks	
ECC04	0.56			0.024		✓	2.86	0.00529	along the specimen	Bleeding
ECC05	0.56		✓	0.027	✓		1.68	0.00751	only near the failure cracks	Cold joints
ECC06	0.56		✓	0.024	✓		2.82	0.00658	only near the failure cracks	Bleeding
ECC07	0.58			0.018	✓		2.27	0.010	along the specimen	
ECC08	0.64			0.015		✓	2.43	0.00465	along the specimen	Cold joints
<b>ECC09</b>	<b>0.62</b>			<b>0.017</b>		✓	<b>2.6</b>	<b>0.015</b>	along the specimen	

\* c/w = cement/water, c/s = cement/stabilizer, c/sp = cement/superplasticizer



Overall ECC trial mix designs and their corresponding compressive behaviours are compared in Table 3-22. ECC09 presented the best performance in terms of achieving acceptable tensile strain capacity and forming microcracks. ECC09 resulted in a tensile strength of 2.6 MPa and an ultimate strain of 0.015. ECC09 illustrated several microcracks developed along the specimen with one final large crack after the tensile test (Fig. 3-41). The additional data for the variation in the uniaxial tensile stress-strain response of ECC09 is shown in Appendix A. The Poisson's ratio of each specimen in ECC09 over the compressive tests are shown in Appendix B.

### **3.6.2.3 Uniaxial compressive properties**

Uniaxial compressive tests were performed on Ø75x150 mm cylinders in all 9 ECC trial mixes. Compressive behaviours such as 28-day compressive strength, modulus of elasticity, and Poisson's ratio (at the strain corresponding to 40% of peak compressive strength) of the ECC were obtained. The compressive stress-strain responses (Fig. 3-43) show that most of the ECC specimens exhibited the typical compressive behaviour of conventional concrete. The effect of workability, bleeding, and cold joints on the material performance under compression are discussed below.

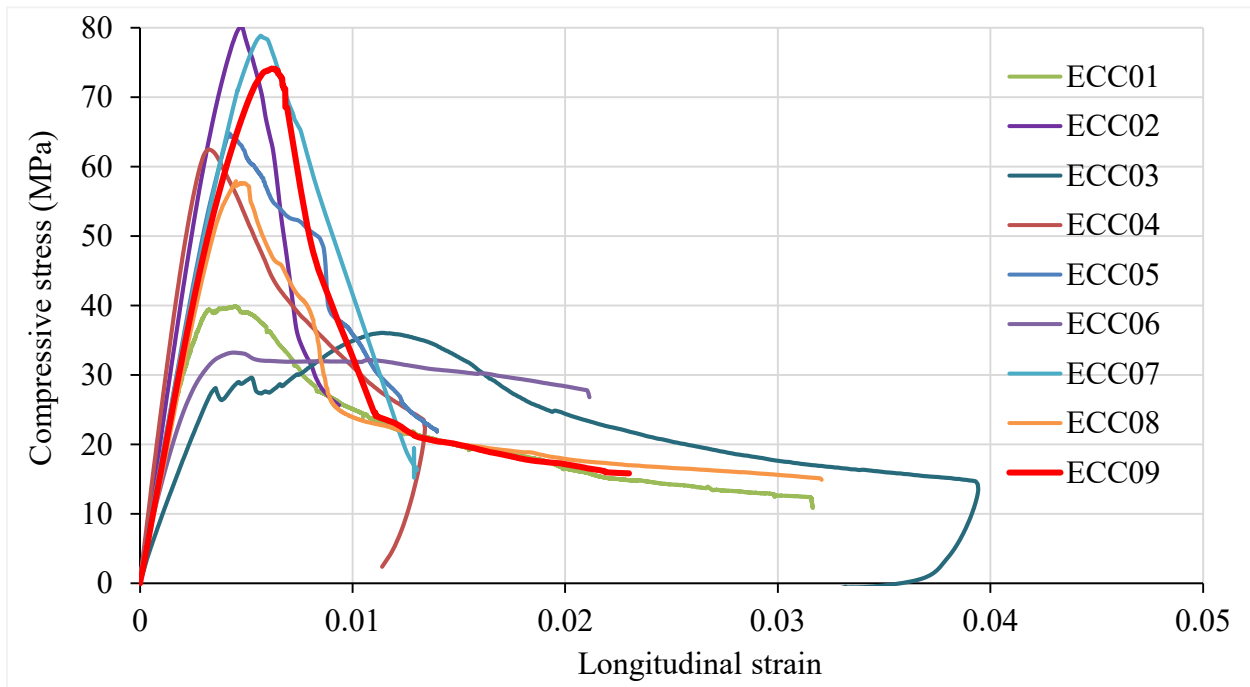


Figure 3-43: Uniaxial compressive stress-strain graph of all ECC trial mixes

The ECC compressive responses suggested that w/c ratio of the mix influences the compressive strength of the material, where the compressive stress tends to decrease as the w/c ratio. ECC01 which was fabricated with the highest w/c of 0.78, resulted in the lower compressive strength of 39.83 MPa. Mixing chemical such as stabilizer and superplasticizer were used to control workability. The effect of stabilizer on compressive responses are not comparable in ECC02 and ECC03, since both ECC presented different behaviours. However, ECC03 which was cast with the most amount of stabilizer presented an unusual compressive behaviour. The optimal ECC09 mix with only 0.63 w/c and superplasticizer achieved a typical concrete compressive behaviour.

Fibre preparation was attempted to reduce the possibility of bleeding in ECC05 and ECC06 mixes. Bleeding due to the overuse of superplasticizer in ECC04 and ECC06 presented different compressive response. ECC06 which experienced the most bleeding showed the lowest compressive strength followed by a rapidly decreasing post-peak behaviour, while ECC04 achieved a compressive strength of 62.47 MPa. The ECC09 mix, having a lesser amount of superplasticizer, resulted in no bleeding and achieved a compressive strength of 74.13 MPa with a typical concrete post-peak behaviour.

Mixing procedures were modified to reduce the possibility of the cold joints due to dry mixtures. Procedures of mixing silica sand with water were conducted in ECC01, ECC02, ECC05, ECC06, and ECC07. Procedures of mixing dry components such as cement, fly ash, and cement with water were conducted in ECC03, ECC04, ECC08, and ECC09. Cold joints only occurred in ECC05 and ECC08 and resulted in a lower compressive strength of 64.78 MPa and 57.91 MPa with non-parabolic post-peak behaviour. The optimal ECC09 mix was conducted according to ECC08 with more mixing water to accommodate the cold joints problem and achieved a compressive strength of 74.13 MPa with a typical concrete post-peak behaviour.

Table 3-23: Summary of ECC trial mixes for compressive responses

Mix ID	Workability		Bleeding		Cold Joints		Max. Compressive Strength (MPa)	Poisson's Ratio (Elastic)	Issue
	c/w* ratio	c/s* ratio	Fibre preparation	c/sp* ratio	Original Mixing procedure	Modified Mixing procedure			
ECC01	0.78			0.012	✓		39.83	0.200	
ECC02	0.63	0.0211		0.024	✓		80.26	0.165	slower curing time
ECC03	0.65	0.0320		0.024		✓	36.08	0.046	
ECC04	0.56			0.024		✓	62.47	0.204	Bleeding
ECC05	0.56		✓	0.027	✓		64.78	0.240	Cold joints
ECC06	0.56		✓	0.024	✓		33.33	0.094	Bleeding
ECC07	0.58			0.018	✓		78.86	0.152	
ECC08	0.64			0.015		✓	57.91	0.141	Cold joints
<b>ECC09</b>	<b>0.62</b>			<b>0.017</b>		✓	<b>74.13</b>	<b>0.153</b>	

\* c/w = cement/water, c/s = cement/stabilizer, c/sp = cement/superplasticizer

Overall ECC trial mix designs and their corresponding tensile behaviours are compared in Table 3-23. Mix ECC09 reached a compressive strength of 74.13 MPa at a strain of 0.00623 with a gradual descending post-peak branch. ACI Committee 363 (2005) defined mixtures with a specified design strength of 55 MPa or more are considered as high-strength concrete. Therefore, ECC09 is considered as a high-strength ECC. A gradual bulging failure, rather than the explosive crushing failure typical of high-strength concrete, was observed. ECC09 resulted in a modulus of elasticity (E) of 16399 MPa, and Poisson's ratio (elastic stage) of 0.153. The additional data for the variation in the uniaxial compressive stress-strain response of ECC09 is shown in Appendix A. The Poisson's ratio of ECC09 throughout the compressive test is shown in Appendix B.

### **3.7 Summary**

The feasibility of ECC fabrication with Western Canada material components was investigated. Mix ECC09 was found to be the optimal mixture, presenting good workability with no bleeding or cold joint problems. The tensile response of ECC09 presented the highest tensile strain capacity with formation of multi-microcracking. Figs. 3-44 and 3-45 showed a prediction of concrete tensile strain with similar tensile strength as ECC09. By comparison, ECC09 achieved up to 234 times higher tensile strain capacity than conventional concrete. On the other hand, ECC09 possessed a typical compressive behaviour of high-strength concrete but with a gradual bulging failure.

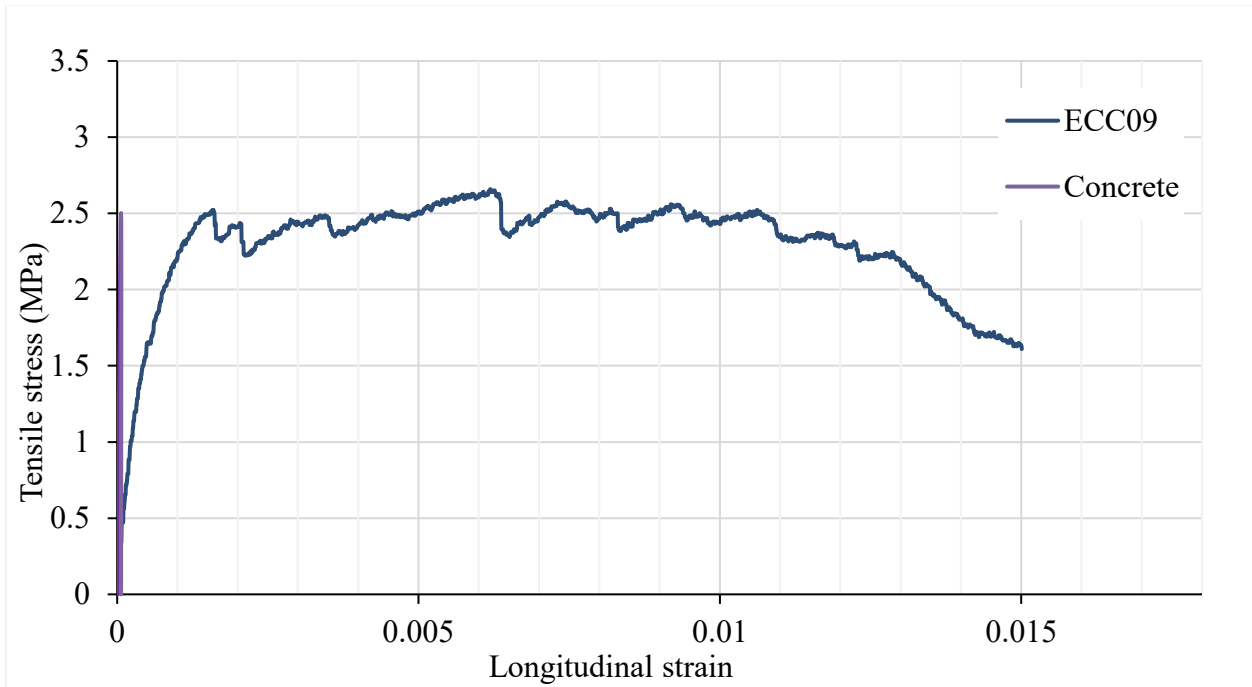


Figure 3-44: Tensile stress-strain response of ECC09 and conventional concrete

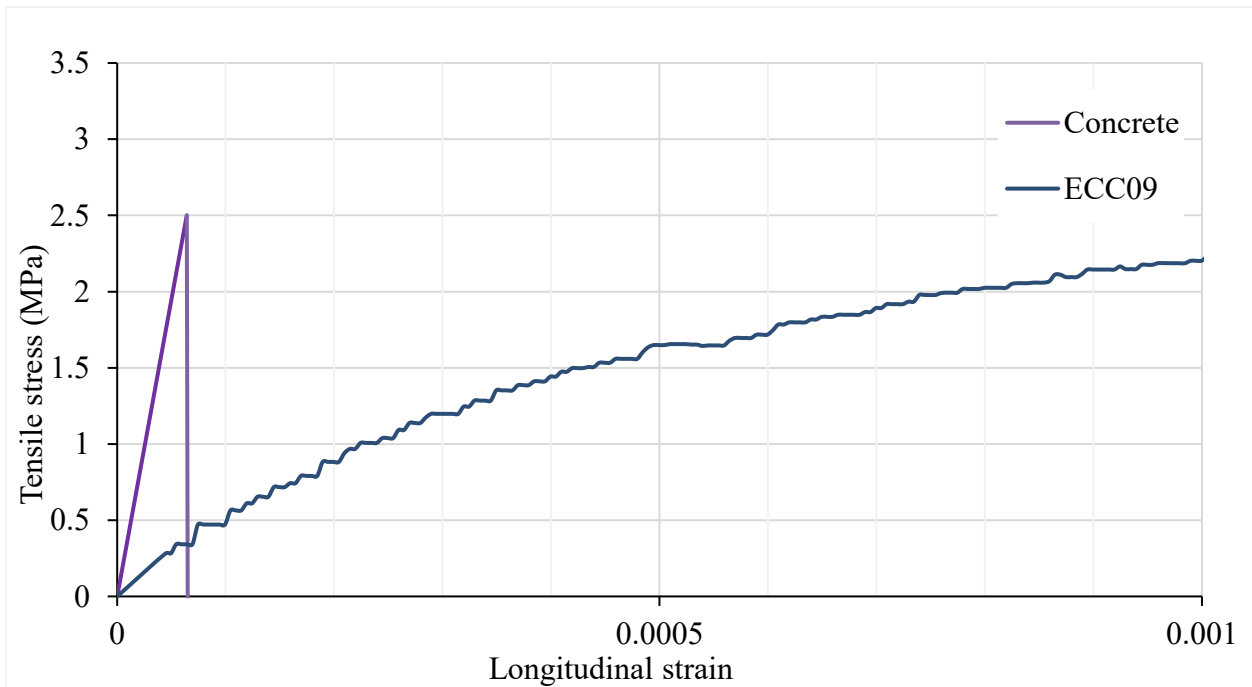


Figure 3-45: Tensile stress-strain response of ECC09 and conventional concrete (close-up)

The mix proportion and mixing procedure of optimal ECC mixture are summarized in Table 3-22 and 3-23. Water-cement (w/c) ratio was proposed to be approximate 0.6 and superplasticizer-cement (sp/c) ratio was proposed to be approximate 0.017 with the following mixing procedure to achieve a good workability and exhibit the best performance of ECC tensile and compressive behaviour. The water/cementitious materials (w/cm) ratio for this mix proportion was found to be 0.25.

Table 3-24: Optimized ECC-M45 mix proportion

ECC-M45 UofA	Cement	Fly Ash	Sand	Water	SP (Superplasticizer)	Fibre
Weight Ratio	1	1.2	0.8	0.6±0.03	0.014-0.018	2% Vol
kg/m <sup>3</sup>	556	667	445	311	6.7	26

Table 3-25: Optimized ECC-M45 mixing procedures

Sequence no.	Activity	Time (min)
1	Charge all sand, fly ash, and cement	3
2	Charge approximately 90% of mixing water	4
3	Mix until material is homogenous	2
4	Charge remaining mixing water and all superplasticizer	4
5	Mix at high RPM* until material is homogenous	4
6	Charge all fibres	2
7	Mix at high RPM until material is homogenous, add water/superplasticizer if necessary	4

\*high RPM (Revolution(s) Per Minute) is recommended to be 50-60 RPM

## CHAPTER 4. CONFINEMENT ON ECC

The ability of a structure to exhibit ductility is an important factor to assess its structural performance under seismic demands. One approach to increase the ductility of a reinforced concrete structure is to have a proper design in which the damage is concentrated at specially detailed joints and critical regions, such as plastic hinges (Park and Paulay 1975). This special detailing prevents shear failures, increases curvature by minimizing the depth of the compressive block in the concrete, and provides a high crushing strain for the concrete through confinement mechanisms. Although there are well-known models to evaluate concrete confinement, such as Mander et al. (1988), similar models for ECC materials are scarce. As the demand and designer interest on ECC materials are increasing, ECC confinement models are necessary.

The only available model for ECC was developed by Motaref et al. (2011) which quantified the confinement effect in ECC cylinders incorporating circular spiral transverse reinforcement. To the knowledge of the author, no models exist for the confinement effect in rectangular columns made with ECC that incorporate rectangular stirrups.

The material characterization presented in Chapter 3 showed that ECC material exhibited a compressive behaviour similar to that of high-strength concrete. The studies on confined high-strength concrete (Yong et al. 1988, Bjerkeli et al. 1990) show that the confined, compressive stress-strain curve of high-strength concrete is different in shape compared to confined normal-strength concrete. Therefore, existing stress-strain models for rectangular confined columns made of normal-strength concrete are not necessarily applicable to high-strength concrete columns.

### 4.1 Scope

The column specimens in this experimental program are casted with the high-strength ECC fabricated in section 3 only. The confinement effects study on ECC columns are conducted on small-scale specimens and square columns with transverse reinforcement ratios ranging from 1 to 2 % only.

## 4.2 Confinement

Transverse reinforcement is traditionally used to provide shear strength, provide a framework for longitudinal bars, and to confine concrete. Concrete is considered as unconfined at low levels of uniaxial compressive stress. This is because of the induced strains to the transverse reinforcement due to the resulting lateral expansion in the concrete are small. The concrete becomes confined when the stresses in the concrete approach the peak uniaxial strength. The transverse strains increase due to progressive internal cracking and expansion in concrete. The restraining pressure of transverse reinforcement produces a confining reaction to the concrete. Previous studies on concrete confinement have demonstrated that the transverse reinforcement can significantly increase the strain at which compressive failure occurs, enhancing strain ductility in compression.

Concrete cylinders with spirals tested by Iyenfar et al. (1970) showed that the increase of strength and ductility with the content of confining steel can be very significant (Fig. 4-1). The concrete is considered as effectively confined in an arch shape between the transverse bars as shown in Fig. 4-2. Therefore, smaller spacing leads to more effective confinement, while larger spacing results in a large volume of unconfined concrete which may spall away (Park and Paulay 1975).

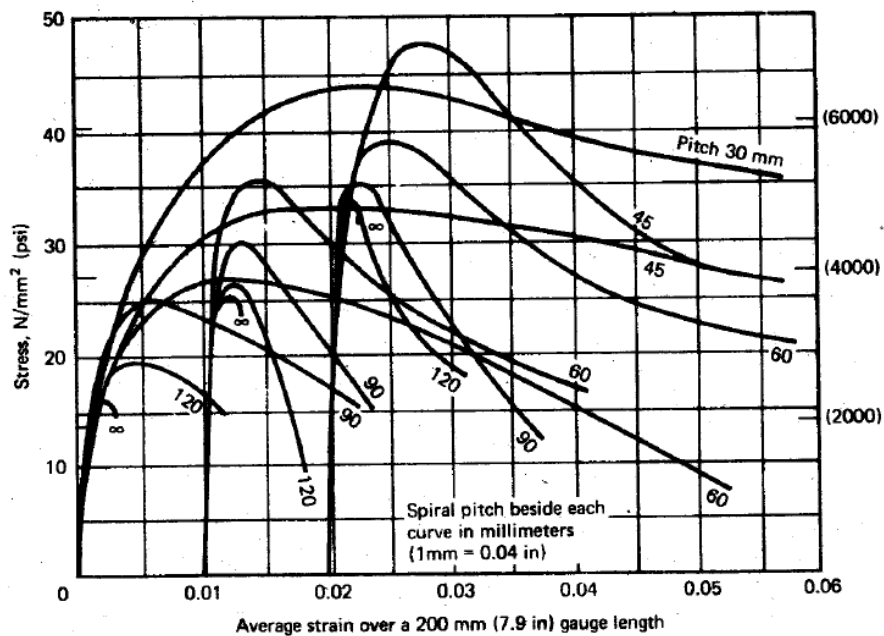


Figure 4-1: Stress-strain curves for concrete cylinders tested by Iyenfar et al. (1970)



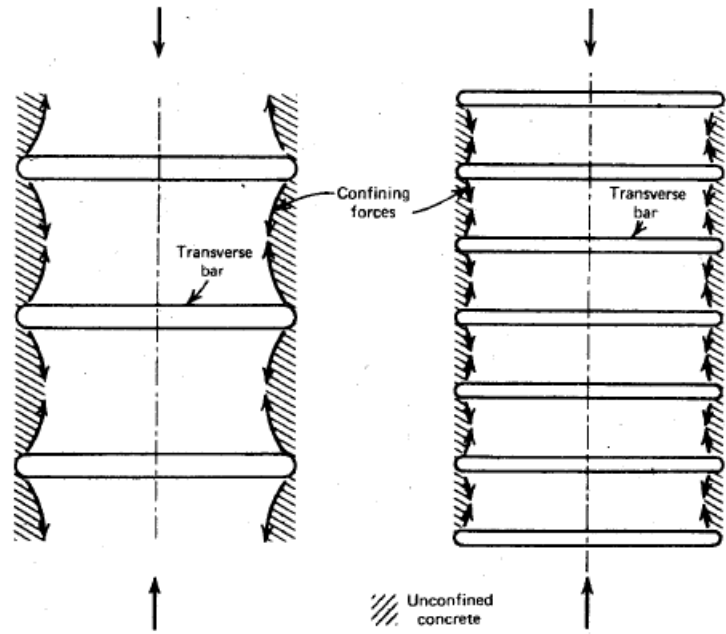


Figure 4-2: Effect of spacing of transverse steel on efficiency of confinement (Park and Paulay 1975)

Concrete prisms with square ties tested by Bertero and Felippa (1964) showed that the effect of transverse steel content on strength is smaller compared to the case in which circular spirals are used to confine concrete. The considerable difference between the confinement by circular steel spirals and that provided by rectangular or square steel hoops is due to their shape. Circular spirals provide a continuous confining pressure around the circumference. Rectangular or square steel hoops can only provide confining reactions near the corners of the hoops because the pressure of the concrete against the side of the hoops tends to bend the sides outwards (Fig. 4-3). Therefore, a considerable portion of the concrete in a rectangular cross section may be unconfined (Park and Paulay 1975).

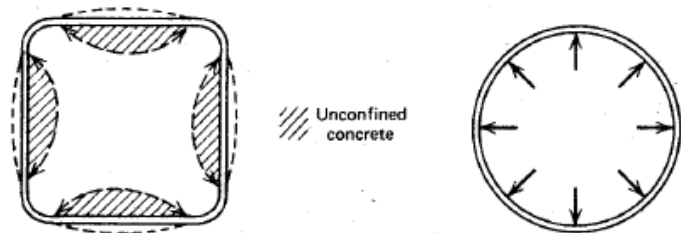


Figure 4-3: Confinement by square hoops and circular spirals (Park and Paulay 1975)

As discussed earlier, confinement by transverse reinforcement has little effect on the stress-strain curve until the peak uniaxial strength of the concrete is approached. The stress-strain behaviour of confined concrete at high strains is a function of several variables, but the ratio of transverse steel content (ratio of cross section of transverse steel to the cross section of concrete) is one of the most important (Park and Paulay 1975) and thus it was set as the main variable in this study. Since circular confined ECC has been studied previously (Motaref et al. 2011), rectangular confinement on square columns is investigated for ECC in this research.

## 4.2.1 Confinement Models – Background

### 4.2.1.1 Mander et al. (1988) Model

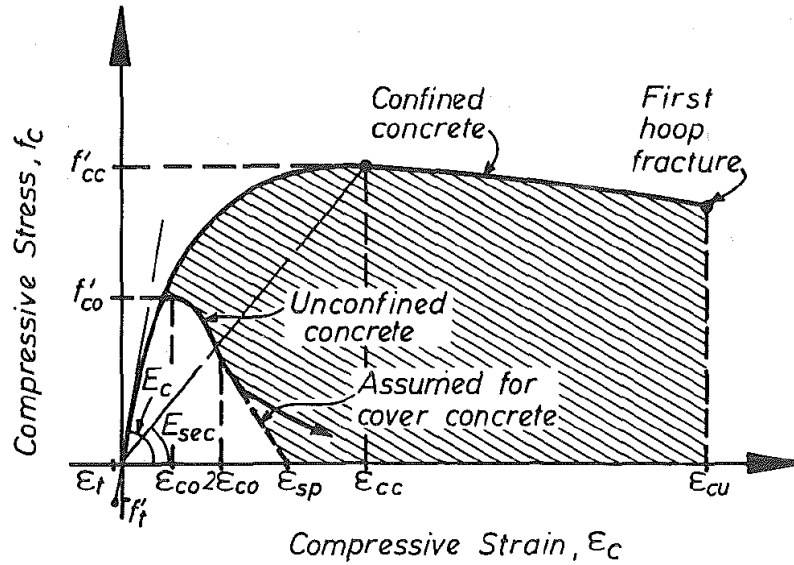


Figure 4-4: Mander et al. (1988) model for confined and unconfined concrete

Mander et al. (1988) presented a theoretical model with the results of an experimental program of some 40 concentric axial compression tests. The program consisted of the axial testing of circular, square, and rectangular reinforced concrete columns. Mander et al. proposed a unified stress-strain approach for confined concrete applicable to both circular- and rectangular-shaped transverse reinforcement. Mander et al. stress-strain model illustrated in Fig. 4-4 is based on a 3-parameter equation suggested by Popovics (1973). The proposed longitudinal compressive concrete stress ( $f_c$ ) and strain ( $\epsilon_c$ ) to describe the entire stress-strain curve in Fig. 4-4 is given by

$$f_c = \frac{f'_{cc} x r}{r - 1 + x^r} \quad (4-1)$$

where

$$x = \frac{\epsilon_c}{\epsilon_{cc}} \quad (4-2)$$

$$r = \frac{E_c}{E_c - E_{sec}} \quad (4-3)$$

$$E_c = 5000\sqrt{f'_{co}} \quad (4-4)$$

$$E_{sec} = \frac{f'_{cc}}{\varepsilon_{cc}} \quad (4-5)$$

and  $f'_{co}$  = the unconfined concrete strength

$\varepsilon_{co}$  = the unconfined concrete strain (generally  $\varepsilon_{co} = 0.002$  can be assumed)

$f'_{cc}$  = compressive strength of confined concrete (defined later).

$\varepsilon_{cc}$  = maximum compressive strain of confined concrete and is defined by

$$\varepsilon_{cc} = \varepsilon_{co} \left[ 1 + 5 \left( \frac{f'_{cc}}{f'_{co}} \right) - 1 \right] \quad (4-6)$$

To determine the confined concrete compressive strength  $f'_{cc}$  (Fig. 4-4), Mander et al. adopted the “five-parameter” multi-axial failure surface developed by William and Warnke (1975) with the ultimate strength surface calculation based on the triaxial tests of Schickert and Winkler (1977). By considering an approach used by Sheikh and Uzumeri (1980) to determine the effective lateral confining pressure on the concrete section, Mander et al. proposed a general solution of the multiaxial failure criterion in terms of the two lateral confining stresses as shown in Fig. 4-7. When the confined concrete core is placed in triaxial compression with equal effective lateral confining stress ( $f'_1$ ) from spirals, circular hoops, or square hoops, confined compressive strength  $f'_{cc}$  is defined as

$$f'_{cc} = f'_{co} \left( -1.254 + 2.254 \sqrt{1 + \frac{7.94f'_1}{f'_{co}}} - 2 \frac{f'_1}{f'_{co}} \right) \quad (4-7)$$

where effective lateral confining stress for sections confined by spirals or circular hoops is given by

$$f_1' = \frac{1}{2} k_e \rho_s f_{yh} \quad (4-8)$$

where effective lateral confining stress for sections confined by rectangular hoops with or without cross ties is given by

$$f_{1x}' = k_e \rho_x f_{yh} \text{ and } f_{1y}' = k_e \rho_y f_{yh} \quad (4-9)$$

and  $\rho_s$  = ratio of volume of transverse confining steel to volume of confined concrete core

$f_{yh}$  = yield strength of transverse reinforcement

$\rho_x, \rho_y$  = ratio of volume of transverse confining steel to volume of confined concrete core is x and y direction respectively

$k_e$  = confinement effectiveness coefficient

For circular hoops

$$k_e = \frac{\left(1 - \frac{s'}{2d_s}\right)^2}{1 - p_{cc}} \quad (4-10)$$

For circular spirals

$$k_e = \frac{1 - \frac{s'}{2d_s}}{1 - p_{cc}} \quad (4-11)$$

Rectangular hoops

$$k_e = \frac{\left(1 - \sum_{i=1}^n \frac{(w_i')^2}{6b_c d_c}\right) \left(1 - \frac{s'}{2b_c}\right) \left(1 - \frac{s'}{2d_c}\right)}{1 - p_{cc}} \quad (4-12)$$

where  $p_{cc}$  = ratio of area of longitudinal reinforcement to area of core of the section

$s'$  = clear vertical spacing between spiral or hoop bars (see Figs. 4-5 & 4-6)

$d_s$  = diameter of spiral between bar centers (see Fig. 4-5)

$w'_i$  = the  $i$ th clear distance between adjacent longitudinal bars (see Fig. 4-6)

$b_c$  and  $d_c$  = core dimension to centerlines of perimeter hoop in x and y directions respectively (see Fig. 4-6)

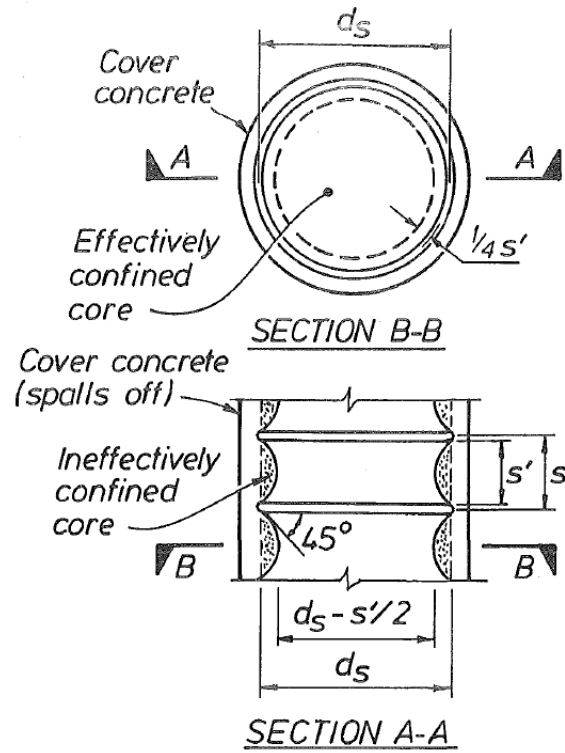


Figure 4-5: Effectively confined core for circular hoop reinforcement (Mander et al. 1988)

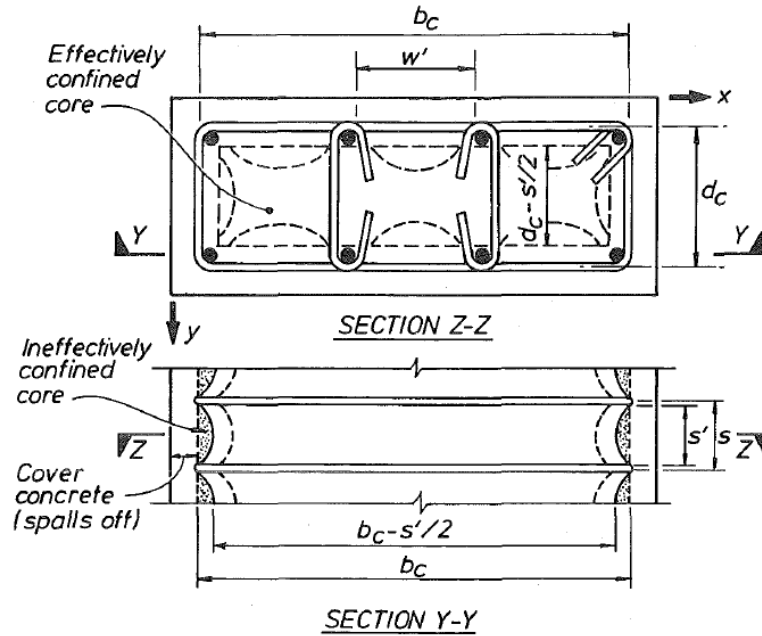


Figure 4-6: Effectively confined core for rectangular hoop reinforcement (Mander et al. 1988)

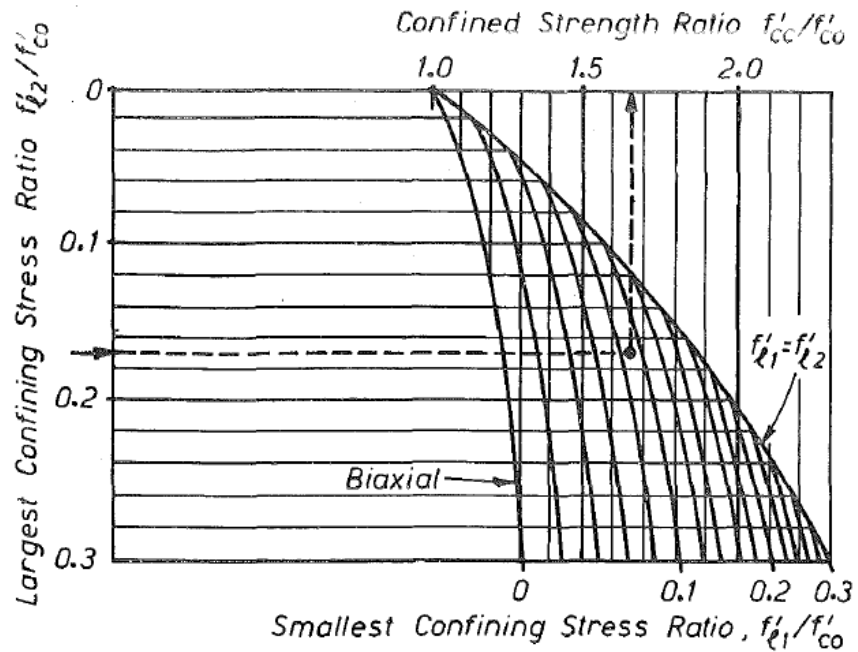


Figure 4-7: Confined strength determination from lateral confining stresses for rectangular sections (Mander et al. 1988)

#### 4.2.1.2 Yong et al. (1988) Model

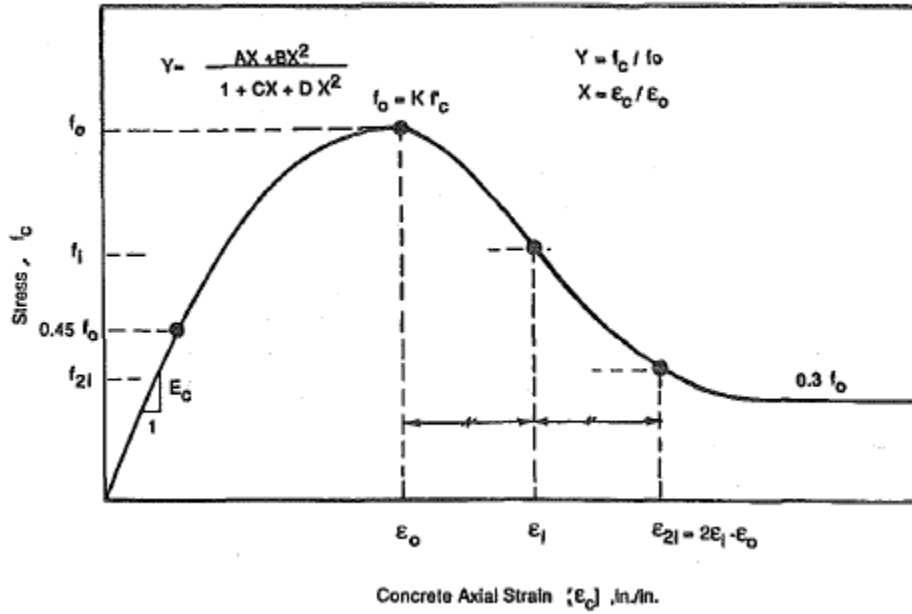


Figure 4-8: Yong et al. (1988) model for confined high-strength concrete

Yong et al. (1988) proposed an empirical model of high-strength concrete with rectilinear confinement subjected to axial compressive load. Yong et al. tested 24 columns made of high-strength concrete with compressive strength ranging from 83.6-93.5 MPa and rectilinearly confined with lateral ties and longitudinal rebars. The proposed stress-strain curve consists of 3 parameters or coordinates such as: (1) peak stress/strain ( $f_0, \epsilon_0$ ); (2) the inflection point on the descending branch ( $f_i, \epsilon_i$ ); and (3) the stress-strain ( $f_{2i}, \epsilon_{2i}$ ) at an arbitrarily selected point on the descending branch. The proposed model consists of two polynomial equations which define the ascending branch and post-peak branch (Fig. 4-8).

$$\begin{array}{l} \text{Ascending branch} \\ \epsilon_c \leq \epsilon_0 \end{array} \quad Y = \frac{AX + BX^2}{1 + (A - 2)X + (B + 1)X^2} \quad (4-13)$$

$$\begin{array}{l} \text{Post-peak branch} \\ \epsilon_c \geq \epsilon_0 \end{array} \quad Y = \frac{CX + DX^2}{1 + (C - 2)X + (D + 1)X^2} \quad (4-14)$$



where

$$Y = \frac{f_c}{f_0}, f_c = \text{concrete stress} \quad (4-15)$$

$$X = \frac{\varepsilon_c}{\varepsilon_0}, \varepsilon_c = \text{concrete strain} \quad (4-16)$$

$$A = E_c \frac{\varepsilon_c}{\varepsilon_0} \quad (4-17)$$

$$E_c = 27.55 w^{1.5} \sqrt{f'_c}; w = \text{unit weight of concrete}$$

$$B = \frac{(A - 1)^2}{0.55} - 1 \quad (4-18)$$

$$C = \frac{(\varepsilon_{2i} - \varepsilon_i)}{\varepsilon_0} \left[ \frac{\varepsilon_{2i} E_i}{f_0 - f_i} - \frac{4\varepsilon_i E_{2i}}{f_0 - f_{2i}} \right] \quad (4-19)$$

$$D = (\varepsilon_{2i} - \varepsilon_i) \left[ \frac{E_i}{f_0 - f_i} - \frac{4E_{2i}}{f_0 - f_{2i}} \right] \quad (4-20)$$

$$E_i = \frac{f_i}{\varepsilon_i} \text{ and } E_{2i} = \frac{f_{2i}}{\varepsilon_{2i}} \quad (4-21)$$

The proposed definition of peak stress  $f_0$  and peak strain  $\varepsilon_0$  in Yong et al. is given as,

$$f_0 = K f'_c \quad (4-22)$$

$$\varepsilon_0 = 0.00265 + \frac{0.0035 \left(1 - \frac{0.734s}{h''}\right) (\rho'' f''_y)^{2/3}}{\sqrt{f'_c}} \quad (4-23)$$

where  $K$  = effective confinement factor

$$K = 1 + 0.0091 \left(1 - \frac{0.245s}{h''}\right) \left(\rho'' + \frac{nd''}{8sd}\rho\right) \frac{f''_y}{\sqrt{f'_c}} \quad (4-24)$$

$f'_c$  = concrete cylinder strength

$s$  = the center-to-center spacing of the lateral ties in inches

$h''$  = length of one side of the rectangular ties in inches

$\rho''$  = volumetric ratio of lateral reinforcement

$f''_y$  = yielding stress of the lateral ties in psi

$n$  = number of longitudinal steel bars

$d$  = nominal diameter of longitudinal steel bars in inches

$\rho$  = volumetric ratio of longitudinal reinforcement

The proposed parameters  $f_i, \varepsilon_i$  and  $f_{2i}, \varepsilon_{2i}$  on the stress-strain curve were obtained using linear regression in Yong et al. is are given by

$$f_i = f_0 \left[ 0.25 \left( \frac{f'_c}{f_0} \right) + 0.4 \right] \quad (4-25)$$

$$\varepsilon_i = K \left[ 1.4 \left( \frac{\varepsilon_0}{K} \right) + 0.0003 \right] \quad (4-26)$$

$$f_{2i} = f_0 \left[ 0.025 \left( \frac{f_0}{1000} \right) - 0.065 \right] \geq 0.3 f_0 \quad (4-27)$$

$$\varepsilon_{2i} = 2\varepsilon_i - \varepsilon_0 \quad (4-28)$$

### 4.2.1.3 Bjerkeli et al. (1990) Model

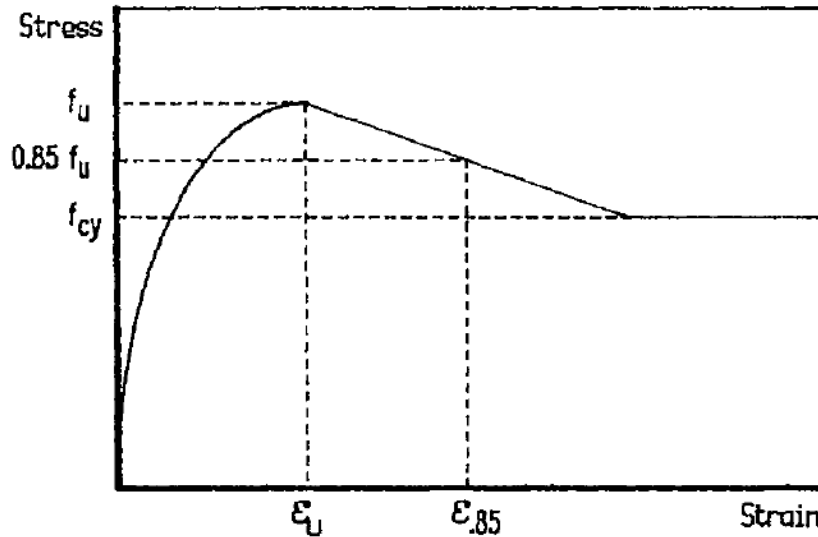


Figure 4-9: Bjerkeli et al. (1990) model for confined high-strength concrete

Bjerkeli et al. (1990) developed a theoretical model to describe the stress-strain behaviour of confined normal density concrete and light weight aggregate concrete. Based on a test program with small-scale and large-scale confined square columns, concrete compressive strength, confining reinforcement ratio, and section geometry were identified as the major three parameters that control the stress-strain behaviour of confined concrete.

Bjerkeli et al. proposed a convenient way of expressing the confining reinforcement ratio by using the idealized “confining pressure”  $f_r$  (Fig. 4-10) which is given by

$$f_r = \frac{A_{sh} f_{sy}}{h' s_p} \quad (4-29)$$

where  $A_{sh}$  = total effective area of hoops ties and supplementary confining reinforcement in direction under consideration with spacing  $s_p$

$f_{sy}$  = yield stress of confining reinforcement

$h'$  = outer size of confined section

$s_p$  = center distance between hoop ties/confining reinforcement

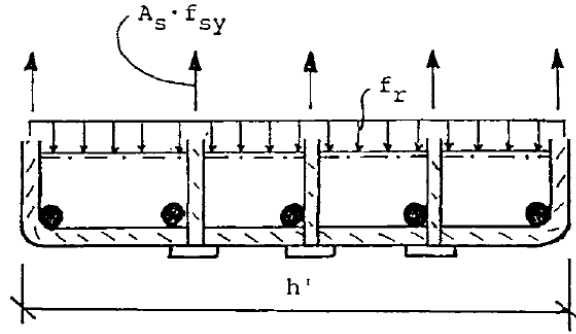


Figure 4-10: Idealized “confining pressures”  $f_r$  (Bjerkeli et al. 1990)

Bjerkeli et al. proposed a “section geometry factor”  $K_g$  to include the influence of the section geometry.  $K_g$  expresses the effective concrete core cross-section after compression arches begin to develop (Fig. 4-11). Both the concrete section geometry and distribution of the longitudinal reinforcement are considered in this factor.  $K_g$  is defined by the larger value of  $K_{g1}$  and  $K_{g2}$  which represents the compression arches between the transverse confinement reinforcement and laterally supported longitudinal reinforcement respectively.

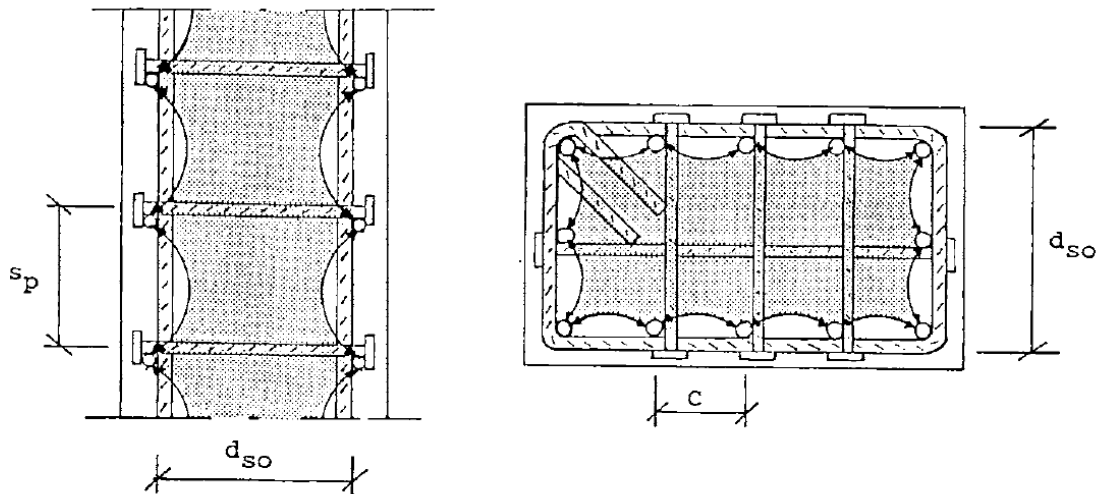


Figure 4-11: Vertical and horizontal section with compressive arches between reinforcement (Bjerkeli et al. 1990)

$K_{g1}$  which corresponds to the development of compression arches in vertical direction between the confinement reinforcement layers can be expressed as (Shah et al., 1983),

$$K_{g1} = 1 - \frac{S_p}{d_{so}} \quad (4-30)$$

where  $d_{so}$  = the shorter outer diameter of hoop ties

$K_{g2}$  which corresponds to the development of compression arches between laterally supported longitudinal reinforcement can be expressed as (Sheikh and Yeh, 1986)

$$K_{g2} = 1 - \frac{n C^2}{5.5 A_c'} \quad (4-31)$$

where  $n$  = number of laterally supported longitudinal bars

$C$  = distance between laterally supported longitudinal bars

$A_c'$  = gross area of concrete section measured to center lone of peripheral hoop

The Bjerkeli et al. stress-strain model is formed by three branches such as ascending branch, descending branch, and a horizontal part (Fig. 4-9)

$$\begin{array}{l} \text{Ascending branch} \\ \varepsilon \leq \varepsilon_u \end{array} \quad \sigma = \frac{E_c}{1 + \left(\frac{E_c}{E_0} - 2\right) \left(\frac{\varepsilon}{\varepsilon_u}\right) + \left(\frac{\varepsilon}{\varepsilon_u}\right)^2} \quad (4-32)$$

$$\begin{array}{l} \text{Post-peak branch} \\ \varepsilon > \varepsilon_u \end{array} \quad \sigma = f_u - Z(\varepsilon - \varepsilon_u) \quad (4-33)$$

$$\text{Horizontal part} \quad \sigma = f_{cy} = 4.87 \frac{d_{so} A_{sh} f_{sy}}{s_p A_c} \quad (4-34)$$

where

$$E_c = 9500 \left(\frac{\rho_c}{2400}\right)^{1.5} (f'_c)^{0.3}; \rho_c = \text{unit weight of concrete in kg/m}^3 \quad (4-35)$$

$$E_0 = \frac{f_u}{\varepsilon_u} \quad (4-36)$$

$$Z = \frac{0.15 f_u}{\varepsilon_{.85} - \varepsilon_u} \quad (4-37)$$

The Bjerkeli et al. model is based on modified expression originally proposed by Martinez et al. (1984), obtained using the standard cube compressive strength. For normal density concrete, the maximum confinement compressive strength  $f_u$  and the corresponding strain  $\varepsilon_u$  can be defined as

$$\begin{aligned} 45\text{MPa} < f'_c \leq 80\text{MPa} & \quad f_u = f'_c + 4 K_g f_r \\ 80\text{MPa} < f'_c < 90\text{MPa} & \quad f_u = f'_c + 3 K_g f_r \end{aligned} \quad (4-38)$$

$$\varepsilon_u = 0.0025 + 0.05 \left( \frac{f_r}{f'_c} \right) \quad (4-39)$$

and

$$\varepsilon_{.85} = \varepsilon'_{.85} + K_g 0.05 \frac{\left( \frac{f_r}{f'_c} \right)}{1 - F} \quad (4-40)$$

$$\varepsilon'_{.85} = 0.0025 \left[ \left( \frac{17.07}{f'_c} \right)^2 + 1 \right] \quad (4-41)$$

$$F = \frac{1}{1 + \left( \frac{1}{f_r K_g} \right)^{1/4}} \quad (4-42)$$

### **4.3 Experimental Program**

A test program was designed to investigate the stress-strain relationship of high-strength ECC members with square ties as transverse reinforcement. A total of sixteen 100 mm x 100 mm x 300 mm ECC columns were tested. The specimens were divided into four sets (each set consisted of 4 columns) that had different transverse reinforcement content: 0%, 1.0%, 1.5% and 2.0%. One additional set of four 100 mm x 100 mm x 300 mm plain concrete square columns, which had the same unconfined peak strength as the ECC columns, was tested as baseline for performance. All specimens were subjected to short-term monotonic axial load until failure.

#### **4.3.1 Geometry**

The columns for this research study were design to have a height to width ratio of 3:1 in order to reduce the boundary effects and minimize the slenderness effect of the specimens as suggested by Lai et al. (2014). Thus, the columns were fabricated to a size of 300 mm in height with a cross-section of 100 mm x 100 mm. Experiments from Yong et. al. (1988) showed that the effect of concrete cover did not affect the confinement stress and strain since the specimens had already experienced major spalling at the early stages of the tests. Therefore, the columns were designed to have no clear cover. To provide clearance for the transverse reinforcement in the 100 x 100 mm molds, the square ties for confinement were designed to be 95 x 95 mm with 135° anchorage at the corners. Four small-diameter (6.35 mm) longitudinal steel bars were placed in the corners of all the specimens to assist positioning and tying the square ties (they were placed also on the specimens with 0% transverse steel ratio). The three sets of columns with 1%, 1.5%, and 2% transverse steel content had a spacing between square ties of 60 mm, 40 mm, and 30 mm, respectively. The cross section and the configuration of ECC columns is shown in Figs. 4-12 and 4-13.

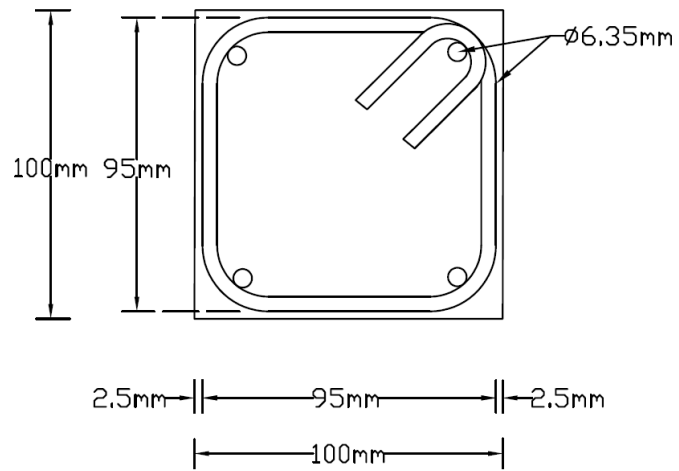


Figure 4-12: Cross-sectional details of specimens

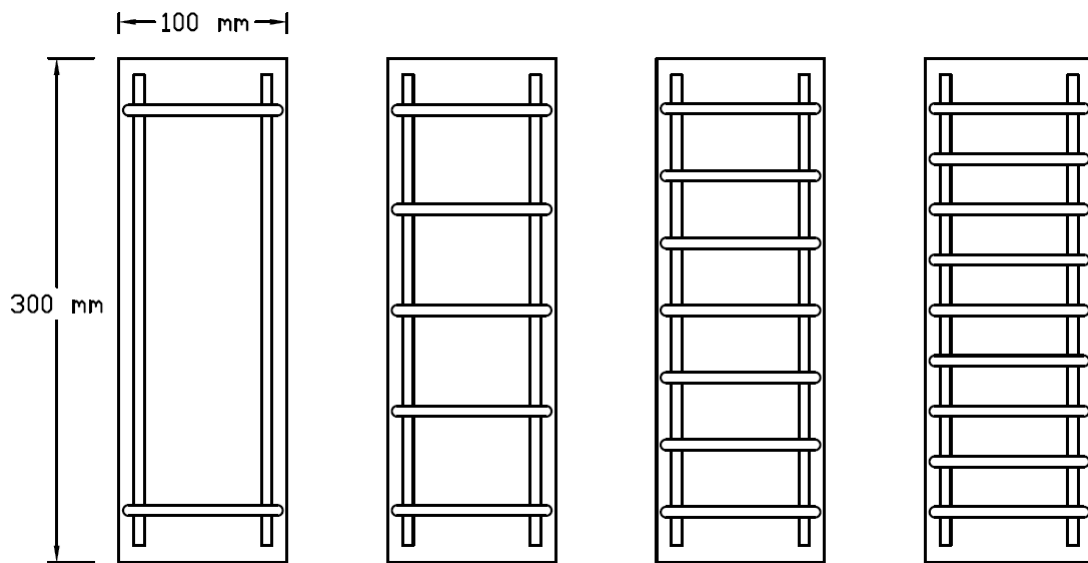


Figure 4-13: cross-sectional details of specimens with 0%, 1%, 1.5%, and 2% transverse steel content



Table 4-1: Specimen geometry and material properties

Specimen	Dimension (length x width x height) (mm)	Lateral steel area ratio	Spacing (mm)	Longitudinal steel rebar	Compressive cylinder strength (MPa)	Yield strength of steel bars (MPa)
Concrete-0%	100x100x300	0%	-	4Ø6.35	72.6	416
ECC-0%	100x100x300	0%	-	4Ø6.35	74.1	
ECC-1%	100x100x300	1.0%	60	4Ø6.35		
ECC1.5%	100x100x300	1.5%	40	4Ø6.35		
ECC-2%	100x100x300	2.0%	30	4Ø6.35		

## 4.3.2 Material

### 4.3.2.1 Reinforcement

The transverse and longitudinal ¼” (6.35mm) steel consisted of deformed bars with an average yielding stress of 416 MPa, ultimate stress of 602 MPa, and Young’s modulus of 190,000 MPa. The transverse steel was tied to the longitudinal rebars using regular wire ties (Fig. 4-14). The prepared steel cages were placed in molds for ECC pouring (Figs. 4-15 – 4-18).



Figure 4-14: Steel cage preparation



Figure 4-15: Steel cages of ECC-0%

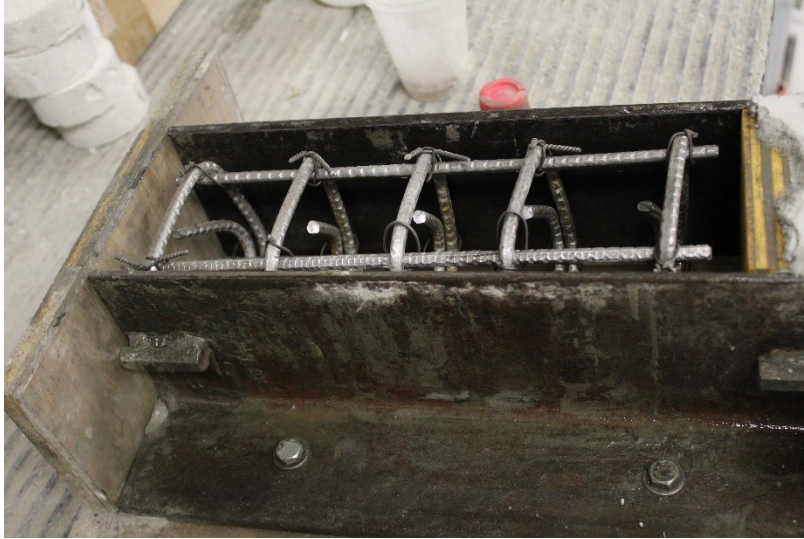


Figure 4-16: Steel cage of ECC-1%



Figure 4-17: Steel cage of ECC-1.5%



Figure 4-18: Steel cage of ECC-2%

#### **4.3.2.1 ECC**

The high-strength mix of ECC09 developed in Chapter 3 was prepared according to the following list of components ( $\text{kg}/\text{m}^3$ ): (1) type GU portland cement (3337 kg), (2) ASTM Class F fly ash (4004 kg), (3) Silica sand (2670 kg), (4) Superplasticizer Glenium 7700 (40 kg), (5) water (2002 kg), and (6) PVA fibres (2% of the volume). The mix was prepared on a 10 L capacity ELRICH intensive mixer model RV02E in the concrete laboratory at the University of Alberta.

The columns were poured horizontally and vibrated on a vibration table as shown in Fig. 4-19. The specimens were kept in a curing room at approximately  $25^\circ\text{C}$  and 95-100% relative humidity until one day before testing. The resulting ECC had a compressive strength of 75 MPa at a 0.00624 strain, an elastic modulus of 16399 MPa, and a Poisson ration of 0.153.





Figure 4-19: Specimen fabrication

#### 4.3.4 Instrumentation and Testing Procedure

To measure the stress-strain compressive response of the specimens, two linear variable differential transducers (LVDT's) with swivel eyelets that permitted rotation were placed opposite each other at the middle section of the specimen. The LVDT's were mounted onto an aluminum frame which was screwed to the specimen. The gauge length of the LVDT's was set to 200 mm. The total deformation of the specimen was calculated by averaging the reading of the two LVDT's. Eight 1/4" thumbscrews with four at each end were screwed into the specimen surface to secure the aluminum frame. Four aluminum bars were used to ensure that the top and bottom plates were parallel with respect to each other. After fixing the aluminum frame on to the specimen, the aluminum bars were released to allow free deformation during the tests. An overall view of the instrumentation of the specimen is shown in Figs. 4-20 and 21.

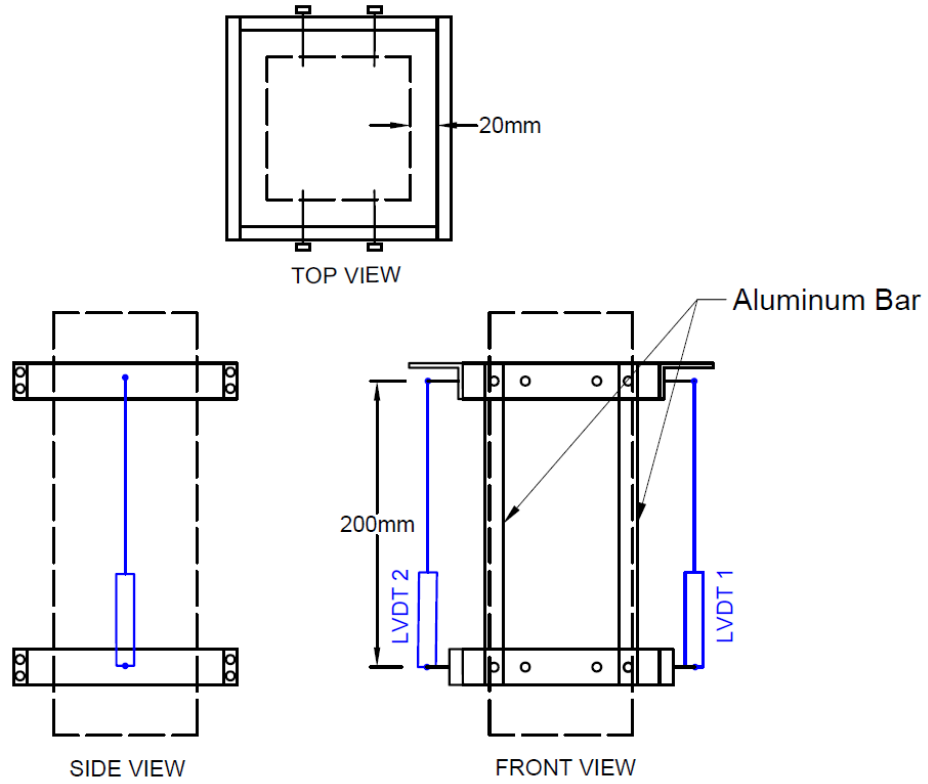


Figure 4-20: Overall 2-D view of instrumentation of specimen

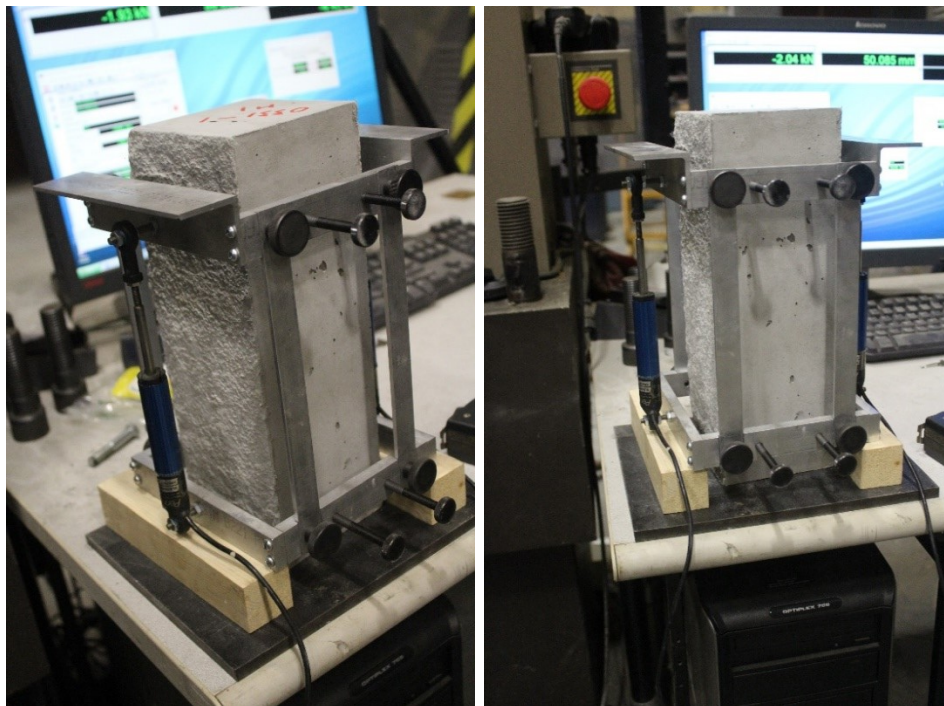


Figure 4-21: Overall 3-D view of instrumentation of specimen

The specimens were loaded under a concentric monotonically increasing axial compressive load in a MTS 815 machine (Fig. 4-22). The tests were conducted in a displacement control system with a loading rate of 0.3 mm/s. The specimens were pre-loaded to reach around 1-2 kN to prevent slipping between the specimen and the load cell. A QuantumX data acquisition system was used to collect the LVDT readings along with axial load values. The tests were terminated when either the load dropped to 40% of the maximum load or when the LVDT's started giving unreasonable readings due to excessive deformation. All specimens were tested at 28 days of age.

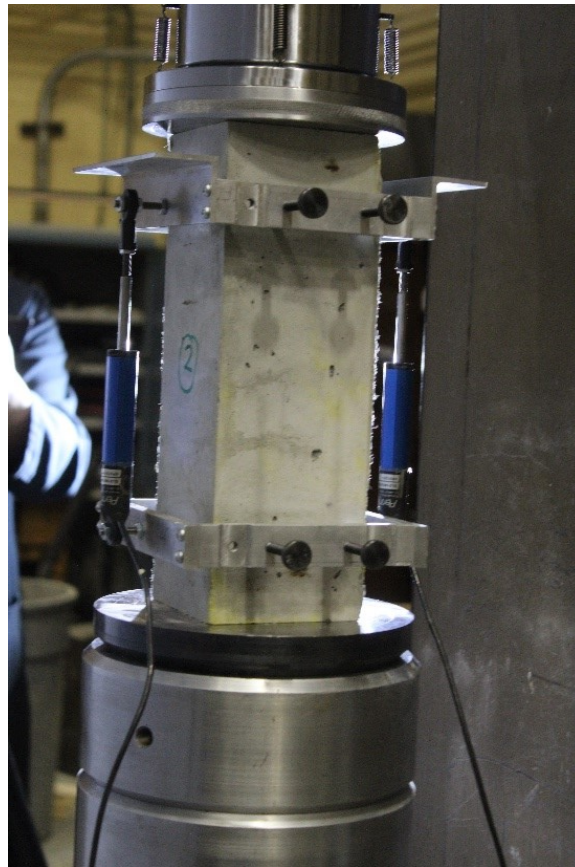


Figure 4-22: General view of specimen testing in MTS 815 machine

### 4.3.5 Result and Discussion

A total of sixteen 100 mm x 100 mm x 300 mm ECC columns were tested under uniaxial compressive load. The compressive load records were obtained from the MTS 815 machine and the compressive strains were calculated from averaging the reading from the two LVDTs. The overall averaged load-displacement results for the ECC and concrete columns are presented in Figs. 4-23 – 4-24 and 4-30 – 4-32. Dividing the force from the actuator by the cross section area, and dividing the displacement from the LVDT by the gauge length, averaged stress-strain relationships were prepared as shown in Figs. 4-25 – 4-31 and 4-33 – 4-35. The averaging process and the variation between each specimen in all four set of ECC columns are shown in Appendix C. A comparison of the stress-strain responses of all tested specimen is shown in Fig. 4-37. The axial compressive test results are summarized in table 4-2.

#### 4.3.5.1 Unconfined Columns

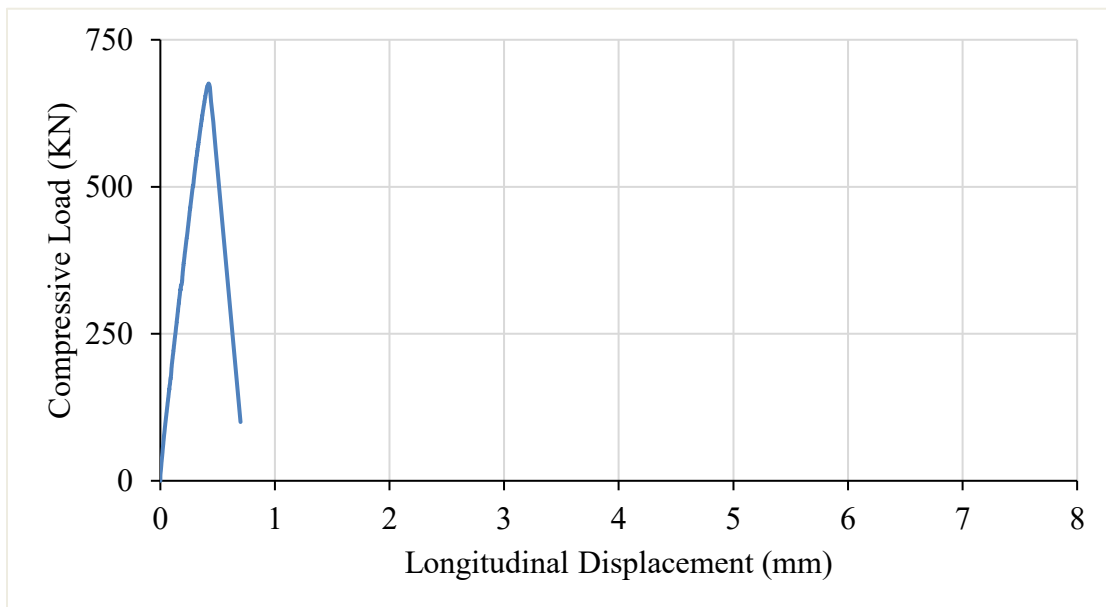


Figure 4-23: Averaged load-displacement response for 0% confinement concrete square column



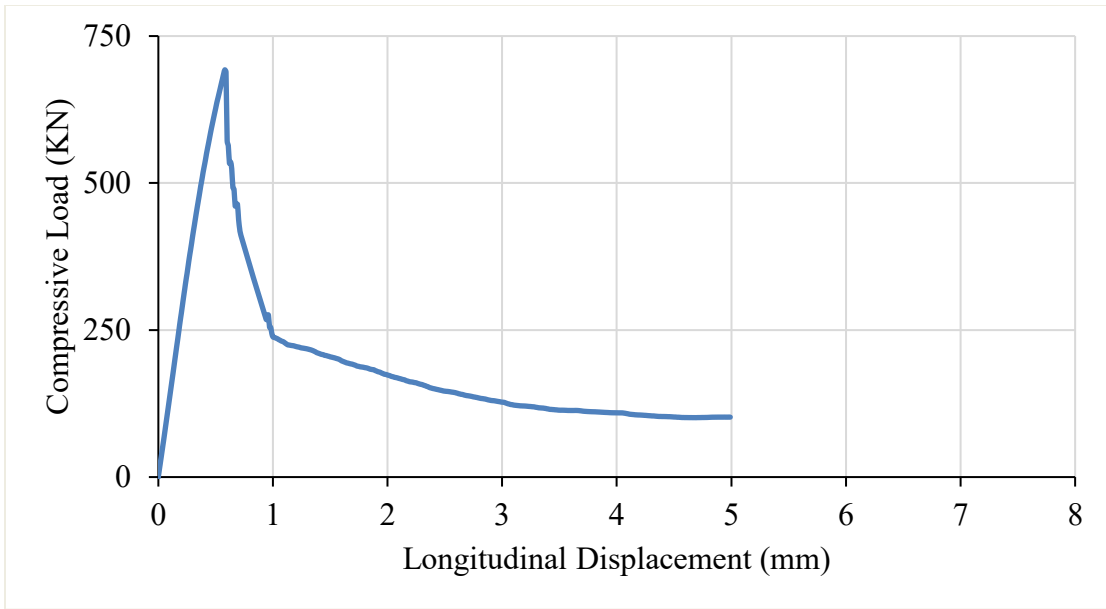


Figure 4-24: Averaged load-displacement response for 0% confinement ECC square column

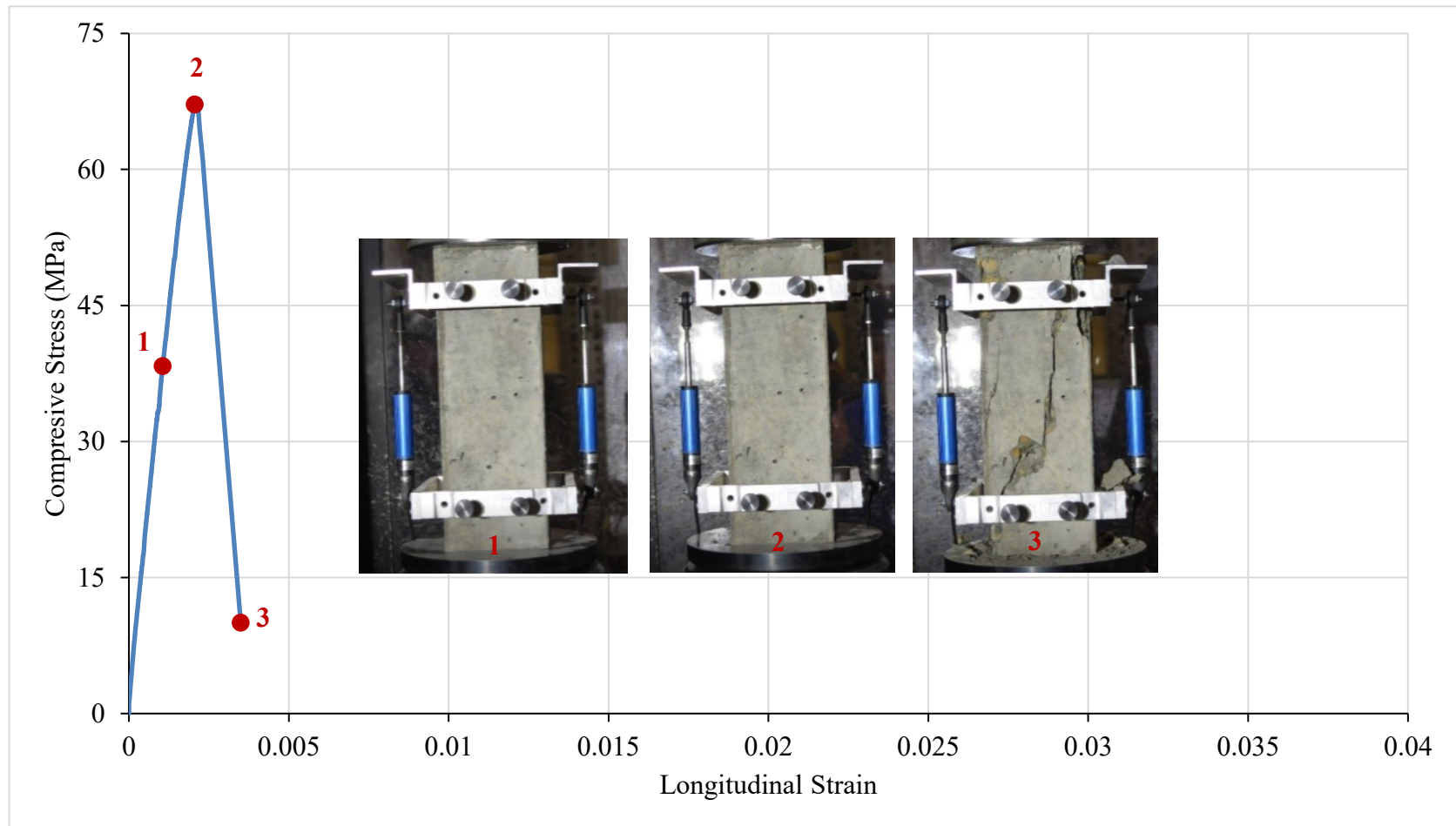


Figure 4-25: Averaged stress-strain response for 0% confinement concrete square column (Concrete-0%)

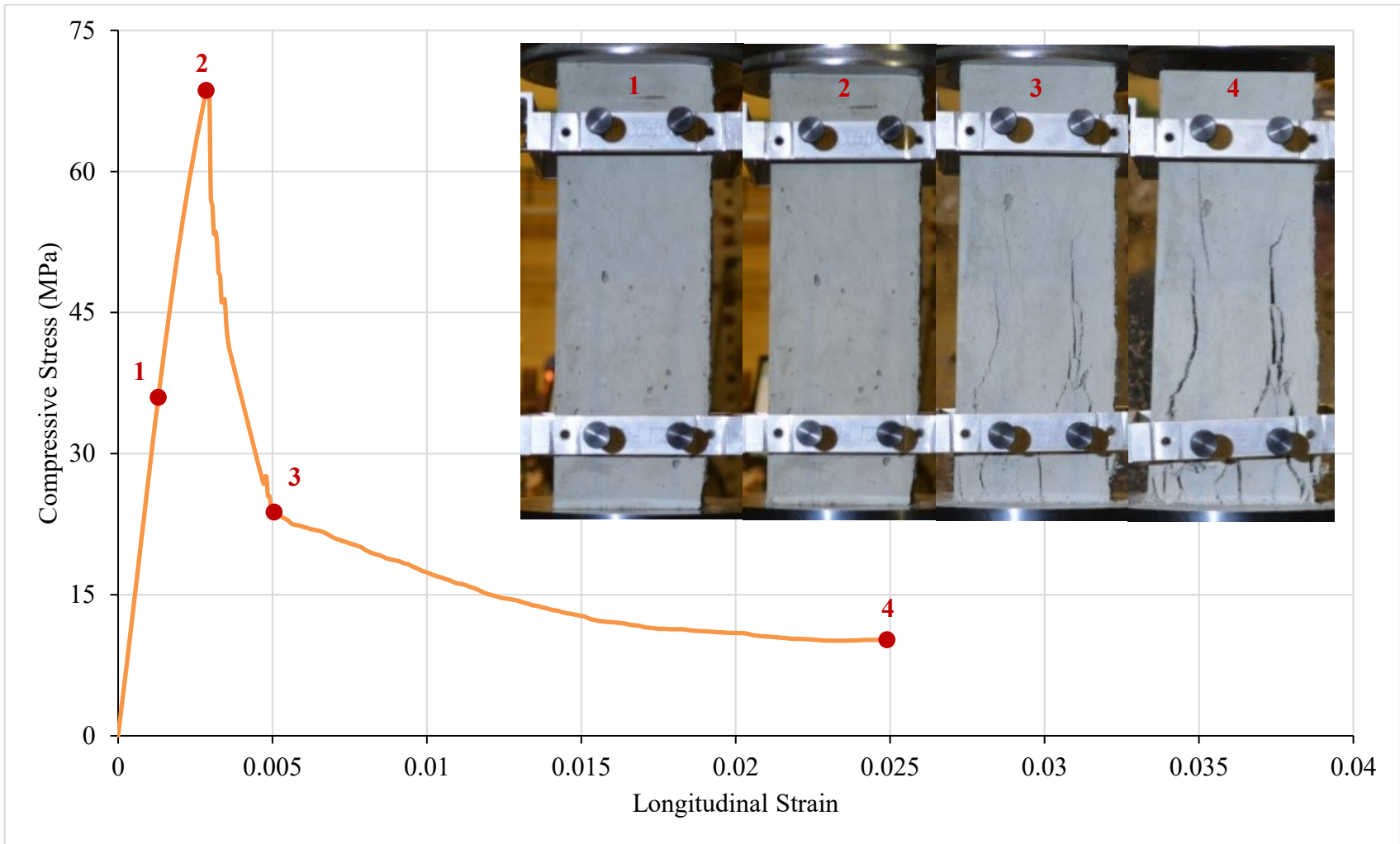


Figure 4-26: Averaged stress-strain response for 0% confinement ECC square column (ECC-0%)

The general behaviour of the unconfined concrete and ECC columns was similar to their compressive cylinder tests in terms of mode of failure. The results showed that unconfined concrete and ECC columns had a similar peak strength and strain. Concrete-0% columns reached a peak compressive stress of 67.56 MPa at a strain of 0.002112 while ECC-0% columns reached a peak compressive stress of 69.26 MPa at a strain of 0.002902. After the peak strength, the Concrete-0% columns had a sudden explosive type of failure at the maximum axial load with a diagonal failure surface (Fig. 4-27). In comparison, ECC-0% columns formed a few longitudinal microcracks at the maximum axial load, which gradually widened. At the plateau-like stage of the stress-strain curve, ECC-0% reached a residual stress of 11 MPa (Fig. 4-26). Overall, the results showed that the strength degradation of unconfined ECC columns was more gradual than in unconfined concrete columns which exhibited explosive failures.

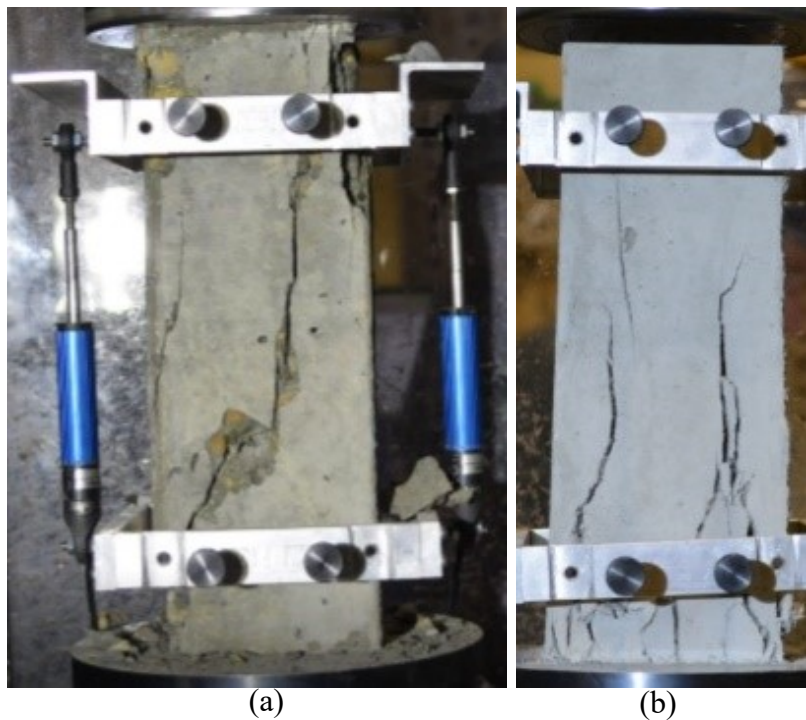


Figure 4-27: Ultimate cracking of (a) concrete-0% and (b) ECC-0%

#### 4.3.5.1.1 Shape Effect

The peak compressive strengths  $f_{c0}$  for unconfined concrete and ECC columns were found to be lesser than their corresponding compressive cylinder strengths  $f'_c$ , with a similar ratio of  $f_{c0}/f'_c = 0.93$  in both cases (Figs. 4-28 – 4-29). The strain at peak stress  $\epsilon_c$  and the Elastic Modulus  $E_c$  for the unconfined concrete and ECC columns were different than the value obtained from the control cylinders as well. The differences in strength, strain, and Elastic Modulus between the unconfined columns and control cylinders can be ascribed to both shape and boundary effects. These effects were observed in suggested by Yong et al. (1988) and Martinez et al. (1984) which tested concrete columns of different sizes, of rectangular and circular shapes, cast with the same material.

The shape effect is due to the stress concentrations present in straight edges. This is a reasonable phenomenon such as the distinct compressive strength obtained between concrete cube and cylinder (Kotsovos, 1983). The boundary effect is due to the influence of the boundary restraints that the loading plates impose onto the specimen. As discussed by Kotsovos (1983), the frictional restraint prevents the lateral expansion of the specimen at the coupon-plate interfaces. The additional restraint effectively “confines” the specimen at boundaries, and thereby providing additional strength. The boundary effect is more pronounced on shorter specimens such as in conventional cylinder testing. In specimens with higher height-to-width aspect ratios, the confining effect of the plates is smaller and leads to a lower strength. This is a more realistic behaviour that correlates better with columns found in frames in regular buildings.

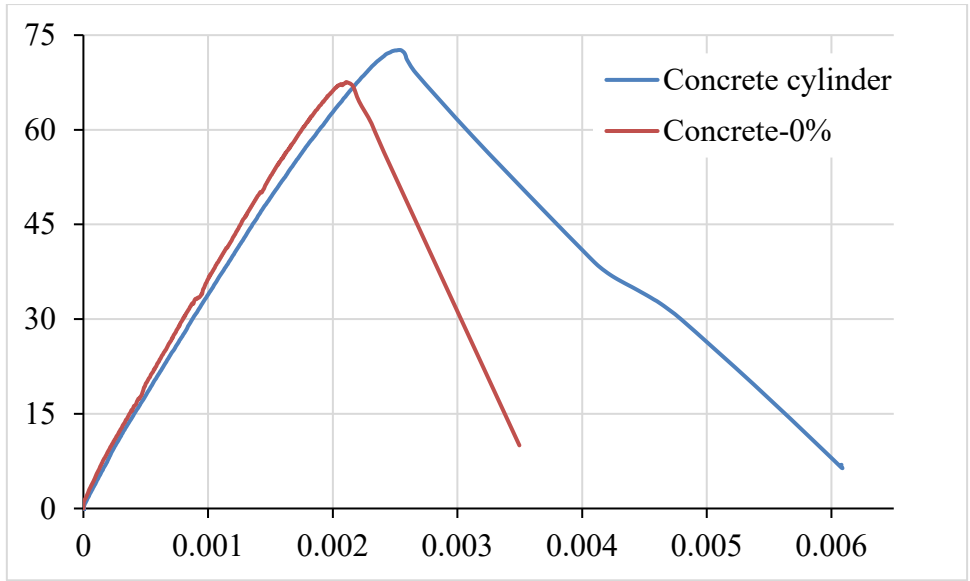


Figure 4-28: Stress-strain graph of concrete cylinder and concrete square columns

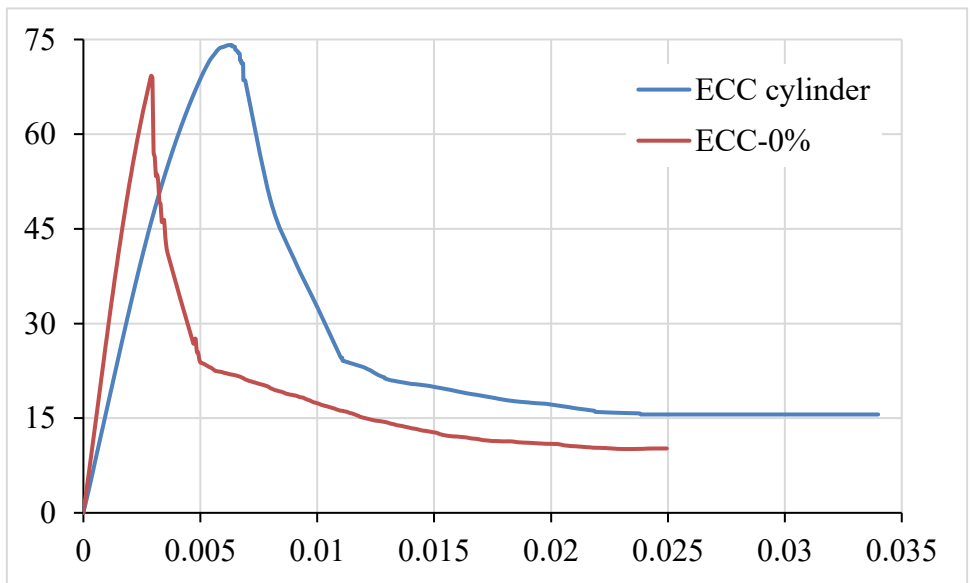


Figure 4-29: Stress-strain graph of ECC cylinder and ECC square columns

#### **4.3.5.2 Confined Columns**

The general behaviour of the confined ECC columns showed four main stages: (1) an initial, ascending, quasi-linear stage; (2) the attainment of peak compressive strength; (3) a gradual post-peak descending branch; and (4) a plateau-like region of residual stress.

The difference in peak compressive strengths in columns ECC-1%, ECC-1.5%, and ECC-2% was minimal and not statistically significant: 70.17 MPa, 70.41 MPa, and 71.38 MPa for ECC columns with 1%, 1.5% and 2% confinement, respectively.

A few microcracks formed on the specimens at the maximum axial load (Fig. 4-36). After microcracking occurred, the cracks developed into larger cracks as the specimen entered the post-peak stage. At the plateau-like stage of the stress-strain curve where cracks began widening, ECC-1%, ECC-1.5%, and ECC-2% reached a residual stress of 35MPa, 48MPa, and 50MPa respectively.

It is important to note that minor cracking and/or crushing at the boundaries was observed before reaching the maximum load (Fig. 4-36) in some of the specimens.

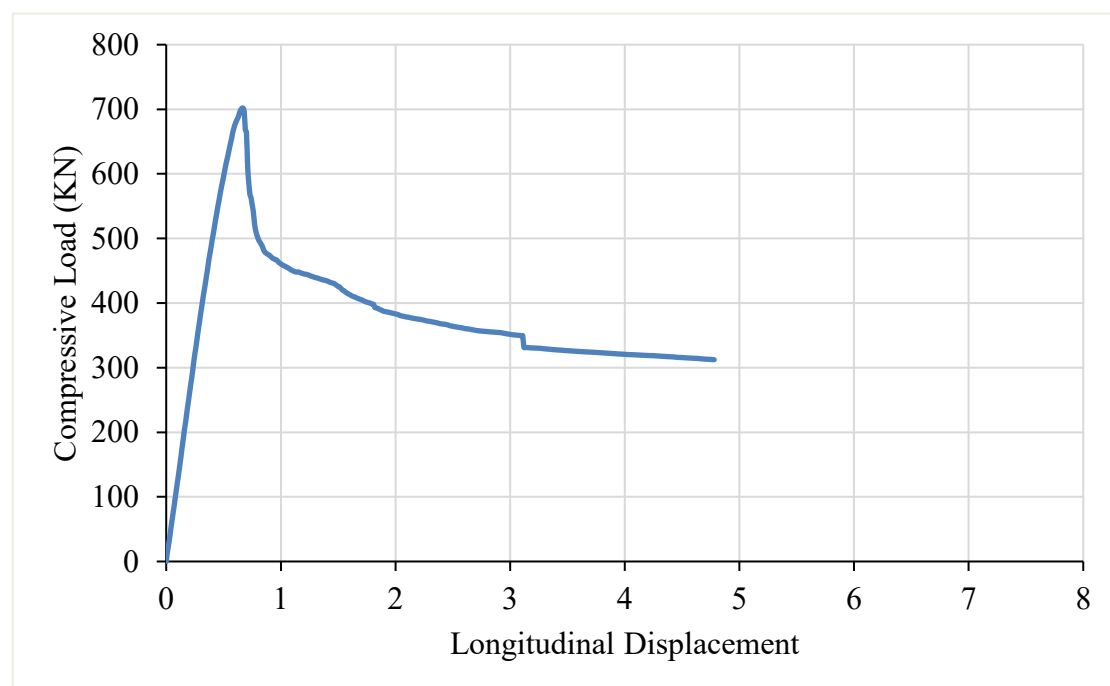


Figure 4-30: Averaged load-displacement response for 1% confinement ECC square column

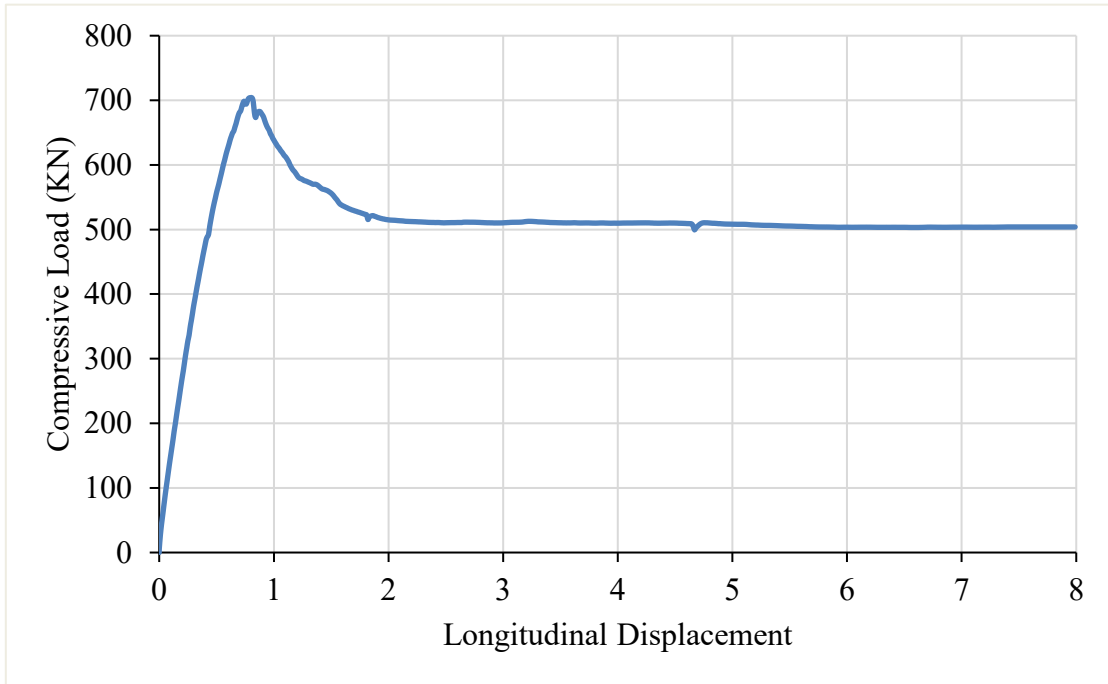


Figure 4-31: Averaged load-displacement response for 1.5% confinement ECC square column

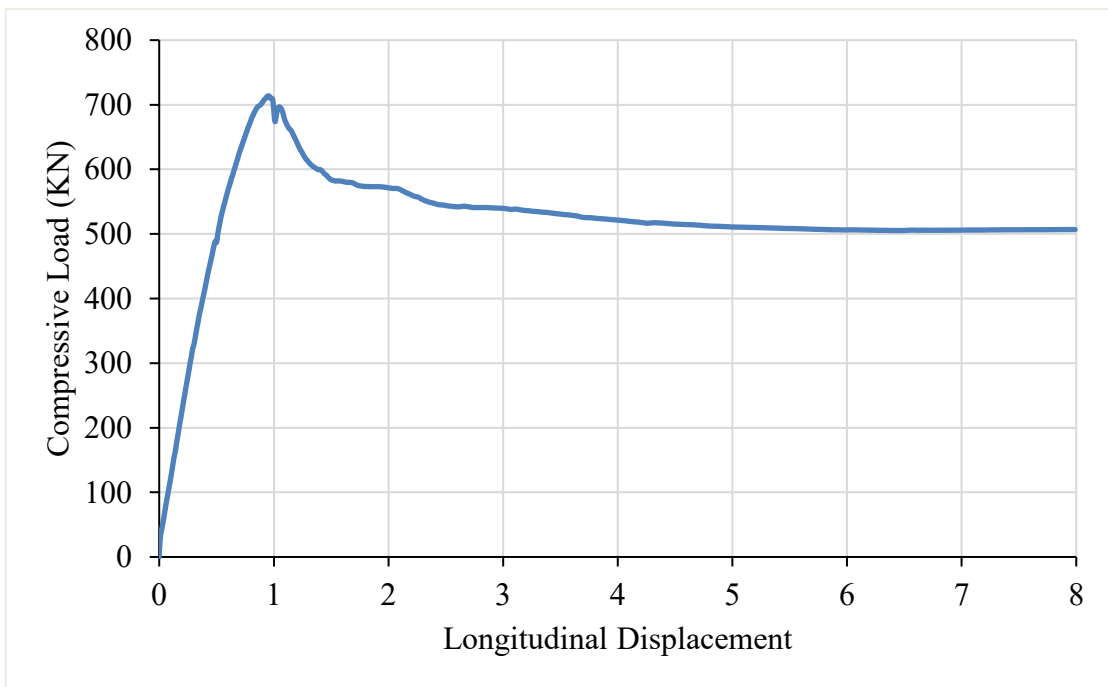


Figure 4-32: Averaged load-displacement response for 2% confinement ECC square column



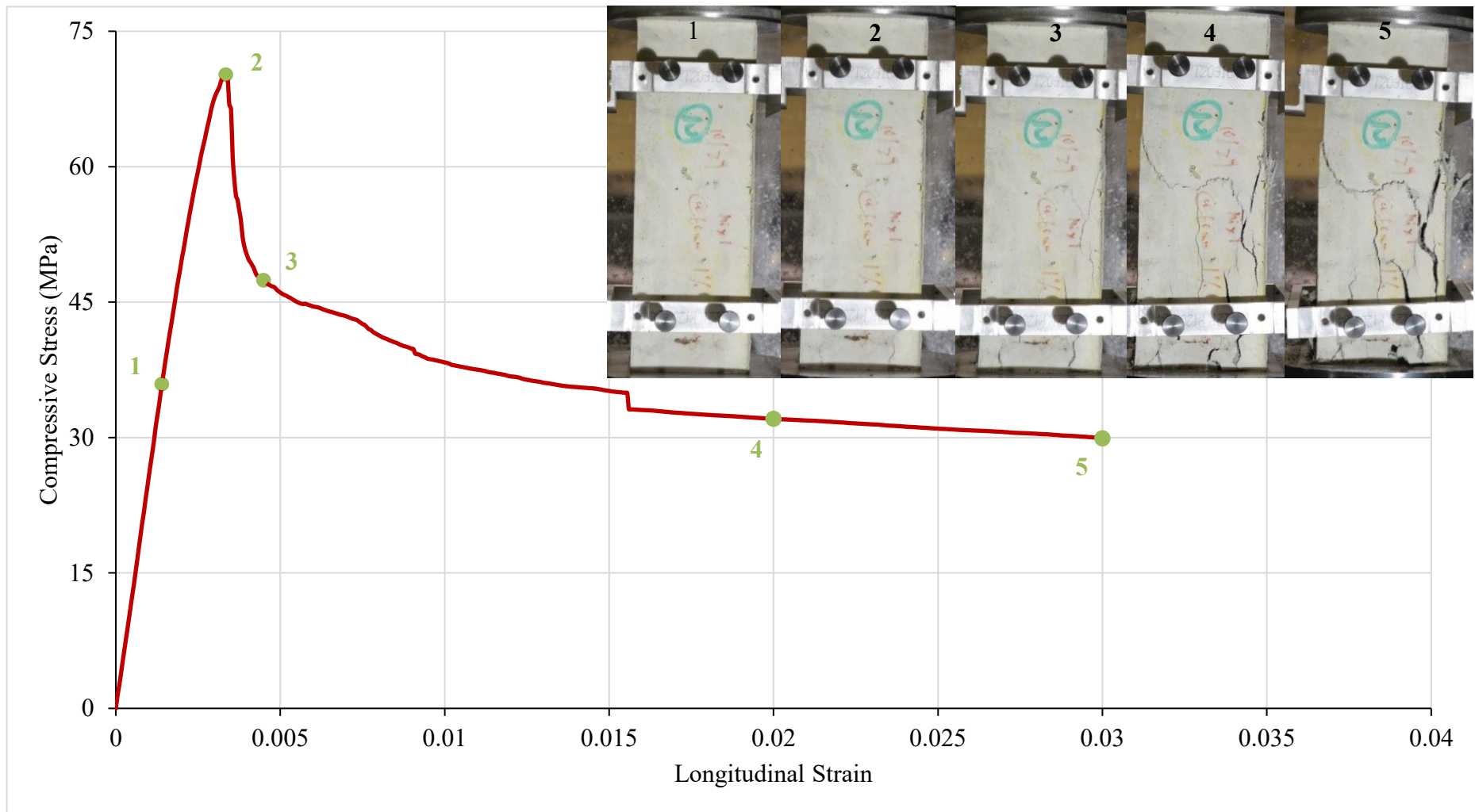


Figure 4-33: Averaged stress-strain response for 1% confinement ECC square column

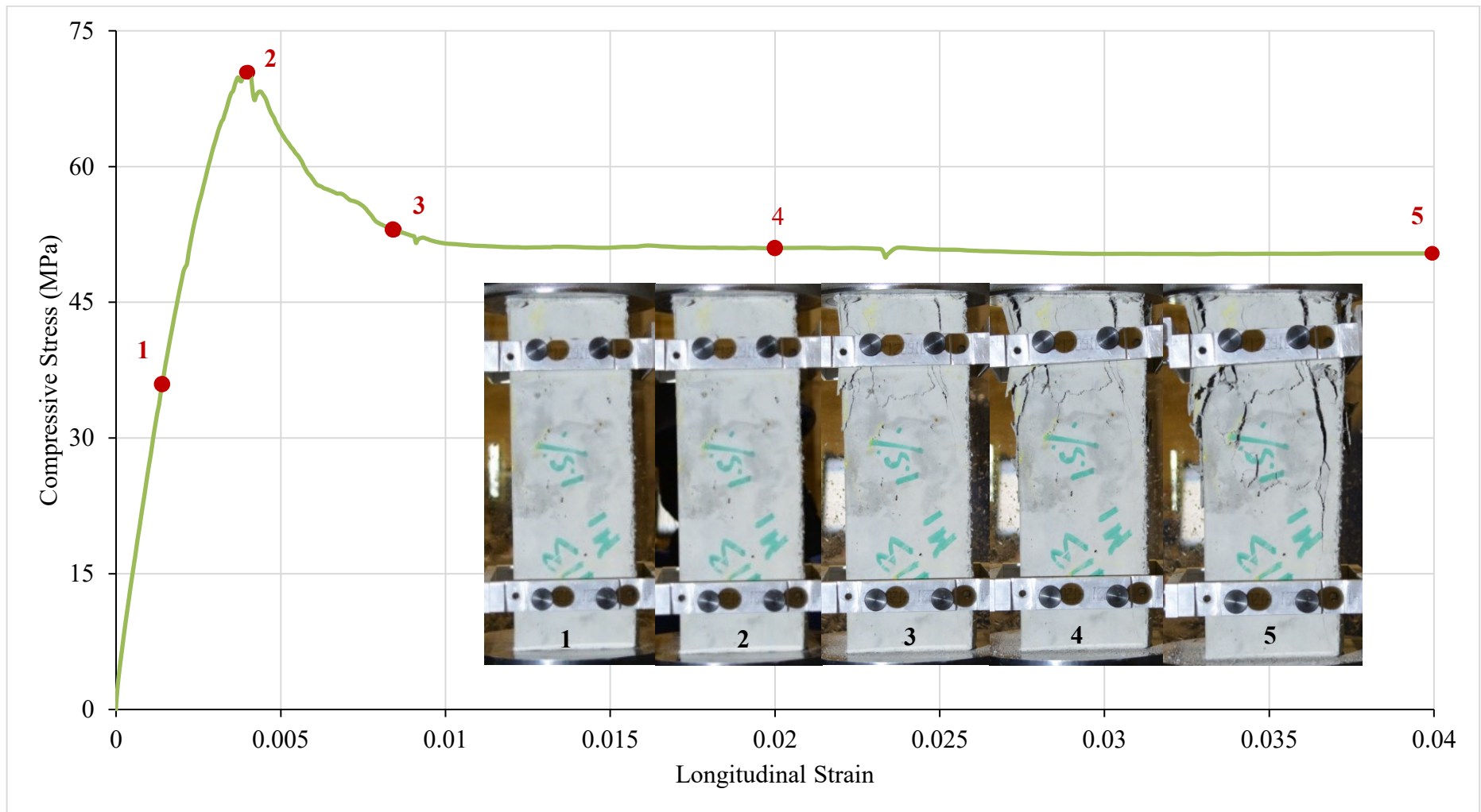


Figure 4-34: Averaged stress-strain response for 1.5% confinement ECC square column

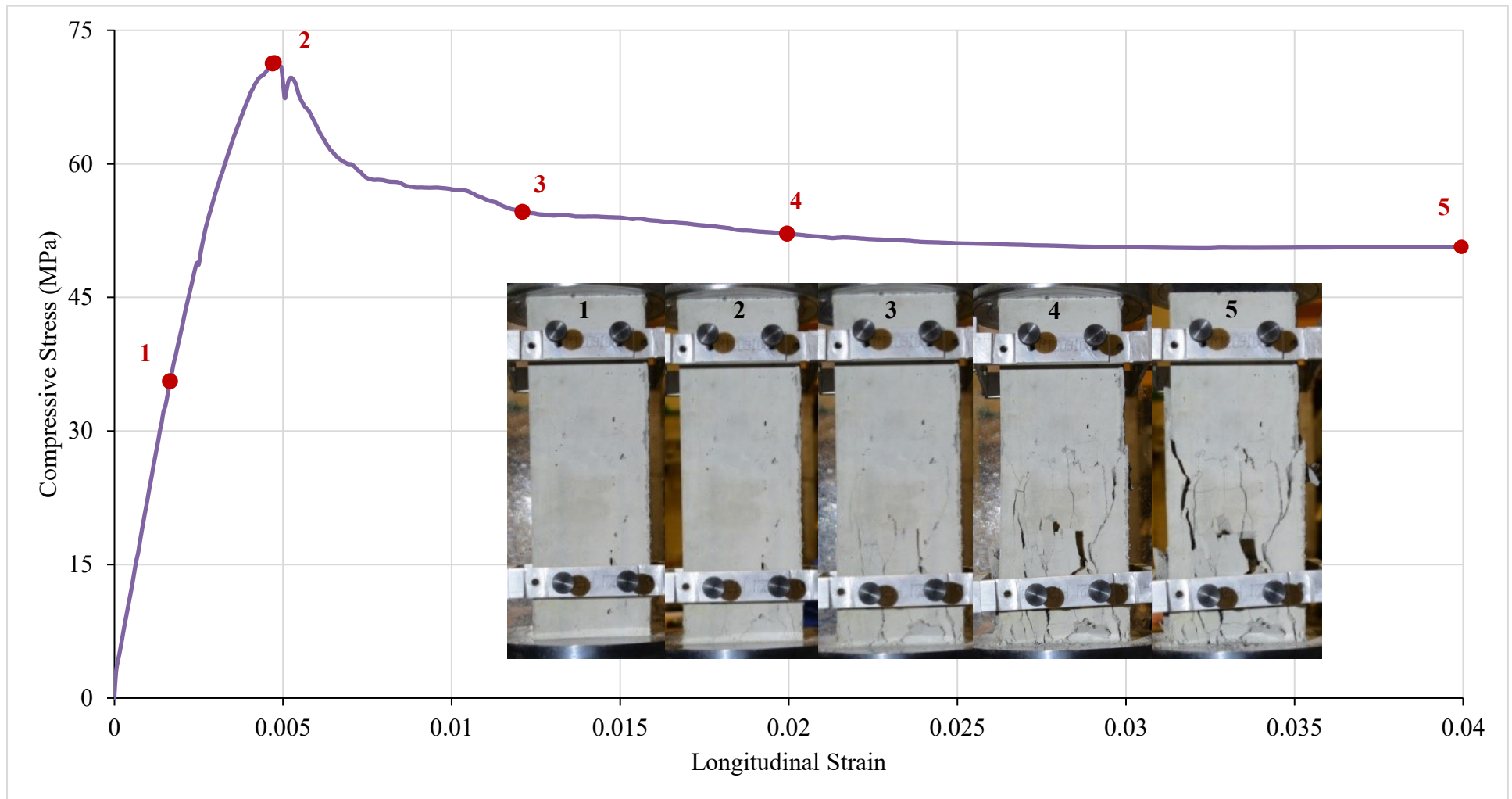


Figure 4-35: Averaged stress-strain response for 2% confinement ECC square column

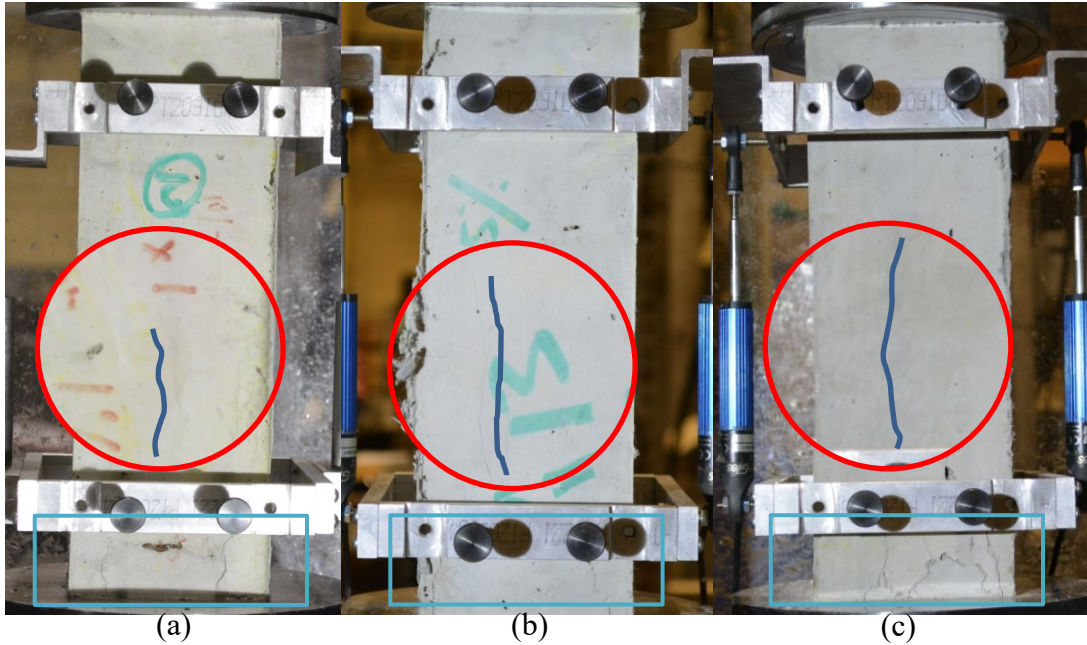


Figure 4-36: Microcracks and boundary conditions at peak load on (a) ECC-1%, (b) ECC-1.5%, and (c) ECC-1.5%

#### **4.3.5.3 Discussion**

The overall stress-strain responses of concrete-0%, ECC-0%, ECC-1%, ECC-1.5%, and ECC-2% are plotted for comparison in Fig. 4-37 and the tests results are summarized in Table 4-2. The confined ECC columns showed a small increase in confined strength compared to unconfined ECC columns which had a peak strength of 69.26 MPa. The comparison of the post-peak responses suggests that the transverse steel content has an effect on stress degradation and residual stress, but not in the pre-peak response nor in the peak strength. ECC-1% shows an increase in residual stress of 218% when compared to ECC-0%, while ECC-1.5% shows an increase in residual stress of 37% when compared to ECC-1%. However, ECC-2% only shows an increase in residual stress by 4% from ECC-2%. This suggests that there is a threshold of the effect from the transverse reinforcement which additional stirrups no longer increase the residual stress capacity.

The ratio of the four longitudinal steels to the cross-sectional area of the columns in this case were 1.26%. The contribution of the longitudinal steels to the overall compressive strength were 8 MPa in total. Since the contribution of the longitudinal steels were small, it was neglected in the stress-strain model study.

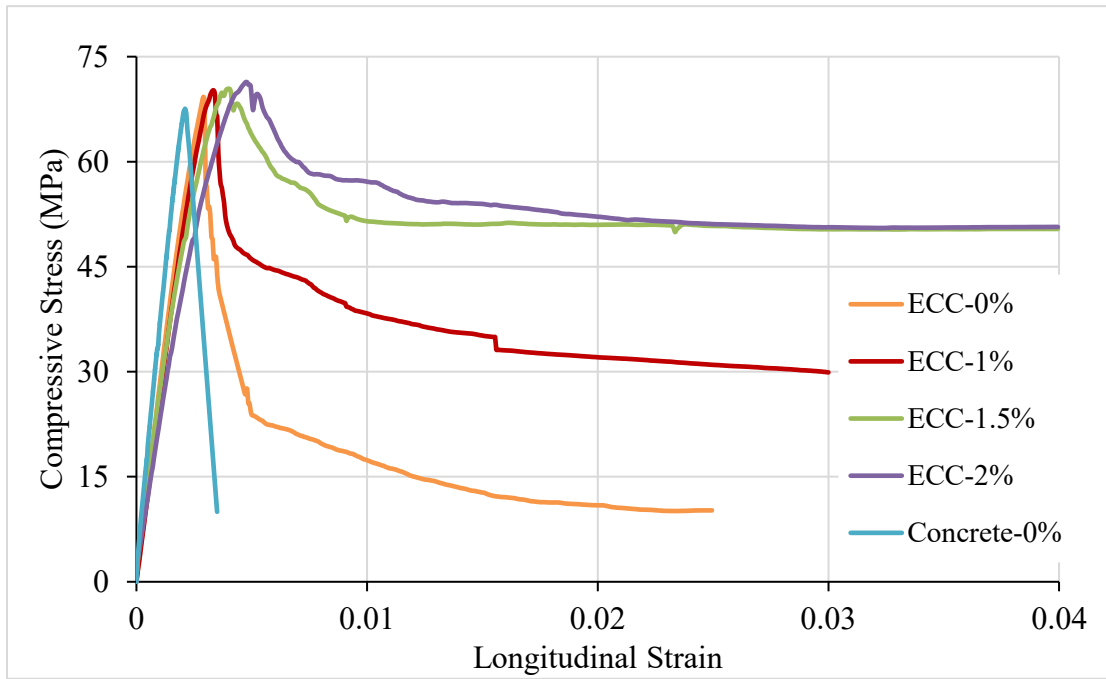


Figure 4-37: Averaged stress-strain response for all square column

Table 4-2: Summary of axial compressive test results

Specimen ID	Modulus of elasticity (E)	Peak compressive stress (MPa)	Strain at peak stress	Residual Stress
Concrete-0%	34476	67.56	0.002112	-
ECC-0%	28201	69.26	0.002902	11
ECC-1%	25374	70.17	0.003352	35
ECC-1.5%	25211	70.41	0.004002	48
ECC-2%	25675	71.38	0.004752	50

## 4.4 Empirical Model for Stress-strain Relationship

There are different existing confinement models for concrete. The model by Mander et al. (1988), developed for normal-strength concrete, is widely used. For high-strength concrete, the models by Yong et al. and Bjerkeli et al. which capture the post-peak degradation and residual strength of this material are available. Due to its simplicity, the Bjerkeli et al. model was selected as a candidate to develop a modified version that able to describe the confined behaviour in ECC columns.

### 4.4.1 Parameters of Stress-Strain Relationship

#### 4.4.1.1 Compressive Strength ( $f_{c.ecc}$ ) for Confined ECC

Bjerkeli et al. presented an equation for compressive strength  $f_u$  for confined normal-density concrete based on cube compressive strength with section geometry factor  $K_g$  and confining reinforcement ratio  $f_r$  (Eq. 38). For confined ECC, the compressive strength  $f_{c.ecc}$  is modified based on the experimental results obtained in this study. The compressive strength  $f'_u$  originally proposed by Bjerkeli et al. is shown below for convenience. Note that  $f'_c$  was originally obtained from cube compressive tests.

$$f_u = f'_c + 4 K_g f_r \quad (4-38)$$

Equation (4-38) can be modified to account for the unconfined compressive strength either from conventional cylinder tests or unconfined ECC column tests. Two versions of the compressive strength equation for confined ECC are discussed next, depending on the type of input available to the designer. Both will provide comparable values of peak compressive strength for confined ECC.

The first version of the compressive strength  $f_{c.ecc}$  equation (4-43) uses a value of unconfined peak strength  $f'_{ecc}$  obtained from standard compressive cylinder tests. Due to the shape effect and boundary effects discussed in section 4.3.5.1.1, a shape factor  $\gamma$  is added to the cylinder strength. The modified the compressive strength  $f_{c.ecc}$  equation for this case is

$$f_{c.ecc} = \gamma f'_{ecc} + C_2 K_g f_r \quad (4-43)$$

In which the shape factor  $\gamma$  is 0.932 in this case, as per the experimental test results. The coefficient  $C_2$  has been determined through statistical regression as 0.156.

The second version of the compressive strength  $f_{c.ecc}$  equation (4-44) is based on the peak strength  $f_{ecc0}$  obtained from the unconfined samples with a height-to-width ratio deemed to minimize boundary effects. In this case, the modified the compressive strength  $f_{c.ecc}$  equation for this case is,

$$f_{c.ecc} = f_{ecc0} + C_1 K_g f_r \quad (4-44)$$

The coefficient  $C_1$  is 0.262.

#### **4.4.1.2 Elastic Modulus ( $E_{ecc}$ )**

The elastic Modulus ( $E_c$ ) for concrete in Bjerkeli et al. model was defined as

$$E_c = 9500 \left( \frac{\rho_c}{2400} \right)^{1.5} (f'_c)^{0.3}$$

For confined ECC, an equation for the elastic modulus of ECC is developed based on the definition from CSA A23.3 Standard (Clause 8.6.2), which provides a simplified equation for the elastic modulus for normal weight concrete as  $E_c = 4500\sqrt{f'_c}$ . By calibrating the latter expression with the experimental results obtained in this study, a best-fit equation to predict the elastic modulus of ECC based on its compressive cylinder strength is:

$$E_{ecc} = 1900\sqrt{f'_{ecc}}$$

#### 4.4.1.3 Regression of parameters in the model by Bjerkeli et al. (1990)

The original equations and coefficients in Bjerkeli et al. (1990) are listed in Table 4-3. Statistical regression was used to obtain the best fit between the model and measured result of the ECC square column tests. The modified Bjerkeli et al. equations are summarized in Table 4-3.

Table 4-3: Equations of Bjerkeli et al. model with the original and modified coefficients

Eq. name	Equation	Coefficient		
		$C_n$	Original	Modified
Maximum confinement compressive strength	$f_u = f_{co} + C_1 K_g f_r$	$C_1$	4.0	0.262
	$f_u = \gamma f'_c + C_2 K_g f_r$	$C_2$	4.0	0.156
Strain at $f_u$	$\varepsilon_u = C_3 + C_4 \left(\frac{f_r}{f'_c}\right)$	$C_3$	0.0025	0.0025
		$C_4$	0.05	0.0217
Strain at $0.85f_u$	$\varepsilon_{.85} = \varepsilon'_{.85} + K_g C_5 \left(\frac{f_r}{f'_c}\right) \frac{1}{1-F}$	$C_5$	0.05	0.015
Parameter for $\varepsilon_{.85}$ calculation	$\varepsilon'_{.85} = C_6 \left[ \left(\frac{C_7}{f'_c}\right)^2 + 1 \right]$	$C_6$	0.0025	0.0025
		$C_7$	17.07	16.92
Residual stress	$\sigma = f_{cy} = C_8 \frac{d_{so} A_{sh} f_{sy}}{s_p A_c}$	$C_8$	4.87	6.34*

\* According to the maximum residual from the experiment data,  $f_{cy} \leq 0.7f_u$



#### 4.4.2 Summary of Empirical Model for Rectangularly Confined High-Strength ECC in Square Columns

The proposed stress-strain curve for rectangularly confined high-strength ECC in square columns is similar to that of the original model by Bjerkeli et al. It consists of an ascending branch, descending branch, and horizontal part that represents the residual stress (Fig. 4-38).

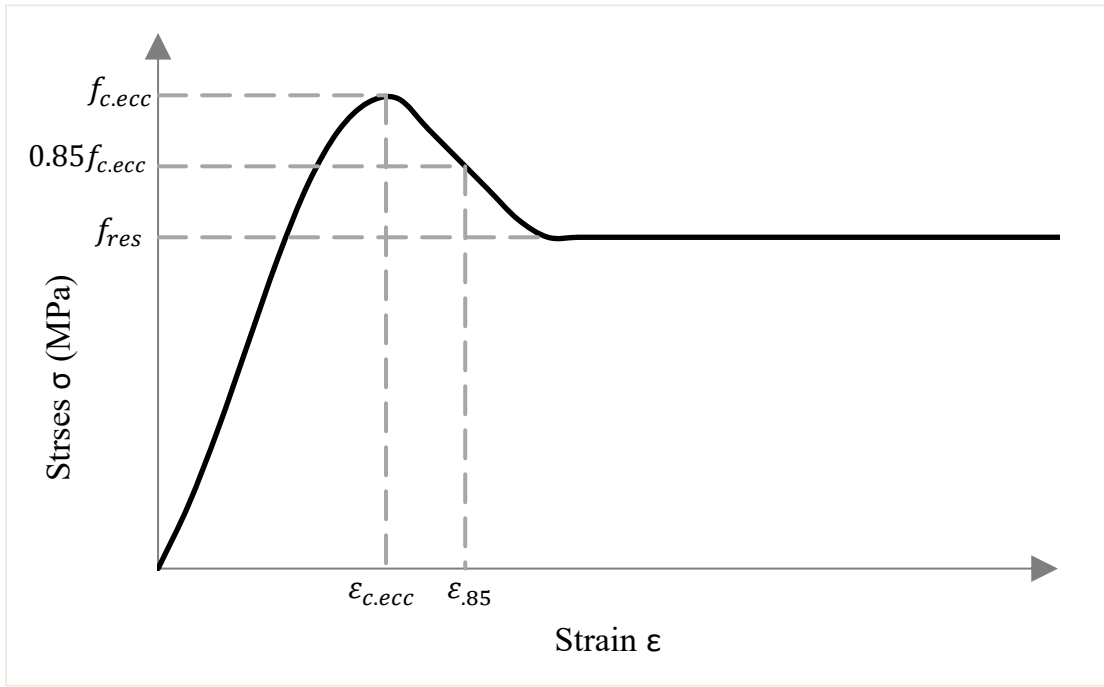


Figure 4-38: Proposed confinement model for Rectangular Confined High-Strength ECC in Square Columns

Ascending branch

$$\varepsilon \leq \varepsilon_{c.ecc}$$

$$\sigma = \frac{E_{ecc}}{1 + \left(\frac{E_{ecc}}{E_0} - 2\right) \left(\frac{\varepsilon}{\varepsilon_{c.ecc}}\right) + \left(\frac{\varepsilon}{\varepsilon_{c.ecc}}\right)^2} \quad (4-45)$$

Post-peak branch

$$\varepsilon > \varepsilon_{c.ecc}$$

$$\sigma = f_{c.ecc} - Z(\varepsilon - \varepsilon_{c.ecc}) \quad (4-46)$$

Horizontal part

$$\sigma = f_{res} = 6 \frac{d_{so} A_{sh} f_{sy}}{s_p A_{ecc}} \leq 0.7 f_{c.ecc} \quad (4-47)$$

where

$$E_{ecc} = 1900\sqrt{f'_{ecc}} \quad (4-48)$$

$$E_0 = \frac{f_{c.ecc}}{\varepsilon_{c.ecc}} \quad (4-49)$$

$$Z = \frac{0.15 f_{c.ecc}}{\varepsilon_{.85} - \varepsilon_{c.ecc}} \quad (4-50)$$

The maximum confinement compressive strength  $f'_{c.ecc}$  and the corresponding strain  $\varepsilon_{c.ecc}$  can be defined as

$$\text{Version 1} \quad f_{c.ecc} = f_{ecc0} + 0.262 K_g f_r \quad (4-51)$$

$$\text{Version 2} \quad f_{c.ecc} = \gamma f'_{ecc} + 0.156 K_g f_r ; \gamma = 0.932 \quad (4-52)$$

$$\varepsilon_{c.ecc} = 0.00273 + 0.014 \left( \frac{f_r}{f'_{ecc}} \right) \quad (4-53)$$

and

$$\varepsilon_{.85} = \varepsilon'_{.85} + K_g 0.00943 \frac{\left( \frac{f_r}{f'_{ecc}} \right)}{1 - F} \quad (4-54)$$

$$\varepsilon'_{.85} = 0.00289 \left[ \left( \frac{17.25}{f'_{ecc}} \right)^2 + 1 \right] \quad (4-55)$$

$$F = \frac{1}{1 + \left( \frac{1}{f_r K_g} \right)^{1/4}} \quad (4-56)$$

The confining pressures  $f_r$  and section geometry factor  $K_g$  are defined as.

$$f_r = \frac{A_{sh} f_{sy}}{h' s_p} \quad (4-55)$$

where  $A_{sh}$  = total effective area of ties and supplementary confining reinforcement in direction under consideration with spacing  $s_p$

$f_{sy}$  = yield stress of confining reinforcement

$h'$  = outer size of confined section

$s_p$  = center distance between hoop/ties confining reinforcement

$K_g$  is defined by the larger value of  $K_{g1}$  and  $K_{g2}$  which represents the compression arches between the transverse confinement reinforcement and laterally supported longitudinal reinforcement respectively.

$$K_{g1} = 1 - \frac{s_p}{d_{so}} \quad (4-56)$$

where  $d_{so}$  = the shorter outer diameter of hoop ties

$$K_{g2} = 1 - \frac{n C^2}{5.5 A_{ecc}'} \quad (4-57)$$

where  $n$  = number of laterally supported longitudinal bars

$C$  = distance between laterally supported longitudinal bars

$A_{ecc}'$  = gross area of ECC section measured to center line of peripheral hoop

The proposed empirical model for rectilinearly confined high-strength ECC in square columns was compared to the experimental curves in Figs. 4-39 – 4-41. The model yields reasonable results for the ascending branch, descending branch, and horizontal part.

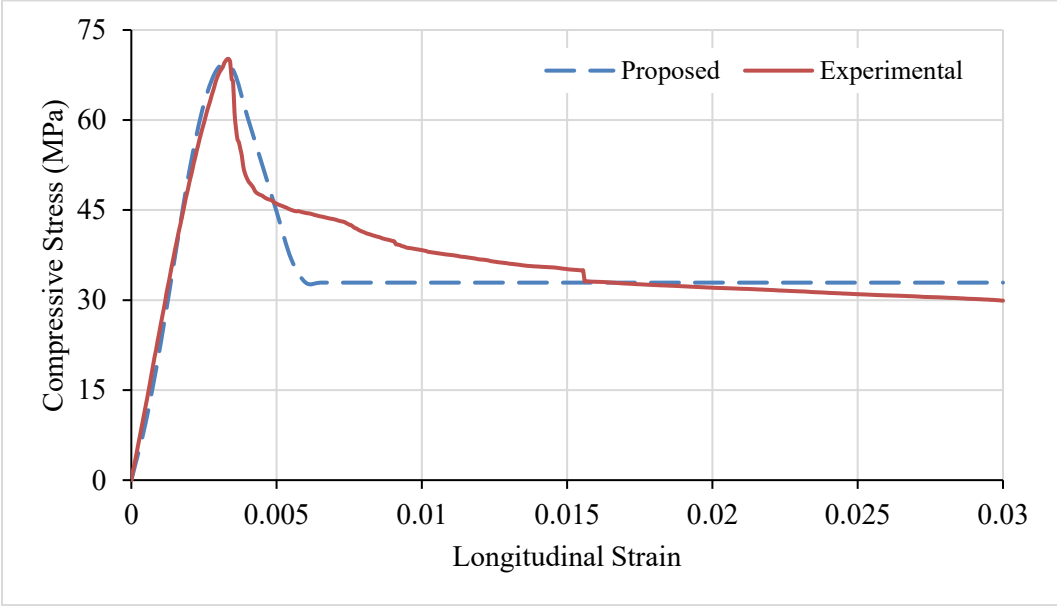


Figure 4-39: Comparison between ECC-1% test result and proposed model

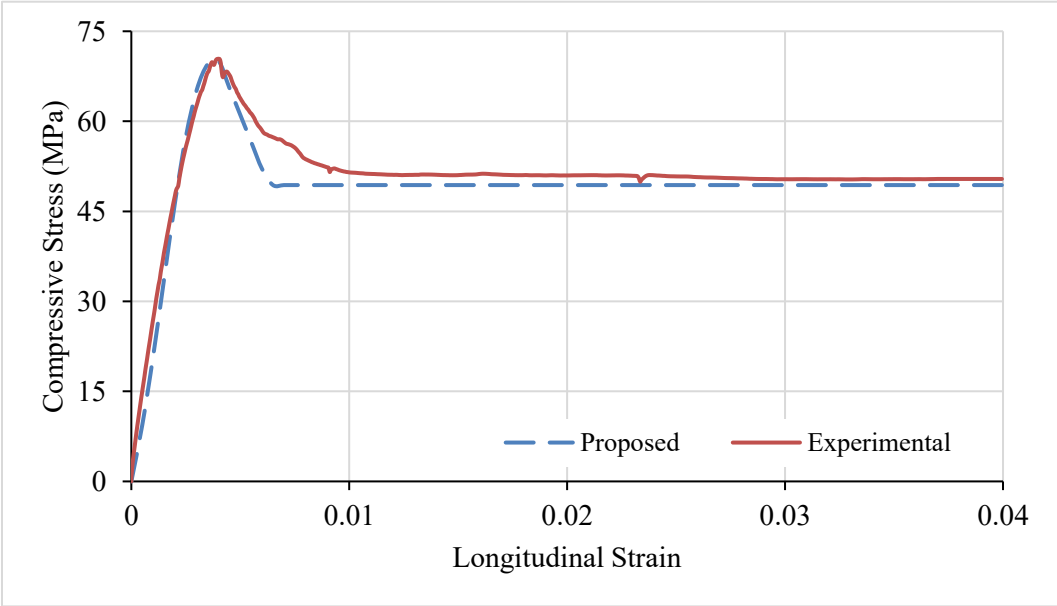


Figure 4-40: Comparison between ECC-1.5% test result and proposed model

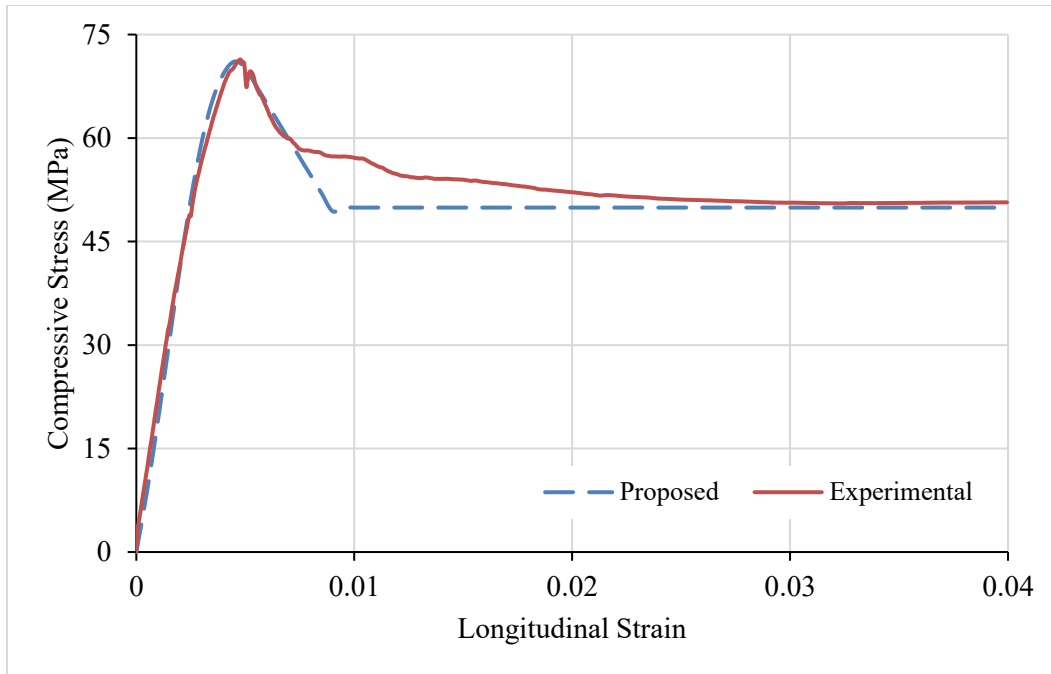


Figure 4-41: Comparison between ECC-2% test result and proposed model

## Notation for the proposed ECC confinement model

$A_{ecc}$	= gross area of ECC section, mm <sup>2</sup>
$A_{ecc}'$	= gross area of ECC section measured to center lone of peripheral hoop, mm <sup>2</sup>
$A_{sh}$	= total effective area of hoops ties and supplementary confining reinforcement in direction under consideration with spacing $s_p$ , mm
$C$	= distance between laterally supported longitudinal bars, mm
$d_{so}$	= the shorter outer diameter of hoop ties, mm
$E_{ecc}$	= Elastic Modulus of ECC, MPa
$f_{ecc0}$	= compressive strength of the corresponding unconfined column, MPa
$f'_{ecc}$	= compressive strength of ECC standard cylinders, MPa
$f_{c.ecc}$	= axial compressive strength of the confined ECC column, MPa
$f_r$	= confining pressures, MPa
$f_{res}$	= residual stress of confined ECC column, MPa
$f_{sy}$	= yield stress of confining reinforcement, MPa
$h'$	= outer size of confined section ( $h' = d_{so}$ in this case), mm
$n$	= number of laterally supported longitudinal bars
$K_g$	= section geometry factor
$s_p$	= center distance between hoop ties/confining reinforcement, mm
$\sigma$	= compressive stress, MPa
$\varepsilon$	= compressive strain
$\varepsilon_{c.ecc}$	= compressive strain at $f_{c.ecc}$ , MPa
$\varepsilon_{.85}$	= compressive strain at $0.85f_{c.ecc}$ , MPa

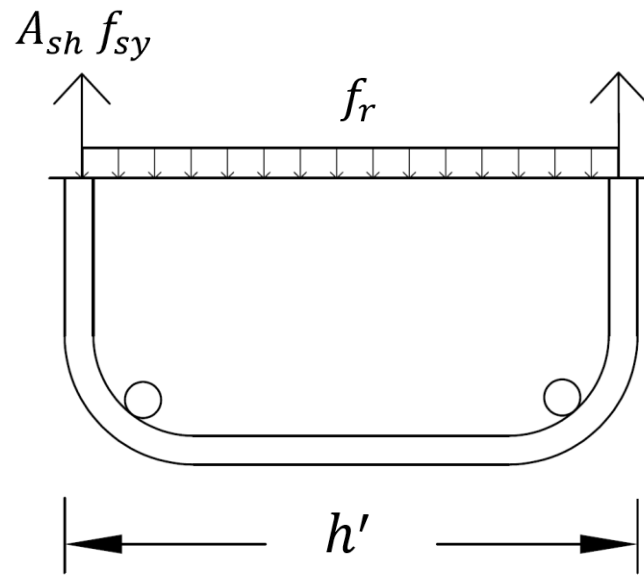


Figure 4-42: Ideal "confining pressures"  $f_r$

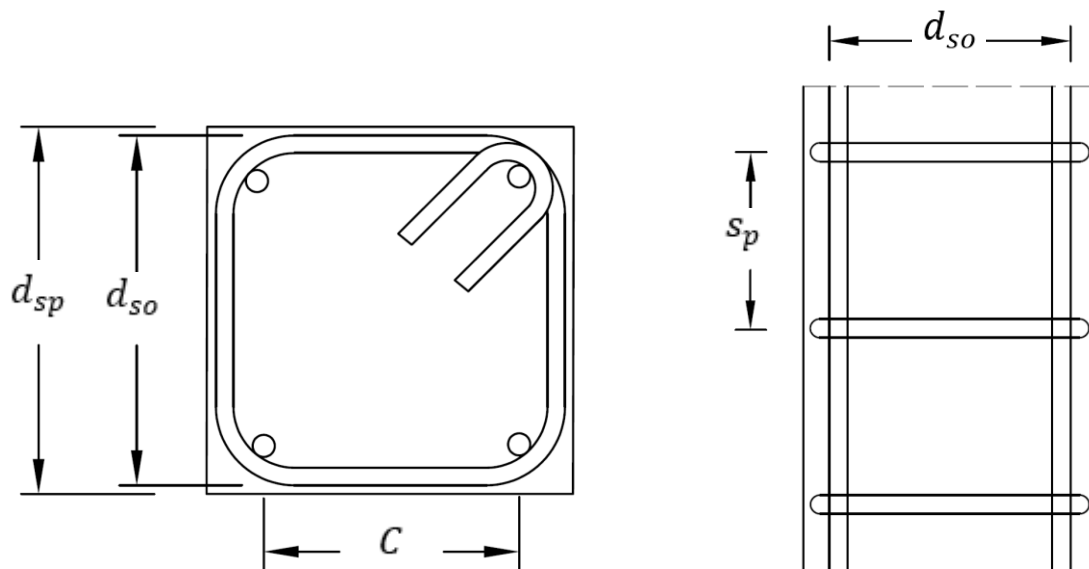


Figure 4-43: Horizontal and vertical column cross-section

## CHAPTER 5. VALIDATION AND PARAMETRIC ANALYSIS

Under an earthquake, ground accelerations induce large stresses in structures due to inertial forces, and cause damage in reinforced-concrete structures through concrete cracking and spalling, yielding of the reinforcement, and plastic deformations. If the structure is adequately designed, the damage will be concentrated at specific regions, it will be able to sustain repeated loading cycles through significant nonlinear behaviour without significant degradation of strength. The critical regions in which damage is concentrated are known as plastic hinges, often located at the ends of beams and columns. Once the rotational capacity of the plastic hinges is exhausted or sufficient plastic hinges are developed, the structure will exhibit a local or global collapse mechanism. Collapse mechanisms that lead to the greatest structure ductility are preferred. In conventional RC construction, ductility is primarily achieved by (i) ensuring that the amount and placement of reinforcement that produces the smallest size of the compressive zone for the design loads, which enables the achievement of large curvature values; (ii) using mild reinforcement to enable large longitudinal strains, avoiding premature fractures; and (iii) by confining of the concrete through reinforcing spirals, stirrups, and jackets to increase the crushing strain and delaying failure in compression.

If the structure is made of reinforced-ECC (RECC), resilience and damage resistance of the ECC material against spalling and cracking is expected to be greater than those of conventional concrete. Due to the lack of studies about ECC in compression, a research on the performance of confined ECC was conducted in previous section to develop a confinement model for ECC. This model is one of the first studies to investigate the behaviour of confined ECC at the element level for rectangular columns with rectangular stirrups.

At the system (structure) level, an enhanced performance in terms of cracking and spalling can be expected if the structure is made of ECC. As an alternative to full-scale experimental testing of ECC structures, finite-element analysis models can be used to study the performance of a whole structure in a parametric analysis. A computer simulation of two frames, one made with reinforced-ECC (RECC) and another made with conventional reinforced-concrete (RC), is conducted and the responses of both models are compared to investigate the structural response of ECC at the system level. Open-source, finite-element software OpenSEES is used to conduct the



study. Static and dynamic analysis were developed to evaluate the ductility capacity and predict the seismic performance of the frames. Prior to the parametric analysis, validation of the methodology and material models will be conducted using the experimental results obtained in the previous section.

## **5.1 Scope**

This parametric study is a preliminary study to the FEA modelling of a full-scale RECC structure. Therefore, only two plastic hinges at the supporting columns are investigated. This parametric study is conducted with the ECC material modelling according to the experimental material characterization from section 3. The confined ECC material is modeled with the empirical stress-strain responses of ECC columns subjected to monotonic axial load only from the experimental program in section 4. Under tension, ECC is assumed to start cracking at the region where there are no transverse steels. Therefore, the tensile response of confined ECC is assumed to be same as unconfined ECC and independent on the transverse steel effects.

## 5.2 OpenSEES Software

OpenSEES is an open-source, freely available, and object-oriented software framework for earthquake engineering simulation using finite element methods. It has been developed since 1997 by the Pacific Earthquake Engineering Research (PEER) Centre at the University of California, Berkeley (McKenna and Fenves, 2000). Key aspects of model-building, material models, element formulation, and solution algorithms that pertain to the validation and parametric studies discussed in this chapter will be discussed here. Further details about the program and syntax can be readily found in the OpenSEES Manual (Mazzoni et al. 2006).

## 5.3 OpenSEES Modelling

### 5.3.1 Frame Elements

#### Non-Linear Beam-Column Element

The Non-Linear Beam-Column element refers to the distributed plasticity model which considers the spread of nonlinear behaviour along the elements (Mazzoni et al. 2006). The *NonlinearBeamColumn* element allows setting Gauss integration points along the element for finite-element analysis, assigning cross-section, and defining geometric coordinate-transformation options. The syntax in OpenSEES for the *NonlinearBeamColumn* element is

```
element nonlinearBeamColumn $elemID $iNode $jNode $numIntgrPts $secTag  
$transfTag
```

## 5.3.2 Material

### 5.3.2.1 Uniaxial Material

This represents a material with uniaxial stress-strain or force-deformation relationship (Mazzoni et al. 2006). The following are the materials were used in this model to represent the structural materials of the frame.

#### Steel02 Material

*Steel02* material is one of the steel and reinforcing-steel material options in OpenSEES. It is used to construct a uniaxial steel material based on the Giuffré-Menegotto-Pinto (1973) model with isotropic strain hardening including a transition zone from elastic to strain hardening portions (Mazzoni et al. 2006). *Steel02* material allows customization of mechanical properties such as yield strength ( $F_y$ ), modulus of elasticity ( $E$ ), strain-hardening ratio ( $b$ ), and parameters to control the transition from elastic to plastic branches ( $R_0$   $cR_1$   $cR_2$ ). The syntax in OpenSEES for the *Steel02* material (Fig. 5-1) is

```
uniaxialMaterial Steel02 $matTag $Fy $E $b $R0 $cR1 $cR2
```

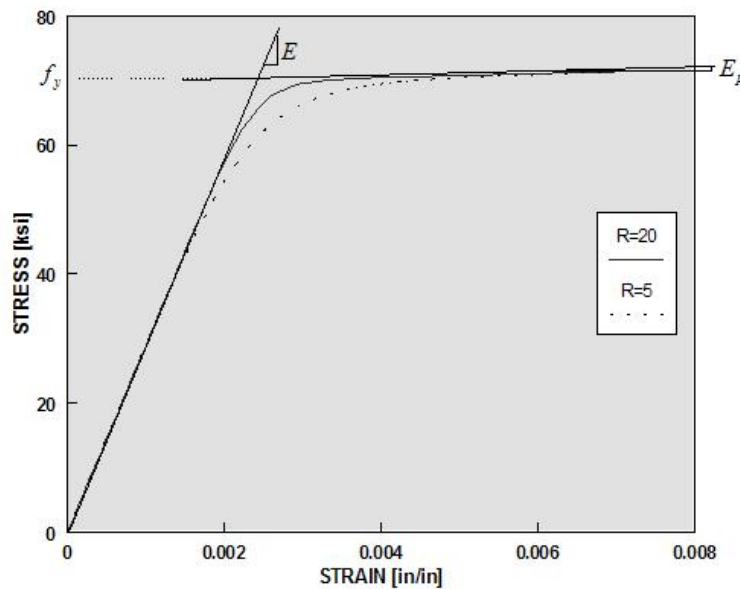


Figure 5-1: Uniaxial material Steel02 in OpenSEES (Mazzoni et al. 2006)

## Concrete02 Material

*Concrete02* material is one of the concrete material options in OpenSEES. *Concrete02* material is a Kent-Scott-Park (1971) concrete model with degrading linear unloading/reloading stiffness (Hisham and Yassin, 1994). *Concrete02* material also includes linear tension softening which is most suitable to represent typical concrete properties. *Concrete02* material allows customization of concrete mechanical properties such as concrete compressive strength ( $f_{pc}$ ), concrete strain at maximum strength ( $\epsilon_{psc0}$ ), concrete crushing strength ( $f_{pcu}$ ) and corresponding strain ( $\epsilon_{psU}$ ), the tensile strength, and tension softening stiffness ( $E_{ts}$ ). The syntax in OpenSEES for the *Concrete02* material (Fig. 5-2) is

```
uniaxialMaterial Concrete02 $matTag $fpc $epsC0 $fpcu $epsU $lambda $ft $Ets
```

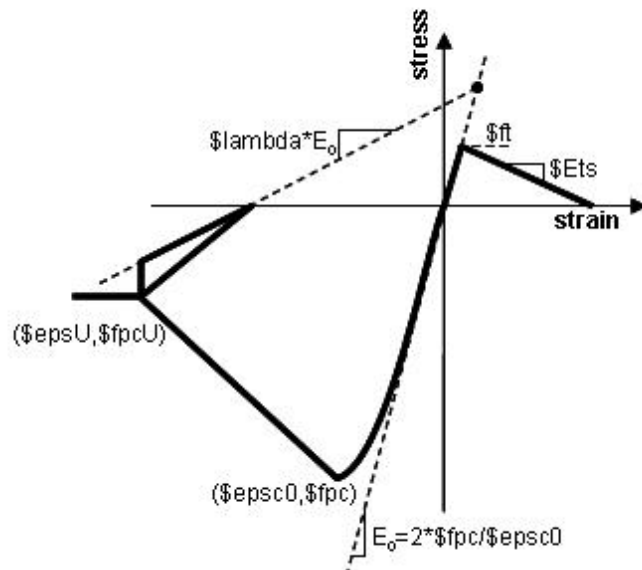


Figure 5-2: Uniaxial material Concrete02 in OpenSEES (Mazzoni et al. 2006)

## ECC01 Material

*ECC01* (Han et al. 2003) is the only available material option in OpenSEES that can simulate the strain-hardening behaviour in tension that ECC exhibits. *ECC01* material allows customization of tensile and compressive material properties such as tensile cracking stress ( $\mathbf{sigt0}$ ), strain at tensile cracking stress ( $\mathbf{epst0}$ ), peak tensile stress ( $\mathbf{sigt1}$ ), strain at peak tensile stress ( $\mathbf{epst1}$ ), ultimate tensile strain ( $\mathbf{epst2}$ ), compressive strength ( $\mathbf{sigc0}$ ), strain at compressive strain ( $\mathbf{sigc0}$ ), ultimate compressive strain ( $\mathbf{epsc1}$ ), and other parameters ( $\mathbf{alphaT1}$   $\mathbf{\$alphaT2}$   $\mathbf{alphaC}$   $\mathbf{alphaCU}$   $\mathbf{betaT}$   $\mathbf{betaC}$ ) to control the unloading curve in tensile and compressive zones.

The syntax in OpenSEES for the *ECC01* material (Figs. 5-3 and 5-4) is

```
uniaxialMaterial ECC01 $IDconcCover $sigt0 $epst0 $sigt1 $epst1 $epst2  
$sigc0 $epsc0 $epsc1 $alphaT1 $alphaT2 $alphaC $alphaCU $betaT $betaC
```

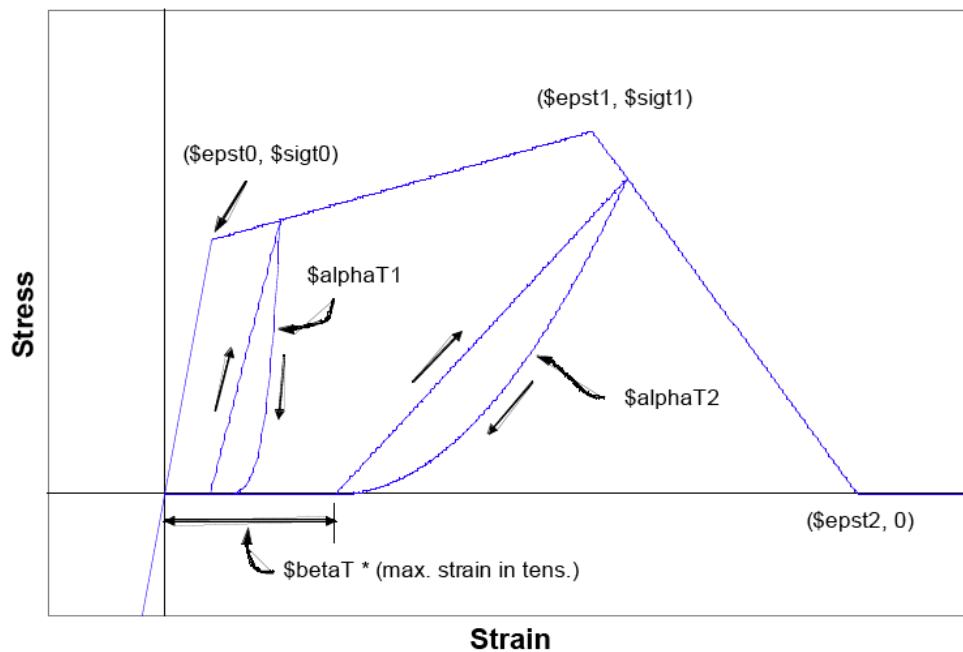


Figure 5-3: Uniaxial material ECC01 (Tension) (Mazzoni et al. 2006)

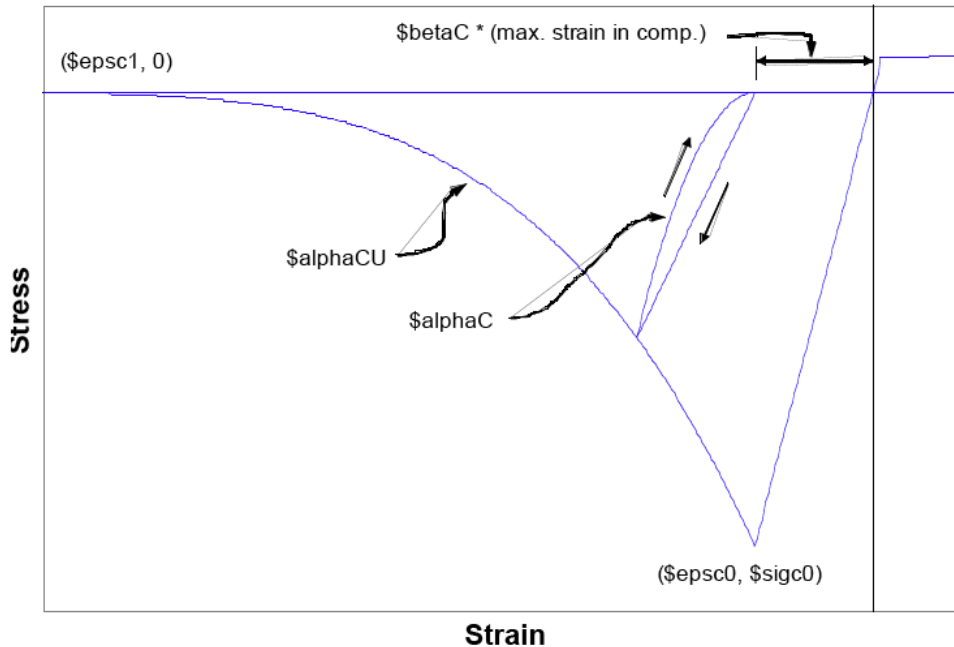


Figure 5-4: Uniaxial material ECC01 (Compression) (Mazzoni et al. 2006)

### 5.3.3 Section Modelling

*Section* command is used to construct a stress-resultant force-deformation response at a cross-section of a beam-column element. There are various options of sections in this command such as elastic, fibre, wide flange, plate fibre, etc. (Mazzoni et al. 2006).

*FiberSection* allows a cross-section to be divided into smaller regions for which the material response is integrated to give stress resultant behaviour. These small regions can be defined as fibre, patch, or layer sections in this command. The *fiber* subcommand allows generating a single fibre. The *patch* subcommand allows generating a number of fibres over a geometric cross-section in different shape patches such as quadrilateral, rectangle, or circle. The *layer* subcommand allows generating a row of fibres along a straight line or a circular arc (Mazzoni et al. 2006). Dimensions, materials, and numbers of fibres (layers/patch) can be specified in these subcommands. An example of beam and column fibre sections is shown in Fig. 5-5. An example of the syntax in OpenSEES for *FiberSections* is

```

section fiberSec $id {

    patch quadr $matTag $nfCoreZ $nfCoreY -$coreY $coreZ -$coreY -$coreZ
    $coreY -$coreZ $coreY $coreZ

    layer straight $matTag $numBarsInt $barAreaInt -$coreY $coreZ $coreY
    $coreZ }

```

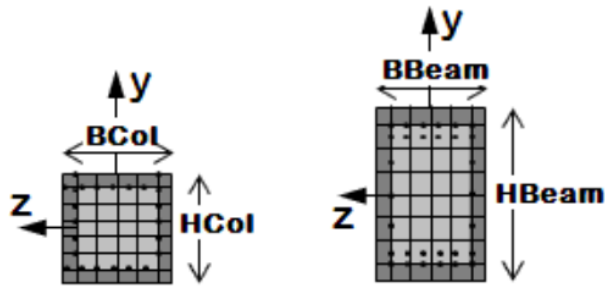


Figure 5-5: Example of fibre sections (Mazzoni et al. 2006)

### 5.3.4 Applying Mass and Load

#### 5.3.4.1 Mass

The masses of the columns, beams, slabs, etc. can be assigned to a frame as a lumped mass to each corresponding node / degree of freedom using *mass* command. The syntax in OpenSEES for *mass* is

```

mass $nodeID $MassNode 0.0 1.0 0.0 0.0 0.0;

```

#### 5.3.4.2 Load

Loads can be applied to a frame using the *Pattern* command to construct a load pattern object which allows customization of different time loading pattern options. There are two types of patterns used in this model for load application: plain and uniform excitation.

##### Plain Pattern

*Plain* pattern is one of the pattern options that offers different load conditions such as nodal loads (*load*), element loads (*eleload*), and single-point constraint (*sp*). The syntax in OpenSEES for *Pattern* is

```

pattern Plain $patternTag $tsTag {
load...
eleLoad...
sp...
}

```

### Uniform Excitation Pattern

*UniformExcitation* pattern allows the time series information of the earthquake such as the time step of the ground motion, the input file of the ground motion, ground-motion scaling factor, as well as the ground motion direction. The syntax in OpenSEES for the *UniformExcitation* pattern is

```

set AccelSeries "Series -dt $dt -filePath $GMfile -factor $GMfact"; #
time series information

pattern UniformExcitation $IDloadTag $GMdirection -accel $AccelSeries ;#
create Uniform excitation

```

## 5.3.5 Analysis Command

### 5.3.5.1 Static Analysis

A static pushover analysis is conducted through applying static load to a structure without considering the mass or damping matrices. An inverted triangular lateral force profile can be selected if it is assumed that the lateral response of the structure is governed by the first mode of vibration for instance.

### 5.3.5.2 Dynamic Analysis

A dynamic analysis is conducted through applying a seismic load in terms of ground motion to a structure with the considering of the mass and damping matrices.

### Rayleigh Damping Command

A widely use damping model for multi degree-of-freedom system, Rayleigh damping, can be used to assign damping to a frame. Rayleigh damping refers to a viscous damping assuming a linear combination of the mass and stiffness (Rayleigh 1877). The syntax in OpenSEES for *rayleigh* is

```

rayleigh $alphaM $betaKcurr $betaKinit $betaKcomm;

```



#### **5.3.5.4 Recorder**

The resultant parameters from FE analysis can be recorded and stored using *recorder* command with the options of node recorder, element recorder, or plot recorder. The *Node* recorder is able to record the response of a number of nodes at every converged step (Mazzoni et al. 2006). The *Element* recorder allows measuring responses at a specific fibre in the section of the element. The *Plot* recorder allows a graphical window for the plotting of the results during analysis.

### **5.4 Validation**

Three validation studies are presented next. The first two have been conducted by others and they illustrate the feasibility of finite-element models developed using the OpenSEES framework to represent the dynamic and pseudo-static behaviour of structural elements made with confined ECC, possessing circular cross-sections. The third is a validation study conducted by the author in which the performance of the confinement model for rectangular columns is compared to the experimental results obtained earlier.

#### **5.4.1 Element level (bridge column)**

Motaref et al. (2011) tested four segmental concrete cantilever columns of circular sections with plastic hinges incorporating ECC and other advanced materials (Fig. 5-6). The test results were compared to the predicted response calculated using an OpenSEES model, which included a confined ECC model developed for circular columns proposed by Motaref et al. (2011). The tensile capacity of the ECC was neglected. The displacement and base shear results obtained from an OpenSEES pushover analysis (Fig. 5-7) showed a reasonable agreement with the test results.

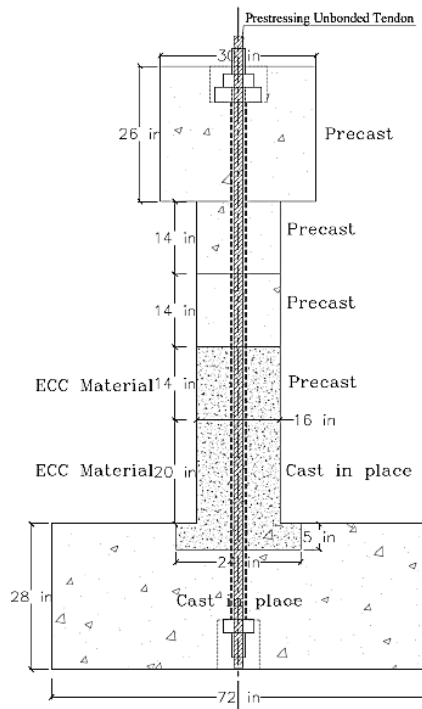


Figure 5-6: Concrete cantilever column with ECC plastic hinge (Motaref et al. 2011)

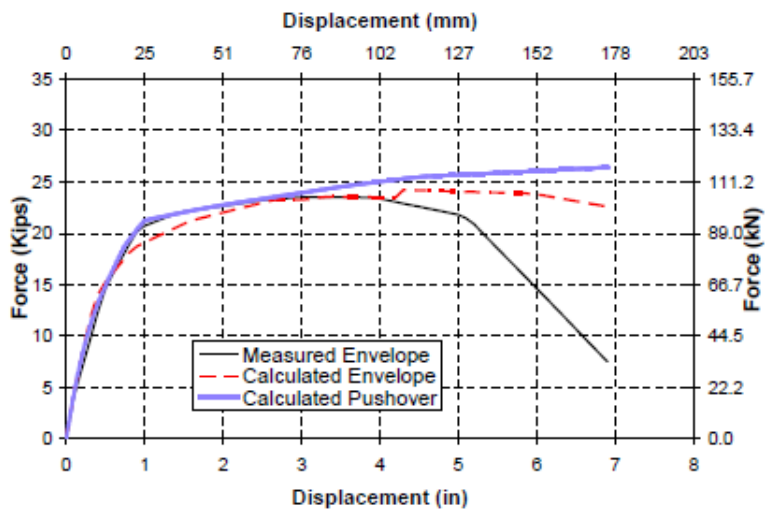


Figure 5-7: Displacement and base shear of a tested column with ECC plastic hinge (Motaref et al. 2011)

### 5.4.2 System level (dynamic testing of a 4-span bridge)

Cruz-Noguez and Saiidi (2010) tested a four-span bridge incorporating plastic hinges made with ECC and other different advanced materials. An analytical model of the bridge subjected to a dynamic excitation consisting of a record of the Northridge earthquake with a PGA of 1.0g was developed in OpenSEES (Fig. 5-8). Since the bridge column had circular cross-sections, a ECC material model developed by Motaref et al. (2011) was used while neglecting the tension capacity of the ECC. The calculated displacement and base shear of the SMA Bent (a two-column pier reinforced with shape-memory alloy and ECC) obtained from the OpenSEES model shows a reasonable correspondence in comparison to the experimental results (Fig. 5-9).

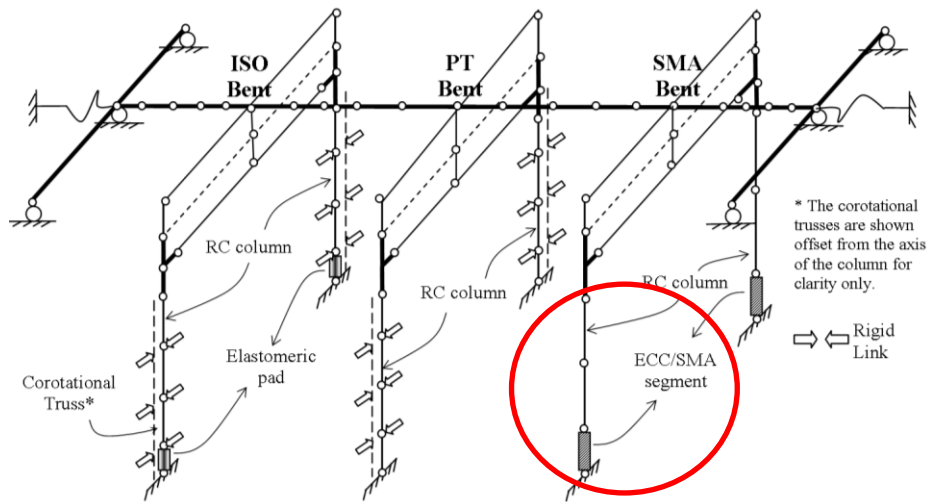


Figure 5-8: Configuration of the tested four-span bridge (Cruz-Noguez and Saiidi, 2010)

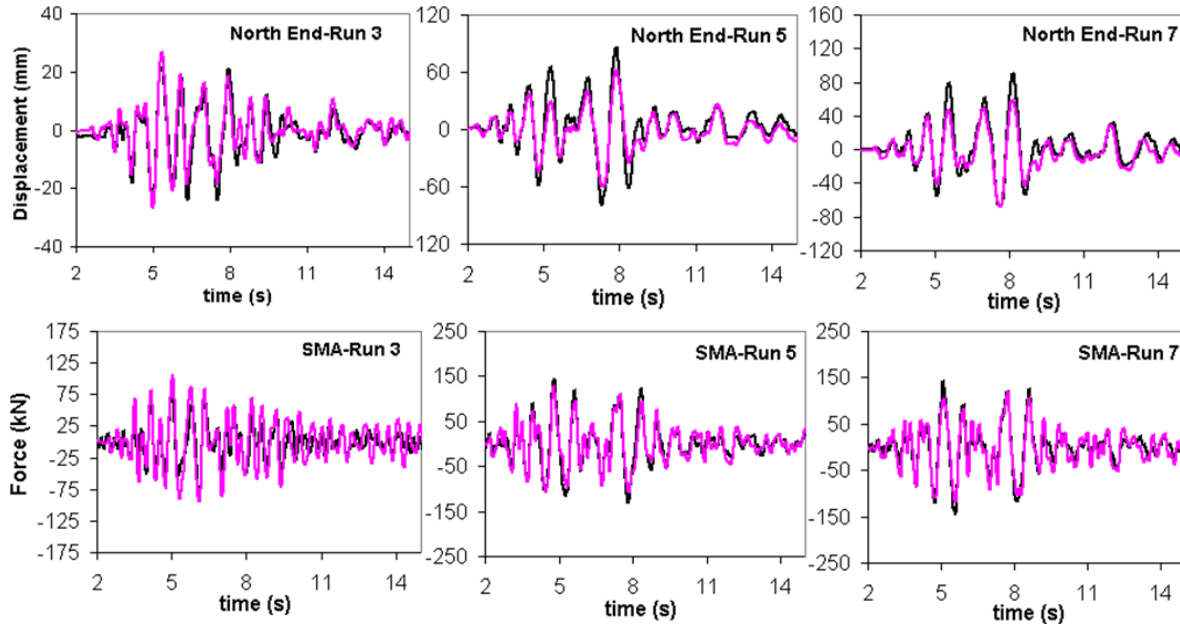


Figure 5-9: Displacement and base shear of SMA Bent. Black line: measured; purple line: calculated (Cruz-Noguez and Saiidi, 2010)

#### 5.4.3 Element level (rectangular cross-section under axial compression)

The validation studies conducted by Cruz-Noguez and Saiidi (2010) and Motaref et al. (2011) were performed for ECC columns with circular cross-sections. There are no validation studies for rectangular elements made with ECC since no experimental studies for this type of geometry and reinforcement are available in the literature.

To investigate the suitability of the confinement model developed in Chapter 4, a FE model was conducted in OpenSEES to simulate the response of the rectangular columns made of confined ECC under axial compression. The ECC confinement was modeled using the *Concrete02* material discussed earlier in section 5.3.2. No tensile response was defined for the *Concrete02* material since the columns were in pure compression and the fibre-section approach was used to model the columns. The resulting model was used to predict the compressive responses of the ECC column specimens and compared to the experimental responses discussed in Chapter 3.

Four 100 mm x 100 mm x 300 mm square ECC columns with 0%, 1%, 1.5%, and 2% transverse steel confinement were modeled as subject to a uniaxial compressive load. *NonlinearBeamColumn* elements and *fiber-sections* were used to model the columns. The

analytical load-displacement results were compared to the experimental ones (Figs. 5-10 a-d). The OpenSEES analytical results show a reasonable correspondence to the experimental response in terms of the compressive load-displacement response.

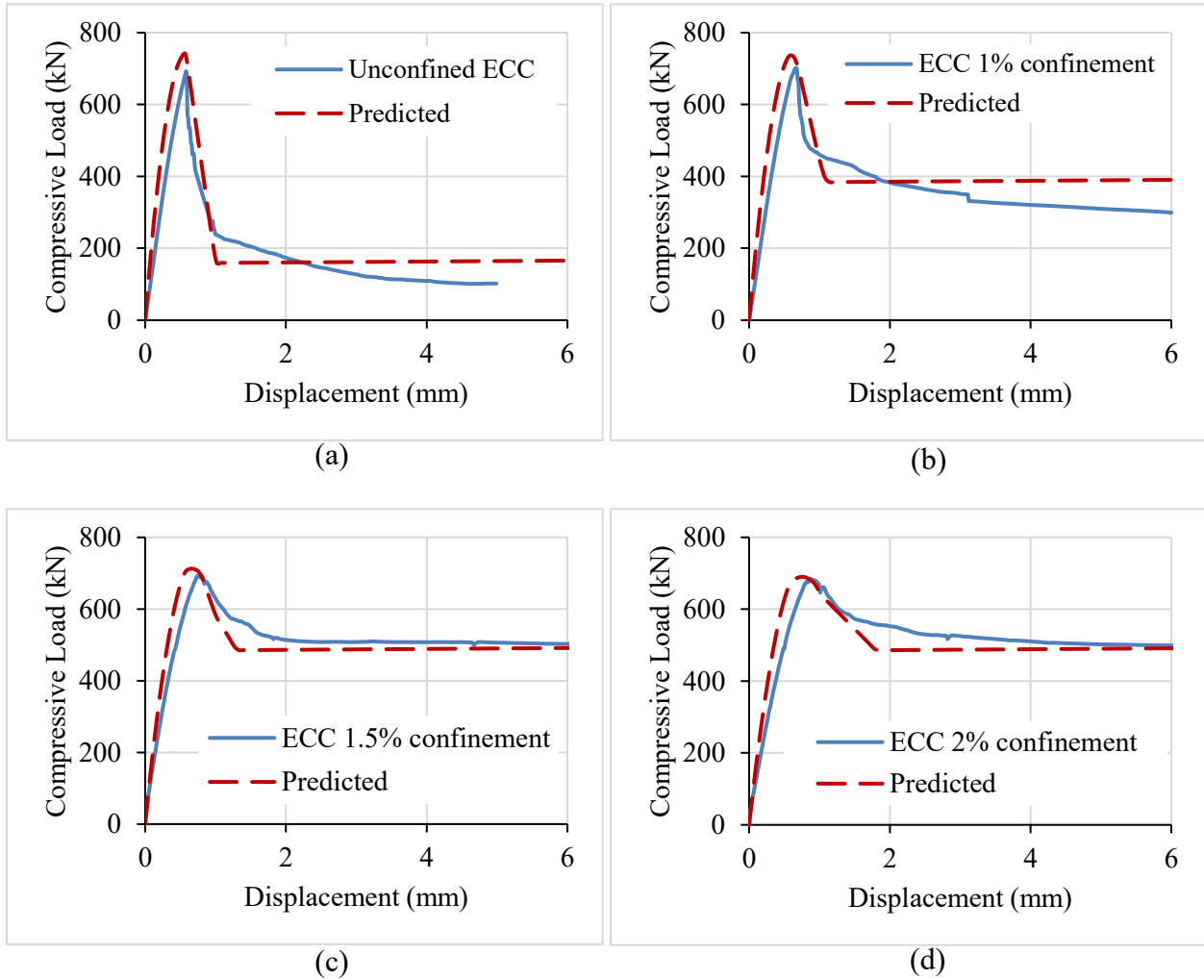


Figure 5-10: Load-displacement curve of ECC square columns with (a) unconfined material, (b) 1% confinement, (c) 1.5% confinement, (d) 2% confinement

Although *Concrete02* can represent well the response of confined ECC in compression, it should be noted that the disadvantage that this material has is its inability to represent the response of ECC in tension. *Concrete02* has a post-peak tensile descending branch, which is typical of conventional concrete that exhibits tension softening, but cannot simulate the tensile stress-strain response of ECC.

## 5.5 Frame Modelling

Two 2-D frames, one made with ECC and reinforced with steel (RECC) and another made with conventional concrete and reinforced with steel (RC) were developed and analyzed using OpenSEES. The typical frame is a one-bay, 7-storey frame with a total height of 98 ft (8.1 m) as shown in Fig. 5-11. The frame has 24 in (165.5 mm) x 24 in (165.5 mm) square columns and 24 in (165.5 mm) x 42 in (289.6 mm) beams. All reinforcement consists of #8 ( $\text{\O}25.4$  mm) steel bars with 2.5 in (17.24 mm) concrete cover. Both support columns are assumed to be fully fixed to the ground. All columns were assumed to be confined with 1.5% transverse steel content.

The steel was assumed to have a yield strength of 460 MPa, modulus of elasticity of 200,000 MPa, and a strain-hardening ratio of 0.01. The unconfined concrete had a peak compressive strength of 72.6 MPa at 0.00254 strain, and ultimate stress of 6.895 MPa at 0.006 strain, properties which were assumed to be equal to the concrete cylinder compressive tests described in Chapter 4. The confined concrete had a peak compressive strength of 107 MPa at 0.0065 strain, and an ultimate stress of 33 MPa at 0.0135 strain, which were calculated using a high-strength confinement model for concrete (Bjerkeli et al. 1990). The tensile behaviour of concrete was assumed to be linear elastic until a tensile strength of 2.5 MPa at a strain of 0.000075.

The compressive properties of unconfined ECC were obtained from the unconfined ECC square column specimens described in Chapter 4, which had a peak compressive strength of 69.26 MPa compressive strength at 0.0029 strain. The compressive properties of confined ECC was obtained from the confined ECC square column tests with 1.5% transverse reinforcement described in Chapter 4, which had a peak compressive strength of 70.41 MPa at 0.004 strain which. The tensile properties of ECC were obtained from the tensile coupon tests described in Chapter 3, which had a linear behaviour until a peak tensile stress of 2.5 MPa at 0.0125 strain, followed by a tensile strain ductility till an ultimate strain of 0.017.

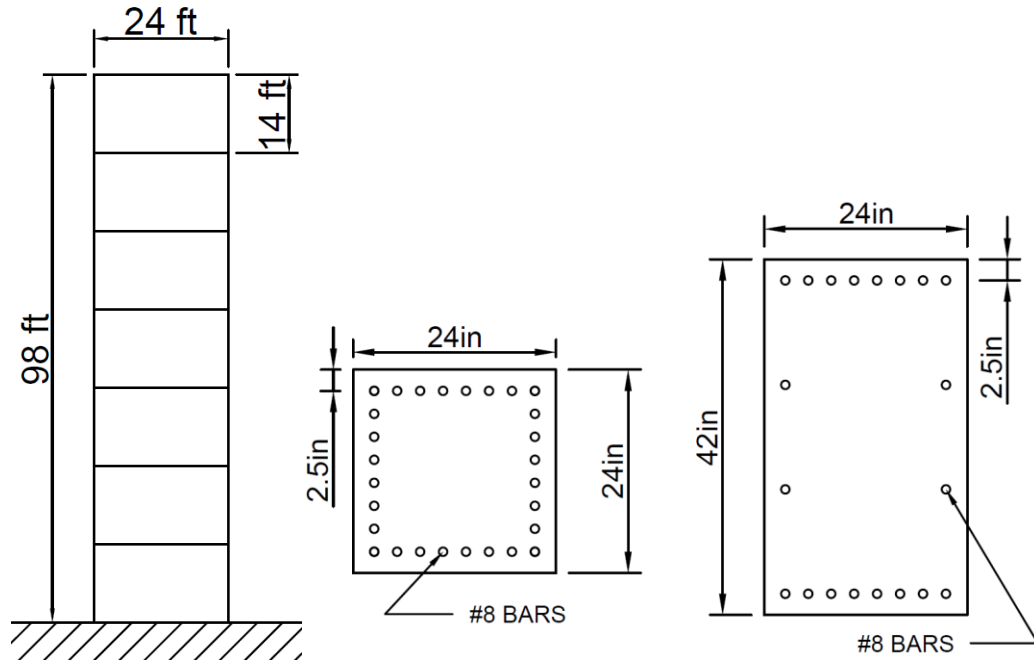


Figure 5-11: Geometry of a 7-storey building with cross sections of columns and beams

Creating the FE model of the 7-storey building model in OpenSEES consisted of three steps of modeling: (section 5.4.1) building the frame and defining fixity supports, (section 5.4.2) defining mass and gravity loads, (section 5.4.3) applying external load, and (section 5.4.4) recording analysis results.

## 5.4.1 Building the Frame

### 5.4.1.1 Frame Elements

Beams and columns of the frame were modelled using *NonlinearBeamColumn* elements. Each element of the frame was set to have five integration points with linear geometric coordinate-transformation.

### **5.4.1.2 Material Properties**

#### 5.4.1.2.1 Steel

*Steel02* material was used to represent the #8 reinforcement bars in the frame. The reinforcement bars were assumed to have a yield strength of 460MPa, modulus of elasticity of 200,000MPa, and strain-hardening ratio of 0.01 (Fig. 5-12). The parameters to control the transition were input as the recommended values from OpenSEES:  $R_0=18$ ,  $R_1=0.925$ ,  $R_2=0.15$ .

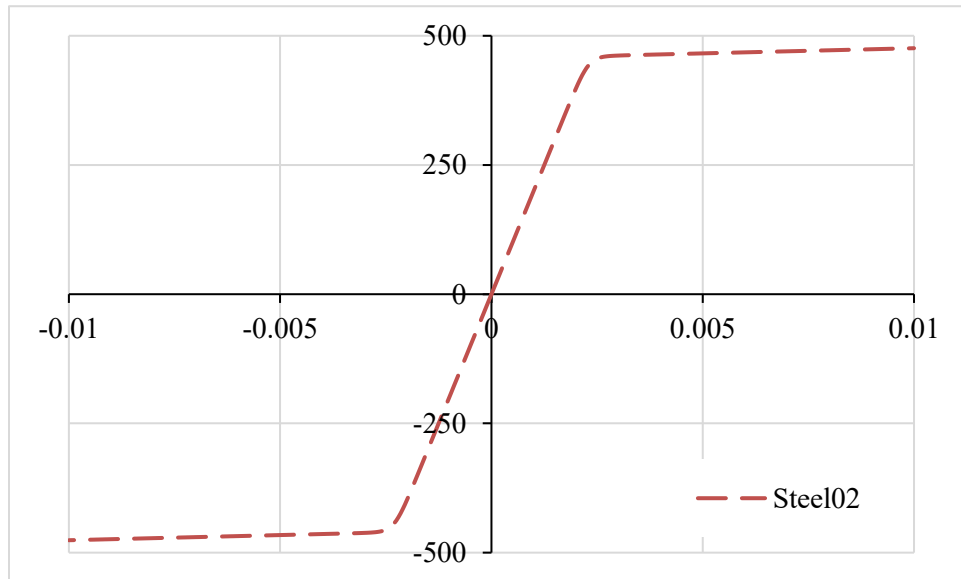


Figure 5-12: Compressive and tensile behaviours of steel bars for OpenSEES



#### 5.4.1.2.2 Concrete

Unconfined and confined concrete materials were modeled using *Concrete02* material. As discussed before, the unconfined concrete material was based on the compressive test on concrete control cylinders from Chapter 3. The compressive behaviour of unconfined concrete material for this model were defined to have a maximum compressive strength of 72.64 MPa at 0.00254 strain, and ultimate stress of 6.895 MPa at 0.006 strain (Fig. 5-13). To prevent numerical instabilities, *Concrete02* assigns a constant residual stress after reaching the crushing strain.

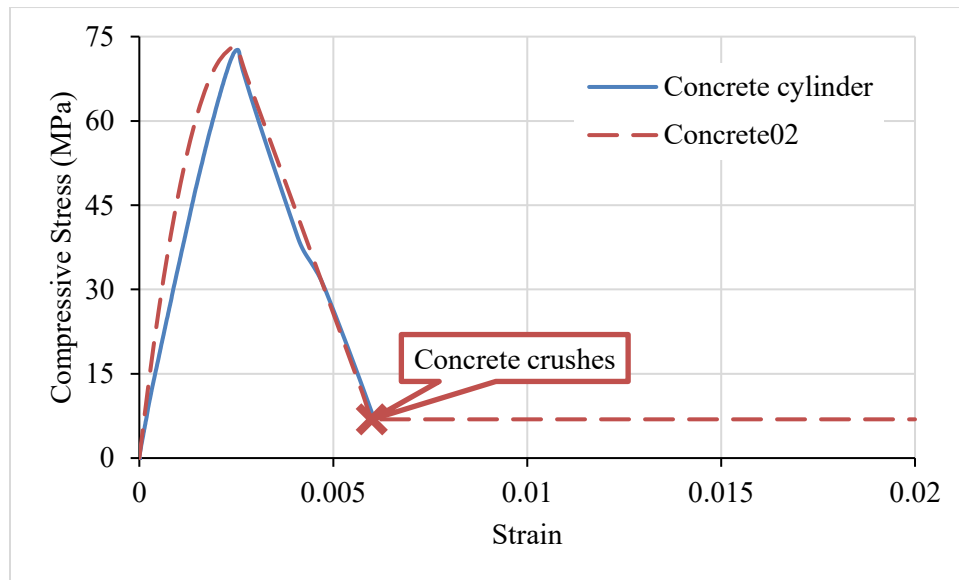


Figure 5-13: Compressive behaviour of unconfined concrete material in OpenSEES

The confined concrete material was calculated using Bjerkeli et al. (1990) model with 1.5% transverse steel content. The compressive behaviour of confined concrete for this model was defined to have a compressive strength of 107 MPa at 0.0065 strain, and an ultimate stress of 33 MPa at 0.0135 strain (Fig. 5-14).

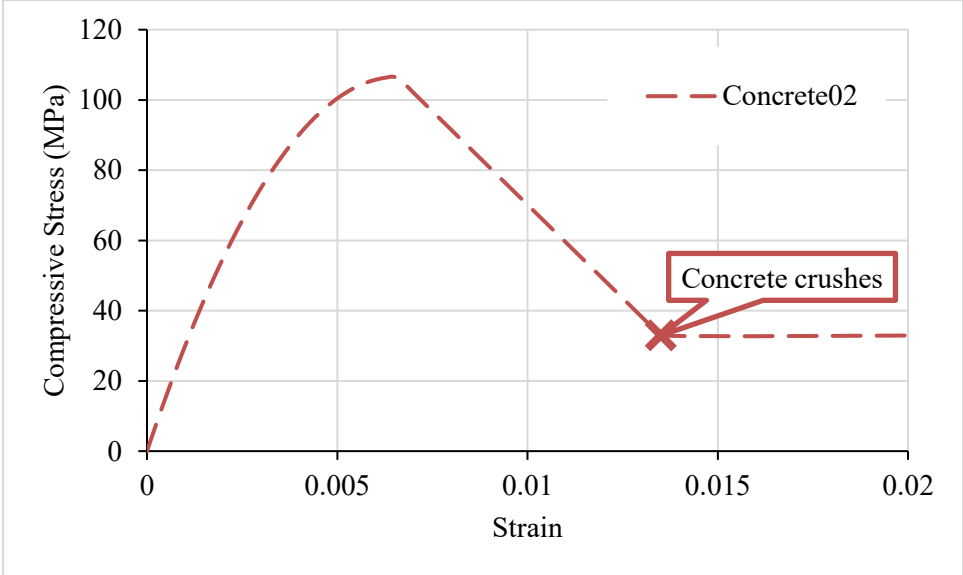


Figure 5-14: Compressive behaviour of confined concrete material in OpenSEES

The tensile behaviour of concrete material for this model was assumed as a typical brittle concrete response with a tensile strength of 2.5 MPa at a strain of 0.000075, followed by tensile softening (Fig. 5-15).

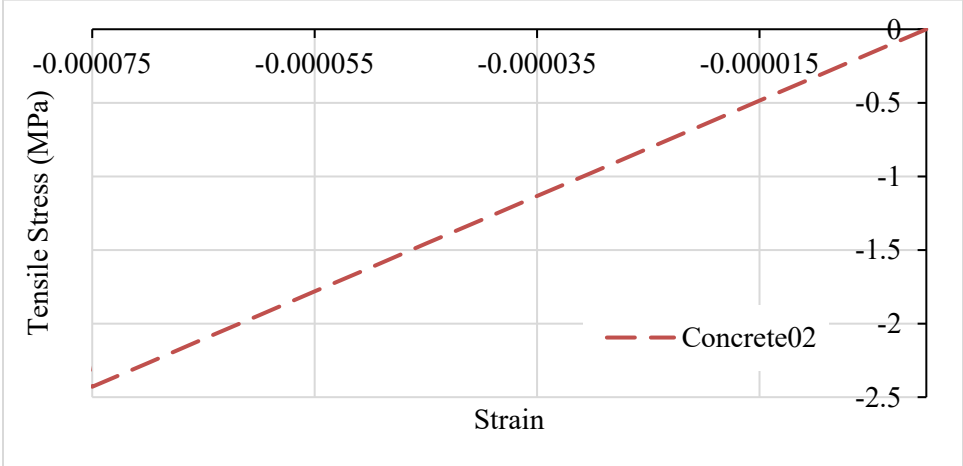


Figure 5-15: Tensile behaviour of concrete material in OpenSEES

#### 5.4.1.2.3 ECC

The validation studies conducted by Cruz-Noguez and Saiidi (2010), and Motaref et al. (2011) considered ECC columns with circular sections. Prior to this work, no validation studies existed in the literature for rectangular elements made with ECC.

As discussed before, the compressive behaviour of unconfined and confined ECC material was defined based on the compressive test on ECC square columns with 0% and 1.5% confinement presented in Chapter 4. *ECC01* and *Concrete02* are two suitable concrete materials to model ECC and its advantages and limitations will be discussed next.

The compressive response of *Concrete02* material (Fig. 5-2) is suitable for modeling the compressive behaviours of unconfined and confined ECC, since it can capture the ascending pre-peak branch and descending post-peak behaviour similar to those of concrete (Fig. 4-37), plus the notable residual compressive stress that confined ECC shows for large values of compressive strain. However, a major drawback is that the material cannot simulate the strain-hardening behaviour of ECC, since it can only represent tension softening.

On the other hand, *ECC01* (Fig. 5-3) allows the simulation of the strain-hardening behaviour of ECC, but the compressive response has a post-peak descending, exponential behaviour that is suitable for unconfined ECC, but can only approximately capture the post-peak residual compressive stress of confined ECC, since the descending branch steadily approaches zero stress. The descending branch is controlled by a coefficient termed **alphaCU** (Fig. 5-3).

In this study, it was decided to use the *ECC01* material for the parametric analysis, in order to be able to simulate the characteristic tensile response of ECC, and make a qualitative assessment of its cracking properties with respect to concrete. A range of exponential terms for the descending compressive branch are investigated to approximate the compressive response.

The compressive behaviour of unconfined ECC for this model was defined to have a compressive strength 69.26 MPa at 0.0029 strain (Fig. 5-15). The small residual stress of the unconfined ECC was neglected since the experimental tests showed that the specimens was already experiencing large cracks beyond the strain of 0.005 (Fig. 4-26). The best fit post-peak curve for unconfined ECC material was obtained with a coefficient **alphaCU** equal to 4.

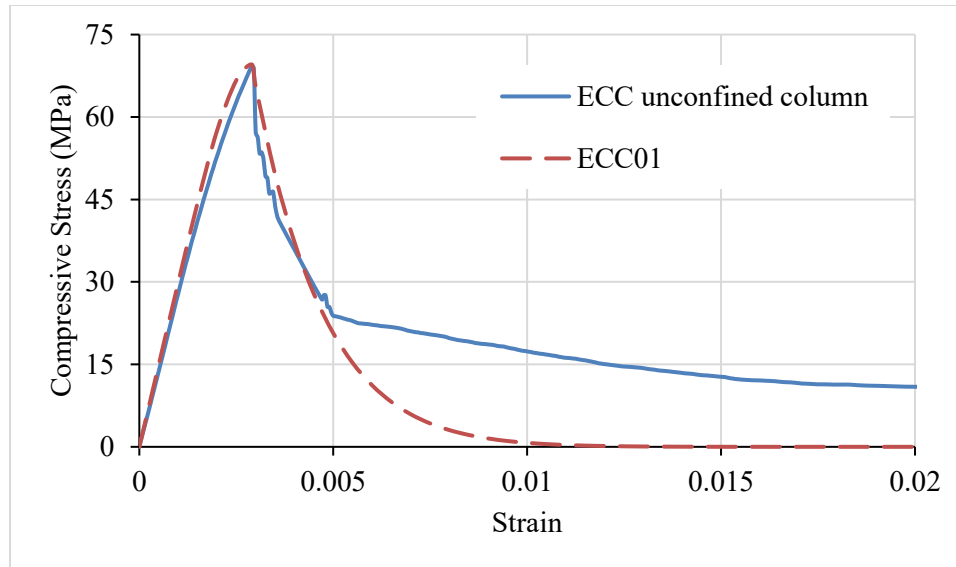


Figure 5-16: Compressive behaviour of unconfined ECC material in OpenSEES

The compressive behaviour of confined ECC with 1.5% transverse steel ratio had a compressive strength of 70.41 MPa at 0.004 strain (Fig. 5-16). An arbitrary, ultimate crushing strain of 0.02 in compression was chosen since the studies of confined columns using modern reinforcing schemes lead to maximum strains of concrete of the order of 0.02 (Chadwell and Imbsen, 2002). In order to accommodate the compressive residual stress of the confined ECC, a range of *ECC01* models with different options in coefficient  $\alpha_{1\text{phaCU}}$  (such as 19, 35, 65, 105) was developed for this analysis (Fig. 5-15). The analysis results for the different compressive branches were compared and discussed in section 5.3.

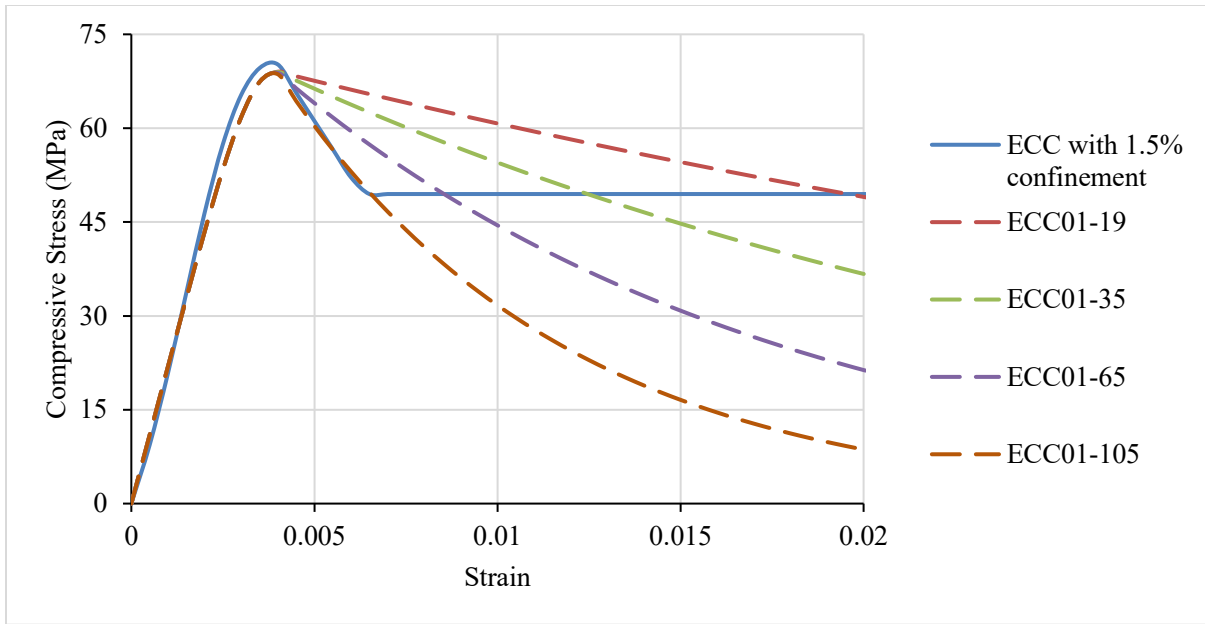


Figure 5-17: Compressive behaviour of confined ECC material in OpenSEES

The tensile behaviour of ECC material was defined based on the tensile test on ECC coupon specimen from Chapter 3. The tensile behaviour of ECC material for this model is defined to have a tensile cracking stress of 2.4 MPa at 0.001 strain, peak tensile stress of 2.5 MPa at 0.0125 strain, and ultimate tensile strain of 0.017 (Fig. 5-18).

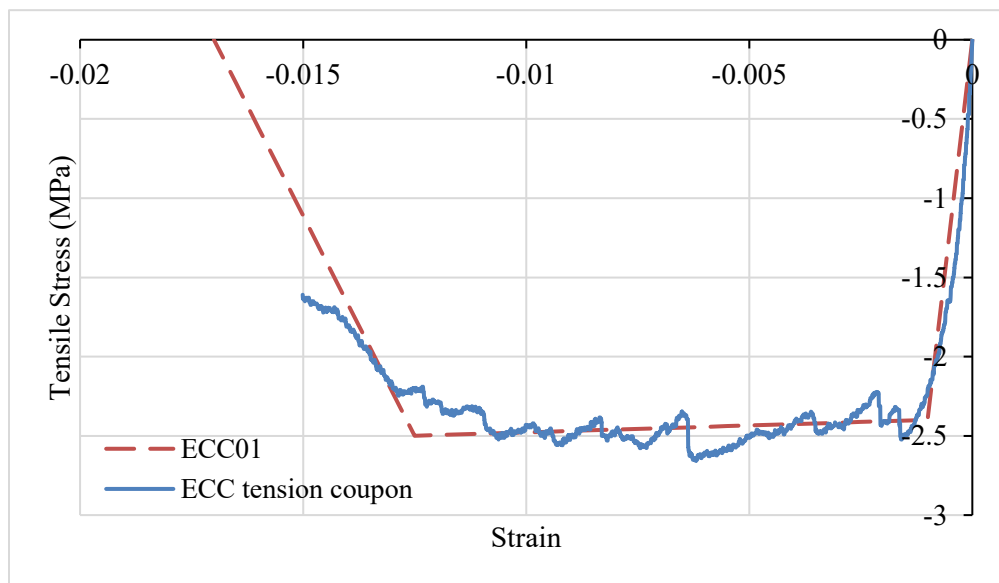


Figure 5-18: Tensile behaviour of ECC material in OpenSEES

### **5.4.1.3 Section Modelling**

Both beam and column sections from Fig. 5-10 were modeled using *FiberSections* into the fibre sections similar to the examples shown in Fig. 5-5. Element cover and core for column and beam sections were both modeled in *Patch* subcommand with 20 fibres in both z- and y-direction. Longitudinal reinforcement #8 bars were modeled as straight lines of fibres in *layer* subcommand where 8 bars on top and bottom and 2 bars on the intermediate layer.

### **5.4.2 Applying Mass and Gravity Load**

#### Mass

The masses of the columns, beams, and slabs were assigned as a lumped mass to each corresponding node using *mass* command.

#### Gravity Load

Gravity load was applied by assigning self-weight on each element using the *pattern* command. *Plain* pattern was chosen to represent the self-weight load on elements with *eleLoad* subcommand. This was modeled with a *beamUniform* load option for uniformly distributed self-weight to the elements. The syntax in OpenSEES for *Pattern* with *eleLoad* is

```
pattern Plain 101 Linear {  
eleLoad -ele $elemID -type -beamUniform 0 -$Qd1Col;      # COLUMNS  
eleLoad -ele $elemID -type -beamUniform -$Qd1Beam; }    # BEAMS
```

The gravity load analysis was set to be static loading with a load-controlled integrator. Newton-Raphson was set to be the numerical algorithms in this case. Convergence tolerance and the maximum number of iterations were specified accordingly. After the gravity load analysis, the time of calculation was reset to zero for other external load analysis to detect the masses.

### 5.4.3 Applying External Load

#### 5.4.3.1 Pushover Analysis

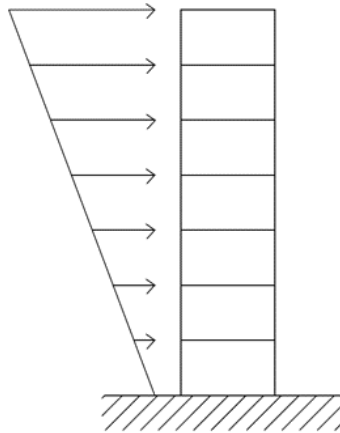


Figure 5-19: Lateral loads on a 7-Storey building in pushover analysis

The inverted triangular load profile was applied through *pattern* command. *Plain* pattern was chosen for this model to use *load* subcommand for applying nodal load on each floor. The syntax in OpenSEES for *Pattern* with *load* is for this model is

```
pattern Plain 200 Linear {  
    load 81 1 0.0 0.0;  
    load 71 [expr 6/7] 0.0 0.0;  
    load 61 [expr 5/7] 0.0 0.0;  
    load 51 [expr 4/7] 0.0 0.0;  
    load 41 [expr 3/7] 0.0 0.0;  
    load 31 [expr 2/7] 0.0 0.0;  
    load 21 [expr 1/7] 0.0 0.0;  
    load 11 [expr 0/7] 0.0 0.0;}
```

The pushover analysis was defined as static loading with a displacement-controlled integrator. Newton-Raphson was set to be the numerical algorithms in this case. Convergence tolerance and the maximum number of iterations were specified accordingly.

### 5.4.3.2 Dynamic Analysis

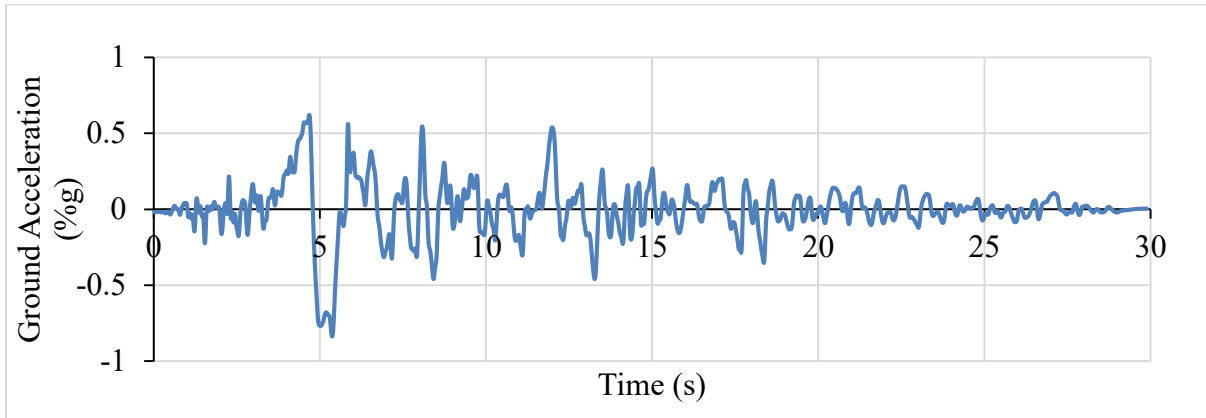


Figure 5-20: Rinaldi record from the Northridge earthquake (1994)

The Rinaldi record from the Northridge earthquake (1994) in California was applied to the frames for dynamic analysis (Fig. 5-20). The earthquake load pattern was input as ground acceleration with time, which was applied to frame using *pattern* command. *UniformExcitation* pattern was chosen in this case to represent the ground excitation.

### Rayleigh Damping Command and Solution Algorithm

Rayleigh damping for this model was defined in the first mode and third mode of the structure with a damping ratio of 2% in both modes.

The dynamic analysis was defined as a transient loading with Newark integrator. Newton-Raphson was set to be the numerical algorithm for solution in this case. Convergence tolerance and the maximum number of iterations were specified as per the Manual's recommendation.

### **5.4.4 Recorder of Analysis Result**

The displacement of the roof and the base shear were recorded using *Node* subcommand with the response options of displacement and reaction respectively. The stress-strain behaviours of the structural materials were recorded using *Element* subcommand with the response option of *stressStrain*. Syntax examples in OpenSEES for *recorder* is



```

recorder Node -file $dataDir/DFree.out -time -node $FreeNodeID -dof 1 2 3
disp; # displacements of free node

recorder Node -file $dataDir/RBase.out -time -nodeRange $SupportNodeFirst
$SupportNodeLast -dof 1 2 3 reaction; # support reaction

recorder Element -file $dataDir/SS8Ele1ConMid.out -time -ele $FirstColumn
section fiber 0 0 $IDconcCore stressStrain; # concrete fiber
stress-strain, node i

```

## 5.6 Finite-Element Analysis Results

Two 2-D frames, one made with RECC and another with conventional RC, were analyzed using OpenSEES. Since the modeling of ECC columns under compression might be overestimated, this finite-element analysis was mainly focused on the structural performance in terms of the tensile responses. Static pushover analysis and dynamic analysis were developed to evaluate the ductility capacity and predict the seismic performance of a full-scale structure. Base shear versus roof drift responses of both frames in static pushover analysis were compared. The overall structural performance and cracking mechanism of concrete and ECC during static pushover analysis and dynamic analysis were investigated as well. Roof displacement of both frames and cracking status over time during the seismic load in the dynamic analysis were studied.

Base columns (column A and B) of the structure were chosen to examine the material cracking in this case. The stress-strain responses of the base columns were studied at fibres located at different points in the column along in the direction of the loading (Fig. 5-21) to examine the spread of cracking.

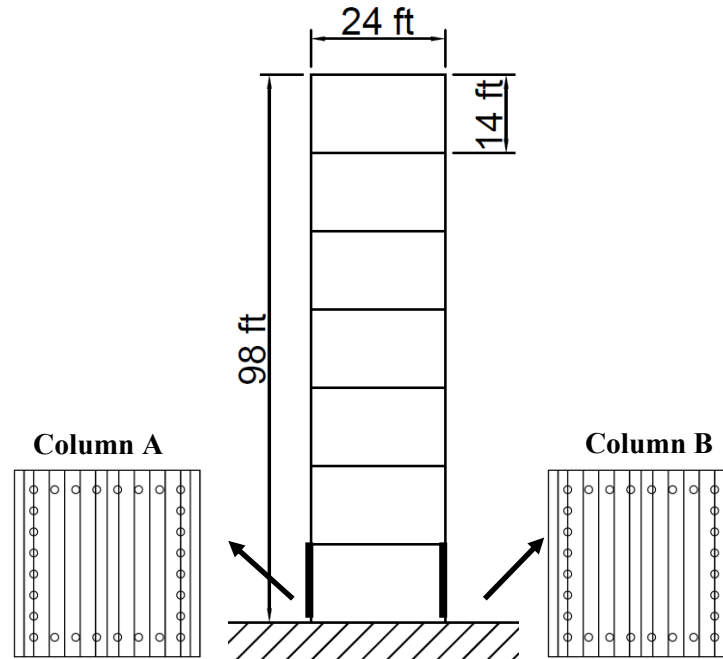


Figure 5-21: Overall view of base column sections for cracking study

### 5.3.1 Static Pushover Analysis

Static pushover analysis is a method to predict seismic capacity and deformation demand of a structure. The structure is pushed in a force- or displacement-controlled manner until the structure fails due to insufficient material strength or a local/global collapse mechanism is formed. The absence of inertial effects, the monotonic character of the loading (as opposed to cyclic or dynamic), and the influence of the choice of load profile can affect the structural responses under the pushover analysis. This implies that this analysis might not be as accurate as a dynamic analysis using ground accelerations as input.

The static pushover analysis in this study was terminated when the first fibre in the confined concrete or ECC core regions achieved their crushing strain in compression, which was defined as 0.006 for confined concrete and 0.02 for confined ECC.

Base shear and drift percentage of the roof were recorded for both the RC and RECC cases. The cracking mechanism of the two base columns was studied by examining the stress-strain behaviour of the material at different fibres in the cross-section.

### 5.3.1.1 Results and Discussion

Figure 5-22 shows the base shear versus roof drift relationships for the RC frame and the associated cracking conditions at both base columns A and B at the ground-column interface. If a given concrete fibre reaches its ultimate tensile strain, it is shown in black color to represent failure in localized crack.

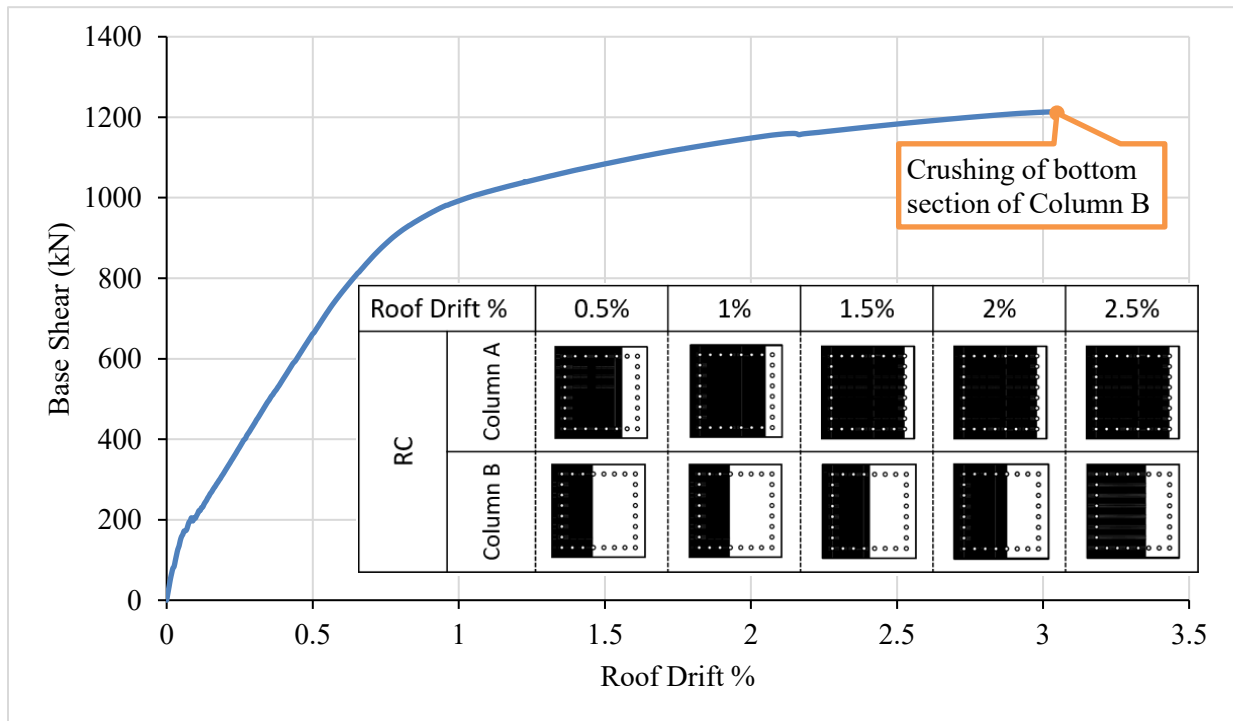


Figure 5-22: Shear-drift graph of RC building with associated cracking conditions

Column A cracked rapidly starting at 0.055% drift while Column B started cracking from 0.093% drift. After 0.5% drift where concrete had experienced significant cracking, both base concrete column A and B continued to crack slowly.

Fig. 5-21 illustrates the base shear versus roof drift responses of the RECC frame with ECC confinement material having different exponential terms for the descending branch (section 5.4.1.2.3).

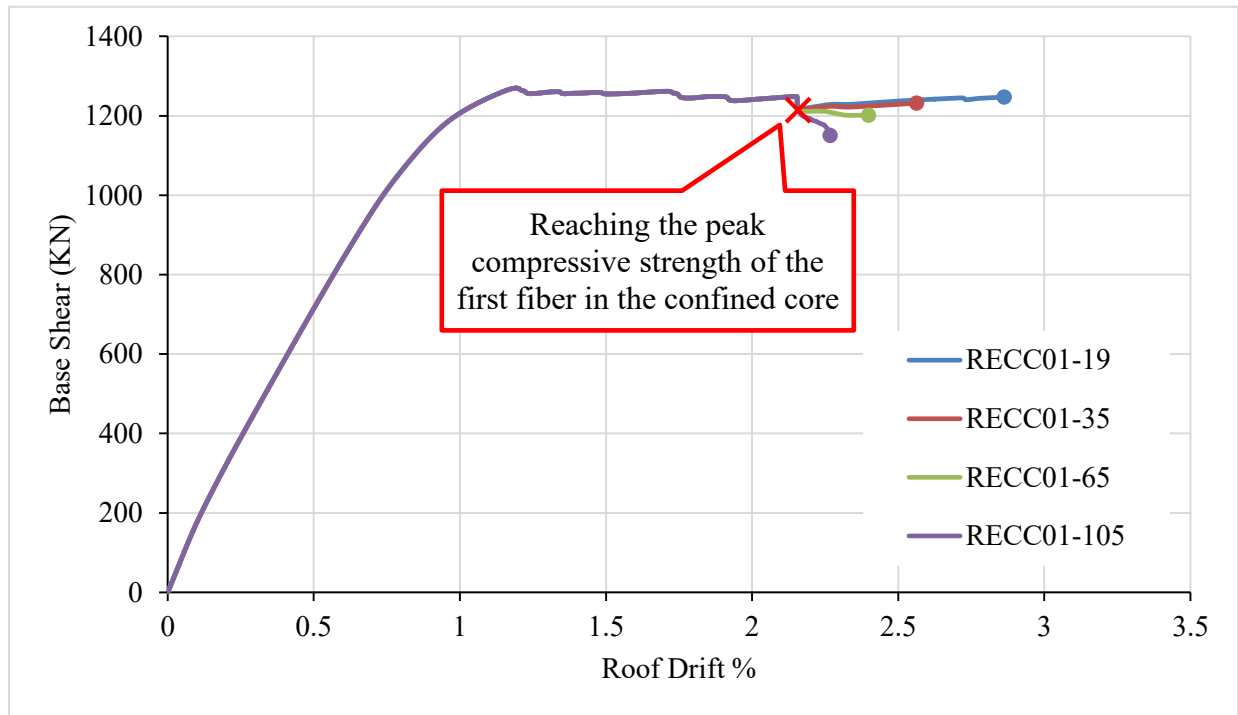


Figure 5-23: Base shear – Roof drift of RECC building

As expected, the responses of RECC01-19, RECC01-35, RECC01-65, and RECC01-105 (the value after the dash corresponds to the value of the parameter **alpha<sub>CU</sub>** in the ECC01 material) are the same until the ECC core fibres reach the maximum compressive stress. After this point, the results show slightly different shear-roof drift responses where RECC01-105 shows a decreasing shear strength and RECC01-19 shows a higher shear versus roof drift relationship. The decreasing shear strength of RECC01-105 is due to its compressive strain-stress curve (Fig. 5-16) which has a lower post-peak strength. In contrast, the higher ultimate shear strength of RECC01-19 is due to its compressive strain-stress curve (Fig. 5-16) which has a higher post-peak strength.

For simplicity, the pushover curve of RECC01-19 was used to investigate the cracking condition. If a given ECC fibre exceeds the ultimate tensile strain of ECC, it is shown in a striped hatch. Note

that values of strain lesser than the ultimate tensile strain correspond to a state in which the ECC is assumed to present multiple microcracks.

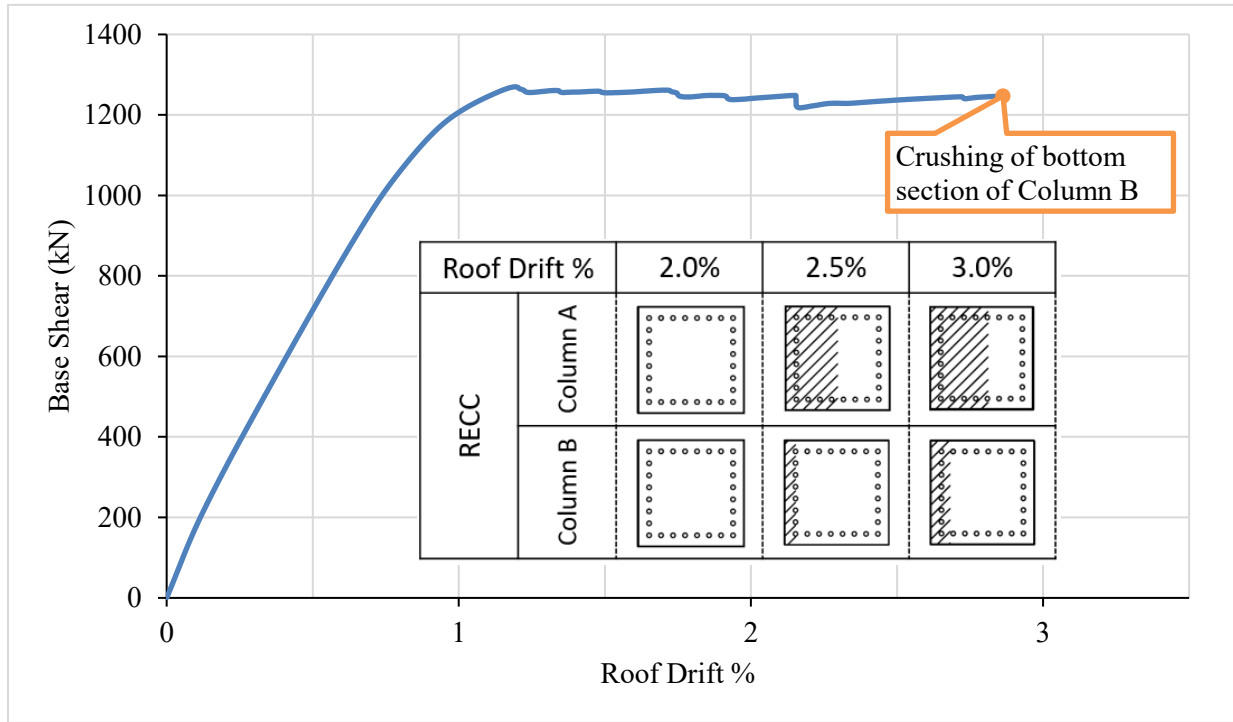
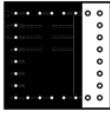
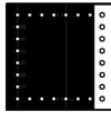
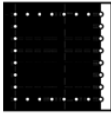
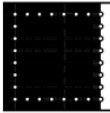
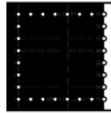
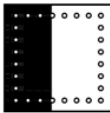
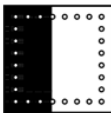
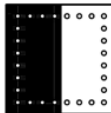
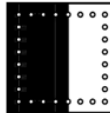
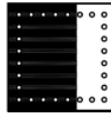
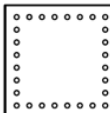
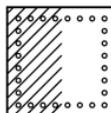
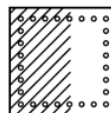
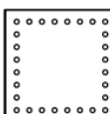
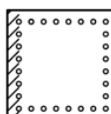
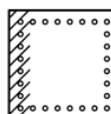


Figure 5-24: Shear-Drift graph of RECC (RECC01-19) building with associated cracking conditions

Figure 5-24 shows the cross-sectional cracking of column A and B in the RECC frame over the pushover analysis. Column A experienced cracking starting at 2.15% drift, which spread rapidly. Column B started cracking gradually from 2.17% drift.

The overall cracking mechanism in Fig. 5-22 and 5-24 is summarized in Table 5-1. In comparison, RC base columns started cracking rapidly from 0.055% while RECC base columns first start cracking gradually at 2.17% drift. When both frames reach failure at ultimate roof drift, RECC columns show a significant reduction in failure cracking than RC columns even at a higher roof drift. The results demonstrate that RECC base columns are able to sustain larger drift with less damage from cracking.

Table 5-1: Summary of RC and RECC base columns cracking

Roof Drift %		0.5%	1%	1.5%	2%	2.5%	3%
RC	Column A						
	Column B						
RECC	Column A						
	Column B						

### 5.4.1 Dynamic Analysis

A dynamic analysis is conducted to investigate the structural behaviour of the RC and RECC frames under seismic load. The Rinaldi record of the Northridge earthquake (1994) in California was applied to the 7-storey frames.

The RECC frame in this case was also modeled with the ECC-19 material model to represent confined ECC. Roof displacement during the earthquake over time was recorded for both the RC and RECC frames. The cracking mechanism of the two base columns (columns A and B) in both cases was studied by examining the stress-strain behaviour of the material at different fibre on the cross-section.

### 5.4.1.1 Results and Discussion

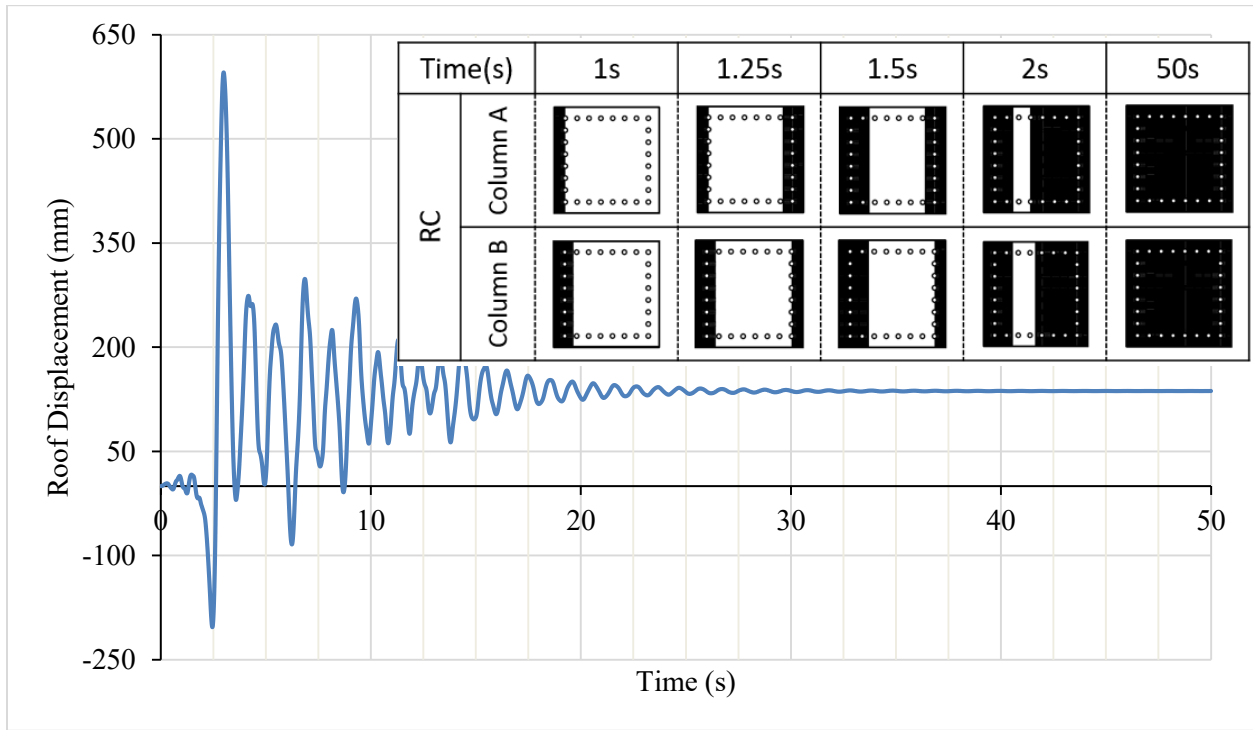


Figure 5-25: Roof Displacement of RC Building with associated Cracking Conditions

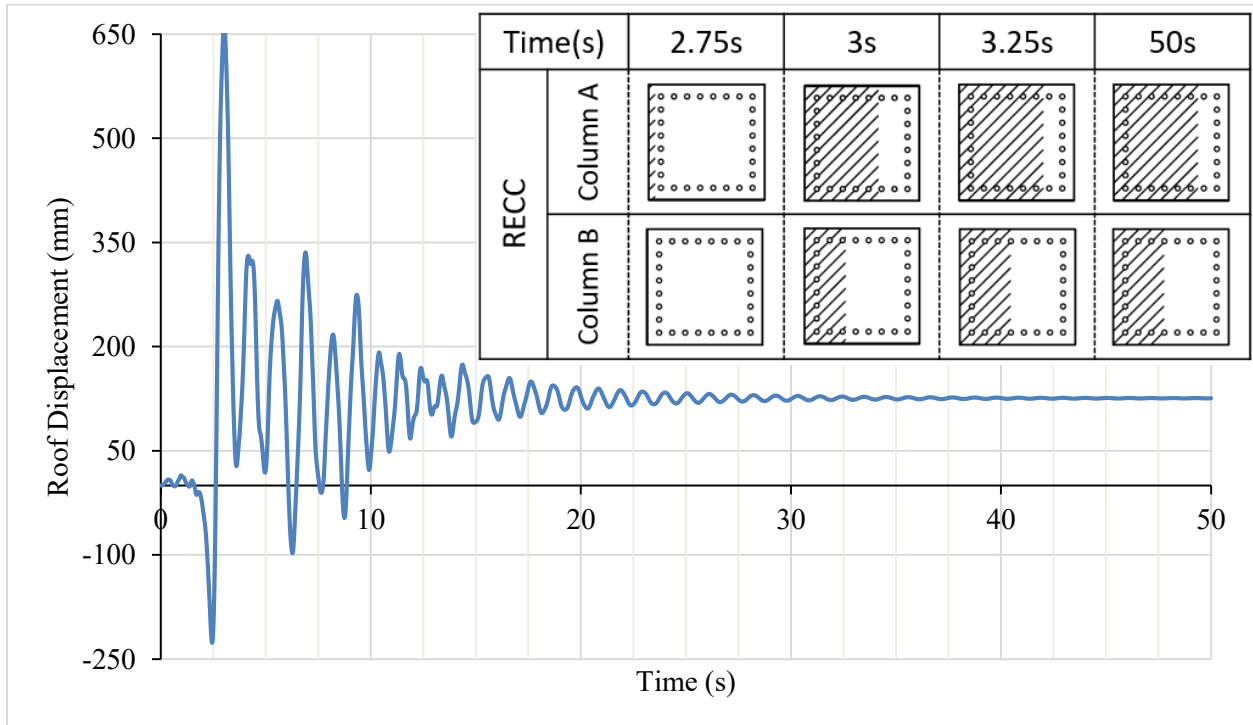


Figure 5-26: Roof Displacement of RECC Building with associated Cracking Conditions

Figure 5-25 and 5-26 illustrate the roof displacements of RC and RECC frames over time under the Northridge earthquake. It is shown that the maximum displacement at the roof for both the RC and RECC buildings during the earthquake are similar. It is noted that the Rinaldi record from the Northridge earthquake is a so-called near-fault seismic motion, which contains a velocity pulse that pushes structures predominantly in one direction. This tends to produce significant residual displacements, such as the ones seen in Figs. 5-25 and 5-26.

Figure 5-25 shows cross-sectional cracking of column A and B in RC frame over time. It shows that the outer part of the RC base column A and B starts cracking at time 1.0 s where the ground vibration starts. Then RC base column A and B experience significant cracking all over the cross section when RC frame approaching -200 mm roof displacement at 2.5 s. As the result, both RC column A and B have already been fully cracked and possibly spalled from the seismic load by time 2.5 s. Figure 5-26 shows the cross-sectional cracking of column A and B in the RECC frame over time. It shows that RECC base column A and B are able to withstand 200 mm of roof displacement at 2.5 s with no major cracking. RECC base columns have not formed failure cracks until the frame starts approaching 650 mm roof displacement at 2.75 s. As a result, both RECC base column A and B only have been cracked only on one side and result in 73% and 46% damaged area in the left and right base columns, respectively, after the earthquake. The cracking results of RC base columns illustrate that conventional concrete material has already experienced excessive localized cracking only with small ground movement and leads to full damage before the earthquake ended. The cracking state at the RECC base columns indicate that ECC material is able to tolerate some ground movement without forming cracks and thereby results in less damage after the earthquake.



## CHAPTER 6.SUMMARY AND CONCLUSIONS

### 6.1 Summary

Rectangular confinement effect on Engineered Cementitious Composites (ECC) was studied in three main objectives in this research. An experimental study on ECC fabrication with local Western Canada material together with PVA fibres from Japan and material characterization was conducted. An experimental program on small-scale square columns made with optimized ECC and confined with rectangular stirrups was performed. A parametric study of large-scale reinforced-ECC structures with square columns was developed by finite-element (FE) modeling.

The feasibility of future large-scale ECC fabrication with local Western Canada material together with PVA fibres from Japan was studied accompanied by material characterization. Nine trial mixes with different modification on mix proportion and mixing procedure were conducted. Uniaxial tensile and compressive tests were performed on the specimens. The ECC with the best tensile performance was chosen to be the constitutive material used in the column tests. The uniaxial compressive responses of the optimal ECC showed a compressive strength of 74.13 MPa at a strain of 0.00623 with a gradual descending post-peak branch. A gradual bulging failure rather than an explosive crushing failure was observed. ECC09 resulted in a modulus of elasticity (E) of 16399 MPa, and Poisson's ratio of 0.153. According to the definition of ACI Committee 363 (2005), the optimal ECC is considered as a high-strength ECC in this case. The uniaxial tensile responses of the optimal ECC showed a tensile strength of 2.6 MPa and an ultimate strain of 0.015. The cracking of the optimal ECC illustrated microcracks had developed along the specimen after the tensile test. By comparison, the optimal ECC achieved up to 234 times higher tensile strain capacity than conventional concrete.

Sixteen 100 mm x 100 mm x 300 mm ECC square columns, which consisted of one set of unconfined ECC and three sets of confined ECC with 1%, 1.5%, and 2% steel were tested under monotonic axial compressive load. A set of unconfined concrete columns was also tested as control specimens. A test set-up was designed to investigate the behaviours of confined ECC columns and the stress-strain response of rectangularly confined ECC in square columns was studied. An empirical stress-strain model for rectangularly confined high-strength ECC was developed with the test results from the small-scale ECC square columns.

A parametric study on a full-scale reinforced-ECC structure was conducted in an FE software, OpenSEES. A FE validation model of confined ECC in square columns was developed to predict the behaviour of ECC column elements. The analytical results showed a reasonable accuracy in comparison to the experimental results obtained from the experimental programme. By adopting the proposed confinement model, a 7-storey reinforced ECC (RECC) frame with square columns was investigated to study the system-level performance of ECC. Dynamic analyses and static pushover analyses were conducted to study the structural performance of ECC in terms of strength, ductility, and cracking mechanism.

## **6.2 Conclusions**

The following conclusions highlighted the findings and knowledge obtained from this research:

### **6.2.1 ECC Fabrication and Characterization**

1. The mixing procedures and mix proportion of a high-performance and high-strength ECC mix was optimized. As all the steps are reproducible in large-scale manufacturing processes, large-scale ECC fabrication with local western Canada raw materials together with PVA fibres from Japan is deemed to be feasible.
2. Workability, bleeding or cold joints were identified as the main problems in fabricating ECC. The mix proportion and mix procedures of the optimal ECC which presented good workability with no bleeding or cold joint problem were found to be most optimal for fabrication.
3. Overusing chemicals such as superplasticizer and stabilizer to control workability can lead to serious bleeding problems in ECC fabrication. Stabilizer should be omitted in ECC fabrication since it affected the setting time for consolidation. Suitable amount of superplasticizer can accommodate workability for ECC fabrication.
4. Specimens with bleeding or cold joint problem were found to have undesirable behaviour on compressive and tensile behaviours. Specimens with bleeding problem showed lower tensile strain capacities and unusual compressive post-peak responses. Specimens with cold joints showed lower tensile strain capacities, lower compressive strength with non-probably post-peak responses.
5. Water/cement (w/c) ratio was found to have a direct influence in mechanical properties in

ECC. The specimen with the highest w/c ratio had the lowest tensile strain capacity and the lowest compressive strength.

6. Mixing procedures were found to affect the workability which associated with cold joints problem. The original mixing procedure proposed from Li (2008), where silica sand should mix with water before adding other dry components, was not able to accommodate the use of the local western Canada material. The mixing procedure was altered to mix all dry components such as silica sands, cement, and fly ash with water and superplasticizer together. This optimized mixing procedure was found to be a better option for ECC to exhibit a good workability.

### **6.2.2 Confinement effect on ECC**

1. The general behaviour of unconfined ECC columns and unconfined concrete columns presented size effect and boundary effects. In comparison to the unconfined concrete columns, unconfined ECC columns showed a gradual degradation instead of the sudden brittle failure like unconfined concrete columns.
2. The general behaviour of confined ECC columns (ECC-1%, ECC-1.5%, ECC-2%) showed four main stages: (1) an initial, ascending, quasi-linear stage; (2) the attainment of peak compressive strength; (3) a gradual post-peak descending branch; and (4) a plateau-like region of residual stress. The results showed that there is no significant increase in peak strength due to transverse reinforcement. The only strength gain due to the use of more stirrups was observed as a more stable post-peak behaviour in terms of residual stresses.
3. A few microcracks was observed on the all specimens at the maximum axial load. After microcracking occurred, the cracks developed into larger cracks as the specimen entered the post-peak stage.
4. An empirical stress-strain model of rectangularly confined ECC in square column was proposed based on an existing confinement model for high-strength concrete. The maximum compressive strength equation from Bjerkeli et al (1990) model was originally based on the unconfined compressive strength from concrete cubes. It was modified to account for the unconfined compressive strength either from conventional cylinder tests or unconfined ECC column tests in this study.
5. The proposed model showed reasonable correspondence with the test results and was able

to capture the main features of confined ECC rectangular columns with square stirrups.

### 6.2.3 Parametric Study

1. A validation of confined ECC in square columns using was conducted in OpenSEES using *Concrete02* material. The load-displacement results showed a good prediction in comparison to the experimental results.
2. The proposed confinement model of ECC was utilized in RECC frame modeling. Due to the limitation of *Concrete02* material which only allow tension softening, the confined ECC in RECC frame ECC was decided to be modeled with *ECC01* which allows tensile ductility.
3. Although *ECC01* is a better option to model unconfined and confined ECC for rectangular elements for tensile behaviour, the compressive behaviour of *ECC01* only allows zero strength at the ultimate strain. Due to the restraint of the *ECC01*, the confined ECC was modeled into the best fit *ECC01* compressive stress-strain curve to accommodate the residual stress obtained from the experimental results.
4. Static pushover analyses illustrated that ECC formed fewer cracks at larger drift ratios compared to conventional RC. This demonstrated that ECC material can provide ductility to a high degree of deformation while control cracking.
5. Dynamic analyses showed that the RECC frame can reduce cracking during a seismic event, which leads to smaller overall structural damages. This demonstrated the high damage tolerance of ECC.
6. Finite-element analysis for full-scale RECC structure was feasible, as well as the structural performance evaluation of plastic hinges.

### 6.3 Recommendations for Future Work

The following recommendations can be considered for future work:

- ECC fabrication study can be conducted on other type of ECC.
- The experimental results of the small-scale confined ECC columns showed no significant increase in peak strengths. Strain gauges can be installed on the confining stirrups to have a better understanding the confining stress. Further study on the confining stress on ECC can be done to improve the equation of compressive strength of confined ECC.
- An additional number of specimens to be tested and obtain greater statistical significance.
- Further investigation on the size effect and boundary effect on ECC columns can also be done to improve the equation of compressive strength of confined ECC.
- Beside circular and simple square confinement, different other combination of confinement can be performed to investigate the confinement effect on ECC.
- Beside monotonic axial compressive load, cyclic loading can be also applied to confined ECC to understand the unloading behaviour.
- As part of further parametric studies, the source code of *ECC01* in OpenSEES can be modified to accommodate the experimental data and improve the simulation of RECC structures.
- Other plastic hinges of the full-scale RECC structure can be studied to fully evaluate the structural performance and material responses.

## REFERENCES

- ACI Committee 363. (2005). High-Strength Concrete (ACI 363R). Special Publication, 228, 79-80
- ASTM, A. (2014). C469/C469M-14-Standard Test Method for Static Modulus of Elasticity and Poisson's Ratio of Concrete in Compression. USA: ASTM International.
- Avenston, J., Cooper, G. A., & Kelly, A. (1971). Single and multiple fracture in the properties of fiber-composites. Proceedings of the National Physical Laboratory, 15-26.
- BASF official website. MasterGlenium 7700: High-range water-reducing admixture for producing consistent concrete mixtures. Retrieved from: <https://www.master-builders-solutions.basf.us/en-us/products/masterglenium/1727>
- Bertero, V. V., Felippa, C., Roy, H. E. H., & Sozen, M. A. (1964, November). Discussion of Ductility of Concrete. In Proceedings of International Symposium on the Flexural Mechanics of Reinforced Concrete, ASCE-ACI, Miami (pp. 227-234).
- Bjerkeli, L., Tomaszewicz, A., & Jensen, J. J. (1990). Deformation properties and ductility of high-strength concrete. Special Publication, 121, 215-238.
- Boshoff, W.P. & van Zijl, G.P.A.G. (2007). Tensile creep of SHCC. In Proceedings of the Fifth International RILEM Workshop on High-Performance Fiber-Reinforced Cement Composites (HPFRCC 5), Reinhardt, H.W. and Naaman, A.E., Eds., pp. 87–96. RILEM, Paris.
- Chadwell, C.B., Imbsen & Associates. (2002). XTRACT - Cross Section Analysis Software for Structural and Earthquake Engineering". <http://www.imbsen.com/xtract.htm>
- Cruz, C. A. and Saiidi, M. (2010). "Experimental and Analytical Seismic Studies of a Four-Span Bridge System with Innovative Materials" Technical Rep. No. CCEER-10-04, Center for Civil Engineering Earthquake Research, Dept. of Civil Engineering, Univ. of Nevada, Reno, NV.
- Curbach, M. & Jesse, F. (1999). High-performance textile-reinforced concrete. Struct. Eng. Int., 9(4), 289–291.
- De Koker, D., & Van Zijl, G. P. A. G. 2004. Extrusion of engineered cement-based composite material. In Proceedings of the 6th RILEM Symposium on Fiber-Reinforced Concretes (FRC) (pp. 20-22).
- Fischer, G. & Li, V.C. (2002). Effect of matrix ductility on deformation behavior of steel reinforced ECC flexural members under reversed cyclic loading conditions. ACI Struct. J., 99 (6), 781–790.

- Fukuyama, H., Matzuzaki, Y., Sato, Y., Iso, M., & Suwada, H. (2000). Structural performance of engineered cementitious composite elements. In Proceedings of the 6th ASCCS International Conference on Steel–Concrete Composite Structures, March 22–24, Los Angeles, CA.
- Han, T. S., Feenstra, P. H., & Billington, S. L. (2003). Simulation of highly ductile fiber-reinforced cement-based composite components under cyclic loading. *Structural Journal*, 100(6), 749-757.
- Inaguma, H., Seki, M., Suda, K., & Rokugo, K. (2006). Experimental study on crack-bridging ability of ECC for repair under train loading. In *International RILEM Workshop on High Performance Fiber Reinforced Cementitious Composites in Structural Applications* (pp. 499-508). RILEM Publications SARL.
- Johnson, N., Ranf, R. T., Saiidi, M. S., Sanders, D., & Eberhard, M. (2008). Seismic testing of a two-span reinforced concrete bridge. *Journal of Bridge Engineering*, 13(2), 173-182.
- Kamal, A., Kunieda, M., Ueda, N., & Nakamura, H. (2007). Assessment of crack elongation performance in RC beam repaired by UHP–SHCC. In *Proceedings of the Ninth International JSCE Summer Symposium*, September 18, Yokohama National University, Japan.
- Kanda, T., & Li, V. C. (1998). Interface property and apparent strength of high-strength hydrophilic fiber in cement matrix. *Journal of materials in civil engineering*, 10(1), 5-13.
- Kanda, T., Nagai, S., Maruta, M., & Yamamoto, Y. (2011, December). New high-rise R/C structure using ECC coupling beams. In *2nd International RILEM Conference on Strain Hardening Cementitious Composites*, Rio de Janeiro (pp. 12-14).
- Kent, D. C., and Park, R. (1971), "Flexural members with confined concrete", *J. Struct. Div., ASCE*, 97(7), pp. 1969-1990.
- Kim, Y.Y., Fischer, G., & Li, V.C. (2004). Performance of bridge deck link slabs designed with ductile ECC. *ACI Struct. J.*, 101(6), 792–801.
- Kojima, S., Sakata, N., Kanda, T., & Hiraishi, T. (2004). Application of direct sprayed ECC for retrofitting dam structure surface-application for Mitaka-Dam. *Concrete Journal*, 42(5), 135-139.
- Kotsovos, M. D. (1983). Effect of testing techniques on the post-ultimate behaviour of concrete in compression. *Materiaux et construction*, 16(1), 3-12.
- Krenchel, H. & Stang, H. (1989). Stable microcracking in cementitious materials. In *Brittle Matrix Composites 2*, Br&t, A.M. & Marshall, J.H., Eds., pp. 20–33. Elsevier, Amsterdam.

- Kunieda, M. & Rokugo, K. (2006a). Measurement of crack opening behavior within ECC under bending moment. In Proceedings, High-Performance Fiber-Reinforced Cementitious Composites (HPFRCC) in Structural Applications, Fischer, G. & Li, V.C., Eds., pp. 313–322. RILEM, Paris.
- Kunieda, M., & Rokugo, K. (2006b). Recent progress on HPFRCC in Japan. *Journal of Advanced Concrete Technology*, 4(1), 19-33.
- Kurary official website A. Kuralon™ and Kuralon K-II™. Retrieved from: <http://www.kuraray.us.com/products/fibers/kuralon-and-kuralon-k-ii/>
- Kurary official website B. Mechanical Properties of PVA Fiber. Retrieved from: <http://www.kuraray.co.jp/kii/english/07.html>
- Lai, M., Ho, J. C. M., & Pam, H. J. (2014). Experimental studies of spiral-confined HSCFST columns under uni-axial compression. *World Academy of Science, Engineering and Technology, International Journal of Civil, Environmental, Structural, Construction and Architectural Engineering*, 8(6), 576-582.
- Lepech, M. D., & Li, V. C. (2009). Application of ECC for bridge deck link slabs. *Materials and Structure*
- Lepech, M.D., Li, V.C., Robertson, R.E., & Keoleian, G.A. (2007). Design of ductile engineered cementitious composites for improved sustainability. *ACI Mater. J.*, submitted.
- Li, V. C. & Leung, C. K. Y. (1992). “Steady state & multiple cracking of short r&om fiber composites.” *ASCE J. of Engineering Mechanics*, 118 (11), 2246-2264.
- Li, V. C. (1992). “Post-crack scaling relations for fiber reinforced cementitious composites.” *ASCE J. of Materials in Civil Engineering*, 4 (1), 41-57.
- Li, V. C. (1993). From micromechanics to structural engineering-the design of cementitious composites for civil engineering applications.
- Li, V. C. (2003). On engineered cementitious composites (ECC). *Journal of advanced concrete technology*, 1(3), 215-230.
- Li, V. C. (2006). Bendable Composites. *STRUCTURE*, 45.
- Li, V. C. (2008). Engineered Cementitious Composites (ECC) Material, Structural, and Durability Performance.
- Li, V. C., & Wang, S. (2002). Flexural behaviors of glass fiber-reinforced polymer (GFRP) reinforced engineered cementitious composite beams. *Materials Journal*, 99(1), 11-21.



- Li, V. C., Horikoshi, T., Ogawa, A., Torigoe, S., & Saito, T. (2004a). Micromechanics-based durability study of polyvinyl alcohol-engineered cementitious composite. *Materials Journal*, 101(3), 242-248.
- Li, V. C., Mishra, D. K., Naaman, A. E., Wight, J. K., LaFave, J. M., Wu, H. C. & Inada, Y. (1994). "On the shear behavior of engineered cementitious composites." *J. of Advanced Cement Based Materials*, 1 (3), 142-149.
- Li, V. C., Stang, H. & Krenchel, H. (1993). "Micromechanics of crack bridging in fiber reinforced concrete." *J. of Materials & Structures*, 26, 486-494.
- Li, V. C., Wang, S., & Wu, C. (2001). Tensile strain-hardening behavior of polyvinyl alcohol engineered cementitious composite (PVA-ECC). *ACI Materials Journal-American Concrete Institute*, 98(6), 483-492.
- Li, V. C., Wu, C., Wang, S., Ogawa, A., & Saito, T. (2002). Interface tailoring for strain-hardening polyvinyl alcohol-engineered cementitious composite (PVA-ECC). *Materials Journal*, 99(5), 463-472.
- Li, V.C. & Lepech, M. (2004). Crack-resistant concrete material for transportation construction. In *Proceedings of the Transportation Research Board 83rd Annual Meeting, Compendium of Papers CD-ROM, Paper 04-4680*. Transportation Research Board, Washington, D.C.
- Li, V.C. & Yang, E.H. (2007). Self-healing in concrete materials. In *Self-Healing Materials: An Alternative Approach to 20 Centuries of Materials Science*, van der Zwaag, S., Ed., pp. 161–193. Springer, New York.
- Li, V.C., Fischer, G., Kim, Y.Y., Lepech, M., Qian, S., Weimann, M., & Wang, S. (2003). Durable Link Slabs for Jointless Bridge Decks Based on Strain-Hardening Cementitious Composites, RC-1438. Michigan Department of Transportation, Lansing.
- Li, V.C., Lepech, M., Wang, S., Weimann, M., & Keoleian, G. (2004b). Development of green ECC for sustainable infrastructure systems. In *Proceedings of the International Workshop on Sustainable Development & Concrete Technology*, May 20–21, Beijing, China, Wang, K., Ed., pp. 181–192.
- Lin, Z. & Li, V. C. (1997). "Crack bridging in fiber reinforced cementitious composites with slip-hardening interfaces." *J. Mechanics & Physics of Solids*, 45 (5), 763-787.
- Lin, Z., K&a, T. & Li, V. C. (1999). "On interface property characterization & performance of fiber reinforced cementitious composites." *RILEM J. Concrete Science & Engineering*, 1, 173-184.
- Maalej, M. & Li, V.C. (1994). Flexural/tensile strength ratio in engineered cementitious composites. *ASCE J. Mater. Civil Eng.*, 6(4), 513–528.

- Mander, J. B., Priestley, M. J., & Park, R. (1988). Theoretical stress-strain model for confined concrete. *Journal of structural engineering*, 114(8), 1804-1826.
- Martinez, S., Nilson, A. H., and Slate, F. O. (1984). "Spirally reinforced high-strength concrete columns." *ACI Struct. J.*, 81(5), 431-442.
- Mazzoni, S., McKenna, F., Scott, M. H., & Fenves, G. L. 2006. *The Open System for Earthquake Engineering Simulation (OpenSEES) User Command-Language Manual*.
- McKenna, F. and Fenves, G. 2000. An Object-Oriented Software Design for Parallel Structural Analysis. *Advanced Technology in Structural Engineering*: pp. 1-8.
- Menegotto, M. and P. E. Pinto (1973). Method of analysis for cyclically loaded R.C. plane frames including changes in geometry and non-elastic behaviour of elements under combined normal force and bending. *Symposium on the Resistance and Ultimate Deformability of Structures Acted on by Well Defined Repeated Loads*, International Association for Bridge and Structural Engineering. Zurich, Switzerland: 15-22.
- Mitamura, H., Sakata, N., Shakushiro, K., Suda, K., & Hiraishi, T. (2005). Application of overlay reinforcement method on steel deck utilizing engineered cementitious composites-Mihara Bridge. *Bridge and Foundation Engineering*, 39(8), 88-91.
- Mobasher, B., Peled, A., & Pahilajani, J. (2006). Distributed cracking and stiffness degradation in fabric-cement composites. *Materials and structures*, 39(3), 317-33
- Mohd Hisham Mohd Yassin, "Nonlinear Analysis of Prestressed Concrete Structures under Monotonic and Cycling Loads", PhD dissertation, University of California, Berkeley, 1994.
- Mohebbi, A. (2017). *Development and Seismic Evaluation of Pier Systems w/Pocket Connections, CFRP Tendons, and ECC/UHPC Columns* (Doctoral dissertation).
- Monteiro, P. (2006). *Concrete: Microstructure, Properties, and Materials*. McGraw-Hill Publishing.
- Moore, N.C. (2009). Self-healing concrete could toughen infrastructure. *The University Record Online For Faculty and Staff of the University of Michigan*. [http://www.ur.umich.edu/0809/Apr27\\_09/16.php](http://www.ur.umich.edu/0809/Apr27_09/16.php)
- Motaref S, Saiidi M S and Sanders D H (2011). "Seismic response of precast bridge columns with energy dissipating joints Report" No CCEER-11-01 Center for Civil Engineering Earthquake Research, Department of Civil Engineering, University of Nevada, Reno
- Naaman, A.E. and Reinhardt, H.W. (2003). Setting the stage: toward performance-based classification of FRC composites. In *Proceedings of the Fourth International RILEM Workshop on High-Performance Fiber-Reinforced Cement Composites (HPFRCC 4)*, Naaman, A.E. and Reinhardt, H.W., Eds. RILEM, Paris.

- Park, R. and Paulay, T. (1975) "Reinforced Concrete Structures", J.Wiley & Sons, New York
- Parra-Montesinos, G. & Wight, J.K. 2000. Seismic response of exterior RC column-to-steel beam connections. *ASCE J. Struct. Eng.*, 126(10), 1113–1121.
- Popovics, S. (1973). A numerical approach to the complete stress-strain curve of concrete. *Cement and concrete research*, 3(5), 583-599.
- Qudah, S., & Maalej, M. (2014). Application of Engineered Cementitious Composites (ECC) in interior beam–column connections for enhanced seismic resistance. *Engineering Structures*, 69, 235-245.
- Ramirez, C. M., & Miranda, E. (2012). Significance of residual drifts in building earthquake loss estimation. *Earthquake Engineering & Structural Dynamics*, 41(11), 1477-1493.
- Rayleigh, J. W. S. B. (1896). *The theory of sound* (Vol. 2). Macmillan.
- Reinhardt, H.W., Krüger, M., & Große, C.U. (2003). Concrete prestressed with textile fabric. *J. Adv. Concrete Technol.*, 1(3), 231–239.
- Rokugo, K., Kunieda, M., & Lim, S. C. (2005). Patching repair with ECC on cracked concrete surface. *Proc. of ConMat05, Vancouver, Canada [CD-ROM]*.
- Romualdi, J.P. & Mandel, J.A. (1964). Tensile strength of concrete affected by uniformly distributed closely spaced short lengths of wire reinforcement. *Proc. ACI J.*, 61(6), 657–671.
- Romualdi, N.P. & Batson, G.B. (1963). Mechanics of crack arrest in concrete. *Proc. ASCE Eng. Mech. J.*, 89(EM3), 147–168.
- Şahmaran, M., & Li, V. C. (2007b). De-icing salt scaling resistance of mechanically loaded engineered cementitious composites. *Cement and Concrete Research*, 37(7), 1035-1046.
- Şahmaran, M., & Li, V. C. (2008). Durability of mechanically loaded engineered cementitious composites under highly alkaline environments. *Cement and Concrete Composites*, 30(2), 72-81.
- Sahmaran, M., Lachemi, M., Hossain, K., Ranade, R., & Li, V. C. 2009. Influence of aggregate type and size on ductility and mechanical properties of engineered cementitious composites. *ACI Materials Journal*, 106(3), 308-316.
- Sahmaran, M., Li, M., & Li, V. C. (2007a). Transport properties of engineered cementitious composites under chloride exposure. *Materials Journal*, 104(6), 604-611.
- Schickert, G., & Winkler, H. (1977). RESULTS OF TEST CONCERNING STRENGTH AND STRAIN OF CONCRETE SUBJECTED TO MULTI-AXIAL COMPRESSIVE STRESS. *Deutscher Ausschuss für Stahlbeton, Heft 277, Berlin, West Germany*

- Shah, S. P., Fafitis, A., & Arnold, R. (1983). Cyclic loading of spirally reinforced concrete. *Journal of Structural Engineering*, 109(7), 1695-1710.
- Sheikh, S. A., & Uzumeri, S. M. (1980). Strength and ductility of tied concrete columns. *Journal of the structural division*, 106(ASCE 15388 Proceeding).
- Sheikh, S. A., & Yeh, C. C. (1986, May). Flexural behavior of confined concrete columns. In *Journal Proceedings* (Vol. 83, No. 3, pp. 389-404).
- Suda, K., & Rokugo, K. (2005). Anti-carbonization process utilizing direct sprayed ECC applying to railway viaduct involving flexural fatigue cracks. *Concrete Journal*, 43(5), 162-167.
- Sundara Raja Iyengar, K. T., Desayi, P., & Reddy, K. N. (1970). Stress-strain characteristics of concrete confined in steel binders. *Magazine of concrete research*, 22(72), 173-184.
- Suthiwarapirak, P., Matsumoto, T. & Kanda, T., (2002). Flexural fatigue failure characteristics of an engineered cementitious composite and polymer cement mortars. *JSCE J. Mater. Conc. Struct. Pavements*, 718(57), 121–134.
- Takashima, H., Miyagai, K., Hashida, T., & Li, V. C. (2003). A design approach for the mechanical properties of polypropylene discontinuous fiber reinforced cementitious composites by extrusion molding. *Engineering fracture mechanics*, 70(7), 853-870.
- Varela, S., & Saiid'Saiidi, M. (2013). Shear Behavior of Engineered Cementitious Composite Structural Members. In *Second conference on smart monitor, assessment and rehabilitation of civil structures*. Istanbul, Turkey.
- Wang, S. & Li, V.C. (2003). Materials design of lightweight PVA-ECC. In *Proceedings of the Fourth International RILEM Workshop on High-Performance Fiber-Reinforced Cement Composites (HPFRCC 4)*, Naaman, A.E. & Reinhardt, H.W., Eds., pp. 379–390. RILEM, Paris.
- Wang, S. & Li, V.C. (2006a). High early strength engineered cementitious composites. *ACI Mater. J.*, 103(2), 97–105.
- Wang, S. & Li, V.C. (2006b). Polyvinyl alcohol fiber-reinforced engineered cementitious composites: material design & performances. In *Proceedings, High-Performance Fiber-Reinforced Cementitious Composites (HPFRCC) in Structural Applications*, Fischer, G. & Li, V.C., Eds., pp. 65–73. RILEM, Paris.
- Wang, S. (2005). *Micromechanics-Based Matrix Design for Engineered Cementitious Composites*, Ph.D. thesis, University of Michigan, Ann Arbor.
- Wang, S., & Li, V. C. 2007. Engineered cementitious composites with high-volume fly ash. *ACI Materials Journal American Concrete Institute*, 104(3), 233-241.

- William, K. J. and Warnke, E. P. (1975). Constitutive model for the triaxial behavior of concrete. International association for bridge and structural engineering proceedings, 19, 1-30.
- Yang, E. H., & Li, V. C. (2010). Strain-hardening fiber cement optimization and component tailoring by means of a micromechanical model. Construction and building Materials, 24(2), 130-139.
- Yang, Y., Lepech, M., & Li, V.C. (2005). Self-healing of engineered cementitious composites under cyclic wetting & drying. In Proceedings of the International Workshop on the Durability of Reinforced Concrete Under Combined Mechanical & Climatic Loads (CMCL), October 27–28, Qingdao, China, pp. 231–242. © 2008
- Yong, Y. K., Nour, M. G., & Nawy, E. G. (1988). Behavior of laterally confined high-strength concrete under axial loads. Journal of Structural Engineering, 114(2), 332-351.
- Zhou, J., Qian, S., Ye, G., Copuroglu, O., van Breugel, K., & Li, V. C. (2012). Improved fiber distribution and mechanical properties of engineered cementitious composites by adjusting the mixing sequence. Cement and Concrete Composites, 34(3), 342-348.

## APPENDIX A – VARIATION IN MECHANICAL PROPERTIES OF ECC09

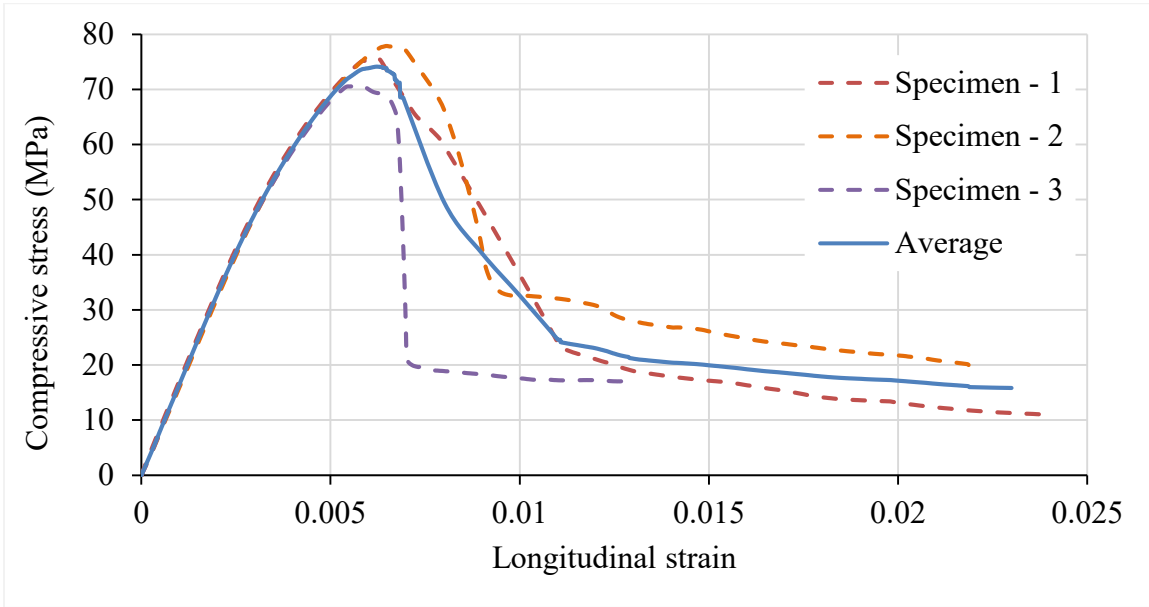


Figure A- 1: Uniaxial compressive stress-strain curves of ECC09

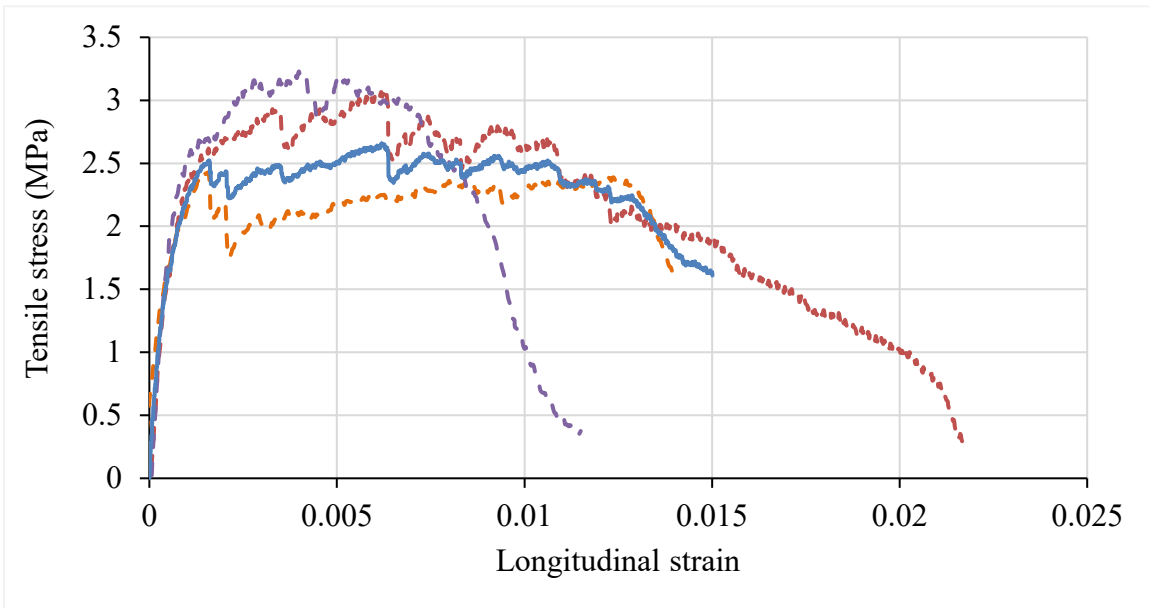


Figure A- 2: Uniaxial tensile stress-strain curves of ECC09

## APPENDIX B – POISSON'S RATIO OF ECC09

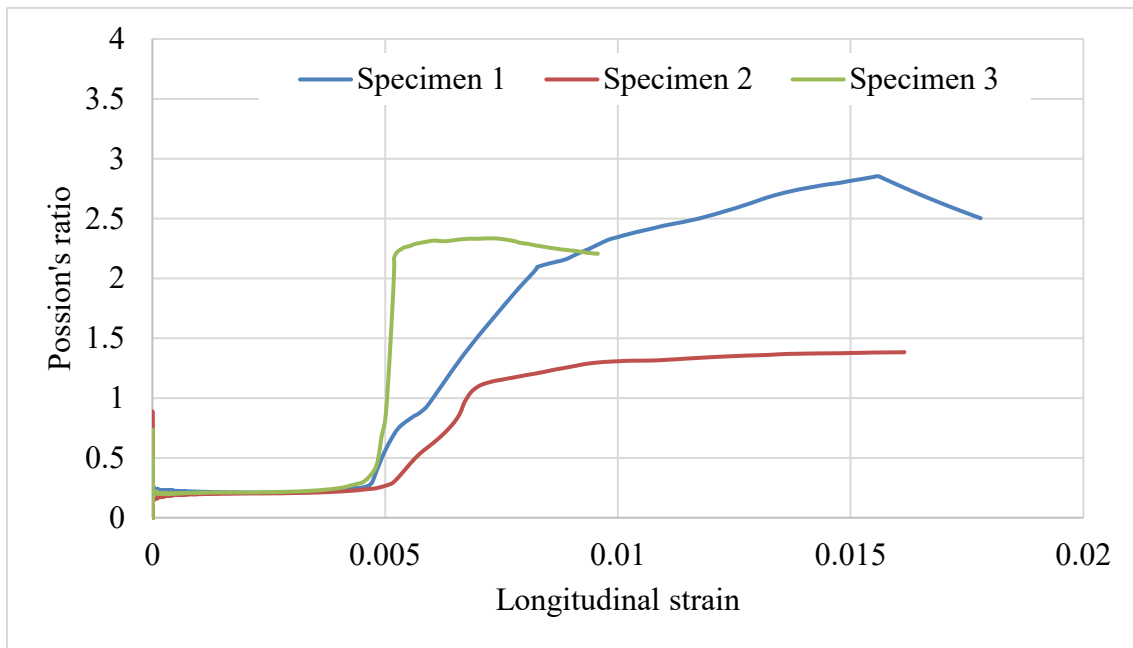


Figure B- 1: Poisson's ratios vs longitudinal strain of three ECC09 specimens

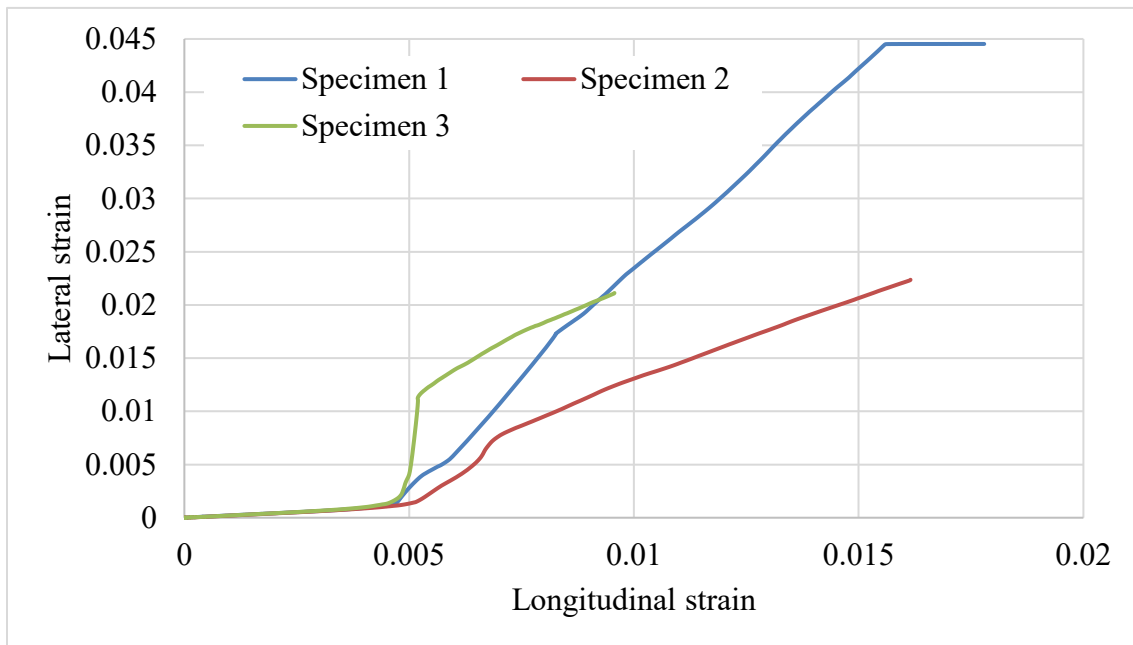


Figure B- 2: Lateral strain vs longitudinal strain of three ECC09 specimens

## APPENDIX C – AVERAGING PROCESS AND TEST VARIATIONS OF TESTED COLUMNS

The averaging of the load-displacement responses or stress-strain responses were computed by averaging the applied loads or stresses at each step of strain which was set to be 0.00005.

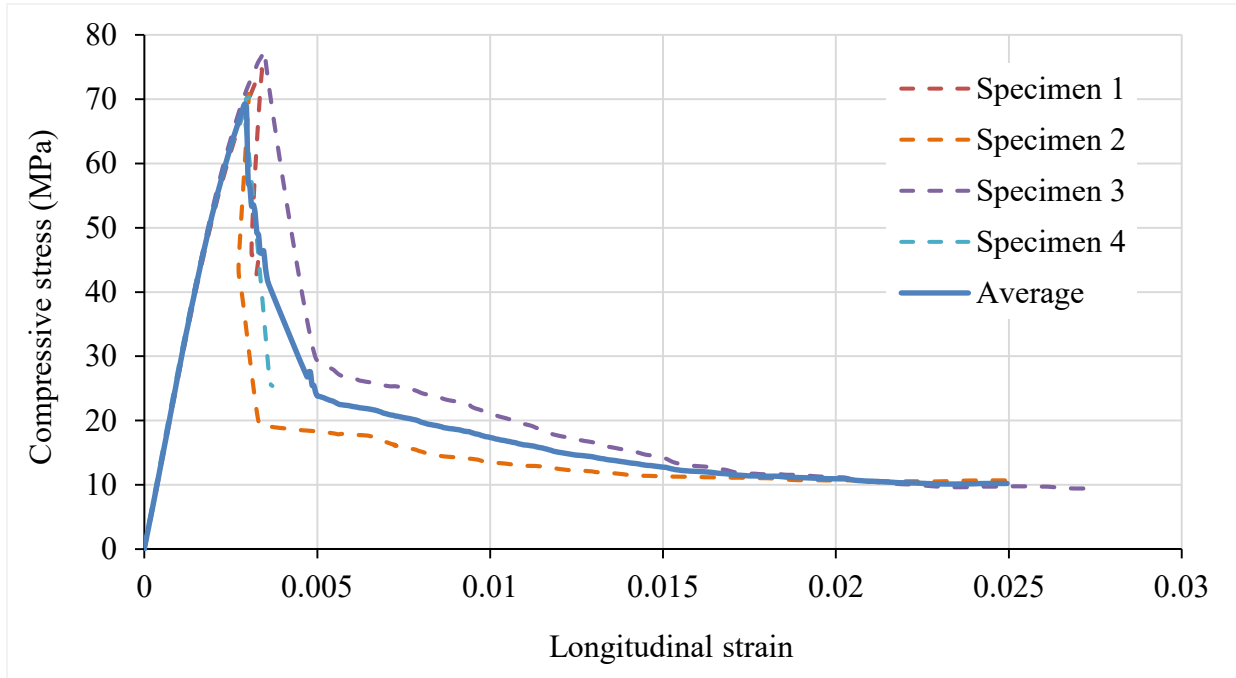


Figure C- 1: Stress-strain curves for 0% confinement ECC square columns



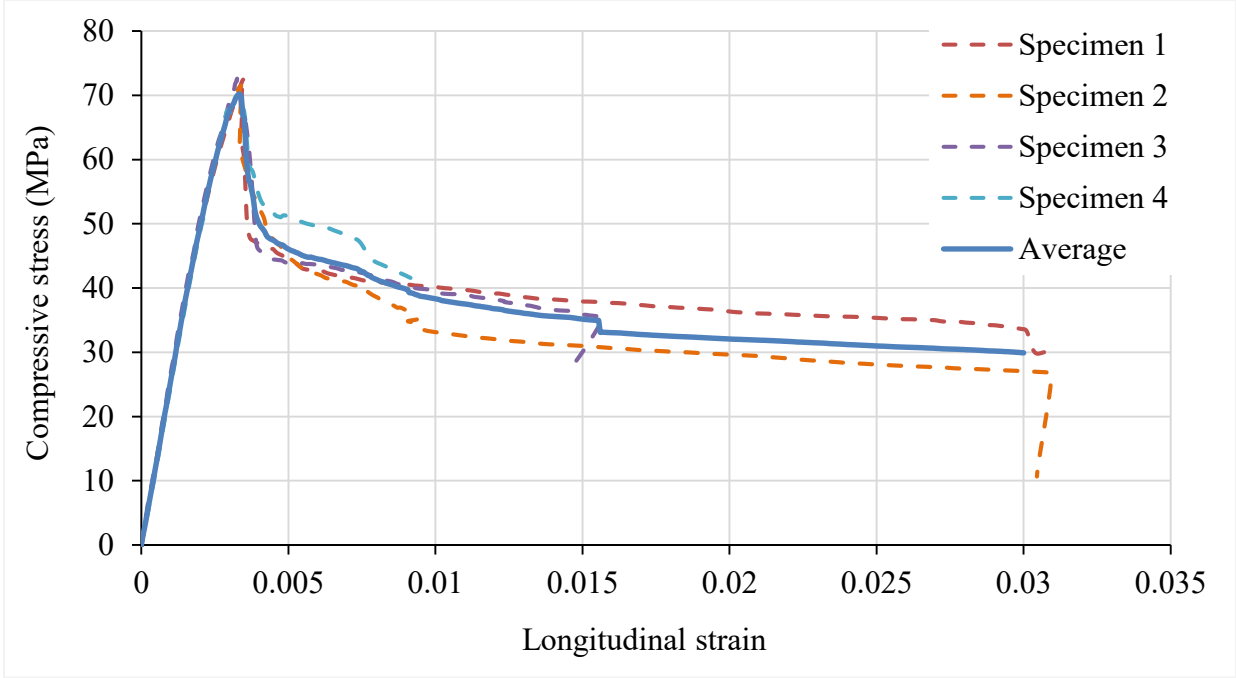


Figure B- 3: Stress-strain curves for 1% confinement ECC square columns

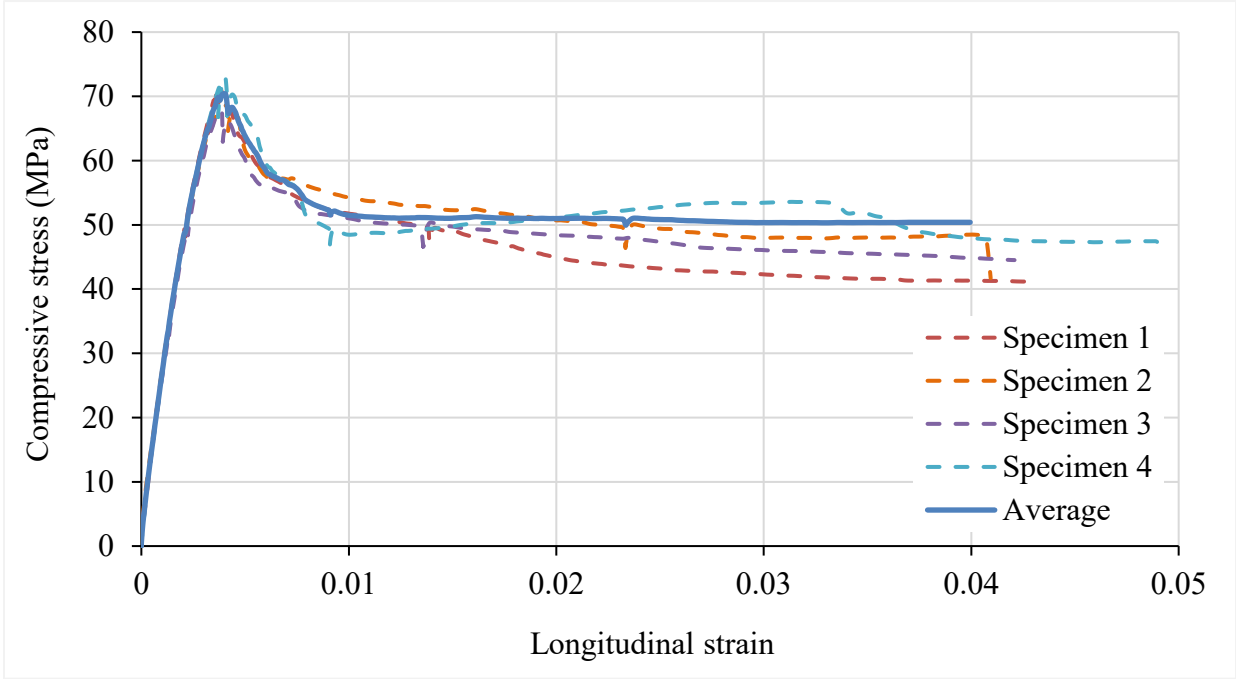


Figure B- 4: Stress-strain curves for 1.5% confinement ECC square columns

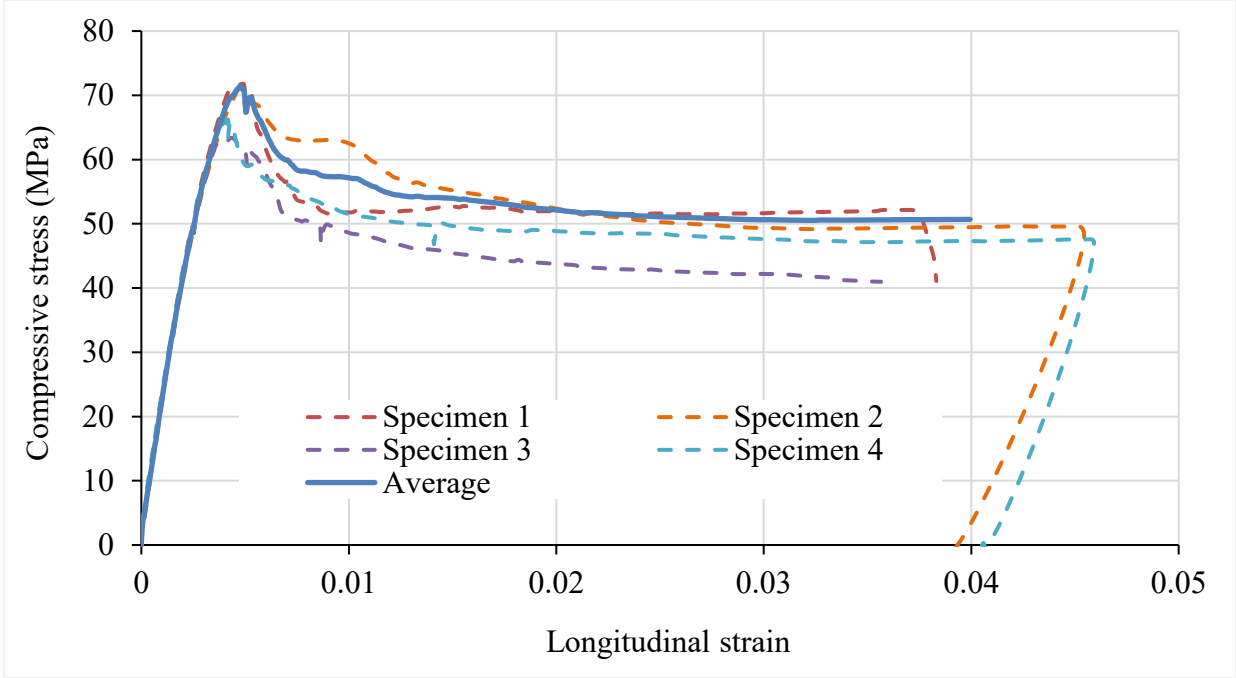


Figure B- 5: Stress-strain curves for 2% confinement ECC square columns